NASA TECHNICAL TRANSLATION

NASA TT F-589

NASA TT F-589

SATELLITE METEOROLOGY

Edited by K. S. Shifrin and V. L. Gayevskiy

Hydrometeorological Press, Leningrad, 1968

NATIONAL AERONAUTICS AND SPACE ADMINISTRATION • WASHINGTON, D. C. • JUNE 1970

SATELLITE METEOROLOGY

Edited by Doctor of Physical Mathematical Sciences K. S. Shifrin
and Candidate of Geographical Sciences V. L. Gayevskiy

Translation of "Sputnikovaya Meteorologiya," Glavnoye Upravl-
eniye Gidrometeorologicheskoy Sluzhyere Pri Sovete Ministrov
SSSR, Ordena Trudovogo Krasnogo Znameni Glavnaya Geofizicheskaya
Observatoriya u.m. A. I. Voyeykov. Hydrometeorological Press,
Leningrad, Trudy 221, 1968

NATIONAL AERONAUTICS AND SPACE ADMINISTRATION

For sale by the Clearinghouse for Federal Scientific and Technical Information
Springfield, Virginia 22151 – CFSTI price $3.00

SATELLITE METEOROLOGY

FOREWORD

In the collection the problems of interpretation of satellite data and the methods of determination of meteorological atmospheric parameters according to the data of satellite measurements are examined, and the results of investigation of radiation processes in the terrestrial surface-atmosphere system are presented. The collection is calculated for specialists working in the field of the physics of the atmosphere, both graduate students and upperclassmen of hydrometeorological institutes and universities.

TABLE OF CONTENTS

Page No.

NASA TECHNICAL TRANSLATION

ACTINOMETRIC EQUIPMENT OF SOVIET WEATHER SATELLITES

V. A. Besking, V. L. Gayevskiy, V. V. Zenkov,
L. B. Krasil'chnikov, B. V. Khlopov, V. A. Khrustalev and G. I. Shuster

ABSTRACT: In the article the authors present the operation principles and main characteristics of actinometric equipment of weather satellites, installed on Soviet satellites Kosmos-122, Kosmos-144 and Kosmos-156. The optical systems are described and illustrated, and the system of collection of actinometric information is analyzed.

The actinometric equipment of Soviet meteorological satellites serves for /3* measuring the earth's and atmosphere's own outgoing radiation, the outgoing shorwave radiation reflected by the earth and its atmosphere, and the effective radiation temperature of the terrestrial surface or clouds. In accordance with the above-mentioned purposes of the equipment it operates in three spectral bands. The values measured in the 0.3-3 μ spectral band are the energy brightness and density of the flow of reflected shortwave radiation. In the 3-30 μ spectral band the energy brightness and outgoing radiation flow density are measured. The effective radiation temperature is determined by measuring the effective brightness in the 8-12 μ spectral band.

All types of the above-mentioned actinometric measurements are carried out by two types of actinometric instruments which are included in the equipment.

The first type is a narrow-angle instrument (brightness meter) with an instantaneous field of vision angle of 4° × 5° with a working viewing angle in the direction, perpendicular to the flight trajectory of the satellite amounting to ±66°.

* Numbers in the margin indicate pagination in the foreign text.

The second type is a wide-angle instrument (flow density meter) with an angle of vision of 136-140°.

In order to increase the reliability of the equipment all the instruments are used in sets of two. The instruments of the duplicating set may be turned on on command from the earth. The optical diagrams of the longwave channel of the instrument of the first type and the instrument of the second type, explaining their working principle, are given in Figures 1 and 2.

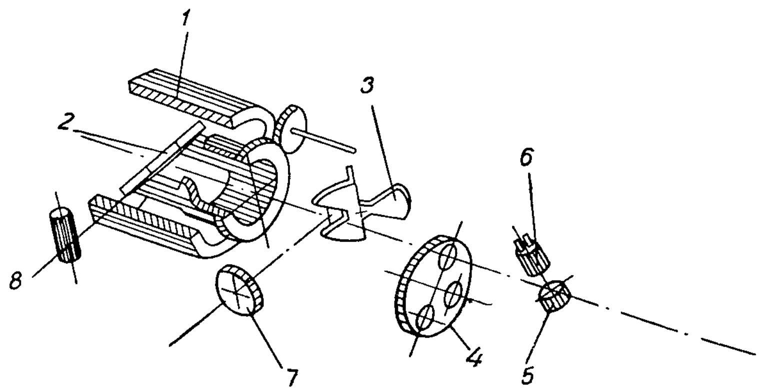

Figure 1. Optical Diagram of a Narrow-Angle Instrument.

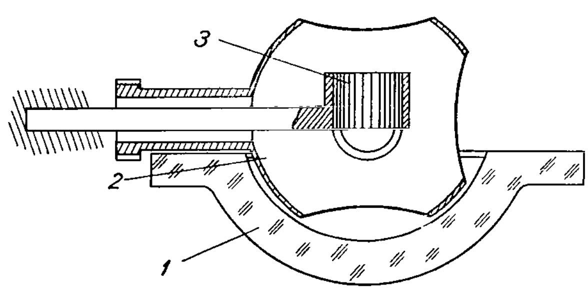

Figure 2. Optical Diagram of a Wide-Angle Instrument.

The optical systems of the actinometric instruments serve for limiting the angles of the field of vision, limiting the spectral band, concentrating the flow of radiation on the frequency transformer flow receivers, and for the instruments of the first type it is used also for calibration and collection of information by means of scanning.

The principal elements of the optical system (Figure 1) are:

1) a cylindrical streamlined shell made of the KRS-5 crystal, which makes the instrument airtight and enables us to scan and calibrate;

2) the scanning mirror of a conical shape, which compensates the divergence of the beam which passed through the streamlined shell;

3) the mirror three-leaf modulator;

4) filters for separating the spectral bands in measurements and calibration; /4

5) extra-axial parabolic mirror;

6) bolometer;

7) cosmic window made of the KRS-5 crystal;

8) calibrating light source unit.

The optical system of a shortwave channel is the simplest one, since in this channel it is not necessary to switch over the filters and use a two-beam system.

The optical systems of the instrument of the second type are identical and they differ only by the materials used in them and the filter covers. The corresponding diagram is given in Figure 2, where 1 is the filtering streamlined shell , 2 is the modulator, 3 is the bolometer.

The satellite on which the actinometric equipment is installed, rotates around the earth on a circular orbit (mean flight altitude is 600 km) and is oriented with respect to the earth in such a way that the optical axis of the instruments are constantly directed vertically downward.

The orientation of the satellite along the path excludes its rotation around the vertical axis.

The diagram of the collection of actinometric information by the wide-angle and narrow-angle instruments is presented in Figure 3.

The survey of the terrestrial surface by the narrow-angle instrument along the satellite's flight trajectory is carried out by the movement of the satellite itself, while the survey in the perpendicular direction is carried out by means of rocking of the input mirror 2 about the 0-0' axis (Figure 1).

As it had been already mentioned the measurement of energy brightnesses is carried out by a narrow-angle instrument in three spectral ranges (0.3-3, 8-12 and 3-30 μ over two independent channels as the result of which the 8-12 and 3-30 μ ranges are combined in one of the measuring channels and are separated by the exchange of the corresponding filters. /5

The flow entering the input of the channel, is modulated by the mechanical modulator with a frequency of 80 cps. The radiation of the modulator in the 0.3-3 μ spectral range is practically absent, as the result of which the shortwave flow is modulated down to the zero level when it is overlapped by the light-beam modulator vein.

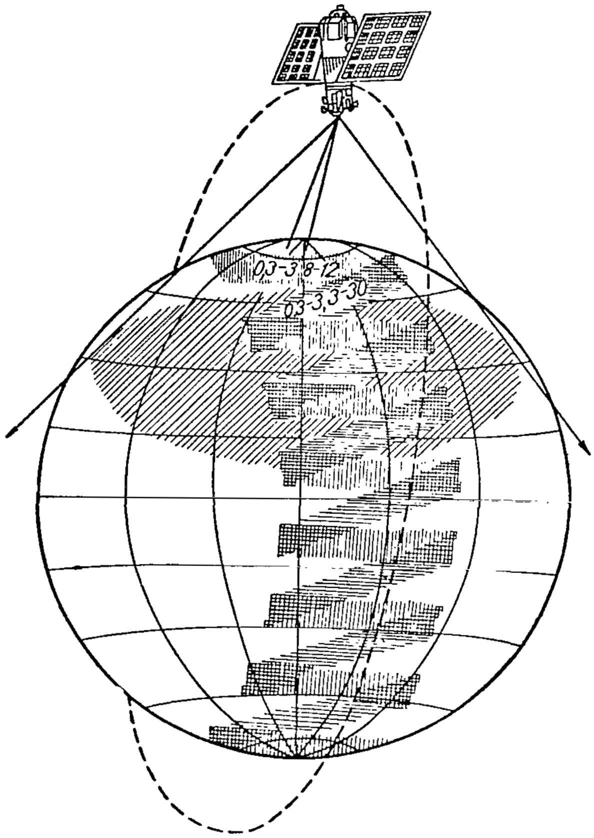

Figure 3. System of Collection of Actinometric Information.

In the 3-30 and 8-12 μ channel the instrument operates according to the two-beam system. In this channel modulation is carried out by means of a mirror modulator by comparing the flows from the earth and from outer space.

The radiation measured and the space radiation arrive through different streamlined windows, however both optical channels are thermally balanced to the maximum, and have an equal quantity of identical elements, which makes it possible to eliminate almost completely the interfering radiation of the optical system parts.

The modulated flow falls on the receiver of the bolometric type and causes the appearance at the outputs of the bolometric bridge of an alternating voltage, which is thereupon amplified, rectified, and filtered in the electrical unit, and then delivered to the output of the equipment in the form of a direct voltage measuring between 0 and 6 V. /6

The work of the shortwave and longwave channels is synchronized in such a way, that at the same time moment both channels receive radiation from the same area on the earth. Inasmuch as in the longwave channels there are two independent spectral ranges, the frequency of the scanning lines of the 0.3-3 μ channel is twice as large as the frequency of the lines of the 8-12 μ or 3-30 μ channel.

The measurement of the density of the radiant flow arriving from the earth into the outer space, is carried out by the wide-angle non-scanning instrument with two spectrum bands of 0.3-3 and 3-30 μ , for which purpose two optical systems are built into the instrument, which are directed at the same area on the earth. The input channels of these systems are hemispheric streamlined shells, made of quartz and KRS-5 with an intercepting coating, functioning as filters.

The radiant flow included in these optical systems is modulated with the frequency of 64 cps and comes to the bolometric receiver. The modulation level for the wide-angle heat channel is determined by the temperature of the modulator, which under established conditions is approximately equal to the temperature of the instrument's body.

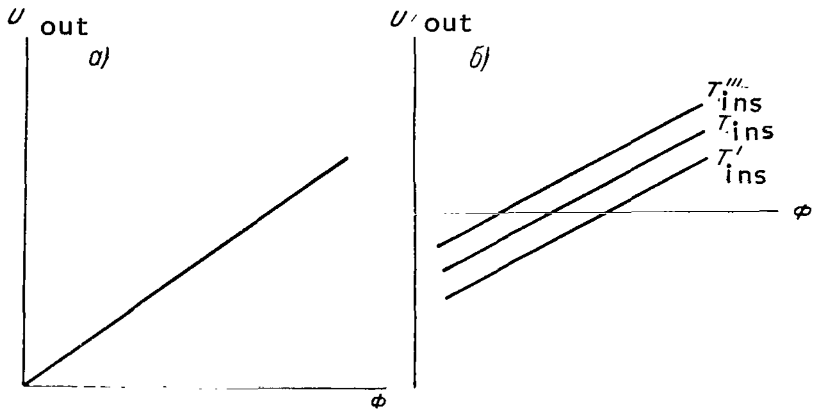

Figure 4. Input Characteristics of Actinometric Equipment.

In the 3-30 μ spectrum band the radiation of the modulator is commensurable with the incoming radiation, and may be either smaller or greater than the incoming flow. Since the receiver reacts to the difference between the two flows, for the purpose of eliminating the ambiguity of the sign of the outgoing signal into the 3-30 μ channel we introduce a supporting voltage generator, the work of which is synchronized with the rotation of the modulator. The phase indicator circuit, supplied by this generator, delivers the voltage changed in a jump, which is determined by the sign of the output signal. In the 0.3-3 μ band the modulator radiation is equal to zero, as the result of which in this band the sign of the output signal may be only positive.

On the basis of the above, it is not hard to represent (Figure 4a) the output characteristics of instruments of the first type and the shortwave instrument of the second type, which in the unreal case of complete thermal equilibrium, identity of elements of optical channels of the two-beam system, and linearity of the amplification circuit are determined by the equation

$$U_{out} = k\Phi$$

where U_{out} is the output voltage, k is the coefficient of conversion of the flow into voltage, Φ is the flow of radiation entering the instrument. /7

For the longwave instrument of the second type

$$U_{out} = k(\Phi - \Phi_{ins}),$$

where Φ_{ins} is the flow dependent on the temperature of the instrument body.

The family of the output characteristics of this instrument is presented in Figure 4b.

The constancy of the value of the conversion coefficient is affected by a number of factors, such as for example, the constancy of the amplifier amplification coefficient, sensitivity of the bolometer, and optical characteristics of the optical elements.

It is impossible to maintain the constancy of these factors during the entire service life of the actinometric equipment, as the result of which in a narrow-angle instruments periodic calibration is provided for, and in wide-angle instruments, where it is very difficult to carry this out, but where the optical system is simpler, the electrical calibration of the amplification circuit is provided. To exclude the variability of the characteristics of actinometric equipment elements in processing information it is advisable to use the ratio between the output voltage and the voltage obtained during periodic calibration and standardization, performed every seven minutes. The standardization signals are obtained when the scanning mirror moves to a 90° angle from the nadir with the simultaneous turning on of the silicon standard lamp. In standardization, in order to exclude the interfering signals from the body of the standard lamp a quartz filter is introduced before the parabolic mirror.

Simultaneously with the standardization of the narrow-angle instrument, the calibration of the wide-angle instrument is carried out in the process of which a standard calibrating voltage with the frequency of 64 cps is delivered to the input of the wide-angle instrument amplifiers.

The output voltages of the actinometric equipment are transmitted into the telemetric system over 8 channels in the form of positive polarity voltages from 0-6 V, and interrogated in it with a frequency of 8 cps for channels of the narrow-angle instrument and with a frequency of 2 cps for channels of the wide-angle instrument.

For information interpretation, a synchronous signal channel is provided for in the instrument, over which discrete voltage levels between 0 and 6 V with a 2 cps interrogation frequency in this channel are delivered to the telemetric equipment. The synchronous-signal channel assures the separation of information, corresponding to various sectors of the spectrum, marks the work period of the standardization system, and determines the sign of the radiation in the 3-30 μ wide-angle channels.

The temperature of the actinometric equipment is measured in five points over special channels.

The geographical tying in of information is carried out by means of comparison of the signals, delivered by the unit of the single time aboard, with the signals of the line mark, mixed into the basic information.

The relative root-mean-square measurement error, determined under laboratory conditions during calibration of the equipment on a single day, amounts to about 0.5%. This error is random and has been calculated without taking into account the systematic error, which may be connected with the calibration process.

Naturally, the random error during the entire service life of the equipment on the satellite, connected with aging of its elements, may increase somewhat.

PRINCIPLES OF CALIBRATION OF LONGWAVE ACTINOMETRIC INSTRUMENTS ON WEATHER SATELLITES

L. B. Krasil'shchikov

ABSTRACT: In the article the author presents the principles of the method of calibration of longwave actinometric instruments of the satellites by means of laboratory vacuum simulators of the black radiation and examines the requirements presented to the calibrating equipment.

The longwave actinometric instruments of Soviet weather satellites measure the outgoing radiation. /8

Depending on the angle of the field of a vision of the instrument either the energy brightness of the earth's-atmosphere system is measured or the energy density of the radiation flux [1].

The brightness is measured in spectral bands of 3-30 and 8-12 μ, and flux density is measured only in the 3-30 μ range. Before they are installed on the satellites, the actinometric instruments must be calibrated on the ground.

Calibration of the instruments consists of determining the conversion coefficients or conversion factors for changing over from the values of the output voltage to the measured values of the energy or effective brightness and the energy density of the flux.

The calibration is performed experimentally, since the calculated determination of conversion coefficients gives only approximate values.

The conversion factors are a function of time, instrument temperature, and the feed voltage.

Due to the above-mentioned causes, in determining the totalities of the conversion factors (calibration curves) it is necessary, as a parameter, to prescribe the temperature of the instruments and the feed voltage. To make an allowance for the influence of spontaneous variations of the conversion factor with time, periodic electrical calibration of the amplification circuits is provided for in the actinometric wide-angle instruments, and in the narrow-angle instruments, the periodic standardization by a constant radiation flux. The initial calibration and standardization signals, in their turn dependent on the temperature and the feed voltage, are determined during the calibration.

The longwave channels of the actinometric equipment operate in limited, but wide spectral ranges, as the result of which the reproducible calibration may be achieved when strictly conditioned radiators are used as the sources.

The best source of radiation, possessing a strict dependence of the radiated flux on the temperature, and its known spectrum distribution, is the absolutely black body. This circumstance, as well as the elimination of the multiple reflections between closely located receiver and radiator under the calibration conditions, require the use of an absolutely black body as the model's radiator. /9

If the radiator is an absolutely black body, the radiating flux, picked up by the receiver is proportional to the difference $T_1^4 - T_2^4$, where T_1 is the temperature of the radiator, and T_2 is the temperature of the receiver. Hence it follows that the output voltage depends both on the temperature of the radiator and on the temperature of the receiver. In general the output voltage may be a complex function of the temperature of the instrument's body, because on it depends also the sensitivity of the receiver and the capacitor's amplification coefficient. If we consider, that the temperature of the body $T_b \approx T_2$, then

$$U = k(T_2)\left(T_1^4 - T_2^4\right)\Omega, \tag{1}$$

where Ω is the aperture of the instrument. In devices, where the comparison is made with a cold radiator of a constant temperature when the optical channels of measurement and comparison are identical

$$U = k(T_2)\left(T_1^4 - T_c^4\right)\Omega, \tag{2}$$

where T_c is the temperature of the cold radiator.

As it follows from expressions (1) and (2) in both cases the output voltage depends on the temperature of the receiver, however in the second case this dependence is determined only by the $k(T_2)$ function, which often may be quite close to a constant value.

Plotting of the calibration curves with the use of an absolutely black radiator should be carried out varying the radiation flux directed into the instrument by varying the temperature of the radiator, and not by varying the aperture Ω, since in actual practice the actinometric instruments are used with a constant temperature.

By making calibration conditions similar to the conditions of the work of the actinometric instrument, we decrease substantially the errors connected with the selectivity of the receiving device, especially in the 8-12 μ band.

As it has been already mentioned, during calibration we should establish a relationship between the output voltage and the effective brightness. In the 8-12 μ band, by effective brightness we should understand

$$\frac{1}{\pi}\int_{\lambda_1}^{\lambda_2} f(\lambda, T)\, d\lambda,$$

where λ_1 and λ_2 are boundaries of the range, determined by the spectral characteristics of the instrument. Since the instrument does not possess a strict П-shaped spectral characteristic, the position of points λ_1 and λ_2 may be indicated quite indefinitely.

A specific calibration characteristic is obtained, if as an independent variable we adopt the value of the energy brightness of an absolutely black radiator $B = \sigma T^4/\pi$ milliwatt/cm^2·steradian. This value does not depend on the spectral characteristics of the actinometric instruments themselves, as the result of which it was adopted as an independent variable in plotting the characteristics, both in the 8-12 μ and in the 3-30 μ bands. This calibration characteristic plotting principle is all the more justified, by the fact that actually the changing and measured value during calibration is the temperature of the black radiator T. The value of the effective brightness, when necessary, may be calculated according to the known value B with a certain approximation.

Since in all wide-angle instruments the angle of the field of vision is constant, equal to the aperture angle, and amounts to 140°, in calibrating wide-angle instruments we adopt as the independent variable the density of current Φ, coming from the black radiator in a solid angle with an opening of 140°, $\Phi = 0.885\ \sigma T^4$ milliwatts/cm^2. Value Φ does not depend on the instrument's own spectral characteristics. /10

For calibration under conditions similar to the actual working conditions of the equipment on the satellite, it is required that the input windows of the instruments (streamliners), creating an additional modulated flow, would perform a thermal exchange with the external medium only by means of radiation. Exchange by means of convection or heat conductivity of the air should be excluded. In this case the temperature of the shells would be established close to their temperature on the satellite, if the conditions of the radiant heat exchange of the shells themselves, and their frames during calibration would not differ substantially.

We can use the calibration curves obtained by means of an absolutely black body, for determining the energy brightness of grey radiators.

The calibration curves of a wide-angle instrument are absolutely applicable for only a grey and a simultaneously isotropic radiator.

On the basis of the above, we can see that the calibration process consists of determination of the output voltage U_{out} as a function of the temperature of the black radiator T_{rad}, the temperature of the instrument's body T_{ins} and of the feed voltage U_{fd}, determination of the standard signal $U_{st} = f(T_{ins}, U_{fd})$ and a determination of the calibration signal $U_c = f(T_{ins}, U_{fd})$. The calibrating equipment is based on black spherical radiators with a variable temperature and cold radiators, cooled with liquid nitrogen.

The coefficient of radiation of a spherical radiator according to [2] is equal to

$$\varepsilon = \frac{1+\sqrt{1-\left(\frac{d}{D}\right)^2}}{1+\sqrt{1-\left(\frac{d}{D}\right)^2}+\left(\frac{d}{D}\right)^2\frac{1-\varepsilon_k}{2_k}}, \quad (3)$$

where D is the diameter of the sphere, d is the diameter of the opening, ε_k is the coefficient of radiation of the internal coating of the sphere.

The dependence of the coefficient of radiation of the cavity on the coefficient of radiation of the coating under a different d/D ratio is presented in Figure 1.

We should note, that the cold radiator, operating actually as radiation absorber, should have a high absorption coefficient, while a high radiation coefficient in this case has no substantial significance. This reduces the requirements to the nonselectivity of the internal coating of the sphere in the longwave region of the spectrum, since the sphere radiates when $\lambda_{max} \approx 25\mu$, and absorbs radiation, which has a $\lambda_{max} \approx 10\ \mu$. The ε_k value of the enamel used with 25 μ was not determined, but this, as it follows from the above, is not very important.

Construction of imitators of black radiation with large output windows, having an $\varepsilon \geq 0.95$, is quite a feasible task. With an opening 200 mm in diameter in order to obtaine $\varepsilon = 0.98$ we require a sphere 400 mm in diameter, painted with an enamel paint with $\varepsilon_k = 0.8$.

As it had been already noted the calibration of actinometric instruments should be performed under the conditions which imitate the heat exchange in outer space.

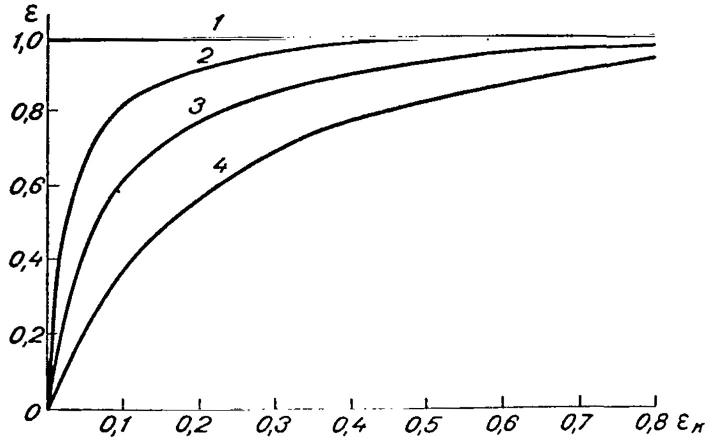

Figure 1. Dependence of the Radiation Coefficient of a Cavity on the Radiating Capacity of its Internal Coating.

1) $\frac{d}{D}=0$; 2) $\frac{d}{D}=0{,}1$; 3) $\frac{d}{D}=0{,}5$; 4) $\frac{d}{D}=0{,}8$.

For this purpose we should eliminate the transmission of a heat to gas. The natural way of attaining this is by placing the instruments calibrated together with the spherical radiator into a vacuum. /11

Let us evaluate the required vacuum, which should be maintained in the system.

As we know [3], the heat conductivity of air begins to depend on air pressure p, when the main free pass of molecules $\bar{\lambda}$ becomes approximately equal to the distance between the walls.

Let us assume that in our case $\bar{\lambda}$ = 2 cm, whereas on the basis of $\bar{\lambda} = 1/\sqrt{2}\pi n\delta^2$, where n is the number of molecules in a unit of volume, δ is the effective diameter of the molecule, we have

$$n = \frac{1}{\sqrt{2}\,\lambda\pi\delta^2} \approx 6{,}5 \cdot 10^{13}\ 1/\text{cm}^3,$$

which corresponds to $\approx 2 \cdot 10^{-3}$ Torr.

With a further decrease of pressure, beginning with this value, the heat conductivity of gas in the vacuum system described decreases. What residual pressure will prove satisfactory? Apparently, it will be a pressure, when the transmission of heat by heat conductivity through gas is substantially smaller than transmission of heat by radiation. Heat transmission by radiation is proportional to the difference of the force powers of the temperature, and transmission by heat conductivity is proportional to the difference in temperatures. Evidently the greatest ratio $q = T_1 - T_2/T^4{}_1 - T^4{}_2$ corresponds to the worst calibration.

Since $q = \frac{1}{(T_1^2+T_2^2)(T_1+T_2)}$, for the calculation we should take the smallest T_1 and T_2.

In our case T_1 = 0°C and T_2 = - 196°C. According to [3] heat transmission by heat conductivity through gas is equal to /12

$$W = \alpha \varkappa p \sqrt{\frac{273}{T_2}} (T_1 - T_2) \text{ watts/cm}^2 \tag{4}$$

where α is the accommodation coefficient, $\alpha \approx 1$, κ is the heat conductivity of the free molecules for air (κ = $16.6 \cdot 10^{-6}$ watts/cm^2 degrees), p is the pressure in Torrs.

Assuming that $W = 0.1\sigma(T_1^4 - T_2^4)$, we have

$$p = \frac{0{,}1\sigma \cdot 4T_1^3}{\alpha\varkappa \sqrt{\frac{273}{T_2}}} \approx 6 \cdot 10^{-4} \text{ Torr}$$

The residual pressure of the order of 10^{-4} Torr. during calibration of actinometric instruments is easily maintained by a simple vacuum device, containing a preliminary rarefaction pump VN461M and a high-vacuum pump VA01-1.

Let us evaluate the accuracy of obtaining the conversion factor, which we get during calibration. The general expression for the value of the conversion factor γ_1 in$\cdot$cm^2 ster/volts of a narrow-angle instrument, obtained as the result of calibration, will be

$$\gamma_1 = \frac{\pi U_{out}}{\sigma\varepsilon \left(T_1^4 - T_x^4\right)}. \tag{5}$$

The value of the conversion factor γ_2 in cm^2/watts of the wide-angle instrument

$$\gamma_2 = \frac{U_{out}}{\sigma\varepsilon \left(T_1^4 - T_\kappa^4\right) \sin^2 \frac{\vartheta}{2}}, \tag{6}$$

where U_{out} is the output voltage, σ is Stephan-Boltzmann's constant, ε is the radiation coefficient of the calibration radiators, T_1 is the radiator temperature, T_B is the temperature of the instrument's body, T_c is the temperature of the cold radiator, ϑ is the aperture of the wide-angle instrument.

Assuming that $T_1^4 - T_c^4 \approx T_1^4$, we have for the narrow-angle instrument a relative root-mean-square error, or the variation coefficient

$$\frac{\sigma_{\gamma_1}}{\gamma_1} = \sqrt{\left(\frac{\sigma_{U_{out}}}{U_{out}}\right)^2 + \left(\frac{\sigma_\varepsilon}{\varepsilon}\right)^2 + \left(\frac{4\sigma_{T_1}}{T_1}\right)^2}. \tag{7}$$

Accordingly the variation coefficient in calibrating the wide-angle instrument is equal to

$$\frac{\sigma_{\gamma_2}}{\gamma_2}=\sqrt{\left(\frac{\sigma_{U\text{out}}}{U_\text{out}}\right)^2+\left(\frac{\sigma_\varepsilon}{\varepsilon}\right)^2+\left(\frac{2\sigma_\vartheta}{\tan\vartheta}\right)^2+\left(\frac{2\sigma_{T_1}}{T_1-T_k}\right)^2}. \quad (8)$$

We may prove, that assuming that $\sigma_x = \Delta x/2$, where σ_x is the root-mean-square error of measurement of each variable, and Δx is the confidence range, we have for the narrow-angle instruments $\sigma_{\gamma_1}/\gamma_1 \approx 2\%$, and for the wide-angle instruments $\sigma_{\gamma_2}/\gamma_2 \approx 8\%$. /13

REFERENCES

1. Vetlov, I. P.: "Investigation and Outgoing Radiation by Means of the Kosmos-122 Satellite,: *Meteorologiya i Gidrologiya,* No. 1, 1967.
2. Blokh, A. G.: *Osnovy Teploobmena Izlucheniyem* [Principles of Heat Transfer by Radiation], GEI, 1962.
3. Dashman, S.: *Nauchnyye Osnovy Vakuumnoy Tekhniki* [Scientific Principles of Vacuum Technology] *IL* (Foreign Literature Press), 1950.

INFORMATION PROPERTIES OF SCANNING INFRARED EQUIPMENT OF WEATHER SATELLITES

A. A. Kmito and V. S. Stepkin

ABSTRACT. In the process of measurements of the radiant flow a part of the information is lost. In the article, the authors determine the root-mean-square error of the quantam signal. They obtained the expression for the dynamic errors in measurements. The errors caused by the action of the unstabilizing factors, are examined applicably to the two channel optical system. The measure for indeterminancy is the convention entropy. The probability of detection of the signal is evaluated under the condition of independence of the signal and noise, and also under the action of the normally distributed radiant flow and noise on the system. The authors obtained an expression for the probability of detection of the signal and determined the loss of information, caused by the indeterminancy in detection of the signal. In conclusion they give a complete expression for the evaluation of information properties of the equipment of weather satellites.

The scanning infrared equipment, intended for measuring the value of the radiant flux and obtaining a thermal map of the underlying surface, may be considered as a channel for conversion and transmission of information on the values measured. For the analysis and synthesis of this equipment, we may use the information theory apparatus. The main advantage, indicating the rationality of the use of this apparatus, consists of the possibility of taking into account the random character not only of the measurement errors but of the measurement value also. /14

In the process of measurement the radiant flux falling on the input pupil of the instrument, is transformed in it to an electrical signal, which is the carrier of information on the size of the flux. The amount of information contained in the signal, according to [1], is written down in the following way:

$$H_{\Delta}(\Phi)=\sum_{i=1}^{N} p(u_i)\log p(u_i), \tag{1}$$

where $p(u_i)$ is the probability of the appearance of signal u_i, N is the number of levels of quantization of the signal.

During the measurement of the radiant flux a part of the information is lost. The information loss is caused by measurement errors and indeterminancy in detecting the signal.

The errors in measuring the absolute value of the radiant flux are posed by the quantization of the signal in time and with respect to the level, by the limited sensitivity of the equipment and its time lag, respectively, and also by the action of the noises and the unstabilizing factors. Let us examine them.

Quantization of the signal with respect to time, without taking into account the dynamic characteristics of the equipment, is carried out on the basis of A. V. Kotel'nikov's theorem, assuming that the spectrum of the signal with a length T is included in the frequency band between 0 and ω_B. We obtain the absolute root-mean-square error of determination of the input radiant flux $\delta\Phi_f$, caused by this, using Rayleigh's theorem [2], in the following form:

$$\delta\Phi_f = \frac{1}{\pi T} \int_{\omega_B}^{\infty} |F(i\omega)|^2 d\omega, \tag{2}$$

where $|F(i\omega)|$ is the amplitude-frequency spectrum of the flux.

In the case when the correlation function of the radiant flux measured (which is often performed in actual practice) is approximated by the exponential dependence of the form of /15

$$R(t) = R(0)e^{-\alpha|t|}, \tag{3}$$

the signal's spectral density is expressed [3] by the formula

$$|F(i\omega)| = \frac{R(0)}{\pi} \frac{\alpha}{\alpha^2 + \omega^2}, \tag{4}$$

where R(0) is the dispersion of the radiant flux measured.

Taking this into account, we rewrite expression (2) in the following manner:

$$\delta\Phi_f = \frac{\alpha^2 R^2(0)}{\pi^3 T} \int_{\omega_B}^{\infty} \frac{d\omega}{(\alpha^2 + \omega^2)^2}. \tag{5}$$

In measuring the radiant flux by equipment, the dynamic properties of which may be characterized by the inertia coefficient τ, we introduce dynamic errors, dependent on the specific features of interpretation of the results obtained [3]. If the instantaneous readings of the signal are interpreted as the instantaneous magnitudes of the value measured, the root-mean-square error of it is expressed by the formula

$$\delta u = \left[R_1(0) - \frac{1}{\tau} \int_0^\infty e^{-\frac{t}{\tau}} R_1(t)\, dt \right]^{1/2}. \tag{6}$$

Let us consider that approximation of the free type is correct, and take into account that dispersion of the inertial instrument readings $R_1(0)$ is connected with the dispersion of the measured value R(0) [3] by the relationship

$$R_1(0) = \frac{k^2(\omega)\, s^2(\omega)\, R(0)}{1 + \alpha\tau}. \tag{7}$$

Then the dynamic error of the measurement of instantaneous values of the radiant flux will be

$$\delta\Phi_d = \frac{1}{s(\omega)\, k(\omega)} \sqrt{\alpha\tau R_1(0)}. \tag{8}$$

where $s(\omega)$ is the volt sensitivity of the receiver with the given modulation frequency ω, $k(\omega)$ is the transmission function of the electric channel.

Quantization of the signal according to the level, caused by the limited sensitivity of the equipment, results in the appearance of errors in the measurement of its amplitude values. Taking into account, that the threshold sensitivity of the equipment examined $\Delta\Phi_{thr}$ does not undergo any substantial changes in the working range and that the quantization errors with respect to level within the limits of the quantization steps are distributed uniformly, for evaluating this error we may use the known [2] formula

$$\delta\Phi_a = \frac{\Delta\Phi_{thr}}{2\sqrt{3}}. \tag{9}$$

Measurement errors, caused by the action of the disturbing factors, depend on the design of the structural diagram of the equipment, including the optical path, determining its resistance to noises. The latter is especially high in the two-channel optical system, which is ordinarily used in the scanning equipment of weather satellites. In this system the input radiant flux Φ /16
is reflected from the scanning mirror m_1, and the standard flux Φ_0 is reflected from the fixed mirror m_2. These fluxes pass through optical filters f_1 and f_2, and modulated by the mechanical interrupter M, which provides for the alternating arrival of these fluxes on the collecting mirror m_3, which directs the flux to the receiver. The electrical signal, generated by the receiver,

arrives at the electric circuit of the equipment, and is then transmitted over the telemetric system, the errors of which are not examined here. The principal equation of the equipment, collected according to the system indicated, evidently will have the following appearance:

$$u=c_1\left[p'_{m_1}p'_{f_1}B-p'_{m_2}p'_{f_2}B_0+\frac{A}{A_0}\sigma\left(A_{m_1}b_{m_1}\varepsilon_{m_1}T^4_{m_1}-A_{m_2}b_{m_2}\varepsilon_{m_2}T^4_{m_2}\right)\right]. \qquad (10)$$

where $c_1 = \omega A_0 s(\omega)k(\omega)p'_{m_3}$; B and B_0 are energy brightnesses at the input; ω is the angle of the field of vision of the equipment; A and A_0 are the areas of the input pupil and receiver, respectively; σ is the radiation low constant.

The efficiencies of the elements of the optical channel are designated with p' with the corresponding indices, the temperature is T, the radiating capacity is ε, the area is A and the coefficients making an allowance for the share of radiation in the spectral range selected are b.

In case the values included in formula (10) are independent, the absolute root-mean-square error of measurement of the radiant flux $\delta\Phi_B$, caused by the action of the additive noises δu, the randomly changing external actions, and instability of the standard flux $\delta\Phi_0$, will be

$$\delta\Phi_B=\frac{c_2}{c_1}\sqrt{\begin{aligned}&(p'_{m_1}B\delta p'_{f_1})^2+(p'_{f_1}B\delta p'_{m_1})^2+(p'_{f_2}B_0\delta p'_{m_2})^2+(p'_{m_2}B_0\delta p'_{f_2})^2+\\&+(p'_{m_2}p'_{f_2}\delta B_0)^2+\frac{\sigma^2\bar{A}^2\bar{b}^2}{\pi^2A_0^2}\{[4\bar{T}^3_{m_1}\bar{\varepsilon}_{m_1}\delta(T_{m_1}-T_{m_2})]^2+[(T^4_{m_1}-T^4_{m_2})\delta\bar{\varepsilon}_{m_1}]^2\}+\\&+\left(\frac{\delta u}{c_1}\right)^2+\left(\frac{u\delta k(\omega)}{c_1k(\omega)}\right)^2+\left(\frac{u\delta s(\omega)}{c_1s(\omega)}\right)^2+\left(\frac{u\delta p'_{m_2}}{c_1p'_{m_2}}\right)^2\end{aligned}}. \qquad (11)$$

We note, that from the formula obtained it follows that the optical system has the highest noise resistance if the radiation of mirrors m_1 and m_2 themselves is equal, and also if the coefficients of transmission of both filters are equal ($\varepsilon_{m_1} = \varepsilon_{m_2} = \bar{\varepsilon}$, $T_{m_1} = T_{m_2}$ and $p'_{f_1} = p'_{f_2} = p'_f$). In this case the amplitude of the output signal u is determined by the difference of the radiant fluxes $\Phi - \Phi_0$. The relative root-mean-square error, caused by the action of the factors examined, in this case will be minimum and equal to

$$\frac{\delta(\Phi-\Phi_0)}{(\Phi-\Phi_0)}=\sqrt{\left(\frac{\delta k(\omega)}{k(\omega)}\right)^2+\left(\frac{\delta s(\omega)}{s(\omega)}\right)^2+\left(\frac{\delta u}{u}\right)^2+\left(\frac{\delta p'}{p'}\right)^2}, \qquad (12)$$

From the latter relationships we can see that the errors depend substantially on the signal-to-noise ratio at the output of the equipment, increasing at the beginning of the measurement band.

In evaluating the total error of measurements we should sometimes take into account the fact that the mechanical modulation of the radiant flux results in the loss of information on the value measured at those time moments when the flux is overlapped by the modulator's veins. The value of the modulation error decreases with the increase of the modulation frequency ω according to the relationship /17

$$\delta\Phi_{M} = \Phi\left(1 - \cos\pi\frac{\Omega}{\omega}\right), \tag{13}$$

where Ω is the principal value of the change in the input radiant flux.

The total measurement error results in the fact that after obtaining the results there remains a certain indeterminancy with respect to the values of the radiant flux present. The over-all measure of the results in determinancy is the conventional entropy, which represents the sum of particular conventional entropies weighted by the corresponding probabilities, i.e.,

$$H_{\Delta}(\Phi/z) = \sum_{j=1}^{N} p(z_j) H_{\Delta}(\Phi/z_j), \tag{14}$$

where $z = \Phi + \delta\Phi$ is one of the possible results of measurement, $p(z_j)$ is its probability,

$$H_{\Delta}(\Phi/z_j) = \sum_{i=1}^{N} p(u_i/z_j) \log p(u_i/z_j),$$

$p(u_i/z_j)$ is the conventional probability of the fact that the value of u_i occurred within the i-th range, if we know that the measurement result corresponded to the j-th interval z.

Determination of the conventional probability $p(u_i/z_j)$ is connected with the necessity of constructing particular laws of probability distribution z. A conventional probability $p(z_j/u_i)$ is determined more simply. As the result of conversion from probability $p(u_i/z_j)$ to probability $p(z_j/u_i)$ we obtain the following expression for determining the conventional entropy:

$$H_\Delta(u/z) = \sum_{j=1}^{N}\sum_{i=1}^{N} p(z_j/u_i)\,p(u_i)\log\frac{p(z_j/u_i)\,p(u_i)}{\sum\limits_{i=1}^{N} p(z_j/u_i)\,p(u_i)}\,. \tag{15}$$

From expression (15) it follows that for calculating the conventional entropy we should have a law of distribution of the sum $u + \delta u$. Within the limits of the quantization range we can assume, that the value of the signal is extributed according to a uniform law. We assume that the law of the error measurement distribution is normal. This assumption in general does not contradict the error theory. Then, as it is shown in [4], the conventional probability $p(z_j/u_i)$ will be equal to

$$\begin{aligned} p(z_j/u_i) = \frac{1}{2}\Big\{ & (j+1)\,\mathrm{erf}\left[(j+1)\frac{m}{\sqrt{2}}\right] - 2\,\mathrm{erf}\left(j\frac{m}{\sqrt{2}}\right) + \\ & + (j-1)\,\mathrm{erf}\left[(j-1)\frac{m}{\sqrt{2}}\right] + \sqrt{\frac{2}{\pi}}\,\frac{1}{m}\times \\ & \times\left(e^{-(j+1)^2\frac{m^2}{2}} - 2e^{-j^2\frac{m^2}{2}} + e^{-(j-1)^2\frac{m^2}{2}}\right)\Big\}, \end{aligned} \tag{16}$$

where $m = \Delta/\sigma$ is the parameter, Δ is the quantization step, σ is the root-mean-square error, erf(t) is the tabulated Laplace function.

At the input pupil of the instrument the radiant flux arrives, representing a mixture of radiations of the underlying surface and atmospheric radiation. In this case the latter is an interference. Atmospheric radiation is transformed in the instrument in the same way as the principal signal. Let us assume, that the atmospheric radiation is subject to the normal law with the mathematical exploitation m_n and the standard deviation σ_n (for the spectral range selected). This assumption was made from the condition, that from the point of view of obtaining information this law is the most favorable, and in this case we evaluate the work of the instrument under the worst possible conditions. We have /18

$$f(\Phi_a) = \frac{1}{\sigma_n\sqrt{2\pi}}\,e^{-\frac{(\Phi_a - m_n)^2}{2\sigma_n^2}}\,.$$

As a result of the conversion of the radiant flux into electrical signal, the envelope of the error signal will have the following appearance

$$f(u_a) = \frac{(u_a - m_n)}{a\sigma}\,e^{-\frac{(u_a - m_n)^2}{2\sigma^2}}, \tag{17}$$

where u_a is the noise voltage, a is the coefficient of conversion of the radiant flux into the electrical signal.

In addition to the interference which is external with respect to the instrument, there are instrumental noises among which are the noise of the radiation receiver, and the electronic system noise. The distribution of the envelope of this noise according to work [5] is subject to the law

$$f(u_{\text{n}})=\frac{u_{\text{n}}}{n^2}e^{-\frac{u^2_{\text{n}}}{2n^2}}, \tag{18}$$

where n is the mean square value of the noise.

The interference signal and the noise are independent, therefore the envelope of the interference signal and noise total will be distributed according to the following law

$$f(r_0)=\frac{r_0}{\sigma^2_{\Sigma}}e^{-\frac{r_0^2}{2\sigma^2_{\Sigma}}},$$

where

$$r_0=\sqrt{u^2_{\text{n}}+(u_{\text{a}}-m)^2}, \qquad \sigma^2_{\Sigma}=n^2+\sigma^2a^2. \tag{19}$$

Further, let us assume that the value of the radiant flux from the decomposition element has been distributed according to the normal law with mathematical expectation m and root-mean-square deviation σ. This assumption is adopted, proceeding from the fact that under the normal distribution law we obtain the maximum of information on the size of the flow. Then as the result of conversion of the radiant flow into the electrical signal, at the output of the radiation receiver we obtain the distribution of the envelope of the signal in the following form

$$f(u)=\frac{(u-m)}{\sigma^2a^2}e^{-\frac{(u-m)^2}{2\sigma^2a^2}}. \tag{20}$$

We assume that at the output of the radiation receiver we observe an oscillation, which will represent either the mixture of the signal and the noise resultant, or the noise alone.

The distribution of the probability of the envelope of the signal and noise in this case is also subject to Rayleigh's law /19

$$f(E)=\frac{E}{\sigma_1^2}e^{-\frac{E^2}{2\sigma_1^2}},$$

where

$$E = \sqrt{u_n^2 + (u_a - m_n)^2 + (u - m)^2},$$
$$\sigma_I^2 = \sigma_n^2 a^2 + n^2 + \sigma^2 a^2.$$

This sum, having passed through the synchronous detector with the conversion law

$$z = \beta E,$$

where β is the conversion coefficient, we will have a distribution in the form of

$$f(z) = \frac{z}{\sigma_I^2 \beta} e^{-\frac{z^2}{2\sigma_I^2 \beta^2}}.$$

To determine the probability of detection of the signal let us find the threshold level. We shall obtain its value according to the probability of the false alarm.

Let us assume, that the instrument is acted upon by the noise only. Then the probability of false alarm is equal to

$$F = \int_{r_{thr}}^{\infty} \frac{r_0}{\sigma_\Sigma^2} e^{-\frac{r_0}{2\sigma_\Sigma^2}} dr_0 = e^{-\frac{r_{thr}}{2\sigma_\Sigma^2}}.$$

Hence

$$r_{thr}^2 = 2\sigma_\Sigma^2 \ln F,$$
$$u_n^2 + u_f^2 = 2\sigma_\Sigma^2 \ln F + m_f^2 \tag{21}$$

The value of function F may be determined from the ratio

$$F = \frac{\text{the number of permissible gradations skipped}}{\text{number of gradations}}.$$

Then the probability of detection of the signal will be determined as

$$p = \int_{r_{thr}}^{\infty} \frac{z}{\sigma_I^2 \beta} e^{-\frac{z^2}{2\sigma_I^2 \beta^2}} dz.$$

As the result of integration we obtain

$$p=\frac{1}{\sigma_1^2\beta}\left[1-\sigma_1^2\beta^2 e^{-\frac{(r_{\text{thr}}-u)^2}{2\sigma_1^2\beta^2}}\right]=\frac{1}{\sigma_1\beta}\left[1-\sigma_1^2\beta^2 e^{-(k_0-k)^2}\right], \tag{22}$$

where k is the signal-to-noise ratio.

The amount of information lost as the result of ambiguity in detection of the signal is equal to

$$H_\Delta(p)=\sum_{k=1}^{N} p_k \log p_k.$$

In this way, the amount of information which may be obtained at the output of the infrared instrument, taking into account the action of the above-examined factors will be determined from the expression /20

$$I(\Phi/z)=\sum_{j=1}^{N}\sum_{i=1}^{N} p(z_j/u_i)\,p(u_i)\log\frac{p(z_j/u_i)}{\sum_{i=1}^{N} p(z_j/u_i)\,p(u_i)}-\sum_{k=1}^{N} p_k \log p_k.$$

Using the above relationships it is not difficult to evaluate the information properties of specific models of equipment in the meteorological satellites.

REFERENCES

1. Venttsel', Ye. S.: *Teoriya Veroyatnostey*, [The Theory of Probabilities], 1962.
2. Solodov, A. V.: *Teoriya Informatsii i Yeyo Primeneniye k Zadacham Avtomaticheskogo Upravleniya i Kontrolya*, [Theory of Information and its Application to Problems of Automatic Regulation and Control], Nauka Press, Moscow, 1967.
3. Shendrovich, I. M.: "Errors in the Measurement of Hydrometeorological Elements, Represented by Random Functions", *Trudy NIIGMP*, Issue 15, 1966.
4. Rabinovich, V. I.: "Determination of the Amount of Information During Uniform Distribution of the Value Measured and Normal Distribution of Errors," *Izmeritel'naya Tekhnika*, No. 10, 1963.
5. Jamison, D. E. *et al.*: "Physics and Technology of Infrared Radiation," *Sovetskoye Radio*, 1965.

STATISTICAL CHARACTERISTICS OF THE SCANNING INFRARED EQUIPMENT SIGNALS

G. P. Vimberg, Yu. A. Dranishnikov, V. I. Ivanov and V. V. Puchkov

ABSTRACT: In order to determine the effective indications of recognition of various radiating surfaces (cloudiness, underlying surface) according to the results of IR-equipment measurements of the experimental weather satellite Kosmos-122 the authors carried out the calculations of the following characteristics: one-dimensional laws of distribution of the amplitudes of the signal and their numerical characteristics, mathematical expectation, dispersion and central moments of the third and fourth orders; coefficients of correlation for all the second moment of distribution, asymmetry, and excess; autocorrelation functions of the amplitude of the signal along and across the direction of scanning of the IR-equipment. In the article the authors give the characteristics of the initial material and present the results of their calculations.

The infrared scanning equipment of the television type, installed on the experimental weather satellite KOSMOS-122, measured the outgoing radiation of the earth's atmosphere system in the spectral range of 8-12 μ. /21

The results of the measurements made by means of these equipments were represented in the form of a brightness image of the band of IR-equipment survey band (the infrared picture of clouds and their underlying surface), which enables us to trace the cloudiness fields above the terrestrial globe, and also in the form of absolute values of signals at the output of the equipment, yielding information on the temperature of the underlying surface and the upper boundary of the clouds [1, 2].

We know [3, 4], that the outgoing radiation in the above-mentioned spectral range depends on a number of parameters, such as the temperature of the underlying surface and the coefficient of its radiation, the vertical distribution of the temperature, pressure, and moisture of the air, the total ozone content, and others. As the result of this the interpretation of infrared pictures of clouds and underlying surface in a number of cases is difficult and is not always unambiguous [5, 6].

All the above mentioned parameters, which determine the outgoing radiation in the 8-12 μ transparency window of the atmosphere, varies substantially in time and space, these variations bearing a random character. Therefore it is natural, that in order to obtain objective characteristics of the fields of cloudiness and the temperature of the radiating surface we require the use of statistical methods of interpretation and analysis of the results of measurements performed by means of IR-equipment on satellites, which in its turn will enable us to automate the latter, and to preevaluate the probability of recognition of various shapes and types of clouds against the background of the underlying surface.

The determination of the effective features of detection of various underlying surfaces requires the knowledge of such statistical characteristics, as for example the laws of distribution of the signal amplitudes, the functions of the interelement and interline correlation, the spectral functions, and so forth. For this purpose we developed programs for calculating the following on the M-20 electronic computer:

1) of single dimension laws of distribution of the amplitudes of the signal and their numerical characteristics, and also of the mathematical expectation, dispersion, and central moments of the third and fourth orders;

2) the correlation coefficients for all four moments of distribution of point 1, asymmetry, and access; /22

3) autocorrelation functions of the amplitudes of the signal along and across the scanning direction;

4) interline correlation and mutual-correlation functions in the two directions.

Here we use the relationships known from mathematical statistics [7]:

For mathematical expectation

$$m_1 = \frac{1}{n} \sum_{i=1}^{n} U_i, \tag{1}$$

For moments of the ν-th order when $\nu \geq 2$

$$m_\nu = \frac{1}{n} \sum_{i=1}^{n} (U_i - \overline{U})^\nu. \tag{2}$$

The non-displaced evaluations of the moment of distribution of the signal amplitudes were calculated with the formulas

$$M_1 = m_1, \tag{3}$$

$$M_2 = \frac{n}{n-1} m_2, \tag{4}$$

$$M_3 = \frac{n^2}{(n-1)(n-2)} m_3, \tag{5}$$

$$M_4 = \frac{n(n^2-2n+3) m_4}{(n-1)(n-2)(n-3)} - \frac{3n(2n-3) m_2^2}{(n-1)(n-2)(n-3)}, \tag{6}$$

where m_1, m_2, m_3 and m_4 are determined from relationships (1) and (2).

The asymmetry in excess of distribution point 1 were determined from the expressions

$$G_1 = \frac{\sqrt{n(n-1)}}{n-2} q_1, \tag{7}$$

$$G_2 = \frac{n-1}{(n-2)(n-3)} [(n+1) q_2 + 6], \tag{8}$$

where $q_1 = \frac{m_3}{m_2^{3/2}}$ and $q_2 = \frac{m_4}{m_2^2} - 3$. are selected coefficients of asymmetry and excess.

The correlation coefficients between the selected values of the analog of signal U_i and U_j were calculated with the formula

$$r_{i,j} = \frac{m_{i,j}}{s_i s_j}, \tag{9}$$

Here s_i and s_j are standard deviations of values U_i and U_j ($i = 1, 2, \ldots, n$, $j = 1, 2, \ldots, n$).

The calculation of autocorrelation and mutual correlation functions is performed with the expressions /23

$$\rho_x(\tau) = \frac{\frac{1}{k} \sum_{i=1}^{k} [U_x(t_i+\tau) - U_x(t_i)]^2}{M_{2x}}, \tag{10}$$

$$\rho_{xy}(\tau) = \frac{\frac{1}{k} \sum_{i=1}^{k} \{[U_x(t_i+\tau) - U_x(t_i)][U_y(t_i+\tau) - U_y(t_i)]\}}{\sqrt{M_{2x} M_{2y}}}, \tag{11}$$

where x and y designate the direction along and across the scanning direction respectively.

The undisplaced second moments M_2 are determined with formula (4). In all the above given relationships n signifies the number of selected values of the output signal U_i.

The distribution laws and all the numerical characteristics were determined in the selection of values of the envelope of the output signal from the elements being determined. The volume of this sample was selected as variable and amounted to 10, 50, 100, and 200 counts of the signal envelope from the rectangular sectors of the cloud field or background with dimensions of 15 × 100; 75 × 150; 150 × 150; and 150 × 300 km respectively.

In order to determine the correlation functions on the cloud field or a sector of the background we selected a square measuring 450 × 450 and 600 × × 600 km. In these squares the autocorrelation function was calculated for the first lines in two (with respect to x and y) mutually perpendicular directions.

In the investigation of the interline correlation we used counts of the signal envelope from lines 1-2, 1-3, 1-4, ..., 1-30, in both directions.

To determine the mutual correlation function we took the readings of the signal from the first lines with respect to x and y.

As the initial material for calculating the statistical characteristics we used the analog records of the absolute value of the signal along the scanning lines of the infrared equipment and infrared pictures of clouds and underlying surface, obtained as the result of measurements on two loops (1,602 and 1,678) from the experimental weather satellite KOSMOS-122 on 11 and 16 October 1966.

The preparation of the initial material for performing the calculations consisted of the following stages:

determination of the readings of the absolute value of the signal along the scanning line,

determination of the number of gradations for obtaining the numerical value of the absolute value of the signal until the level of quantization along the lines,

the time and geographical tying-in of infrared pictures of cloudiness and underlying surface,

the time tying-in of the absolute value of the signal to the infrared pictures of clouds, the selection of typical radiating surfaces according to the infrared pictures of clouds and underlying surface,

separation of characteristic radiating surfaces into individual squares and selection of the corresponding absolute signal values.

Since the absolute values of the signals of the infrared equipment are represented in the form of analog records on a movie film, for their statistical processing it is necessary to select a number of readings of the absolute values of the signals, along the scanning line and to determine the number of gradations for obtaining the numerical value of the absolute signal value at every level of quantization along the lines. /24

The number of readings of absolute signal values along the scanning lines of the infrared equipment was determined, proceeding from the resolution of the infrared equipment on location.

We know [8] that

$$\left.\begin{aligned} \Delta y &= \frac{2H\tan\frac{\delta y}{2}}{\cos\gamma} \\ \Delta x &= \frac{2H\tan\frac{\delta x}{2}}{\cos^2\gamma + \cos\gamma\sin\gamma\tan\frac{\delta x}{2}} \end{aligned}\right\} \quad (12)$$

where Δy and Δx are the length and width of the element of resolution of this equipment on location, H is the height of the satellite's flight, γ is the scanning angle varying within the limits from 0 to $\pm 40°$, δy and δx are the angular resolution of the equipment along axis y and x, when $H \approx 600$ km, $\delta y = \delta x = 1.5°$ and $\gamma = 0°$, we obtain from the expression (12), that $\Delta x = \Delta y \approx \approx 15$ km. Consequently, the number of readings of the absolute signal values along the scanning line should be not less than

$$n = \frac{L}{\Delta x}, \quad (13)$$

where L is the length of the scanning line on location.

On the basis of this we have

$$n = \frac{2 \cdot 600\tan 40°}{15} \approx 66.$$

The decrease of the resolution with respect to area on the edges of the scanning lines was taken into account by increasing the dimensions of the squares but preserving the number of measurements in them.

The number of gradations for obtaining the numerical magnitude of the absolute signal value was selected, proceeding from the considerations of optimum relationships between the quantization step with respect to amplitude of the infrared equipment signal and the thickness of the analog record of the video signal on the movie film. In this case this relationship is selected in such a way that

$$\Delta h \geqslant \delta, \tag{14}$$

where Δh is the quantization step of the absolute signal value with respect to amplitude, δ is the thickness of the curve record ($\delta \approx 0.25$ mm). When the width of the working part of the film is 27 mm we obtain $N \leq 108$ gradations.

The quantization of the analog records of the video signals by the infrared equipment was performed by means of an electronic converter from analogs to the figures of the silhouette type.

In actual practice the number of readings of the analog record of the video signal along the scanning lines varied in the 60-68 range, while the number of video signal quantization levels was equal to 100. The quantization step in this case corresponds to the variation of the radiation temperature of the radiating surface by about 1°C.

The time and geographical tying-in of infrared pictures of clouds and underlying surface was performed on the basis of orbital data and the time when the equipment was switched on or off. The time tying-in of absolute values of the signal to the infrared pictures of the clouds was performed according to the time marks present in both types of information. /25

As the radiating surface investigated by means of the infrared pictures of clouds and underlying surface we selected the cloudless sectors of seas and oceans, cloudless sectors of the continents, cyclonic cloudiness above dry land and ocean, frontal cloudiness above dry land and oceans, and intramass cloudiness above dry land and ocean.

The results of the calculations of statistical characteristics of infrared equipment signals are given in Figures 1-5, and the numerical characteristics of the law of distribution of signal amplitudes above the radiating surfaces investigated are given in Table 1.

In Figure 1-4 we present the distribution curves of the probabilities of the infrared equipment signal (solid curves) and the curves of the normal distribution of the signal probabilities (dashed curves), plotted according to the mathematical expectation and standard deviation. Along the axis of the abscissa we measure off the values of the signals in conventional units, along the axis of the ordinates the frequencies corresponding to them.

From Figures 1-4 we can see, that in individual occasions the curves corresponding to the real law of distribution of probabilities of the signals almost coincide with the curves corresponding to the normal law of distribution of probabilities. These are mostly the cases of open sectors of watery surfaces and continents, and also of the solid uniform cloud field. But for cyclonic and frontal cloudiness the real law of distribution of probability of the signal does not agree with the normal law.

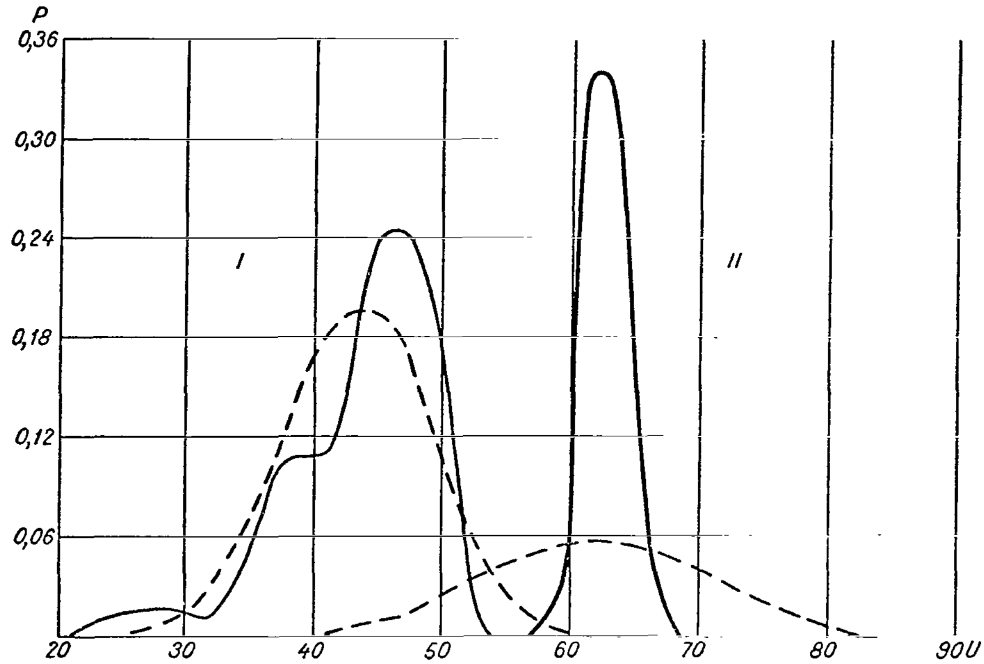

Figure 1. The Laws of Distribution of the Video Signals From the Waters' Surface. I, Pacific Ocean: 64-82° S., 110-107° W; 2 hrs. 40 min. $\bar{u}$ = 42.39, σ = 5.96; II, Open Sector over the Mediterranean Sea: 32-35° N, 29-27° E, 10 hrs. 00 min, $\bar{u}$ = 60.89, σ = 9.7.

From Table 1 we can see that the radiating surfaces investigated, as it should have been expected, differ from one another primarily by the mathematical expectation and dispersion of signals of the infrared equipment. The higher is the radiating surface located, i.e., the lower is the temperature of its radiation, the smaller is the mathematical expectation of the signal above it, and the more uniform character is exhibited by the radiating surface, the smaller signal dispersion it has. /27

The dependence of the initial moment of the first order from the temperature of the radiating surface, which is to be investigated in the future, indicates, apparently the change in the law of distribution of infrared equipment /29
signals above the various radiating surfaces in relation to the latitude of the observation spot, the season, and the time of the day.

TABLE 1. NUMERICAL CHARACTERISTICS OF THE LAWS OF DISTRIBUTION OF INFRARED EQUIPMENT SIGNAL AMPLITUDES ABOVE THE RADIATING SURFACES INVESTIGATED.

Type of Radiating Surface	M_1	M_2	M_3	M_4	G_1	G_2
Pacific Ocean	42,4	6,0	—253,3	5 474,0	—1,2	1,3
Pacific Ocean with insignificant cloudiness	51,4	8,7	—1 150,0	94 584,0	—1,7	13,4
Mediterranean Sea with insignificant cloudiness	60,9	9,7	—9 785,0	1 047 386,0	—10,6	114,9
Continent, North Africa	66,0	2,1	2,8	67,1	0,3	0,2
Continent, South America with insignificant cloudiness	61,0	4,6	—1 338,0	136 312,0	—13,3	288,8
Continent of the center of the European Territory of USSR	43,7	4,8	—106,5	2 496,0	—1,0	1,8
Western Coast of So. America with insignificant cloudiness	52,8	6,6	—1 069,0	122 142,0	—3,7	60,2
Northeastern Caucausus	46,4	2,4	15,4	181,2	1,2	2,8
Cyclone above the West Siberian Lowlands	26,2	4,4	10,6	1 665,0	0,30	1,6
Cyclone above the Atlantic Ocean	33,1	10,5	315,4	27 401,0	0,2	—1,0
Frontal cloudiness above the Pacific Ocean	40,3	5,8	—651,8	48 605,0	—3,1	35,0
Frontal cloudiness above the European Terr. of the USSR	23,3	8,6	—252,3	49 532,0	0,6	2,2
Solid cloudiness of stratiform type above the Pacific Ocean	34,5	5,8	142,6	2 956,0	0,8	—0,3
Solid cumuliform and stratiform cloudiness above the Bellinghausen Sea	45,7	2,4	1,7	123,6	0,1	0,4
Solid cloudiness in the rear of a cyclone above the Atlantic Ocean	23,3	9,9	1 224,0	67 857,0	1,3	4,2
Thick cumuliform cloudiness above South America	20,9	10,8	684,0	37 571,0	0,6	—0,2
Thick cumuliform cloudiness above Turkey	39,8	14,7	—2 208,0	275 446,0	—0,7	2,9
Cumuliform cloudiness with breaks above North Africa	51,2	28,8	621 160,0	531 144 373,0	26	771,0
Cumuliform cloudiness with breaks above South America	52,1	11,4	—1 056,0	101 480,0	0,7	3,0
Cumuliform cells above Atlantic Ocean	62,4	23,1	427 074,0	368 293 407,0	34,7	1294,0

Tr. Note: Commas indicate decimal points.

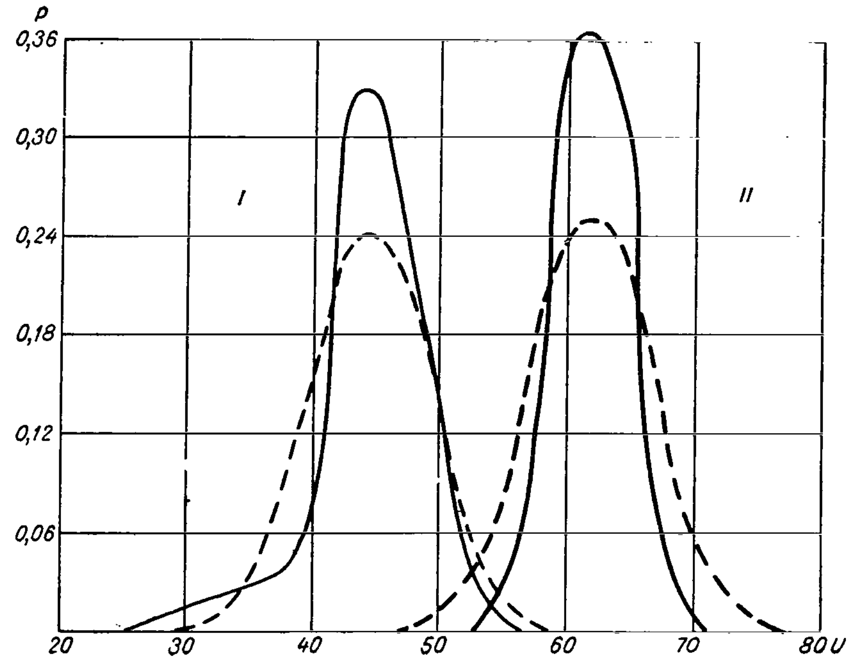

Figure 2. Laws of Distribution of Video Signals from the Surface of the Dry Land. I, Continent (Center of the European Territory of the Soviet Union), 10 hrs. 08 min., $\bar{u}$ = 43.68, σ = 4.78; II, Continent (South America); 39-36° S, 68-66° W, 6 hrs 05 min., $\bar{u}$ = 61.01; σ = 4.65.

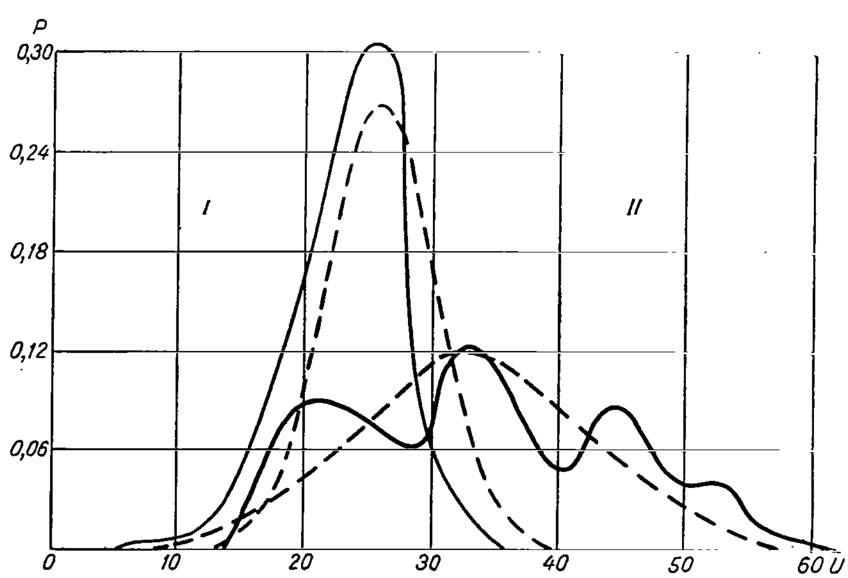

Figure 3. Laws of Distribution of Video Signals from a Cyclone. I, Cyclone Above the West Siberian Lowlands, $\bar{u}$ = 26.2, σ = 4.38, II, Cyclone Over the Atlantic Ocean; 48-54° N, 22-14° W, 9 hrs. 15 min., $\bar{u}$ = 33.14, σ = 10.49.

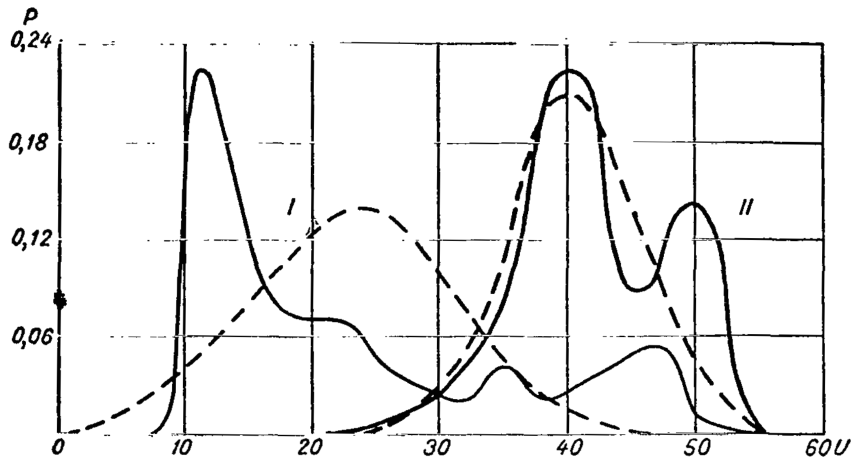

Figure 4. Laws of Distribution of the Video Signals from the Frontal Cloudiness. I, Frontal Cloudiness Above the European Territory of the Soviet Union: 10 hrs. 6 min.-10 hrs. 14 min., $\bar{u} = 23.29$, $\sigma = 8.58$; II, Frontal Cloudiness Above the Pacific Ocean: 43.5-54° S, 162-176° E, 1 hr., $\bar{u} = 40.31$, $\sigma = 5.76$.

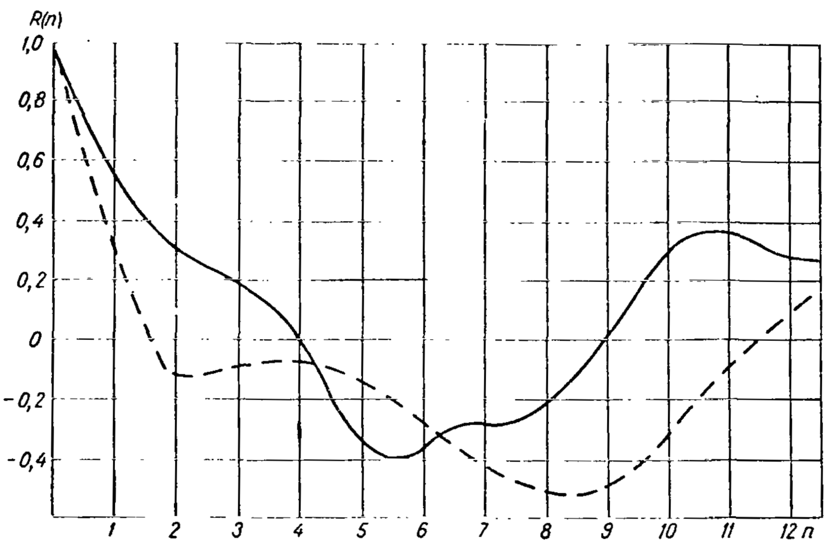

Figure 5. Laws of Distribution of Video Signals from Cyclonic Cloudiness, Cumulus Cloudiness, and Ocean Surface.

From Table 1 we can also see that the law of distribution of the infrared equipment signals is closer to normal in proportion to the uniformity of the character of the radiating surface. The presence of cloudiness above the surface of the continent or the ocean results in a sharp increase of the central moments of the forth order, especially in the case of cumuliform cloudiness with breaks. The latter, taking into account what was said about the initial moments of the first and the second order, enables us to hope for a possibility of automatic recognition of cloudiness according to the measurement data by means of scanning infrared equipment on satellites.

In Figure 5, we give the interelement automatic correlation functions according to two mutually perpendicular directions, calculated according to the readings of the video signal from the cyclones, located above the Atlantic Ocean.

The solid curve on this figure represents the autocorrelation function along the scanning line and the dotted curve represents that taken across the scanning line.

As we can see from the figure both functions have a fluctuating character. The fluctuations of the autocorrelation functions along the scanning line have a certain periodicity with a half period, equal to six measurement elements. The correlation range along the scanning line amounts to about 4 elements, and across to two elements. The value of both autocorrelation functions decreases by two times practically on the second element already.

In conclusion we note that in order to obtain more representative statistical characteristics of the signals of the infrared scanning equipment on weather satellites it is necessary to carry out further calculations for various underlying surfaces and shapes and types of clouds above them during different seasons and in different latitudes.

REFERENCES

1. Vetlov, I P.: "Investigation of Cloudiness and Outgoing Radiation by Means of the Cosmos-122 Satellite," *Meteorologiya i Gidrologiya*, No. 1, 1967.
2. Vetlov, I. P.: "Meteorological Observations from Satellites," *Meteorologiya i Gidrologiya*, No. 4, 1967.
3. Kondrat'yev, K. Ya.; O. A. Avaste; M. P. Federova and K. Ye. Yakushev skaya: *Pole Izlucheniya Zemli Kak Planety* [The Radiation Field of the Earth as a Planet], *Gidrometeoizdat Press*, Leningrad, 1967.
4. Kondrat'yev, K. Ya.; Ye. P. Borisenkov and A. A. Morozkin: *Prakticheskoye Ispol'zovaniye Dannykh Meteorologicheskikh Sputnikov* [Practical Utilization of Weather Satellite Data], Gidrometeoizdat Press, Leningrad, 1966.
5. Malkevich, M. S.: "Certain Problems of Interpretation of the Earth's Outgoing Radiation Field", I. Determination of the Temperature with the the Underlying Surface and the Height of the Upper Boundary of the Clouds," *Trudy GGO*, Issue 166, 1964.
6. Kondrat'yev, K. Ya.; Ye.P. Novosel'tcev and N. Ye. Ter-Markaryants: "Determination of the Temperature of the Underlying Surface and Clouds from Weather Satellites," *Trudy GGO*, Issue 196, 1966.

7. Kramer, G.: *Matematicheskiye Metody Statistiki* [Mathematical Methods of Statistics], IL Press, 1948.
8. Kmito, A. A.: *Metody Issledovaniya Atmosfery s Ispol'zovaniyem Raket i Sputnikov* [Methods of Investigation of the Atmosphere Using Rockets and Satellites], Gidrometeoizdat Press, Leningrad, 1966.

AUTOMATIC PROCESSING OF INFRARED INFORMATION COMING FROM WEATHER SATELLITES

V. F. Goverdovskiy and B. D. Panin

ABSTRACT: The article is devoted to automation of processing of satellite information by means of electronic computers. They examined the algorithm and the results of processing of IR-information from meteorological satellites Kosmos-122 and Kosmos-144 by means of the VNIIEM-3 electronic computers. They show that in the field of radiation temperature the cloud systems are traced. The radiation temperature agrees with the temperature of the ground level layer of air in cloudless regions and reflects the thermal regime of the upper boundary of the clouds. The contrasts in the field of the radiation temperature reflect the boundaries and specific features of the underlying surfaces of various types, and make it possible to refine the analysis of cloud fields.

The intensive development of methods of investigation of weather forming processes on the global scale by means of weather satellites has posed a number of problems connected with the reception, processing, systematization, interpretation, and utilization of satellite data. /30

One of these problems, which is important today, is the automation of the processing of satellite information by means of electronic computers. Modern weather satellites deliver such a great amount of information, that the processing of this information for operative use without the employment of electronic computers is practically impossible.

In the present article we examined the algorithm and the results of automatic processing of infrared information from weather satellites KOSMOS-122 and KOSMOS-144 by means of the VNIIEM-3 electronic computer.

The algorithm of automatic processing of IR-information is subdivided into two individual parts, each of which provides for a number of operations, performed in a certain sequence.

The First Part of the Algorithm is preliminary and includes the performance of the following operations.

a. *Rerecording of information to be processed in the computer's memory.* During the communication periods the scientific and service information is recorded on magnetic tape by means of special devices. Then this information is rerecorded in the computer's memory according to a special program. This program provides for the selection of specific types of information, its sorting and rerecording into the electronic computer's memory. The performance of this program assures the selection and ordered recording from 80 scanning lines of the following forms of information masses: scientific information (IR), information on the time at which the measuring was carried out (time marks), information on orientation of the satellites in space, information of the voltage levels at the equipment centers, used later on for calibration and standardization.

The information from 80 scanning lines is used later on for forming the frames.

In addition the information on the time check and the oribtal data are introduced into the memory of the electronic computer.

b. *Decoding of the time marks, control, and restoration of information.* /31
These operations assure the tying in of the service and scientific information in time, and also the rejecting of distorted information.

The Second Part of the Algorithm provides: calibration and standardization of measurements, separations of contrast in the field studied (radiation temperature), formation of the nodes of the grid, averaging, geographical tying in, and presentation of the processing results.

a. *Calibration and Standardization.* The calibration of the signals of service and scientific information is performed by comparing them with control levels.

Standardization of scientific information signals into degrees of radiation temperature is carried out by two methods.

By the first method the standardization is carried out by means of a signal from a control radiator.

The second method provides for the use of data of ground calibration of the equipment.

b. *Bringing out the contrasts.* The consecutive analysis of each measurement enables us to bring out the sharp changes of the signal on the scanning lines. These changes in the signal correspond to the contrast in the field of outgoing radiation, which in the majority of the cases coincides with the boundaries of the radiating surfaces of various types. The processing algorithm provides for determination on the scanning lines of the position and value of such sharp signal changes, and also the calculation of the values of the contrast corresponding them in the field of radiation temperature between the thermally nonuniform surfaces, for example, on the boundaries of the cloud cover, boundaries between the water and dry land, and so forth.

If the signal increases, then this change (contrast) is assigned the plus (+) sign, and if the signal decreases, then the contrast is assigned the minus (-) sign. The values of the contrast are tied-in in time. The minimum values of the temperature drops, which are considered contrasts, may be changed on the discretion of the operator.

During processing, the finding of the reverse scanning lines and the coordination of information from the forward and reverse scanning lines is provided for.

c. *Formation of nodes and averaging of information.* After separation of the contrast and coordination of the scanning lines the nodes are formed in the scanning lines and the information is averaged. For this purpose the scanning line is divided into 20 intervals, each of which contains an approximately equal quantity of measurements. In each of these 20 intervals the measurements are averaged, and the mean values of the signals are referred to the middle of the intervals, which are considered the nodes of the scanning lines.

The averaged values in the intervals are assumed to be the values of the signal in the nodes of the scanning line. The tying-in of the averaged values in time is carried out according to the known time of the beginning and end of the scanning lines by means of interpolation. Thereupon, the values of the signal in the node of the lines are averaged with respect to four neighboring scanning lines into a single averaged line. When the scanning lines are averaged the values of the contrasts may be also averaged or we may select the maximum contrast with their sign from all the four scanning lines.

d. *Geographical Tie-in.* The geographical tying-in is performed by means of relationships, which assure the conversion from the satellite system of coordinates into the geocentric system, and then to the geographical coordinates. In this processing we are to introduce the corrections to the values of the radiation energy taking into account the scanning law and the position of the satellite in space (through the distortion of the expansion /32
element).

However, experimental processing of IR information from the KOSMOS-122 and KOSMOS 144 satellites showed that these corrections are insignificant, and therefore this part of the algorithms was not carried out.

e. *Presentation of the Results.* The concluding part of the algorithms of the automatic processing of IR information from meteorological satellites provides for a presentation of the results of processing in the form which is convenient for practical use.

To present the results of processing of weather satellite IR-information processing the alphabet digital printing mechanism was used (ADPM). The information obtained from 80 lines, according to the above, is recounted into 20 averaged lines, which are printed by means of the ADPM in the form of a frame.

To present the measurement results from each averaged scanning line we use four printed lines on the paper tape of the ADPM.

In the first line we designate with points the positions of the nodes of the scanning lines (every 5-6 printed symbols); here also by a colon we indicate the position of the heat contrast.

In the second line under the corresponding node we print the values of the radiation temperature in the degrees of the absolute scale and the centigrade scale.

In the third line under the mark of the position of the thermal contrast (on the first printed line) we print its value in degrees (with a two digit figure) with its own sign.

In the fourth line with letters m and p we designate the meridian and parallel of the center of the conventional frame.

On each frame we print the Moscow time during which the information was obtained, as well as the latitude and longitude of the center of the frame. The general appearance of the processing of the results presented in the above-mentioned way, is portrayed in Figure 1.

When necessary the processing results may be printed on large scale blank maps of various projections. For this purpose the algorithm provides for the transformation of the grid of nodes with an allowance for the projection and scale of the map, and also of the position of the observation region.

The algorithm of the automatic procession of IR-information has been developed by the authors of the present article together with Ye. L. Urman Ye. S. Burkovskiy, and V. A. Tarulin to be used in the VNIIEM-3 electronic computer. On the basis of this algorithm we developed a program by means of which we carried out the processing of IR-information from the KOSMOS-122 and KOSMOS-144 satellites on the VNIIEM-3 electronic computer.

Some results of this processing are given below.

The processing of a single frame (80 lines) of IR-information up to printing the results takes about 2 minutes on the VNIIEM-3 electronic computer. This enables us to draw the conclusion that by means of an VNIIEM-3 electronic computer the processing of IR-information may be carried out upon the arrival of information between communication periods.

The results of processing of IR-information from KOSMOS-122 and KOSMOS-144 satellites makes it possible to formulate the following basic conclusions. In the radiation temperature field the cloud systems can be traced quite well. The radiation temperature agrees with the temperature of the ground layer of air in cloudless regions and reflects the thermal conditions of the upper boundary of the clouds. As an illustration, in Figures 1 and 2 we present the results of automatic processing of IR-information obtained on the 2nd of July 1966 from the KOSMOS-122 satellite. The synoptic map of the region, in which the satellite observations were carried out is given in Figure 3. /33

Moscow time: 15.27.45
Latitude + 064.1
Longitude + 078.3

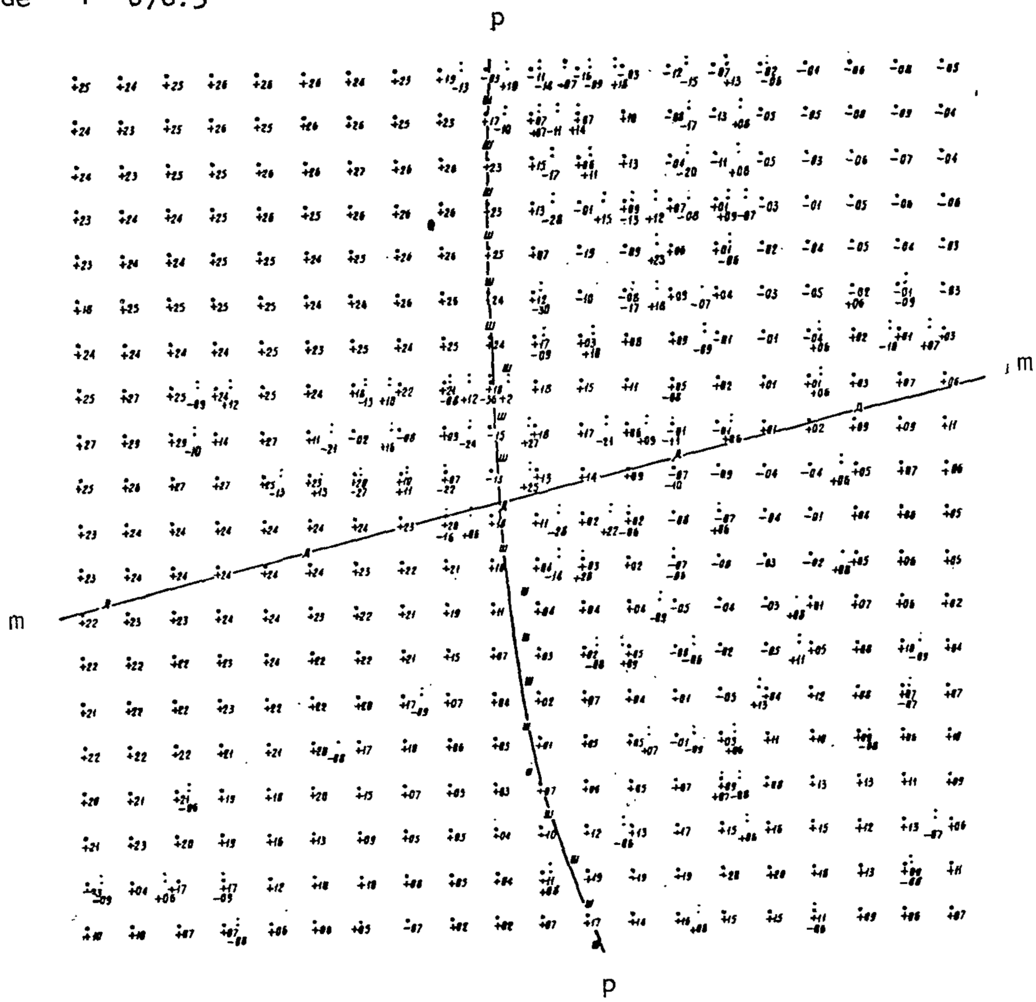

Figure 1. General Appearance of Presentation of the Results of Automatic Processing of IR-Information, Obtained From Weather Satellites KOSMOS-122 and KOSMOS-144. Vertical Line, Latitude; Horizontal Oblique Line, Longitude.

The weather in the observation region was determined by the deep cyclone (the pressure in the center was below 990 millibars) the center of which at 9 hours on the morning of the 2nd of July was at the point with coordinates of 67.5° north and 67° east. In the cyclone zone a well-expressed frontal system was observed with thick cloudiness which deposited precipitation. The warm sector of the cyclone with the ground air temperature above 20°C was characterized mainly by weather with few clouds. By the time of observation (15 hours) the cyclone shifted towards the northeast of the region examined but the weather was still determined by its influence. This can be seen on the diagram of distribution of cloudiness, obtained according to the photographic recording device (PRD) pictures (Figure 4), where we can trace the cloud systems of the warm and cold fronts, and also the solid cloudiness in the center of the cyclone.

/34

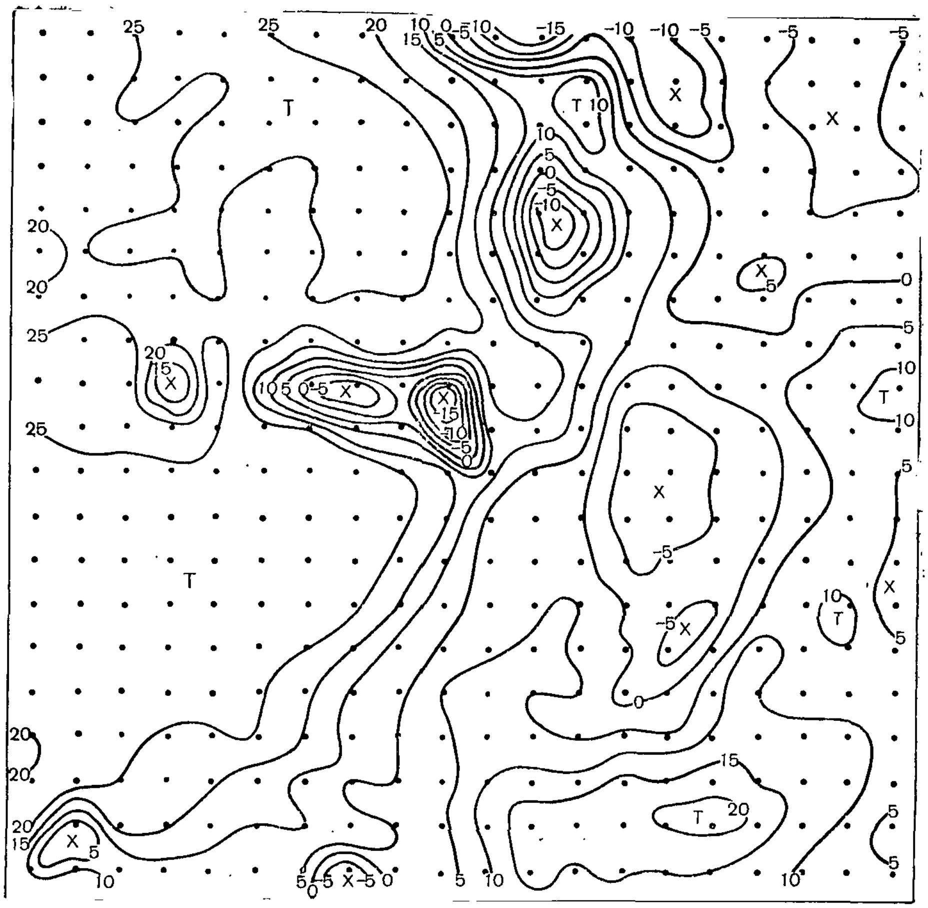

Figure 2. Radiation Temperature Field Plotted According to the Results of Observations From the KOSMOS-122 Satellite.

The results of processing presented in Figure 1, pertain to 15 hours, 27 minutes, 45 seconds of Moscow time. /35

In Figure 1 we present the averaged values of the radiation temperature in the scanning line nodes, the values of the contrasts with their sign and the

directions of the meridian and parallel, passing through the center of the frame. The center of the frame has the coordinates of 64.1° North and 78.3° East. The weather conditions within the limits of this region according to the synoptic map for 15 hours are portrayed in Figure 3. On the synoptic map (Figure 3), we can see that the weather conditions in the northern and southern parts of the region examined differ sharply. In the southern part we observe high values of the ground temperature, of about 25-30°C, whereas in the northern region the ground temperature does not exceed 10°C on the average. In the north of the region solid thick cloudiness predominated, from which precipitation fell in the form of rain. In the south of the region we observed a little-cloudy weather or the cloudiness with breaks. In the south of the region in the zone with a cloudless weather the values of the radiation temperature amounts to 20-25°C on the average. An entirely different picture is observed in the solid cloudiness zone in the north of the region. Here, the /36
difference between the radiation temperature and the ground temperature reaches 10-15°C. We had at our disposal few aerological data, according to which we could judge on the temperature and the height of the upper cloudiness boundary in this region. However, the available radiosonde data showed that even here the processing result in general agreed with the temperature in the upper boundary of the clouds. In Figure 2 we present the field of radiation temperature isotherms. Upon comparing the Figures 2 and 4 we can see that the outlines of the isotherms reflects the principal features in the distribution of cloudiness in the observation region.

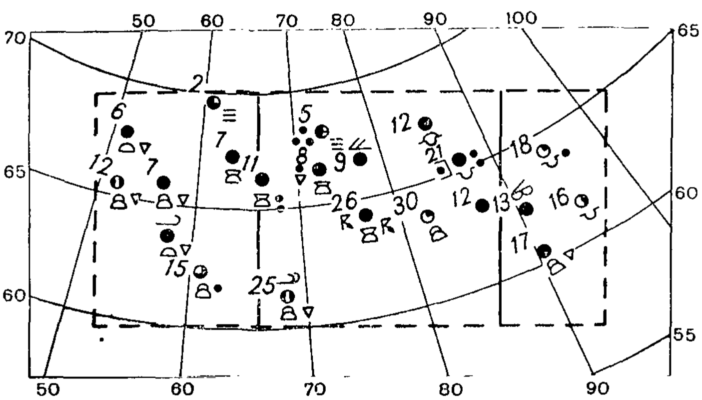

Figure 3. Weather in the Region Covered by Observations of the Kosmos-122 Satellite at 15 hours on 2 July, 1966.

In processing the minimum value of the contrasts, which were printed, was limited to 5°C, i.e., all the signal changes with respect to value, corresponding to the contrast in the temperature field less than 5°C were not taken into account.

From Figure 1, where we give the values of the contrasts in the radiation temperature field, we can see that the contrasts vary with respect to value and sign, especially in regions with cloudy weather. Such a diversity of contrasts reflects the nonuniformity of cloudiness.

In Figure 4 we present the superimposition of the PRD pictures with the distribution of contrast in the radiation temperature field. We note, that in Figure 4 we mark the solid cloudiness outlines

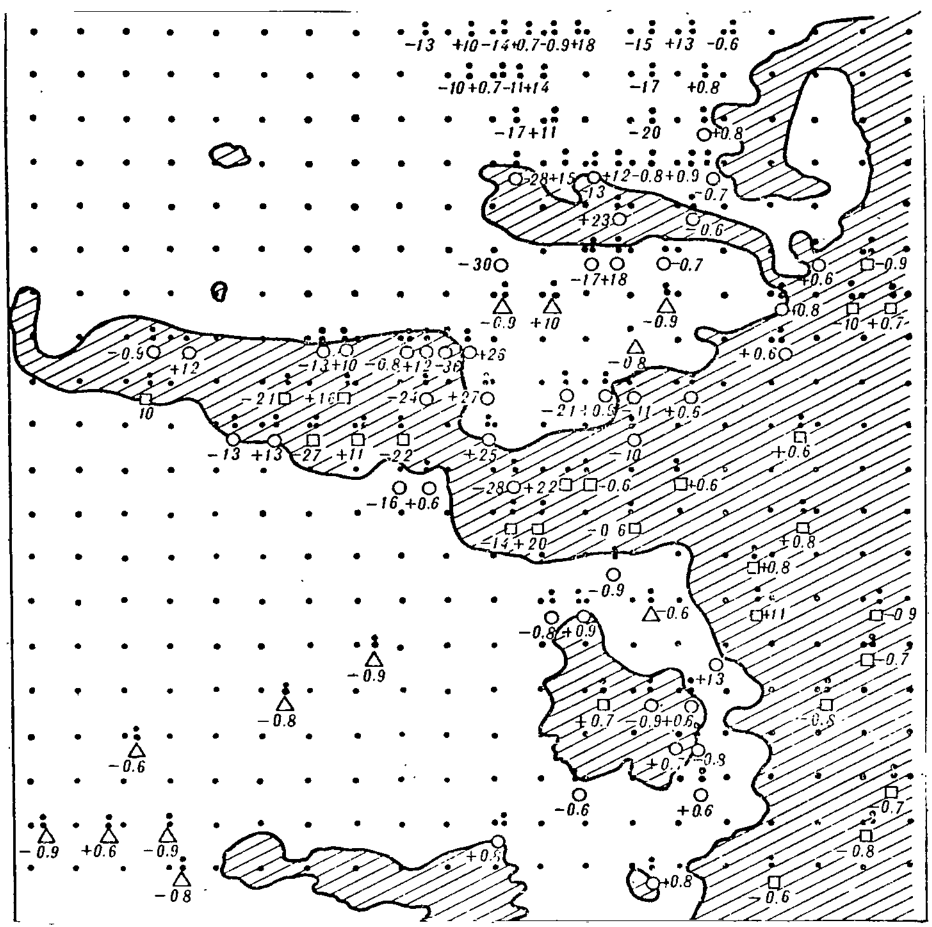

Figure 4. Diagram of Cloudiness, Obtained According to the Picture of the Photographic Recording Device.

It is interesting to analyze the distribution of contrasts in the radiation temperature field in relation to the type of the radiating surface (Figure 4). For this analysis we have selected contrasts at the boundaries of the cloud fields (designated with circles), inside the cloud fields (designated by squares), and in cloudless regions (designated with triangles). The characteristics of the distributions obtained are given in Table 1.

In the process of the analysis we examined separately the positive and negative contrasts, and also the absolute values of the contrasts. The ones with the smallest values were the contrasts in the cloudless regions (8.1°C). The dispersion in these regions also proves the smallest (Table 1). This is quite natural, since the contrasts in cloudless regions are caused by nonuniformities of the underlying surface, which, as a rule, are considerably smaller than the nonuniformities of cloudiness.

TABLE 1. CHARACTERISTICS OF THE CONTRAST IN THE RADIATION TEMPERATURE FIELD ACCORDING TO THE RESULTS OF OBSERVATIONS FROM KOSMOS-122 AND KOSMOS-144 WEATHER SATELLITES.

Type of Surface in the Radiation Temperature Field of Which the Contrast was Examined	Sign of the Contrast	No. of Cases	Mean Value of the Contrast (°C)	Dispersion Degrees^2
Boundaries of the Cloud Fields	Positive	23	11,8	46,75
	Negative	23	14,6	74,84
	Absolute Value	46	13,2	62,79
Inside the Cloud Fields	Positive	11	11,1	29,72
	Negative	15	11,3	41,30
	Absolute Value	26	11,2	36,40
In Cloudless Regions	Absolute Value	12	8,1	1,75

Tr. Note: Commas indicate decimal points.

The mean value of the contrast on the boundaries of the cloud fields and inside the cloud fields with respect to absolute values amount to 11.2° and 13.2°, respectively. /37

In this way the contrasts in the radiation temperature field reflect the boundaries and specific features of the radiation surfaces of various types and make it possible to refine the analysis of cloud fields.

The results of the automatic processing indicate, that the proposed method of IR-information processing makes it possible to analyze the cloud fields.

We note, that the deductions according to the results of automatic processing of IR-information from KOSMOS-122 and KOSMOS-144 satellites were obtained on the basis of the analysis of 50 frames for various regions of the Northern Hemisphere.

EXPERIMENT IN COMPARING THE RESULTS OF MEASUREMENTS FROM THE GROUND, AIRCRAFT, AND SATELLITES

Ye. P. Barashkova and V. L. Gayevskiy

ABSTRACT. In the article the authors give certain results of comparison of shortwave and longwave radiation and temperatures of the underlying surface measured simultaneously on the ground network of actinometric stations, from an airplane and from a satellite above the European territory of the Soviet Union on 17 May, 1967.
The relationship observed between the radiation characteristics at various levels, agree with the evaluations obtained according to the calculation systems.

The scanning instruments installed on a weather satellite enable us to obtain information on the geographical distribution of radiation leaving the earth in the three sectors of the spectrum 0.3-3, 8-12 and 3-30 μ. /38

The outgoing radiation is determined with the properties of the underlying surface and the state of the atmosphere, therefore in order to solve the problem of interpretation of satellite measurements it is necessary to set up a vast complex of investigations in the free atmosphere (by means of aircraft, rockets, balloons and radiosondes) and under ground conditions. Such joint measurements underground, in the free atmosphere from the aircraft and from the satellite, in particular, were performed during the period of the meteor system work in May 1967. In the present article we are making an attempt to compare them. The comparison of the ground, aircraft, and satellite measurements is the easiest for a cloudless atmosphere. In this case we can carry out the quantitative comparison of the ground and the satellite data and in this way to check the various theoretical systems proposed for calculating the outgoing radiation.

When the cloudiness is solid and sufficiently thick the outgoing radiation will be practically determined by the conditions on the upper boundary of the clouds, and to perform the quantitative comparison it is necessary to know the parameters, characterizing the radiation properties of the clouds.

When there is partial cloudiness the quantitative comparisons are practically excluded due to the considerable variagation, and only a qualitative comparison is possible. As a rule, cloudless weather is observed only on small sectors, and therefore quantitative comparison is possible only in individual points. The most interesting in this respect are the points under the satellites, which are in the nadir of the satellite.

When the satellite is at an altitude of 600 km and the angle of vision of the scanning instruments is $3 \times 6°$ the dimensions of the point under the satellite on the surface of the earth are 31.4×62.8 km. The instruments, installed on an airplane, have the working scanning angles within the limits of ±60°. On the ground surface to these scanning angles at the flight height of H corresponds a band with a width of L = 2H tan 60°:

H км	6	7	8	9	10
L км	20.8	24.2	26.9	31.2	34.6

During the maximum altitude of the airplane flight the width of the scanning band overlaps somewhat the width of the point under the satellite. To /39 level off the length of the sectors, the measurement from the airplane, flying with a speed v, should continue for a time t = 63 km/v minutes. With v = = 500 km/hr (8.3 km/min) t = 8 min., while v = 600 km/hr (10 km/hr) t = 6 min.

The measurements from airplanes during the period of passage of the satellite are performed from the maximum altitude of 9-10 km. This altitude is close to the altitude of the upper boundary of the troposphere, and therefore the outgoing radiation obtained from the airplane, differs little from the outgoing radiation of the earth's-atmosphere system measured from the satellite. According to data of [1, 2] the layer of ozone located above the airplane does not introduce any substantial changes in the value of the outgoing radiation fluxes. According to calculations of K. S. Shiffrin and N. P. Pyatovskoya [1], upon passage from the altitude H = 10 km to the altitude of the satellite the ascending shortwave flux changes from 1-9% depending on the height of the sun and the type of the underlying surface. The longwave ascending flux upon passage through the layer of ozone, according to the data of K. Ya. Kondrat'yeva and Kh. Yu. Niylisk [2], changes by 1-1.5%.

Similar equipment is installed on the satellite and the airplane, and therefore, we can perform a direct comparison of the values measured. The ground based measurements are performed by equipment differing from the satellite equipment and the measurement results have different characteristics, therefore, the comparison of ground based and satellite measurements may be performed only by an indirect method. Among the airplane observations we can compare directly the results of pyronometric measurements with the ground observations.

Let us examine in detail the analysis of the results of measurements on 17 May 1967. On this day from 12 hours 41 minutes to 12 hours 47 minutes Moscow statute time, the weather satellite was passing over the European Territory of the Soviet Union (K-156, loop 296). The route of the point under the satellite is presented in Figure 1 by a dashed line, the solid lines delineate the boundaries of the zone, for which information was obtained on the outgoing radiation stop. In the period indicated the ground based actinometric network was in operation. The route of the airplane is shown in Figure 1 by a dashed line. The airplane, from 9 hours 36 minutes to 17 hours 12 min. flew along the Moscow-Voronezh-Rostov on the Don-Voronezh-Kazan'-Sverdlovsk route at an altitude of 9,100 m. The meeting with the satellite occurred at 12 hours, 44 minutes at the point with coordinates ϕ = 50°08' λ = 39°22'. The height of the sun at this moment $H_{\odot}$ = 58.6°. Under the airplane were plowed and green fields, there was a slight haze, above the airplane was a light cloudiness (3/0 Ci), the air temperature at the altitude of the flight t_a = = -38.2°C.

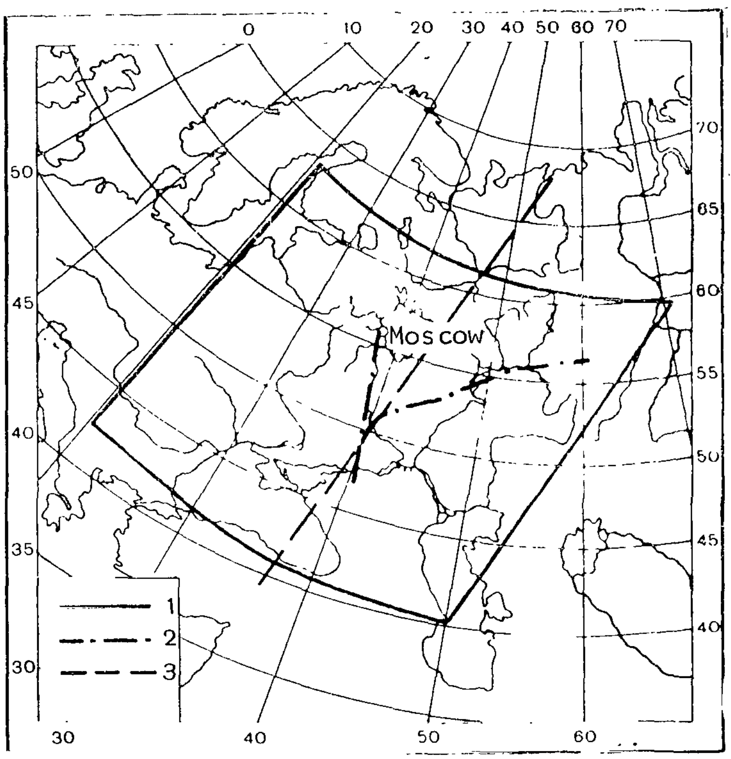

Figure 1. Route of the Point Under the Satellite (3), Route of the Aircraft (2), Boundary of the Information Zone from Loop No. 296 of KOSMOS-156 (1).

The airplane, in addition to actinometric equipment (AC), similar to that installed on the satellite, carried pyronometers, which make it possible to measure the ascending and descending flows of shortwave radiation. These flows may be compared with the ground data.

The comparison of the total of radiation near the underlying surface and the altitude of 9 km shows that with a cloudless sky the total radiation at the altitude of 9 km is greater than at the earth's surface by 10-20%.

$h_{\odot}^{\circ}$	Q	
	$H = 0$ км	$H = 9$ км
40	0,95	1,14
50	1,14	1,34
60	1,27	1,49

With a cloudy sky we observe a different relationship between Q_H and Q_0 depending on the state of the solar disk and the character of the cloudiness. In individual cases in the ground layer we may observe higher values of total radiation. /40

The albedo of the underlying surface according to the data of actinometric network for the moment examined at the European territory of the USSR varies between 13 and 28%. According to the data of aircraft measurements of the albedo of forests and fields along the Rostov on the Don-Benza route is of the order of 13-16%. The appearance of clouds in the field of vision of the pyronometer, installed on the airplane with its receiving surface pointing downwards, results in an increase of the albedo. At the beginning of the flight in the region of Moscow which occurred above alto cumulus clouds, the albedo amounted to 58%.

The geographical distribution of the reflective radiation near the earth's surface $R_k = AQ$ will be determined mainly by the incoming total radiation, since albedo A on the territory examined varies within relatively small limits. The inflow of the total radiation in its turn depends on the geographical coordinates and distribution of cloudiness, and in this case the effect of cloudiness will be the decisive factor. The height of the sun (connected with the latitude and longitude) on the territory examined for the prescribed moment changes from 40 to 64°. On a cloudless sky owing to such a change in the height of the sun the total radiation may increase from 0.95 to 1.32 cal/cm^2 per minute. According to the data of the actinometric network the total radiation varies from 0.02 cal per cm^{2}min (Ladoga, P, 10/10 Sc) to 1.66 cal/cm^2 min (Novo-Pyatigorsk Θ, 10/1 Ci, As, Cu). Consequently, according to /41
the data of the ground network, a minimum of the reflected radiation will be noted in regions with solid cloudiness of the lower level, the maximum in cloudless and a little cloudy regions.

The geographical distribution of the outgoing shortwave radiation, observed from the satellite, will have the opposite character: the regions with the greatest cloudiness will correspond to the greatest values of R_k through the increase of the albedo. If we take into account, that according to the aircraft measurement data upon passage from the cloudless regions to cloudy ones, the albedo changes from 13 to 58%, we should expect that with an unvariable Q the increase of R_k is about fourfold.

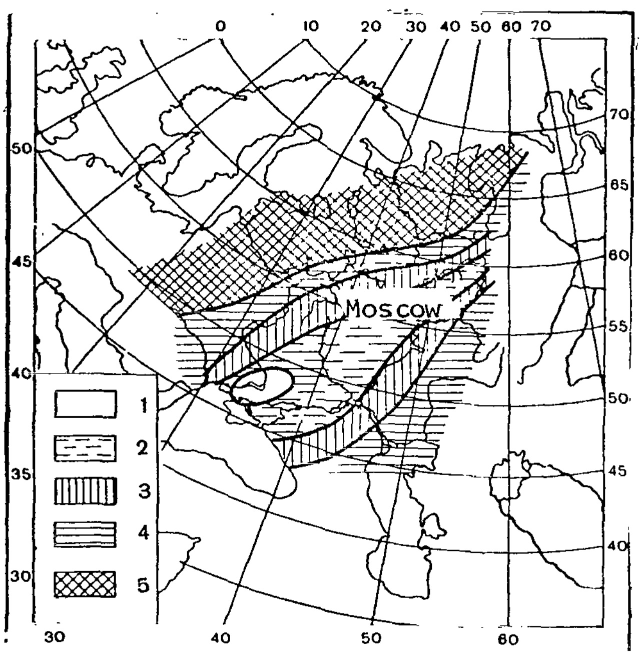

Figure 2. Distribution of Cloudiness Above the European Territory of the USSR on 17 May 1967 at 12 hrs 44 min According to the Moscow Statute Time According to the Ground Based Network Data: 1, cloudless; 2, few clouds; 3, Ci; 4, considerable cloudiness of the lower level; 5, solid cloudiness of the lower level.

In Figure 2 we give the distribution of cloudiness over the European territory of the USSR according to the ground network data. Figures 3a and 3b, on which we give the geographical distribution of the shortwave radiation according to the ground based and satellite data, support the above-mentioned assumption on the character of distribution of shortwave radiation and its relationship with the cloudiness. According to the data of the ground based network the minimum of reflected radiation was observed in the west and northwest regions of the European territory of the USSR, where we observed solid cloudiness of the lower level, the maximum in the southeastern European territory of the USSR, i.e in the cloudless and a little cloudy regions. According to the satellite data, at the southeast of the European territory of the USSR we note the lowest brightnesses of the shortwave radiation. The above mentioned character of distribution of ground and satellite data are somewhat contradicted by the results of comparison of shortwave radiation for the southwestern regions of the European territory of the USSR. Both near the underlying surface and in measurements from the satellite in this region we observe a high reflected radiation. This is /43
caused by the fact that here we observe cumuliform cloudiness with considerable breaks during which sufficiently great values of total radiation near the center line surface, and consequently the reflected radiation, are combined with large values of the albedo during observation from space.

In the point of intersection between the route of the airplane and the satellite we noted a relatively low cloudy weather (3-7 points Ci). The result of the measurements from the airplane in the sector of the spectrum between 0.3 and 3 μ by the scanning instrument in the cal/cm^2 min·ster are given below:

α . . .	—60	—50	—40	—30	—20	—10	0
I_K . .	0.067	0.070	0.070	0.065	0.063	0.061	0.058
α . . .	10	20	30	40	50	60	
I_K . .	0.056	0.058	0.058	0.061	0.061	0.056	

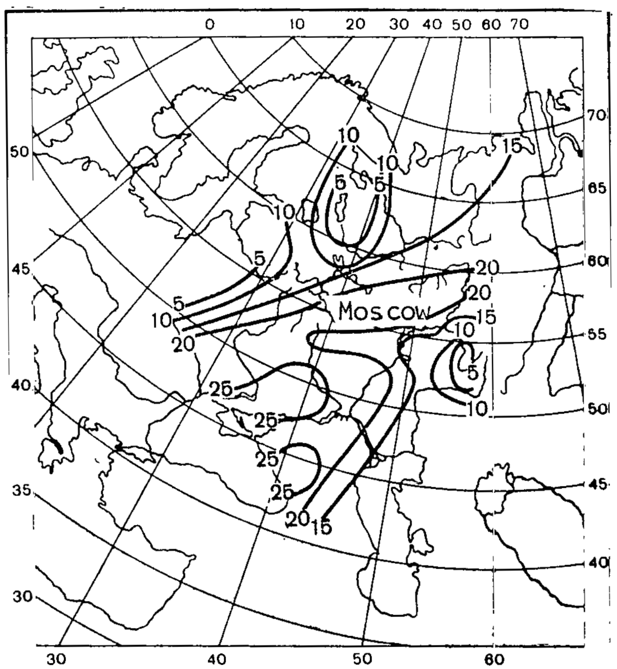

Figure 3a. Distribution of the Reflected Shortwave Radiation According to the Ground Data for 17 May 1967 at 12 Hrs., 44 Min., According to the Moscow Statute Time.

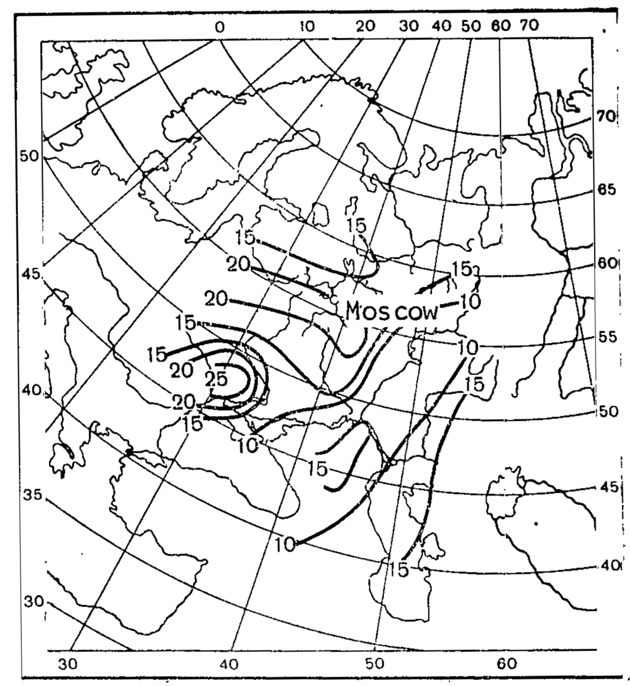

Figure 3b. Geographical Distribution of the Reflected Shortwave Radiation According to Measurements From the KOSMOS-156 Satellite, Loop Number 296, 17 May 1967.

Since I_k depending on the angle changes in relatively narrow bounds, in the first approximation the reflected flow may be adopted as isotropic with a mean value of $\overline{I}_k$ = 0.063 cal/cm^2 min·ster., when $R_k = \pi\overline{I}_k$ = 0.20 cal/cm^{2}min. According to the pyronometer data the ascending current of shortwave radiation at the height of the airplane (H = 9,100 m) is equal to 0.19 cal/cm^{2}min. In this way the value of the ascending current, obtained in measuring with the scanning instrument, is in good agreement with the pyronometric data. According to the ground data, in this region the R_k is equal to 0.22-0.27 cal/cm^{2}min. The ground network data pertains to the standard area covered with green grass, while in the field division of the airplane instruments are also the plowed fields with a lower albedo. The inclusion of the plowed field in the field of vision should result in the decrease of the shortwave reflected radiation which is noted in the comparison of the airplane and ground observations. According to the data of ground measurements in Voronezh and Kamennaya Step' the albedo for green grass amounts to 17% and that of dry soil to 5%. If we consider that the green fields and the plowed fields in the field division of the instrument occupy equivalent areas, the ascending shortwave flux should correspond to the mean value of the albedo of 11% and amount to 0.14-0.17 cal/cm^{2}min. As it follows from the theoretical calculations of K. S. Shifrin and N. P. Pyatovskaya [1], the ascending current of the shortwave radiation above the grassy covered growth with height and with $h_\odot$ = 50° upon the change from 0 to 10 km increases by about 25%. Taking this correction into account we obtain the values of R_k at the airplane level (0.18-0.21 cal/cm^{2}min), which are close to the indications of the airplane pyronometer.

According to the measurements from the satellite the brightness in the nadir is 0.11-0.18 cal/cm^{2}min·ster. Such a discrepancy between the airplane and satellite values is explained by the influence of the cloudiness of the upper level (Ci), located above the airplane. Today we do not possess reliable information on the albedo of clouds of the upper level. According to the data of flight on 21 May 1967, the albedo of Ci changes from 18 to 48%. Such a value of the albedo with Q = 1.45 cal/cm^{2}min, corresponding to the height of the sun of 58°, will assure the values of the reflected radiation of 0.26 -0.70 cal/cm^{2}min.

Results of the measurements in the spectral sector of 8-12 μ, performed from the satellite, yield a concept of the geographical distribution of the radiation temperatures. The radiation temperature, owing to the effect of the layer of the atmosphere and the difference between the radiating capacity of the underlying surface and a unity will be below the true temperature of the surface.

On the basis of the analysis of experimental data V. L. Gayevskiy and Yu. I. Rabinovich [4] arrived at the conclusion that the radiation temperature with a considerable content of water vapor in the atmosphere (5 grams per cm^2) may differ from the true one by 10-15°. The calculations of K. Ya. Kondrat'yev, Ye. P. Novosel'tsev and N. Ye. Ter-Markaryants [5] indicate the /44 systematic discrepancy between the actual and radiation temperature of the underlying surface. On the territory of the Soviet Union during daylight hours in the summer the corrections reach 12-17°, and at night 9-10°C. The difference between the actual and radiation temperature of the clouds in the lower level amounts on the average to 7-8° and does not depend on the season.

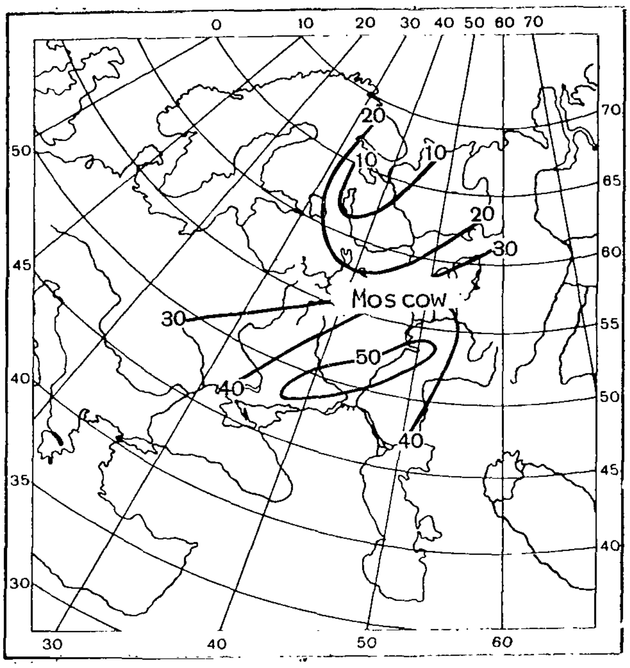

Figure 4a. Geographical Distribution of Soil Temperature According to Ground Data at 12 Hrs. 44 min. Moscow Statute Time 17 May 1967.

The geographical distribution of the radiation temperature, observed from the satellite, is determined by two principal factors: the actual distribution of temperature on the ground surface and the distribution of cloudiness. The distribution of cloudiness according to ground observations is given in Figure 2, and the distribution of the temperature of the underlying surface in Figure 4a. To a certain extent the distribution of temperature reflects the distribution of cloudiness. However, we should note that the zone of maximum temperatures is shifted somewhat to the east from the cloudless and little cloudy regions.

At the hydrometeorological station the temperature of the denuded soil is measured. According to Z. A. Mishchenko's data [6, 7] during the daylight hours in clear weather the temperature of freshly plowed soil is higher than the temperature of the grassy cover by 6-10°; according to observations at the Voyeykovo station [8], on some clear days the difference between the temperature of the surface of bare soil and the grass may reach 11-14°C. On the other hand, the readings of the mercury thermometer during positive vertical gradients of the temperature will be too low. The correction which is a function of the differences between the soil and air temperatures may reach 7-8° [9, 10]. /45 In this way the value of the temperature obtained on bared sectors of the soil, without introduction of corrections would approach the true temperature of the vegetation cover.

In comparing the airplane data with the satellite data in the point under the satellite we should also bear in mind that the scanning continued for a smaller period of time, and that it is required for describing the entire point under the satellite.

According to the satellite data the maximum values of the radiation temperature are noted over the eastern part of the Black Sea and the regions of dry land adjacent to it from the Northeast. This contradicts the fact that the temperature of the dry land during the Summer-Winter period is higher than the temperature of the sea. Possibly, to a certain extent, this contradiction is caused by the difference in the radiating capacity. The secondary maximum, located in the regions of the lower Volga, coincides with the position of the maximum of the soil temperature. The region of the maximum values of the radiation temperature is located in the North-Western zone of Ci. In the distribution of the isopleths of the radiation temperature the distribution of cloudiness is reflected to a certain extent (Figures 2 and 4b). The radiation temperature contrasts reach 30-40°, which agrees with the evaluation by L. V. Murav'yeva and N. Ye. Ter-Markaryants [11], according to the data of which the contrast of radiation temperatures of the underlying surface and the clouds of the lower level in the 8-12 μ sector of the spectrum, during daylight hours in Summer reach 30-45°.

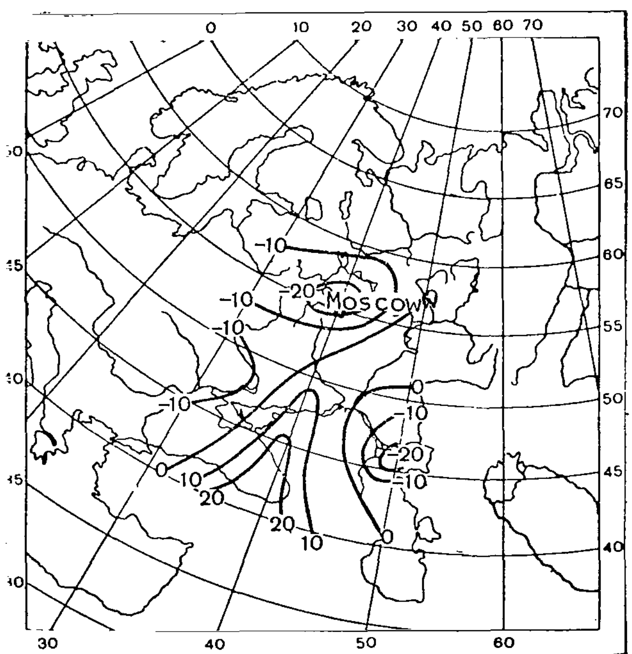

Figure 4b. Geographical Distribution of Radiation Temperature According to Measurements from the KOSMOS-156 Satellite Loop Number 296, 17 May 1967.

In the zone of the lower level cloudiness according to the satellite data the radiation temperature changes from 0 - -15°, which also coincides with the evaluations in work [5]. /46
During the Summer months on the territory of the USSR the radiation temperature of the lower cloudiness according to the data of work [5], varies from -14 to +6°C.

The comparison of radiation temperatures obtained from the airplane and the satellite for the point under the satellite is given below. According to the airplane data, in this region we observe the following radiation temperature at different angles of scanning:

α . . .	—60	—50	—40	—30	—20	—10	0	10	20	30	40	50	60
T_p . .	0.2	3.8	11.0	24.0	32.6	32.6	33.8	33.8	36.2	36.2	32.6	32.6	32.6

Owing to systematic errors in the measurements of T_p with negative angles upon further analysis we use the values of T_p only with positive scanning angles.

The radiation temperature in the region of positive scanning angles is 10 to 15° lower than the soil temperature, obtained from ground measurements. If we take into account that the correction for the effect of the temperature layer remains 10-15° [4, 5], then upon the introduction of this correction we obtain the values of the underlying surface temperature which is close to the observed soil temperature.

The radiation temperature obtained from the satellite in the nadir in this region varies from -11 to +3°C. According to the calculations of work [5] such a temperature in the examined period corresponds to the radiation temperature of the lower cloudiness, although according to the satellite data in this region it is clear, according to the observations from the airplane we note a cloudiness of the upper level, according to the ground data we notice 3-7 points Ci. With the radiating capacity of the clouds of the upper level of the order of $\varepsilon = 0.3$ and in the prescribed soil temperature t_{ss} the radiation temperature of the upper level clouds $T_{p_{Ci}}$ under the mean conditions has the following values:

t_{ss}	31	28	43
$T_{p_{ss}}$	17	15	28
$T_{p_{Ci}}$	-38	-10	-29

Since the value of ε in relation to the thickness of the cloud may vary within a wide range, we should expect that the limits of the measurements of radiation temperature T_p of the cloud level will be wider than those obtained i.e., the T_p observed from the satellite in individual cases may correspond to the cloudiness of the upper level.

As follows from comparison of minimal brightness values from instruments in the 8-12 μ and 3-30 μ ranges, there is a certain connection.

T_p . . .	—30	—20	—10	0	10	20	30
I_{3-30} . .	0.08	0.09	0.11	0.12	0.13	0.15	0.16

Therefore the geographical distribution of intensity in the 3-30 μ channel is analogous to the distribution of the radiation temperature. On the territory of the European part of the USSR I_{3-30} varies from 0.08 to 0.17 cal/ /cm^2 min·ster. The maximum values correspond to the regions with few clouds with a high temperature of the underlying surface, the minimum are observed in the North-Western zone of Ci. The relatively small ranges of the variations of I_{3-30} are explained by the fact that the "high temperature" radiation of the underlying surface experiences a greater weakening in the atmosphere than the radiation which is caused by cloudiness.

Below we give the evaluations of the ascending longwave radiation E↑ in cal/cm^{2}min at the height of the airplane with various heights of the upper boundary of the cloud layer H_{cl} and in cloudless sky (H_{cl} = 0). For the evaluation we have used the formula from works [12, 13] /47

$$E^{\uparrow} = \varepsilon\sigma T_0^4 \cdot 10^{-a\Delta t}, \tag{1}$$

where ε is the radiating capacity, T_0 is the temperature of the underlying surface or the upper boundary of the cloud layer, $\Delta t = T_0 - T_z$, T_z = -38°C the air temperature at the airplane's height, a = 0.0036. The information on the radiating capacity of clouds of various levels were borrowed from work by Ye. P. Novosel'tsev [14].

TABLE 1. ASCENDING LONGWAVE FLUX AT THE LEVEL OF THE AIRPLANE WITH CLOUDS OF VARIOUS LEVELS.

	H_{cl}	T_0	ε	$E^{\uparrow}$	$E^{\uparrow}/\pi$
Surface Below Clouds	0	40	1,0	0,409	0,13
Clouds of the Lower Level	2	8	1,0	0,346	0,11
Clouds of the Middle Level	4	—4	0,8	0,256	0,08
Clouds of the Upper Level	7	—22	0,6	0,175	0,06

Tr. Note: Commas indicate decimal points.

In reality the values of E↑ for the clouds of the upper level should be somewhat higher, since these clouds frequently transmit longwave radiation, coming up from the underlying surface in the lower layers of the atmosphere.

The airplane measurements in the point under the satellite yield the following values of I_{3-30} cal/cm^{2}min·ster:

α	—60	—50	—40	—30	—20	—10	0	10	20	30	40	50	60
I_{3-30}	0.14	0.16	0.19	0.20	0.20	0.21	0.21	0.20	0.20	0.19	0.19	0.16	0.17

As it was in the case of the radiation temperature, owing to the systematic errors, the data with α equal to -50 and -60°C, are too low and have been excluded from further examination. On the basis of these data the ascending longwave flow on the level of the airplane amounts to 0.600 cal/cm^{2}min. This value appears too high, since according to formula (1) even with the maximum value of the underlying surface temperature of 50°C noted during the passage of the satellite, the ascending current of longwave radiation at the level of the airplane does not exceed 0.43 cal/cm^{2}min. From a comparison of the calculations according to formula (1) with the results of the actinometric sounding of work [13], it follows that the accuracy of the calculated values is of the order of ±10%. If the calculation error is assumed to be equal to ±20%, even in that case the values of I_{3-30} measured from the airplane remains substantially higher than the calculated ones.

According to the satellite data in the nadir point I_{3-30} amounts to 0.12--0.13 cal/cm^{2}min·ster., which is considerably lower than the airplane values and is close to the value of $I = E\uparrow/\pi$ = 0.13 cal/cm^{2}min·ster obtained on the basis of the calculations.

Analogous ratios between the ground, airplane and satellite data were obtained for other days as well (Table 2). The materials available to us enables us to compare the ground, airplane, and satellite data in the first approximation. For more accurate comparisons it is necessary to carry out a wider complex of measurements. In particular the measurements of the radiation characteristics at various levels should be accompanied by vertical sounding of the atmosphere by means of an airplane and radiosondes. Since in the majority of the cases even at the maximum altitude of its flight the airplane is below the upper limit of the troposphere, it would be useful to combine airplane measurements with balloon measurements which make it possible to evaluate the transformation of radiation flows observed above the airplane. The problem of the work of the ground actinometric network does not include measurements of such important values which are necessary for comparison, as radiation temperature and the flow of the ascending longwave radiation. In connection with the necessity for checking the calculation methods, used for conversion from one level to the other, the organization of a ground based network of measurements of these elements would be extremely desirable. /48

In order to study the representativity of the data, obtained at the actinometric network, and taking into account the variegated nature of the underlying surface it is necessary also to carry out measurements from the airplane or helicopter at a small altitutde.

TABLE 2. COMPARISON OF THE RESULTS OF MEASUREMENTS IN THE POINT UNDER THE SATELLITE I_0 cal/cm^{2}min·ster, πJ_0, INTERFERENCES, NOISE, $E_P^{\uparrow}$ IN cal/cm^{2}min.

Date	Time, Height of the Sun $h_{\odot}$: Flight Altitude H	Spectral Range, μ	Ground Data	Airplane Data I_0	Airplane Data πI_0
13 May 67	6 hr, 43 min - 6 hr, 59 min.	0,3—3	R_K = 0,02—0,09	0,07	0,22
	$h_{\odot}$ = 20°,	3—30	$E^{\uparrow}$ = 0,52—0,62	0,16	0,50
	H = 8.17 km	8—12	t_{SS} = 9—22°	11—20	—
15 May 67	5 hrs, 38 min - 5 hrs, 45 min.	0,3—3	R_K = 0,09	0,03	0,09
	$h_{\odot}$ = 15°	3—30	$E^{\uparrow}$ = 0,52	0,16	0,50
	H = 7.99 km	8—12	t_{SS} = 9—10°	10	—
17 May 67	12 hrs, 41 min - 12 hrs, 47 min.	0,3—3	R_K = 0,22—0,27	0,06	0,20
	$h_{\odot}$ = 58.6°	3—30	$E^{\uparrow}$ = 0,78—0,89	0,16—0,21	0,50—0,66
	H = 9.1 km	8—12	t_{SS} = 40—50	32—36	—

Airplane Data Interference Noise		Airplane Data $E_p^{\uparrow}$	Satellite Data I_0	Satellite Data πI_0	Satellite Data $E_p^{\uparrow}$	Underlying Surface Under the Airplane	Cloudiness Above the Airplane
0,21	- -	0,23	0,05	0,16	0,17	8 Points Ac, Cu hum., in the Breaks are Forests & Fields	Clear
—	—	—	0,14	0,44	—		
—	- -	—	—10	—	—		
0,10	0,09	0,11	0,02—0,05	0,06—0,15	0,10—0,12	Fields	Clear
—	0,40	0,35	0,14	0,44	—		
—	—	—	—5; —9	—	—		
0,19	—	0,20	0,11—0,18	0,35—0,56	0,34—0,55		
—	0,49	0,41—0,43	0,12—0,13	0,38—0,40	—	Plowed and Green Fields	Clear
—	—	—	—11; +3	—	—		

Tr. Note: Commas indicate decimal points.

REFERENCES

1. Shifrin, K. S. and N. P. Pyatovskaya: "Shortwave Radiation Field Above the Typical Underlying Surfaces," *Trudy GGO*, Issue 166, 1964.
2. Kondrat'yev, K. Ya. and Kh. Yu. Niylisk: "On the Thermal Radiation of the 9.6 μ Absorption Band of Ozone in the Atmosphere", *Problemy Fiziki Atmosfery*, Collection 2, *LGU*, 1963.
3. Shifrin, K. S.; N. P. Pyatovskaya and V. Yu. Kolomiytsov: "Determination of the Flow of Outgoing Shortwave Radiation by Means of a Satellite," *Trudy GGO*, Issue 166, 1964.
4. Gayevskiy, V. L. and Yu. I. Radinovich: "On Estimation of the Influence of the Atmosphere on the Result of Measurement of the Radiation Temperature of the Terrestrial Surface from Satellites," *Trudy GGO*, Issue 166, 1964.
5. Kondrat'yev, K. Ya.; Ye. P. Novosel'tsev and N. Ye. Ter-Markaryants: "Determination of the Temperature of the Underlying Surface and Clouds from Weather Satellites," *Trudy GGO*, Issue 196, 1966. /49
6. Mishchenko, Z. A.: "On the Temperature of the Active Surface in Microclimatic Investigations," *Trudy GGO*, Issue 180, 1965.
7. Mishchenko, Z. A.: "On the Thermal Balance and Temperature of Plants," *Trudy GGO*, Issue 190, 1966.
8. *"Materialy Nablyudeniy GGO"*, [Materials of Observations of the Main Geophysical Observatory], Issue 1. Meteorological and Actinometric Observations in Voyenkovo, 1957.
9. Zubenok, L. I.: "On the Procedure for Measuring the Temperature of the Soil Surface," *Trudy GGO*, Issue 6, 1947.
10. Kondrat'yev, K. Ya. and Z. A. Loginova: "On the Direct Methods of Determination of the Underlying Surface Temperature," *Vestnik LGU*, No. 22, 1956.
11. Murav'yeva, L. V. and N. Ye. Ter-Markaryants: "On the Possibility of Tracing Cloudiness on the Dark Side of the Earth from Weather Satellite lites," *Trudy GGO*, Issue 196, 1966.
12. Barashkova, Ye. P.: "On the Procedure for Calculating Longwave Flows in the Troposphere Under a Cloudless Sky," *Trudy GGO*, Issue 152, 1964.
13. Barashkova, Ye. P.: "Certain Regularities in the Vertical Distribution of the Ascending Longwave Radiation," See the present collection.
14. Novosel'tsev, Ye. P.: "On the Degree of Darkness of the Clouds in the Upper and Middle Level," *Trudy GGO*, Issue 196, 1966.

EXPERIMENT IN USING DATA ON OUTGOING SHORTWAVE RADIATION OBTAINED FROM KOSMOS-122 SATELLITE

K. S. Shifrin and N. P. Pyatovskaya

ABSTRACT. The authors present the shortwave radiation balance of the atmosphere. The calculations were performed on experimental data obtained with a narrow-sector receiver (NSR) aboard the Kosmos-122 satellite. They note good agreement of the measurement data for the field of outgoing shortwave radiation, from the Tiros-IV and Kosmos-122 satellites at different times and with different equipment. The satellite data yield a noticeable anisotropy of the reflection from the water, the brightness increases with the mirror direction. This is the result of both the anisotropy of reflection, and the elongation of the atmospheric indicatrix of diffusion. The processing of data from the Kosmos-122 satellite showed that the albedo, according to the NSR signal, agrees satisfactorily with the known values of the albedo of terrestrial covers, and the value of the radiation heating of the vertical column of the atmosphere coincides with the data of airplane measurements by other authors.

Introduction

The determination of the amount of solar energy, observed by the vertical column of the atmosphere in the terrestrial surface, by means of an instrument located aboard a satellite is a complex problem. The measurements aboard satellites yield individual values of brightnesses of small areas at a wide variety of angles. To convert to the flows of outgoing shortwave radiation (OSR) a special calculation system has been developed at the main geophysical observatory [1, 2]. /50

In the present work we have made an attempt to analyze the data of measurement from satellites and to compare this data with the ground and airplane observations, and also with the climatological calculations. For this purpose we have used the experimental data on the field of outgoing shortwave radiation in the 0.3-3 μ region of the spectrum, obtained by means of a narrow-sector receiver (NSR), installed aboard the Kosmos-122 satellite. These data are interesting by themselves as the characteristic of the OSR field, its space and time variability, and also from the point-of-view of coordinating them with the theoretical system [1, 2].

The Kosmos-122 satellite was launched on 25 June 1966. It was put into a circular orbit 625 km high, tilted to the plane of the equator at an angle of 60°, with a period of rotation around the earth amounting to 97.1 min.

The working principle of the satellite and the methods of obtaining various information are given in work [8].

The actinometric data after operative processing with electronic computers were given in the form of Tables and special maps. The television and infrared pictures of cloudiness after being processed were presented in the form of mounted photographs and maps of the cloud analysis.

Data of Measurements from the Kosmos-122

Let us examine the data on the brightness of the earth's-atmosphere system. For the analysis it is important to have television images of the area viewed together with the NSR readings. We have used the observation data according to the loops for the period from 27 July to 21 September 1966. The /51
initial data in all these occasions are given in the Table 1.

TABLE 1

Date 1966	Number of Loop	Time of Work of the Equipment (Moscow)				Observation Region		Length of Observations (Taking the Breaks into Account (minutes)
		Beginning		End		Latitude	Longitude	
		Hrs.	Min.	Hrs.	Min.	$\phi°$	$\lambda°$	
29 VII	501	6	29	6	36	70 с.—50 N	30 в.—120 E	7
1 VIII	545	5	42	5	48	70 с.—55 N	70 в.—120 E	6
2	560	5	57	6	03	75 с.—55 N	50 в.—110 E	6
7	634	6	00	6	08	60 с.—0	100 в.—150 E	8
16	767	5	17	5	29	10 ю.—30 S	120 в.—145 E	12
17	782	5	40	5	51	70 с.—50 S	70 в.—150 E	11
18	796	3	58	4	23	35 ю.—15 S	120 в.—150 E	25
20	824	1	16	1	37	60 с.—10 S	120 в.—170 E	21
21	853	0	14	0	36	50 с.—15 S	140 в.—170 W	22
25	898	1	00	1	05	60 с.—40 S	110 в.—140 E	5
26	913	1	15	1	42	60 с.—15 S	100 в.—150 E	27
26	927	0	16	0	26	50 с.—45 S	120·в.—170 W	10
11 IX	1160	17	48	18	10	45 ю.—30 N	20 з.—30 E	12
12	1175	18	03	18	19	45 ю.—30 N	20 з.—20 E	16
13	1189	16	41	16	59	50 ю.—20 N	10 з.—30 E	16
15	1220	19	04	19	16	5 ю.—30 N	30 з.—0 E	15
17	1248	16	09	16	32	50 ю.—30 N	20 з.—30 E	23
18	1263	16	25	16	48	40 ю.—10 N	20 з.—20 E	23
20	1292	15	25	15	47	30 ю.—40 N	10 з.—40 E	22
21	1307	16	07	16	16	70 с.—50 N	30 в.—70 E	9

An example of the digital map of radiation data expressed in 10^{-2}cal/ /cm^{2}min·ster is given in Figure 1.

The nephanalysis data on the basis of the television pictures from aboard the satellite are given in Figure 2. On the cloudiness map we have used the system of symbols, corresponding to the four conventional gradations of cloudiness [9].

We should emphasize that the television images are obtained with small resolution, are insufficiently bright, a distortion of the geometry of the picture and the tone of the image. The clouds and cloud systems with a radius of less than 50-100 km were not marked. This in particular is connected with the fact that in a number of cases the television image did not mark the cloudiness, although the brightness signal was very large. The radius of the area viewed by the NSR was about 25 km (according to the under-the-satellite point), and actually the field of vision of the receiver could have been covered with clouds although the television did not show them.

Processing of Data and Their Analysis /53

In order to process the measurement data we have used only the brightnesses, obtained in the point under the satellite, since only for this point did we have the orbital data (height of the sun, latitude and longitude, etc.). This point corresponds in the theoretical system to the $\theta = 0$ angle and accordingly the brightness in it does not depend on the azimuth ϕ.

According to every loop the data were presented in the form of Table 1 of the appendix. In this table we give: the date, number of loop, Moscow time, zenith distance of the sun $i_{\odot}$, coordinates of the place (according to the orbital data, the Kosmos-122 satellite), the mean values of the brightness in the point under the satellite (in 10^{-2} cal/cm^{2}min·ster) according to radiation maps, the state of cloudiness in this point according to the nephanalysis maps of cloudiness plotted on the basis of television pictures from the Kosmos-122 /54 satellite, the appearance of the underlying surface at this point according to the World Atlas [3].

We should note that the position of the nadir (this is precisely the so-called point under the satellite) up to 16 August 1966, for technical reasons was considered to be in the 16th point, and after the 16th of August already in the middle, i.e., between the 14th and 15th points (see Figure 1). In processing the measurement results we have taken in the first case the averages of the nine brightness values, in the second case the averages from 12 values.

These mean values of brightness are subject to extremely great oscillations from point to point depending on the type of the underlying surface and mainly on the cloudiness, as can be seen from Table 1 of the appendix.

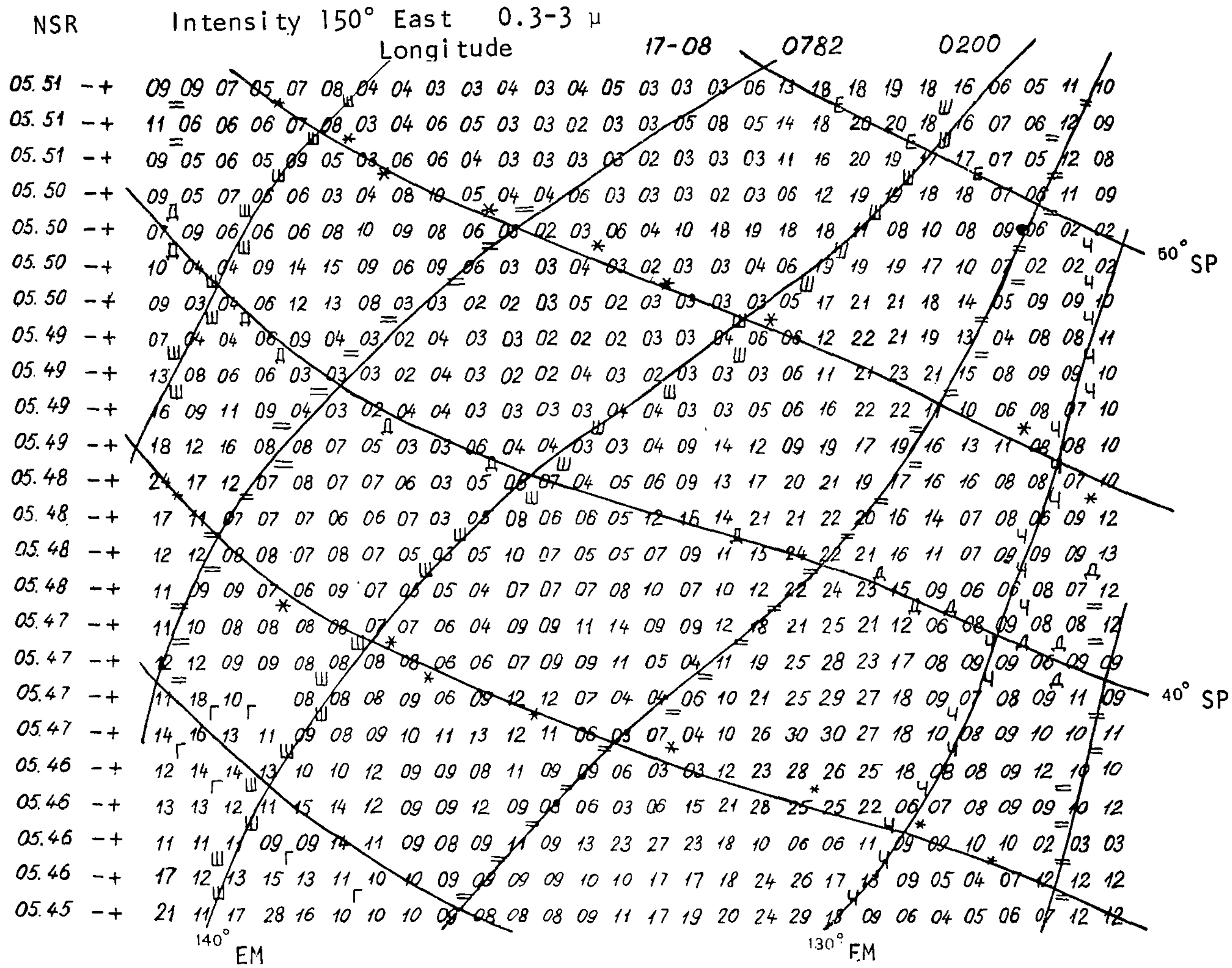

Figure 1. Specimen of the Digital Map of Radiation Data in the 0.3-3 μ Region of the Spectrum Obtained on 17 August 1966 from the Kosmos-122 Satellite.

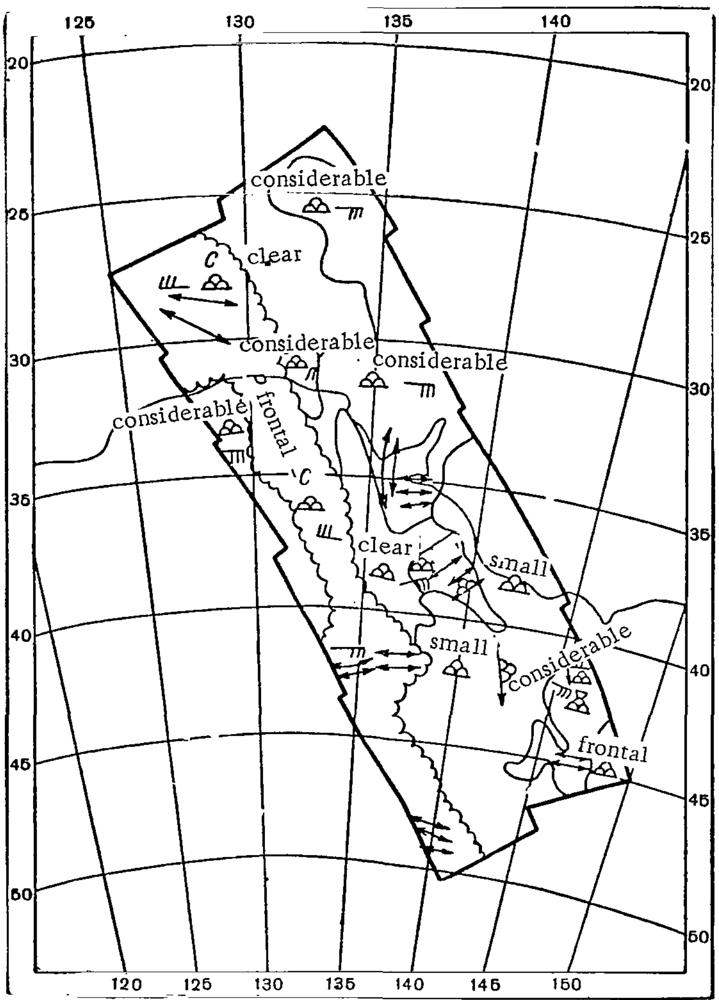

Figure 2. Cloudiness Map Obtained From the Kosmos-122 Satellite on 17 August, 1966, at 5 Hrs., 44 Min. -5 Hrs, 50 Min. Accordin to Moscow Time

As examples, see Figures 3-5, showing samples of brightness field realizations at points beneath the satellite using instantaneous values for several revolutions rather than mean data.

The type of cloud cover and underlying surface at the point in question for revolutions 501, 560, and 583 are presented in Table 1 of the appendix, for revolutions 898 and 913 -- in Table 2 of the appendix.

Figures 3-5 and Tables 1 and 2 of the appendix show that the cloud cover has the greatest influence on brightness and its changes.

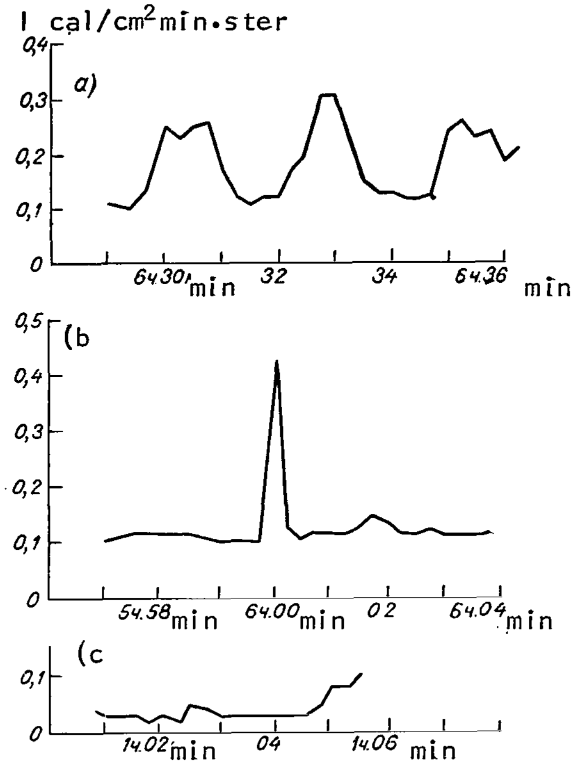

Figure 3. Specimen of Portrayal of the Brightness Field in the Points Under the Satellites (Moscow Time). a, Loop No. 501, 29 July 1966; b, Loop No. 560, 28 July 1966; c, Loop No. 898, 25 July 1966.

According to the mean brightness values in the points under the satellites we have calculated the balance in the radiational heating of the column of the atmosphere. The calculation was performed according to the following formulas.

1) Balance of the earth's-atmosphere system /55

$$\Delta Q = S_0 \cos i - R,$$

where S_0 is the solar constant in cal/cm² min, i is the zenith distance of the sun, R is the flow of outgoing shortwave radiation in cal/cm² min.

Value R was determined according to the values of brightness I, measured from the Kosmos-122 satellite according to the system developed in [2, Tables 1-8 of the appendix].

2) Balance of the column of the atmosphere

$$B = \Delta Q - E^*(1 - A_u),$$
$$E^* = E(1 + 0{,}06),$$

where E is the total illumination of the surface of the earth with shortwave radiation in cal/cm² min, its values for the 0.4-2.5 μ spectral interval are given in Table 3 of work [2]; A_u is the albedo of the underlying surface and /56 clouds. This value was determined according to the values of brightness I, measured from the Kosmos-122 satellite, by means of Tables 1 through 8 of the appendix from work [2].

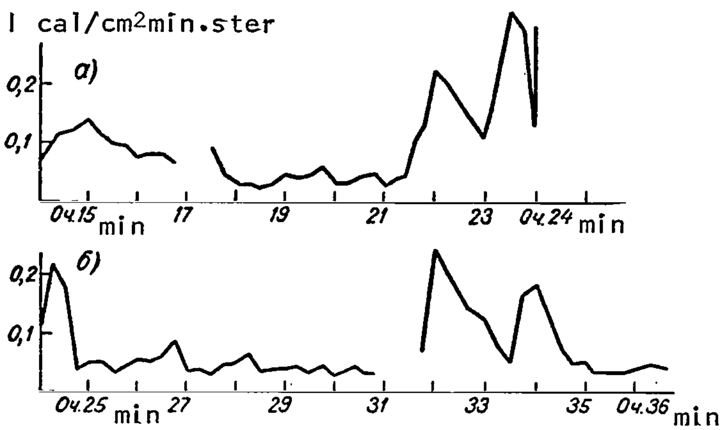

Figure 4. Specimen of Portrayal of the Brightness Field in Points Under the Satellites (Moscow Time), Loop No. 853, 21 August 1966.

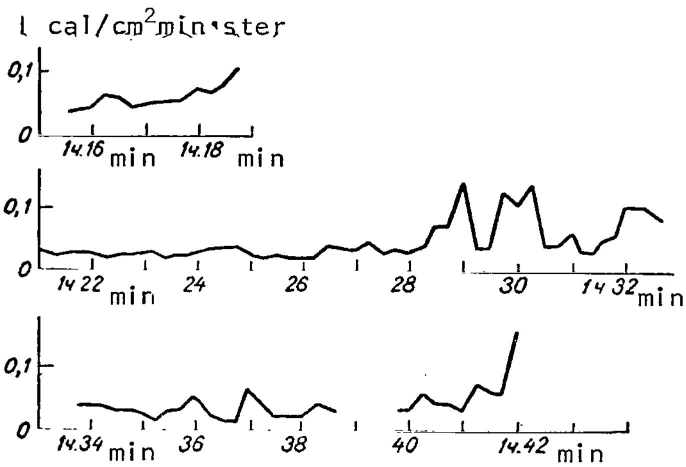

Figure 5. Specimen of Portrayal of the Brightness Field in Points Under the Satellites (Moscow Time), Loop No. 913, 26 August 1966.

The value 0.06 is the addition through radiation, which was not taken into account in [2]. It consists of the following parts: 9% of the total radiation belongs to the spectral region of $\lambda < 0.4\ \mu$, 3.5% to $\lambda > 2.5\ \mu$, i.e., the total addition amounts to 12.5%. Evaluations show that about one half of this value reaches the ground surface.

3) Albedo of the earth's-atmosphere system

$$A_{e-a} = \frac{R}{S_0 \cos i}.$$

4) Radiation heating of the pillar of the atmosphere caused by absorption of solar radiation

$$dT/dt = 0.245\ B \text{ deg/hr}.$$

Here B is in cal/cm^2 min. This formula was obtained by V. G. Kastrov [4].

As an example in Table 2 we give the results of calculations of the values of ΔQ (cal/cm^2 min.), $\partial T/\partial t$ (deg/hr), A_u and A_{e-a} for several points of loops Nos. 767, 898 and 913. The trajectory of these loops passes over the regions of the terrestrial globe with a wide variety of underlying surface (Figure 6).

The detailed results of calculations of the radiation balance of the atmosphere for all the three loops are given in Table 2 of the appendix.

TABLE 2.

No. of the Loop	No. of the Point	A_{e-a}	A_u	ΔQ	$\frac{dT}{dt}$
767 16 VIII 1966	1	0,08	0,09	1,69	0,10
	2	0,13	0,16	1,56	0,10
	3	0,24	0,31	1,24	0,09
	4	0,26	0,30	1,06	0,07
898 25 VIII 1966	1	0,40	0,35	0,16	0,02
	2	0,31	0,35	0,24	0,03
	3	0,26	0,35	0,31	0,04
	4	0,44	0,87	0,26	0,05
913 26 VIII 1966	1	0,19	0,18	0,46	0,04
	2	0,24	0,27	0,73	0,06
	3	0,34	0,42	0,72	0,06

Tr. Note: Commas indicate decimal points.

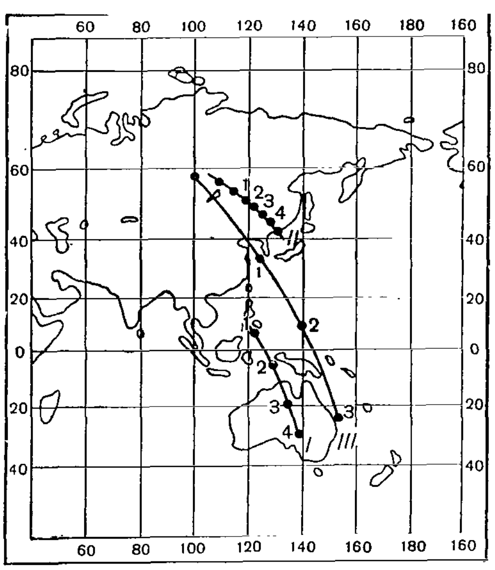

Figure 6. Trajectory of the Flight of Kosmos-122. I, Loop No. 767, 16 August, 1966; II, Loop No. 898, 25 August 1966; III, Loop No. 913, 26 August 1966.

In the cases examined the values of the radiation heating fluctuates within the limits of 0.02-0.1 deg/hr. These values are in satisfactory agreement with the mean values of the radiation heating, obtained earlier by V. G. Kastrov according to the observations during three years in flights on an airplane up to the height of 5 km [4] and N. P. Pyatovskaya according to two years' observations during flights up to the height of 3 km [5, 6]. /57

It is also interesting to compare the values of albedo of surfaces according to the ground observations and climatological calculations with the albedo values obtained from the Kosmos-122 satellite.

During clear days in the region of the Pacific Ocean the albedo according to the Kosmos-122 satellite A_{sat} = 9%, the albedo according to ground data A_{gr} = 7-9%; in Australia (desert region) A_{sat} = 36%, A_{gr} = 28-30%, in Western Siberia A_{sat} = 18%, A_{gr} = 18-20%.

We should note that, in processing the data of measurement from the Kosmos-122 satellite we encountered a number of difficulties, connected first of all with the fact that not all the loops contained data on cloudiness (the TV pictures in radiation maps were often obtained at different times), and disruptions often appeared on radiation maps. Since the orbital data obtained only for the point under the satellite with a space of one minute, it is extremely difficult to tie in the other points to the locality accurately. Moreover, in a number of cases clearly too high values of brightnesses were obtained especially when the sun was low. For example, for loop No. 913 at 1 hr 15 min--1 hr 17 min when the elevation of the sun was less than 5°, the albedo of the underlying surface obtained is greater than 1 (see Table 2 of appendix).

Apparently, the four-point system of cloudiness evaluation selected does not characterize with sufficient accuracy the state of the cloudiness in the region given. For example, in spite of the fact that on the nephanalysis map the 0 point cloudiness (clear) is indicated, in the field of vision of the NSR there may be sectors with cumulus clouds, which increase sharply the readings of the instruments (see for example, Figure 3).

Angular Structure of the Field of Outgoing Shortwave Radiation

The narrow angle instruments, installed aboard a satellite, are scanning in the plane, perpendicular to the satellite flight trajectory. This makes it possible to determine the angle of structure of the OSR field above the uniform underlying surface. As an example we give Figure 7, where we give the indicators of the reflected radiation brightness field above water. These data were obtained from the Kosmos-122 satellite over the Pacific Ocean (29° N and 138° E) on 7 August 1966 (loop No. 634) with the elevation of the sun at 11.5° ($i = 78.5°$). For comparison on the same diagram we give the data from the Tiros-4 satellite for the same elevation of the sun also over the Pacific Ocean and the theoretical curve (Rayleigh), calculated with $\tau_0 = 0.5$ (optical thickness) and albedo A = 0 (according to [10]).

We should note the good agreement between the data of measurements of the OSR field obtained from the Tiros-4 and Kosmos-122 satellites at different times. In Figure 7 we can clearly see the difference of the real OSR field from the Rayleigh field.

The satellite data yield a noticeable anisotropy of the reflection, the brightness grown in the mirror direction. This is the result of both the anisotropy of reflection from the water and from the stretched state of the atmospheric dispersion indicator. This problem is examined in greater detail in work [7].

In conclusion, we should mention the following. The processing of the Kosmos-122 satellite measurement data performed by us indicates that the albedo evaluated according to the NSR signal values coincides satisfactorily with the known values of the ground cover albedos. The value of the radiation heating of the vertical column of the atmosphere coincides with the data of airplane measurements obtained by other authors. /58

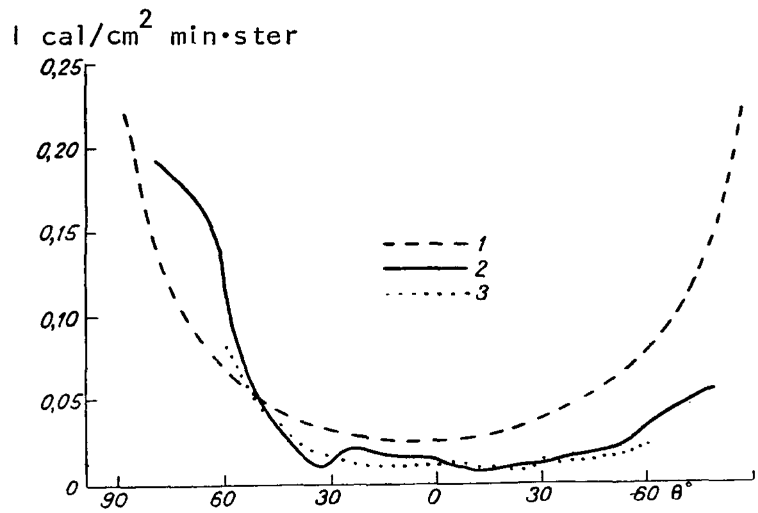

Figure 7. Indicators of Brightness of the Reflected Radiation Field Over Water. 1, Rayleigh Curve; 2, Obtained from the Tiros-4 Satellite; 3, Obtained from the Kosmos-122 Satellite.

REFERENCES

1. Shifrin, K. S.; N. P. Pyatovskaya: "Shortwave Radiation Field Above the Typical Underlying Surfaces," *Trudy GGO*, Issue 166, Leningrad, 1964.
2. Shifrin, K. S.; V. Yu. Kolomiytsov and N. P. Pyatobskaya: "Determination of the Flow of Outgoing Shortwave Radiation by means of a Satellite," *Trudy GGO*, Issue 166, Leningrad, 1964.
3. *Fiziko-Geograficheskiy Atlas Mira* [The Physical Geographical Atlas of the World], Moscow, 1964.
4. Kastrov, V. G.: "Measurement of Absorption of Solar Radiation in the Free Atmosphere up to 3-5 km," *Trudy TsAO*, Issue 8, 1952.
5. Pyatovskaya, N. P.: "Shortwave Radiation Flows in the Free Atmosphere," *Trudy GGO*, Issue 109, 1961.
6. Pyatovskaya, N. P.: "Investigation of the Shortwave Radiation Field in the Free Atmosphere," Author's abstract of the dissertation, *GGO*, Leningrad, 1965.
7. Shifrin, K. S. and V. Yu. Kolomiytsov: "Effect of Anistropy of Reflection from the Underlying Surface on the Determination of the Flow of Outgoing Shortwave Radiation According to Measurement from a Satellite," See the present collection.
8. Aleksandrov, L. A.: "The Meteorological Experiment on a Kosmos-122 Satellite," *Zemlya i Vselennaya*, No. 2, 1967.
9. Kondratyev, K. Ya.; Ye. P. Borisenkov and A. A. Morozkin: *"Prakticheskoye Ispol'zovaniye Dannykh Meteorologicheskikh Sputnikov*, [Practical Utilization of Weather Satellite Data], Gidrometeoizdat Press, Leningrad 1966.

10. Arking, A.: The Angular Distribution of Scattered Radiation as Measured from TIROS Papers of Intern. Sympos. on Radiation in Leningrad, *UGGI, Monogr.*, No. 28, Paris, 1965.

APPENDIX - TABLE 1.

Results of Observation from the Kosmos-122 Satellite in the Point Under the Satellite.

Moscow Time Hrs. Min. Sec.	$i_{\odot}^{\circ}$	Coordinates of the Location: Latitude φ°	Coordinates of the Location: Longitude λ°	Mean Reading I $\frac{cal}{cm^2 min \cdot ster}$	Cloudiness Characteristic	Underlying Surface
			29 July, 1966, Loop No. 501			
6 29 45	62,6	61,9 N	62,3 E	0,16	C, Cumuliform	Middle- and Southern Taiga Western Siberian Pine Forests
6 30 45	59,7	63,4 N	69,4 E	0,22	Boundary between the C and Clear Zones (Principal Cloud Systems)	Sphagnum, in some places forested & clay grassy swamps of the Taiga zone.
6 31 45	56,9	64,4 N	77,1 E	0,12	Clear	Deciduous-spruce, cedar-Northern Taiga Western Siberian Forests
6 32 45	54,2	65,0 N	85,3 E	0,28	C, Frontal Banded Structure	Large, spruce-large, Northern Taiga Western Siberian Forests
6 33 45	51,5	65,1 N	93,8 E	0,14	Clear	Large, Northern Taiga sparse forests with brush and swamp sectors
6 34 45	48,9	64,7 N	102,1 E	0,19	Clear	Large, Middle Taiga forests (brush and mosses)
6 35 45	46,5	63,8 N	110,1 E	0,21	Considerable, Banded Structure	Large, Middle Taiga forests with moss, grass, and brush
6 36 45	44,1	62,5 N	117,4 E		C, Cumuliform	Mountainous Taiga dark coniferous forests

Tr. Note: Commas indicate decimal points.

Moscow Time Hrs. Min. Sec.	$i_{\odot}^{\circ}$	Coordinates of the Location: Latitude φ°	Coordinates of the Location: Longitude λ°	Mean Reading I $\frac{\text{cal}}{\text{cm}^2\text{min}\cdot\text{ster}}$	Cloudiness Characteristic	Underlying Surface
			2 August 1966, Loop No 560			
5 57 45	70,1	62,3 N	56,0 E	0,08	Boundary between the Clear & Considerable Zones	Dark-coniferous Western Ural Forests
5 58 45	66,8	63,7 N	63,2 E	0,11	Clear	Western Siberian Pine Forests
5 59 45	63,5	64,6 N	71,1 E	0,14	Clear	Grassy and Grassy-mossy lowland swamps
6 00 45	60,2	65,1 N	79,4 E	0,16	Considerable, Stratiform	Sphagnum, sometimes forested swamps of the Taiga zone
6 01 45	56,9	65,0 N	87,8 E	0,13	Considerable, Cumuliform	Large-spruce-cedar Northern Taiga Western Siberian Forests
6 02 45	53,7	64,5 N	96,1 E	0,12	Alike, distinctly expressed thick cumulus and cumulonimbus clouds	Large-spruce-cedar Northern Taiga Western Siberian Forests

Tr. Note: Commas indicate decimal points.

APPENDIX - TABLE 1 (Continued)

Moscow Time Hrs. Min. Sec.	$i_{\odot}^{\circ}$	Coordinates of the Location: Latitude φ°	Coordinates of the Location: Longitude λ°	Mean Reading $I \frac{\text{cal}}{\text{cm}^2\text{min}\cdot\text{ster}}$	Cloudiness Characteristic	Underlying Surface
			21 August, 1966, Loop No. 853			
0 24	49,7	19,0 N	168,5 E	0,12	Light, Cumuliform	Water
0 25	48,1	15,6 N	170,0 E	0,05	Same	Water
0 26	46,7	12,3 N	171,4 E	0,04	Same	Water
0 27	45,5	8,9 N	172,8 E	0,06	Light, banded structure	Water
0 28	44,4	5,5 N	174,2 E	0,05	Same	Water
0 29	43,7	2,1 N	175,5 E	0,04	Same	Water
0 30	43,1	1,3 S	176,8 E	0,04	—	Water
0 31	42,9	4,7 S	178,1 E	0,10	—	Water
0 32	42,9	8,1 S	179,5 E	0,15	—	Water
0 33	43,1	11,5 S	179,1 W	0,11	—	Water
0 34	43,7	14,9 S	177,7 W	0,15	—	Water
0 35	44,4	18,3 S	176,2 W	0,05	Considerable, cumuliform large cells	Water
0 36	45,4	21,7 S	174,7 W	0,04	Considerable, banded structure	Water

Tr. Note: Commas indicate decimal points.

APPENDIX - TABLE 2

Results of Calculations of the Radiation Balance of the Atmosphere.

Moscow Time			$i_\odot^\circ$	Coordinates of the Location		Mean Reading I $\frac{\text{cal}}{\text{cm}^2 \text{min} \cdot \text{ster}}$	Cloudiness Characteristic	Underlying Surface	A_{sur} %	R cal/cm² min	ΔQ cal/cm² min	B cal/cm² min	$\frac{dT}{dt}$ deg/hrs.
Hrs.	Min.	Sec.		Latitude φ°	Longitude λ°								
							16 August, Loop No. 767						
5	18	45	23,0	6,6 N	124,2 E	0,05	Considerable, banded structure	Water	9	0,15	1,691	0,406	0,099
5	19	45	23,0	3,2 N	125,5 E	0,08	C, Clearly expressed thick cumulus and cumulonimbus	Water	15	0,24	1,601	0,394	0,096
5	20	45	23,5	0,2 S	126,9 E	0,09	C, Cumuliform & stratiform	Water	17	0,27	1,565	0,389	0,095
5	21	45	24,6	3,6 S	128,2 E	0,11	Boundary of the light & C zones, cumuliform	Water	22	0,32	1,500	0,404	0,099
5	22	45	26,2	7,0 S	129,5 E	0,08	Light, cloud bands (the clouds may be cumuliform cirriform & stratiform)	Water	16	0,24	1,555	0,398	0,098
5	23	45	28,1	10,4 S	130,9 E	0,09	Light, cloud bands	Water	19	0,28	1,484	0,386	0,095
5	24	45	30,4	13,8 S	132,3 E	0,10	Considerable, cumuliform	Water	21	0,30	1,427	0,386	0,094
5	25	45	32,9	17,2 S	133,8 E	0,12	Considerable, cumuliform	Water	27	0,37	1,310	0,368	0,090
5	26	45	35,6	20,5 S	135,3 E	0,13	Clear	Water	31	0,39	1,240	0,380	0,093
5	27	45	38,5	28,9 S	136,9 E	0,12	—	Water	29	0,37	1,195	0,347	0,085
5	28	45	41,4	27,2 S	138,5 E	0,15	Clear	Water	37	0,46	1,040	0,316	0,077
5	29	45	44,5	30,5 S	140,4 E	0,12	Considerable, Cumuliform	Water	30	0,37	1,057	0,297	0,073

Tr. Note: Commas indicate decimal points.

APPENDIX TABLE 2 (Continued)

Moscow Time Hrs. Min. Sec.	$i_\odot$	Coordinates of the Location: Latitude $\varphi°$	Longitude $\lambda°$	Mean Reading $I \frac{cal}{cm^2 min \cdot ster}$	Cloudiness Characteristic	Underlying Surface	A_{sur} %	R cal/cm²min	ΔQ cal/cm²min	B cal/cm² min	$\frac{dT}{dt}$ deg/hrs.
					21 August, Loop No. 853						
0 14 00	72,2	50,5 N	146,0 E	0,17	—	Water					
0 15 00	69,6	47,6 N	149,4 E	0,12	Considerable, stratiform	Water					
					25 August, Loop No 898						
0 59 45	86,5	57,6 N	109,8 E		—	Mountain Tayga Dark Coniferous Southern Siberian Forests					
1 00 45	84,3	55,2 N	114,6 E		—	Middle Taiga Large Forests					
1 01 45	82,1	52,6 N	118,8 E	0,03	Light, cumuliform	Middle Taiga large forests	35	0,11	0,163	0,087	0,021
1 02 45	79,9	49,8 N	122,5 E	0,03	Clear	Mountain large forests	35	0,11	0,240	0,172	0,031
1 03 45	77,8	47,0 N	125,8 E	0,03	Clear	Meadowland steps with brush, elms, Mongolian willow, -forest step	35	0,11	0,311	0,162	0,040
1 04 45	75,7	44,0 N	128,7 E	0,07	Clear	Cedar-broad leaf forests in combination with the spruce-fir forests	87	0,24	0,255	0,216	0,053
					26 August, Loop No. 913						
1 15 45	89,15	57,9 N	100,8 E	0,04	Considerable banded structure	Pine & large-pine Middle Siberian Forests	>1				

Tr. Note: Commas indicate decimal points.

APPENDIX TABLE 2 (Continued)

Moscow Time Hrs. Min. Sec.	$i_{\odot}^{\circ}$	Coordinates of the Location: Latitude φ°	Longitude λ°	Mean Reading cal / cm^2 min · ster	Cloudiness Characteristic	Underlying Surface	A_{sur} %	R cal/cm^2 min	ΔQ cal/cm^2 min	B cal/cm^2 min	$\frac{dT}{dt}$ deg/hrs.
1 16 45	87,12	55,6 N	105,7 E	0,05	Light, cloud bands	Mountain-Taiga dark coniferous Southern Siberian forest	>1				
1 17 45	85,1	53,0 N	110,0 E	0,07	Light, banded structure	Transbicalian Mountain Pinelarge forests	>1				
1 21 45	77,2	41,5 N	122,8 E	0,03	Light, cumuliform	Pine-oak, pine dry forests	32	0,11	0,334	0,167	0,041
1 22 45	75,3	38,4 N	125,2 E	0,03	Light	the same	29	0,11	0,396	0,185	0,045
1 23 45	73,4	35,2 N	127,4 E	0,02	Clear	Mountain oak lime-maple oak forests	18	0,11	0,463	0,179	0,044
1 24 45	71,6	32,0 N	129,4 E	0,03	Clear	Water	23	0,11	0,524	0,220	0,054
1 25 45	69,9	28,8 N	131,3 E	0,02	—	Water	14	0,08	0,609	0,232	0,057
1 26 45	68,2	25,5 N	132,0 E	0,04	Light, cumuliform	Water	30	0,14	0,604	0,261	0,064
1 27 45	66,6	22,2 N	134,6 E	0,03	Clear	Water	17	0,10	0,683	0,245	0,060
1 28 45	65,1	18,8 N	136,2 E	0,09	C, cumuliform & stratiform	Water	46	0,30	0,540	0,225	0,055

Tr. Note: Commas indicate decimal points.

APPENDIX TABLE 2 (Continued)

Moscow Time Hrs. Min. Sec.	$i^\circ_\odot$	Coordinates of the Location: Latitude φ°	Coordinates of the Location: Longitude λ°	Mean Reading I $\frac{cal}{cm^2 min \cdot ster}$	Cloudiness Characteristic	Underlying Surface	A_{sur} %	R cal/cm² min	ΔQ cal/cm² min	B cal/cm² min	$\frac{dT}{dt}$ deg/hrs.
1 29 45	63,7	15,5 N	137,6 E	0,07	the same	Water	30	0,23	0,657	0,228	0,056
1 30 45	62,4	12,1 N	139 E	0,05	Light, cloud bands	Water	19	0,17	0,756	0,236	0,058
1 31 45	61,2	8,7 N	140,0 E	0,07	Clear, cloud bands	Water	27	0,23	0,734	0,239	0,059
1 34 45	58,4	1,5 S	144,0 E	0,04	Considerably, cumuliform	Water	15	0,14	0,907	0,277	0,068
1 35 45	57,7	4,9 S	146,0 E	0,04	C, clearly expressed thick cumulus and cumulonimbus	Water	15	0,13	0,940	0,293	0,072
1 36 45	57,2	8,3 S	147,0 E	0,04	Light, cumuliform	Water	14	0,14	0,945	0,279	0,068
1 37 45	56,8	11,7 S	148,0 E	0,04	Boundary between the light and C zones	Water	13	0,14	0,955	0,273	0,067
1 40 45	56,7	21,9 S	153,0 E	0,06	Considerable, cumuliform (large cells)	Water	20	0,19	0,910	0,277	0,068
1 41 45	57,0	25,2 S	155,0 E	0,12	C, banded structure	Water	42	0,37	0,720	0,258	0,063

Tr. Note: Commas indicate decimal points.

PROBLEMS OF INTERPRETATION OF INFRARED PICTURES OF CLOUDINESS TAKEN FROM WEATHER SATELLITES

L. N. Guseva, V. F. Zhvalev, K. Ya. Kondrat'yev, N.Ye. Ter-Markaryants

ABSTRACT. The authors examined problems connected with the evaluation of the possible deviations of contrasts of radiation temperature of the underlying surface and cloudiness in each specific case from a corresponding most probable contrast.
The author performed an investigation of the influence on the values of the contrasts of radiation temperautres by such factors as the degree of blackness of the underlying surface, the amount of cloudiness, the angle of sighting of the scanning equipment, and the spectral characteristics. In the work the authors obtain for certain regions of the territory of the USSR the most probable corrections to the temperature of the underlying surface and the upper boundary of cloudiness, measured by the radiation method.

One of the main problems solved by means of weather satellites is the tracing of the distribution of the cloudiness over the terrestrial globe. During the daytime this task is performed by means of the usual television cameras, at night this is done on the basis of the data of three-dimensional distribution of the outgoing infrared (thermal) radiation of the earth's-atmosphere system. /66

As we know in most cases the temperature of the upper boundary of cloudiness is lower than the temperature of the underlying surface, as the result of which in the observations from the satellites the cloudiness creates against the background of the terrestrial surface a certain contrast of the flows of outgoing thermal radiation and because of this can be detected from the weather satellite. Interpretation of the data on IR-radiation measured by means of weather satellites, requires overcoming a series of substantial difficulties (caused, in particular, by the considerable space-time variability of the field of outgoing longwave radiation), this had been discussed earlier in our works [1, 3, 4]. Thus, for example, in developing the corresponding measuring equipment, and also for interpretation of energy values determined by means of it, it is necessary to have data on radiation contrasts, which may originate in the earth's-atmosphere system. In works [1, 3, 4] we have carried out the calculations of the most probable values of radiation contrasts at the level of the upper boundary of the atmosphere and for various regions of the territory of the USSR. The initial data (mean monthly many years values) according to the soil temperatures, temperatures and altitudes of the upper boundary of the clouds were obtained by L. N. Guseva, K. Ya. Kondrat'yev, and N. Ye.

Ter-Markaryants [1, 5] on the basis of the use of substantial statistical material. The calculation of the flows of outgoing radiation in the presence of cloudiness of various levels were carried out taking into account the spectral values of the degree of blackness of the clouds, borrowed from the work by Ye. P. Novosel'tsev [2].

The present article consists of two parts. In the first part we present the following questions, pertaining to the problem of radiation (temperature) contrasts:

1) evaluation of the possible deviations from the most probable contrasts of radiation temperatures of the underlying surface and clouds, calculated by us earlier;

2) investigation of the influence on the radiation temperature contrast /67 values of such factors as the degree of blackness of the underlying surface, the quantity of cloudiness, the sighting angle, the spectral characteristics of the measurement equipment;

3) the analysis of the most probable corrections to the temperature of the underlying surface and clouds, measured by the radiation method, obtained by us previously.

The second part of this work is devoted to the analysis of the infrared pictures of the earth obtained from the Nimbus-1 and Kosmos-122 satellites, illustrated (when it is possible) by example of the use of data on radiation temperature contrasts.

1. Evaluation of the Possible Deviations of Radiation Temperature Contrasts from the Mean Values

The probable values of the radiation contrast of clouds against the background of the underlying surface presented by us in a series of works, were calculated using the initial data, representing the mean long range values. In this case we used the mean long range values of both the content of atmospheric components absorbing radiation and distribution of air temperature with altitude, as well as the temperatures of the underlying surface, and also the temperatures and altitudes of the clouds of various levels.

The deviations of the content of the absorbing components of the atmosphere and the stratification of air temperature in each specific case, from the mean values used in the work, will practically have no substantial influence on the values of the calculated contrast, since they have practically no influence whatever on the flows of the outgoing radiation in a cloudless atmosphere and in the presence of clouds. Moreover, the principal contribution to the over-all flow of outgoing radiation in the region of the transparency windows of the atmosphere is made by the radiating surface (the earth or the cloud) [4, 7]. Therefore the principal deviations of the radiation contrasts from their mean values may originate due to the corresponding deviations of the true temperatures of the radiating surfaces. The calculated values of probabilities of such deviations are represented in Figure 1.

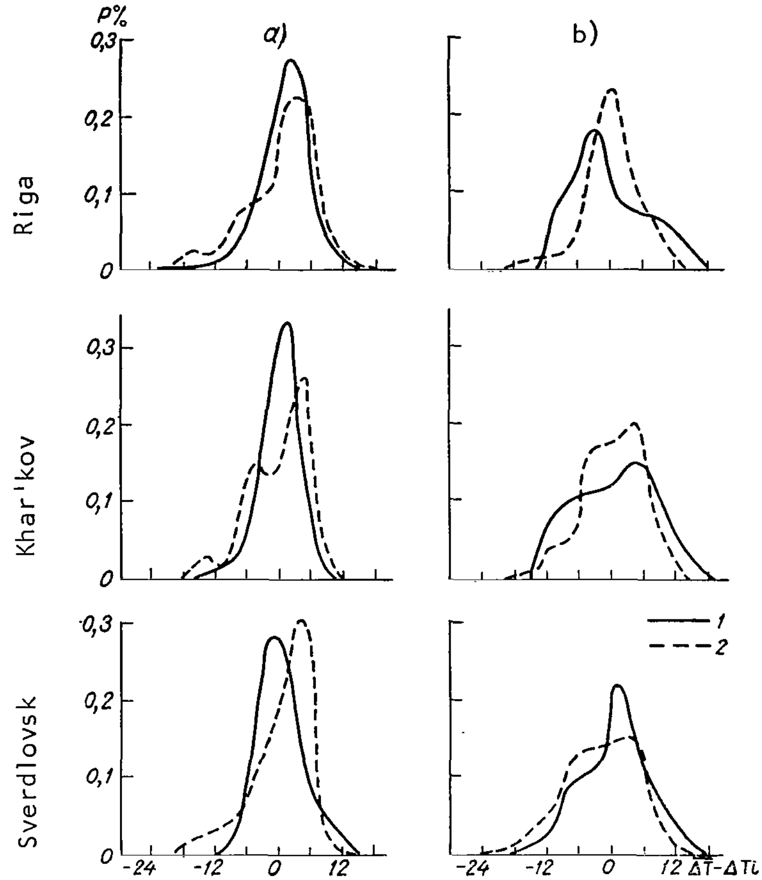

Figure 1. Probability of Distribution of Deviations Between the Values of the Radiation Temperature Contrasts of the Cloudiness Against the Background of the Underlying Surface from the Mean Long-Term Values in Winter (1) and Summer (2). a, Lower Level Cloudiness; b, Middle Layer Cloudiness.

In the clouds of the lower level, as we can see from the curves, the maximum of probability of deviations of the temperature contrast from the mean $\overline{\Delta T}-\Delta T_i$ is expressed more sharply than with clouds of the lower level. During the winter season the clouds of the lower level have insignificant deviations of the values of radiation contrast from the mean values. In general the values of deviations with an approximately 30% probability are included in the 0, -3°C range. In the summer season with an about 50% probability the deviation values are included in the 0, -6° range.

The probability curve of the deviation from the mean value for the clouds of the middle level has a smoother shape. With a probability of about 70% we observe the values of deviations in the range between +6, -6°, practically independently of the season.

The guaranteed value of the mean long-term contrast values for the upper level cloudiness was not calculated because of the small number of observations.

To characterize the values of contrast deviations of the radiation temperatures in each specific case from the average values, and also to characterize the differences of the specific contrast from one another, we give the values of the root mean square deviations of contrast between temperatures of /69 the terrestrial surface and the upper boundary of the cloudiness for certain regions of the USSR (Table 1).

TABLE 1. VALUES OF THE ROOT MEAN SQUARE DEVIATIONS δ OF THE TEMPERATURE CONTRASTS OF CLOUDINESS AND TERRESTRIAL SURFACE FOR EACH MONTH DURING DAYLIGHT (FIRST LINE) AND NIGHTTIME (SECOND LINE).

Point	I	II	III	IV	V	VI	VII	VIII	IX	X	XI	XII
						Lower Level						
Minsk	4,44 4,75	4,61 5,38	6,07 6,16	6,71 6,32	7,81 6,86	8,43 5,48	10,39 3,60	8,62 5,26	5,83 5,29	4,90 3,87	4,36 6,40	5,30 5,66
Sverdlovsk	3,61 4,26	5,8 4,6	4,7 4,0	6,65 4,2	8,8 5,4	10,0 5,17	8,94 7,74	5,9 4,6	4,8 3,7	5,0 3,2	4,4 4,3	3,7 3,7
Aktyubinsk	7,09 4,72	3,71 3,72	3,7 5,9	— 6,79	— 3,96	— —	— 9,2	— 8,5	8,64 5,27	6,4 5,23	3,72 10,8	3,64 4,76
Khar'kov	4,4 3,42	4,74 4,13	5,51 4,1	8,49 4,36	11,7 5,75	12,8 7,52	7,75 4,46	13,3 5,09	7,6 4,41	6,7 4,39	4,44 3,08	4,40 3,68
Volgograd	4,01 4,19	4,2 3,4	4,7 5,4	8,25 5,3	— —	— —	— —	— —	— —	6,27 5,8	4,17 4,3	3,12 4,8
						Middle Level						
Minsk	— —	5,6 7,14	— 5,29	9,18 6,78	6,48 3,74	6,48 5,06	6,16 6,02	8,12 5,5	5,20 5,81	6,56 6,00	5,66 6,08	6,78 5,74
Sverdlovsk	6,72 7,2	5,9 6,08	7,26 6,31	6,9 6,06	8,98 6,21	11,1 7,08	9,74 6,64	6,38 7,85	6,2 5,48	5,9 6,08	7,25 6,78	6,98 5,5
Aktyubinsk	6,5 7,8	— 5,9	5,6 10,06	— —	— 5,01	5,6 5,6	— 4,5	— 4,4	— 4,3	6,9 6,2	— 6,9	7,1 6,5
Khar'kov	6,7 7,02	6,0 6,2	10,4 5,91	9,45 5,92	10,7 6,76	11,2 5,75	13,7 5,7	11,6 6,02	10,4 6,19	6,67 6,46	7,4 7,32	6,87 8,15
Volgograd	6,2 6,6	7,9 6,2	8,5 6,4	7,7 5,7	8,5 5,5	13,8 5,5	— 7,9	— 5,3	6,5 6,6	8,0 5,2	6,9 6,8	9,9 10,04

Tr. Note: Commas indicate decimal points

$$\sigma = \sqrt{\frac{(\overline{\Delta T} - \Delta T_i)^2}{n}}, \tag{1}$$

where $\overline{\Delta T}$ is the mean monthly value of the contrast $(t^\circ_e - t^\circ_{cl})$, ΔT_i is the difference between t_e and t_{cl} in each specific case.

The σ values both for the day and for the night in the annual variations have the maximum values in the summertime, the minimum in winter. The annual variations of σ during the day is expressed better than at night. In this case during the wintertime the greater values of σ are observed during the nighttime. Thus, the mean long-term radiation contrast values may be used for interpretation of the infrared measurements from satellites, since the most probable values of deviations in each specific case are included within the $\pm 3^\circ$ range. Only for the cloudiness of the middle layer do we observe a somewhat larger values of deviations, reaching $\pm 6^\circ$. Taking into account the errors of the modern weather satellite equipment, the contrasts, having deviations of $\pm 6^\circ$ from the average, may be used in the interpretation of the values measured.

2. Effect of Various Factors on the Values of Radiation Temperature Contrasts

a. *Degree of blackness of the underlying surface.* The study of the natural underlying surfaces of the earth, as it has been shown in a number of works [1, 2, 7, 8], differs from the study of the absolutely black body. In the calculation of the probable values of the contrasts, the radiation of the underlying surface was assumed by us to be the radiation of an absolutely black body. Therefore the question arises on the error resulting from this assumption. Possessing data on the spectral variations of the radiation coefficients of various types of natural surfaces, such as water, soil with a vegetation cover, desert [10], and using the solution of the transfer equation in the following form: /70

$$I^{\uparrow}_{\Delta\lambda} \approx P_{\Delta\lambda}(\omega) \left[\varepsilon_{\Delta\lambda} \int_{\lambda_1}^{\lambda_2} E_\lambda (T_e)\, d\lambda + (1 - \varepsilon_{\Delta\lambda}) I^{\downarrow}_{\Delta\lambda} + \sum_{i=1}^{n} \left\{ \int_{\lambda_1}^{\lambda_2} E_\lambda (\overline{T}_i)\, d\lambda \right\} \Delta_i P_{\Delta\lambda} \right., \tag{2}$$

where $\varepsilon_{\Delta\lambda}$ is the coefficient of radiation of the surface for the $\Delta\lambda$ wavelength range, $I^{\downarrow}_{\Delta\lambda}$ is the counter-radiation of the atmosphere at the level of the underlying surface, $P_{\Delta\lambda}$ is the function of transmission in the spectral region of $\Delta\lambda$, ω is the total water vapor content in the atmosphere layer, $E_\lambda(T)$ is the radiation of the absolutely black body with the T temperature, T_e is the temperature of the terrestrial surface, $\overline{T}_i$ is the mean temperature of the i-th layer of the atmosphere, $\Delta_i P_{\Delta\lambda} = P(\omega_{i-1}) - P(\omega_i)$.

We carried out calculations, as the result of which we obtained the values of the radiation temperature contrasts of the clouds against the background of the underlying surface with various radiating capacities thereof. The initial data required for the calculations were taken according to the model of the standard atmosphere ARDC-1959.

In Table 2 we present the values of the differences of the radiation temperatures at the level of the upper boundary of the atmosphere for an absolutely black surface, taking into account the actual spectral variations of the radiating capacities for certain types of natural surfaces. These differences Δt characterize the errors of determination of the contrast of clouds against the background of the terrestrial surface, arising when we do not take into account the radiating properties of the natural surfaces.

TABLE 2. ERRORS Δt OF THE VALUES OF RADIATION TEMPERATURE CONTRAST OF CLOUDS AGAINST THE BACKGROUND OF THE TERRESTRIAL SURFACE THROUGH FAILURE TO ALLOW FOR THE RADIATING PROPERTIES OF THE NATURAL SURFACES.

Spectral Range, μ		Type of Surface				
		1	2	3	4	5
3,5—4,0	$I^{\uparrow}_{\Delta\lambda}$ $\frac{\text{microwatt}}{\text{cm}^2\ \text{ster}}$	12,6	12,6	10,4	13,4	13,7
	t°_{rad}	12,0	12,0	8,5	13,5	14,0
	Δt°	2,0	2,0	5,5	0,5	
4,5—5,0	$I^{\uparrow}_{\Delta\lambda}$ $\frac{\text{microwatt}}{\text{cm}^2\ \text{ster}}$	55,1	58,3	55,8	60,7	61,5
	t°_{rad}	8,5	10,5	9,0	11,0	11,5
	Δt°	3,0	1,0	2,5	0,5	
8,0—13,0	$I^{\uparrow}_{\Delta t}$ $\frac{\text{microwatt}}{\text{cm}^2\ \text{ster}}$	3440,9	3371,5	3151,6	3489,1	3555,0
	t°_{rad}	8,0	6,5	3,0	8,5	9,5
	Δt°	1,5	3,0	6,5	1,0	

Remarks: Designated in the Table: 1, Soil with Vegetation Cover; 2, Desert; 3, Sloping Sandy Shore; 4, Water; 5, Absolutely Black Body.

Tr. Note: Commas indicate decimal points.

As we can see from Table 2, such natural surfaces as soil with a vegetation cover, desert and water in comparison with the absolutely black body yield a radiation temperature which as a rule is 0.5-3°C too low. A more substantial error is obtained for the sloping sandy shore (up to 6.5° in the 8.1-13.0 μ /71 region). Accordingly the values of the contrasts of radiation temperatures of clouds of the lower level and the clouds of the vertical development, the radiations of which were assumed to be absolutely black, upon allowance for the radiating properties of the underlying surface will be decreased by the values of the errors presented in Table 2.

For clouds, possessing a specific degree of IR-radiation transmission (middle and upper level) differences in the contrast values will be substantially less.

Thus, the relatively small values of the errors (0.5-3.0°) for such surfaces as desert, soil with vegetable cover and water, make it possible for the interpretation of the IR-data from satellites to use the precalculated probable values of contrasts of clouds against the background of an absolutely black underlying surface. This is all the more substantiated, because the values of the errors lie within the bounds of the accuracy of measurements corresponding to the present satellite infrared equipment [9].

b. *Amount of cloudiness*. Let us go on to the examination of the effect of the amount of cloudiness on the values of radiation contrast of the clouds against the background of the terrestrial surface.

In detecting cloudiness at night time from the satellite according to the outgoing radiation data in a number of cases we can actually observe not the solid cloud massifs but regions with partial cloudiness. In this connection the process of interpretation of measurement data is rendered more complicated. Moreover, the measuring equipment of the satellite possesses a certain three-dimensional resolution. Therefore it is practically impossible to detect partial cloudiness when the dimensions of the nuclei are smaller than the resolution of the equipment. However, partial cloudiness affects the readings of the radiometers, reducing the radiation temperature of the earth's surface. Let us give the calculated values of the intensity of outgoing radiation in the atmosphere's transparency window with clouds of various levels, different degree of cloudiness, and also the corresponding values of the radiation temperature contrast of the clouds against the background of the underlying surface. (Table 3).

As we can see from Table 3, the radiation temperature contrast (according to the absolute value) decreases substantially with the decrease of the amount of cloudiness in the area of the radiometer's field of vision. Moreover, the different amount of clouds of various levels provides conditions for an outgoing radiation intensity similar with respect to value. Thus, for example, in the region of Leningrad in July, 7 points of cloudiness of the lower level create the same radiation intensity as 4 points of the middle level and 6 points of the upper level.

Similar relationships are noted also in the radiation temperature contrast values of the clouds against the terrestrial surface background. In connection with this the interpretation of data of outgoing radiation measurements in the presence of clouds with breaks without employment of additional information may prove erroneous. As additional materials in the interpretation we may use, for example, the values of the probability of distribution of amounts of cloudiness above the given territory.

TABLE 3. EFFECT OF THE AMOUNT OF CLOUDINESS ON THE VALUE OF THE OUTGOING RADIATION FLOWS I AND CONTRAST OF RADIATION TEMPERATURES ΔT OF THE CLOUDINESS AGAINST THE BACKGROUND OF THE UNDERLYING SURFACE. (8.0-13.0 μ)

	Cloudiness Points	Leningrad			Ashkhabad			Yakutsk		
		Lower	Middle	Upper	Lower	Middle	Upper	Lower	Middle	Upper
January										
I microwatt/cm^2 ster	10	2280	2060	2170	2620	2410	2760	1650	1330	—
	8	2310	2134	2222	2664	2496	2776	1544	1288	—
	6	2340	2208	2274	2708	2582	2792	1438	1246	—
	4	2370	2282	2326	2752	2668	2808	1332	1204	—
	2	2400	2356	2378	2796	2754	2824	1226	1162	—
	0	2430	2430	2430	2840	2840	2840	1120	1120	—
ΔT°	10	3,0	8,0	6,5	3,7	8,0	4,2	—16,0	—9,7	—
	8	2,5	6,5	4,5	2,2	5,2	2,5	—16,0	—9,0	—
	6	2,0	4,5	4,2	1,2	3,7	1,0	—13,0	—7,5	—
	4	1,5	3,0	2,0	0,7	1,7	1,0	—9,8	—6,0	—
	2	0,5	1,5	1,0	0,2	0,7	0,5	—6,5	—4,5	—
July										
I microwatt/cm^2 ster	10	2950	2850	3050	3540	3490	—	3060	2940	3070
	8	3048	2968	3128	3666	3626	—	3144	3048	3152
	6	3146	3086	3206	3792	3762	—	3228	3156	3234
	4	3244	3204	3284	3918	3898	—	3312	3264	3316
	2	3342	3322	3362	4044	4034	—	3396	3372	3392
	0	3440	3440		4170	4170	—	3480	3480	3480
ΔT°	10	7,0	9,5	6,0	9,5	10,5	—	7,0	9,3	7,0
	8	5,5	7,0	3,8	7,5	6,0	—	7,0	8,0	6,0
	6	3,5	4,5	2,3	5,5	4,0	—	4,0	5,5	4,5
	4	1,7	2,5	1,0	3,0	2,0	—	3,0	4,0	3,0
	2	0	0,5	0,2	1,0	0,0	—	1,5	2,0	2,0

Tr. Note: Commas indicate decimal points.

c. *Sighting angle*. Let us now examine the dependence of the infrared radiation fluxes in the atmospheric transparency windows and the corresponding /72 radiation contrast of clouds against the background of the underlying surface on the sighting angle. The angular dependence of the values of outgoing radiation for various sectors of the spectrum and for various models of the atmosphere was calculated by many authors [7]. In this connection it is interesting to evaluate the influence of deviation of sighting from the normal on the calculated probable values of radiation contrast of clouds against the background of the terrestrial surface, since for detection of cloudiness from the satellite infrared narrow angle scanning equipment is used (with a specific scanning angle). As the result of scanning the image of the earth at the edges of the infrared frame is obtained at a certain angle to the radiating surface.

We have calculated the intensity of the outgoing radiation with a cloudless atmosphere and clouds of various levels in the transparency windows of the atmospheres at various sighting angles (0, 10, 30, 45, 60, 82°). The maximum angle of the deviation of the sighting from the nadir (0°) is selected within the bounds of visibility of the earth from the 5 milibar level (the upper level in the calculations). We have adopted the spherical symmetry of the vertical distributions of temperature and air pressure, and also of the absorbing components in the atmosphere. The spectral coefficients of the degree of blackness of the clouds of the middle and the upper layer were assumed to be independent of the angle.

In Figure 2 we present the dependence of the outgoing radiation intensity at the level of the upper boundary of the atmosphere under different angles I_θ with respect to the intensity at normal sighting $I_{\theta=0}$ for two transparency windows. /73

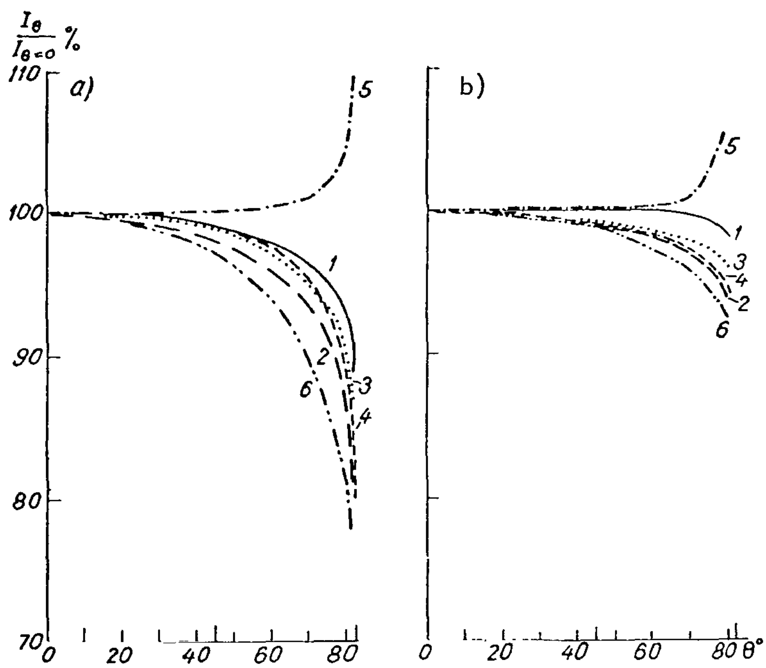

Figure 2. Relative Angular Distribution of the Intensity of Outgoing Radiation in the Atmospheric Transparency Windows of 8.0-13.0 μ (a) and 3.5-4.0 μ (b). 1, Leningrad, January; 2, Leningrad, July; 3, Ashkhabad, January; 4, Ashkhabad, July; 5, Yakutsk, January; 6, Kiev, July.

The principal family of curves, characterizing certain regions of the territory of the USSR, detects a decrease of the values of the intensity with the increase of the angle of sighting, i.e., it illustrates the effect of the "darkening" nearer to the edge of the earth. The curve for the Yakutsk region during the winter period has a reverse course, i.e., it characterized the "lightening" at the edge of the earth.

With the increase of the sighting angle the optical pass of the ray increases, i.e., the mass of the absorbing gas increases, as the result of which the contribution of the terrestrial surface towards the outgoing radiation decreases and the contribution of the atmosphere relatively increases. Since usually the air temperature in the troposphere drops with altitude, the absolute value of the atmospheric radiation decreases with the increase of the sighting angle.

The resulting intensity of the outgoing radiation, as a rule, also decreases. But in the presence of sufficiently powerful temperature inversions in the atmosphere (as it takes place in Yakutsk in the winter) with appreciable sighting angles the radiation of the atmosphere increases sharply against the background of the decrease of the terrestrial surface radiation, which results in an increase of the resulting intensity of the outgoing radiation, i.e., we observe the effect of "lightening" nearer to the edge of the earth.

The dependence of the outgoing radiation on the sighting angle in the 3.5-4.0 μ region is substantially smaller than in the 8.0-13.0 μ region.

In Figure 3 we present the angular dependence of the radiation temperature contrast values of the clouds of the lower level. We observe a considerable decrease of the contrast (up to 7°) or the increase during the inversion up to 6° upon the increase of the angle from 0° to 82° in the 8.0-13.0 μ window. /74

In all the cases the calculations exhibit a smaller angular dependence in the winter time and a somewhat greater in the summer.

In the contrast values in comparison with the radiation intensities it is still more noticeable, that the angular dependence in the 3.5-4.0 μ range is substantially smaller than in the 8.0-13.0 μ range.

Thus, the 3.5-4.0 μ transparency window from the point of view examined is more advantageous when scanning equipment is used for detecting cloudiness during nighttime.

The results of the calculations show that in interpreting IR-data of meteorological satellites, especially in the 8.0-13.0 μ region, we should take into account the angular dependence of temperature contrasts for sighting angles greater than 60-65°.

Thus, for infrared scanning equipment, installed on Soviet weather satellites, where the maximum angle of deviation from the nadir amounts to 45°, the maximum errors in the contrast values resulting from the angle of sighting are within the bounds of +1 to -2°. At the same time for the satellite actinometric equipment, in which the working scanning angle amounts to about 78°, the errors at the edges of the scanning region attain +4, -6°. Therefore, the absolute values of the intensities (or radiation temperatures) with scanning angles greater than 60°, will be substantially distorted and in the interpretation should be examined with an allowance for the corresponding corrections.

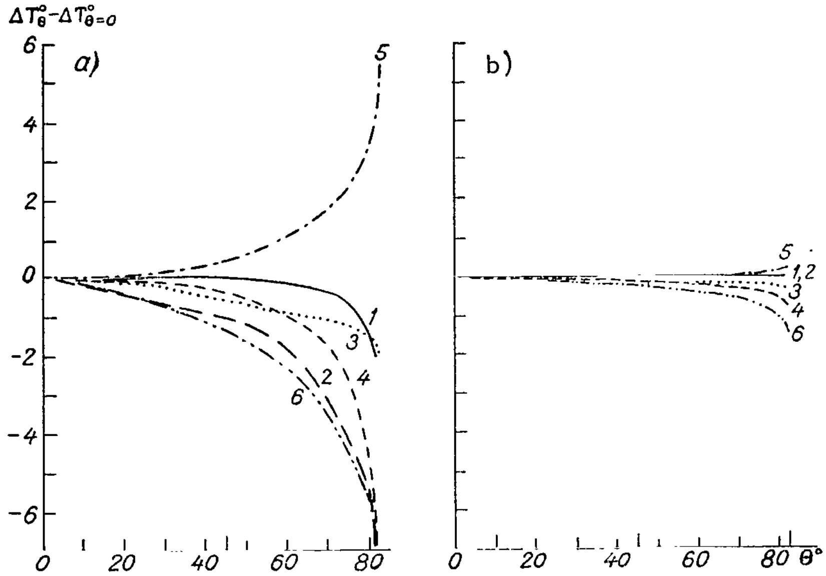

Figure 3. Angular Dependence of the Radiation Temperature Contrast of the Cloudiness of the Lower Level Against the Background of the Underlying Surface in 8.0-13.0 μ Atmospheric Transparency Windows (a) and 3.5-4.0 μ Windows (b). The Symbols are the same as in Figure 2.

d. *Spectral Characteristics of the Measuring Equipment.* The infrared scanning equipment enables us to carry out measurements of the outgoing radiation in specific sectors of the spectrum, which is attained by the use of filters and bolometers with the required limits of transmission and spectral sensitivity. In connection with the fact that the values of the spectral transmission of the τ_λ system filter-bolometer within the bounds of the spectral sensitivity depends substantially on the wavelength, the spectral composition of the radiation reaching the instrument undergoes substantial changes in it. As the result of this, the values of the integral intensities of the outgoing radiation, obtained according to the measurements from the weather satellites, will differ from the actually observed or calculated ones for the upper boundary of the atmosphere. The possible effects of the spectral characteristics of the equipment on the measurement results shall be evaluated with an /75 example of two specific variations of instruments, installed on Soviet weather satellites.

The spectral transmission of one of the instruments encompasses a spectrum range of 7.0-12.0 μ. The transmission curves of the system is characterized by the maximum transmission of 60% at the wavelength of about 10.0 μ. The calculations performed (Table 4) indicate that the filter-bolometer system decreases approximately by two times the value of the intensity of radiation I, arriving at the input of the instrument. With negative temperatures of the radiating surface the equipment underestimates the effective temperatures by 0.5-1.3°, whereas with positive temperatures it overestimates the temperatures by 1.0° on the average.

For another instrument the transmission of radiation in the 8.0-13.0 μ with a maximum of about 8.7 μ is characteristic. The spectral characteristics of the filter-bolometer system change the effective temperature by 0.5-0.7°.

TABLE 4. EFFECT OF THE SPECTRAL TRANSMISSION τ_λ OF THE FILTER-BOLOMETER SYSTEM ON THE VALUE OF THE TEMPERATURES MEASURED BY THE RADIATION METHOD.

Point	Months	Cloudiness	I	$\sum_{i=1}^{n} I_\lambda \tau_\lambda = I_\tau$	t°_{rad}	t°_τ	t°_{true}	t°_{8-13}
System I. Spectral Sensitivity (7-12 μ)								
Leningrad	I	Clear	2177	854	—12,0	—12,5	—7,7	—10,5
		Lower	2047	800	—15,8	—15,0	—11,3	—13,5
		Middle	1884	716	—18,7	—20,0	—23,1	—18,5
Yakutsk	I	Clear	1044	380	—42,2	—43,0	—44,7	—44,5
		Lower	1484	564	—29,0	—29,0	—26,9	—28,5
		Middle	1209	453	—36,5	—37,0	—32,0	—37,8
Ashkhabad	VII	Clear	3807	1534	15,0	16,0	23,4	19,0
System II. Spectral Sensitivity (8-13 μ)								
Leningrad	I	Clear	2432	1485	—10,5	11,0	—7,7	—10,5
		Middle	2056	1251	—18,5	—19,0	—23,1	—18,5

Tr. Note: Commas indicate decimal points

Since the sensitivity of both the first instrument and the second one are substantially lower than the above mentioned errors resulting from the spectral characteristics of the system, in actual practice they may be disregarded. However, with different comparison of the calculation data with the results of measurements by means of the corresponding satellite equipment we should coordinate with sufficient accuracy the spectral ranges of both ones and the others. In the opposite case errors may originate which are substantial for certain problems. Thus, if the measurement results by means of the first instrument (Table 4, range 7.0-12.0 μ) are compared with the data of calculations in the 8.0-13.0 μ range, the errors originating in the effective temperature range 3.0° to 3.5°. /76

In Table 4 we have used the following symbols:

I is the intensity of the outgoing radiation (microwatts/cm^2ster.) in the 7-12 μ and 8-13 μ range;

t°_{rad} is the radiation temperature in the upper boundary of the atmosphere corresponding to the intensity of the outgoing radiation;

t°_τ is the radiation temperature taking into account the spectral transmission of the filter-bolometer system;

t°_{8-13} is the radiation temperature at the upper boundary of the atmosphere in the 8-13 μ range;

t°_{true} the actual temperature of the radiating surface.

3. Corrections to the Temperature of the Underlying Surface and Clouds, Measured by the Radiation Method

In determining the temperature of the radiating surface from satellites a substantial role is played by allowance for the errors, introduced by the transformation of radiation in the atmosphere. The evaluations of such errors, caused by the absorption of radiation, are given in work [6] for the underlying surface and the upper boundary of the clouds of the lower level, the radiation of which was considered to be absolutely black. The values of the errors are determined as the averages for the day and the night. The evaluation of the error in determination of the temperature by the radiation method for clouds, which possess a certain radiation transmission is certainly interesting. We have performed the calculations of the flows of outgoing radiation and radiation temperatures at the level of the upper boundary of the atmosphere at nighttime for certain regions of the USSR and found the required errors. The results are given in Figures 4-5 (recurrence curves) and in Table 5.

The smallest errors in determination of the temperatures of the underlying surfaces and lower level cloudiness occur in the 3.5-4.0 μ transparency window: in 50-60% of the cases we note an error within the limits of 0-1.5°. At the same time in the 8.0-13.0 μ region the most probable error amounts to 3-4° at night. /79

For the middle level cloudiness, which has a certain transmission, the most probable errors in determination of the temperature in the 3.5-4.0 μ transparency window reach 8° in the 4.5-5.0 μ window they amount to -6°, and in the 8.0-13.0 window they decrease to -3, -4°. In this way in the 8.0-13.0 μ transparency window the errors will be the smallest, which is caused by the non-blackness of the "transparent" clouds in the determination of their temperature by the radiation method.

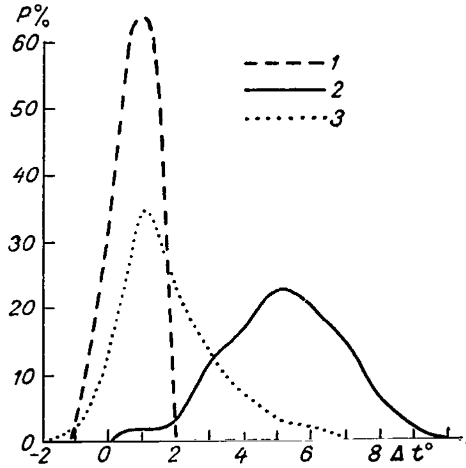

Figure 4. Probability of Distribution of Errors in Determination of the Temperature of Underlying Surface by the Radiation Method at Night Under a Cloudless Sky in Various Atmospheric Transparency Windows. 1, 3.5-4.0 μ ; 2, 8.0-13.0 μ ; 4.5--5.0 μ

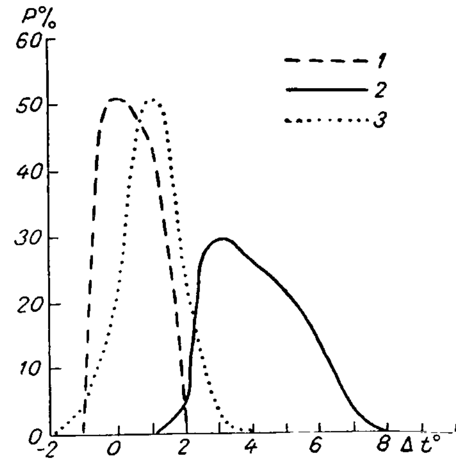

Figure 5. Probability of Distribution of Errors in Determining the Temperature of the Upper Boundary of the Lower Level Cloudiness by the Radiation Method at Night. The Symbols are the same as in Figure 4.

TABLE 5. CORRECTIONS Δt TO THE TEMPERATURE OF THE RADIATING SURFACE, DETERMINED BY THE RADIATION METHOD FROM WEATHER SATELLITES. (The first line for 3.5-4.0 μ, second line for 4.5-5.0 μ, third line for 8.0-13.0 μ).

Point	ΔT° Jan.	Apr.	July	Oct.	Point	ΔT° Jan.	Apr.	July	Oct.
Underlying Surface									
Alma Ata	0,1 0,6 2,8	0,7 1,7 6,2	1,3 4,0 7,0	0,4 0,9 5,4	Irkutsk	1,4 0,8 3,2	0,2 2,0 5,7	1,1 3,1 5,6	0,2 0,9 5,7
Ashkhabad	0,0 0,5 3,8	1,0 2,6 5,1	1,4 3,9 6,4	0,7 1,7 3,7	Kiev	0,6 1,6 5,6	0,7 1,2 6,2	1,2 4,2 8,7	1,2 1,7 6,9
Volgograd	0,6 1,6 2,9	0,8 1,5 5,0	1,4 4,8 7,4	1,2 2,0 4,9	Kuybyshev	0,6 1,1 4,6	0,2 0,5 4,7	1,2 3,9 8,4	0,4 1,4 6,4

Tr. Note: Commas indicate decimal points.

TABLE 5 (Continued)

Point	ΔT° Jan.	Apr.	July	Oct.
Leningrad	0,8	0,3	1,4	1,0
	2,3	0,8	3,9	1,5
	3,8	3,8	7,4	5,0
Novosibirsk	0,5	0,1	0,9	0,1
	0,5	0,1	1,7	0,1
	0,8	2,6	4,7	4,4
Odessa	0,2	0,9	1,0	1,1
	1,4	0,6	3,9	1,4
	4,2	4,6	6,5	3,9
Omsk	0,5	0,2	1,0	0,3
	1,0	0,2	3,0	0,8
	2,0	3,2	6,5	4,8
Riga	0,7	0,6	1,3	1,2
	1,4	1,1	3,6	1,9
	3,4	1,2	8,3	4,9
Sverdlovsk	0,7	0,4	1,7	0,3
	1,2	0,4	3,6	0,8
	4,7	4,9	7,7	5,6
Tbilisi	0,1	1,3	1,3	1,3
	0,6	2,8	4,8	2,3
	6,1	7,3	6,8	5,5
Khar'kov	0,1	0,6	1,1	0,7
	—2,4	0,8	4,3	1,4
	1,8	5,4	7,4	4,9
Khabarovsk	0,6	0,8	1,2	0,9
	1,8	1,3	4,2	1,3
	3,6	4,5	7,8	4,1
Yakutsk	0,3	—1,2	1,1	0,3
	1,2	0,4	3,1	1,3
	2,8	3,4	6,6	7,3

Lower Level Cloudiness

Point	ΔT° Jan.	Apr.	July	Oct.
Alma Ata	0,5	0,3	0,5	0,4
	1,5	0,6	0,8	0,9
	3,8	4,8	3,5	4,9
Ashkhabad	0,5	0,3	1,4	0,0
	0,5	0,1	2,4	0,0
	3,0	4,3	4,9	3,0
Volgograd	0,7	0,3	0,7	0,4
	1,2	0,6	1,0	0,2
	3,2	4,0	3,2	3,7
Irkutsk	1,5	0,2	1,4	0,0
	1,5	1,0	1,4	0,8
	4,2	5,2	6,9	4,8
Kiev	0,6	0,8	1,0	0,2
	1,4	0,8	1,8	0,7
	5,1	5,1	6,0	5,2
Kuybyshev	0,5	0,1	0,8	0,3
	0,5	1,1	1,0	0,8
	5,0	4,6	4,3	5,6
Leningrad	0,2	1,0	0,4	0,7
	1,4	1,0	4,1	1,2
	3,2	3,0	2,9	3,2
Novosibirsk	0,4	0,3	1,2	0,9
	1,2	0,3	1,7	0,9
	1,9	2,8	4,2	3,0
Odessa	0,6	0,1	1,1	0,6
	1,1	0,1	2,1	0,6
	3,2	3,6	4,1	2,9
Omsk	1,1	0,5	0,8	0,3
	1,1	1,0	1,3	0,8
	3.1	3,0	4,8	2,8
Riga	0,6	0,4	1,4	0,1
	1,6	1,0	2,2	0,4
	3,3	3,2	6,4	3,9
Sverdlovsk	0,5	0,3	1,4	0,7
	1,5	1,1	2,2	1,0
	5,5	4,1	6,2	5,0
Tbilisi	1,0	0,3	1,0	0,2
	1,3	1,0	1,5	0,2
	5,5	6,0	2,5	4,4
Khar'kov	0,9	0,0	1,0	0,4
	0,4	1,0	2,5	0,9
	2,4	4,0	5,5	3,9
Khabarovsk	1,1	0,1	1,2	0,3
	2,1	0,4	2,2	0,5
	4,1	3,4	4,9	3,3
Yakutsk	0,6	0,2	0,8	0,2
	1,6	0,7	1,0	1,2
	4,6	3,7	5,5	7,2

Middle Level Cloudiness

Point	ΔT° Jan.	Apr.	July	Oct.
Alma Ata	—5,1	—7,7	—12,5	—10,3
	—5,1	—7,2	—11,2	—8,3
	—3,1	—2,9	—8,7	—5,3
Ashkhabad	—5,0	—10,4	—8,1	—9,1
	—5,0	—9,4	—6,1	—8,6
	—3,2	—5,4	—3,6	—5,1

Tr. Note: Commas indicate decimal points.

TABLE 5 (Concluded)

Point	Δt° Jan.	Δt° Apr.	Δt° July	Δt° Oct.
Volgograd	—3,5	—5,8	—11,1	—9,4
	—2,2	—5,1	—9,8	—9,4
	—0,8	—2,6	—6,5	—7,4
Irkutsk	—0,7	—13,2	—7,7	—7,6
	0,0	—11,2	—7,0	—6,1
	2,3	—7,2	—1,5	—2,6
Kiev	—4,7	—6,8	—7,2	—8,5
	—4,2	—5,8	—6,2	—7,0
	—0,7	—1,8	—7,2	—3,0
Kuybyshev	—1,7	—7,5	—8,0	—5,5
	—1,2	—6,5	—7,2	—4,5
	1,8	—4,5	—2,2	—1,0
Leningrad	—6,6	—8,6	—9,7	—8,4
	—5,1	—7,1	—8,7	—6,4
	—3,6	—5,6	—5,2	—5,4
Novosibirsk	—1,3	—7,5	—9,7	—8,3
	—1,5	—6,5	—8,2	—6,3
	—1,8	—5,0	—5,2	—3,8
Odessa	—6,9	—7,5	—13,0	—6,5
	—5,2	—6,3	—10,3	—6,2
	—3,7	—4,0	—8,3	—4,5
Omsk	—0,4	—7,1	—8,6	—7,9
	0,5	—6,1	—8,1	—6,4
	1,0	—4,6	—3,3	—4,4
Riga	—8,3	—7,2	—8,7	—7,3
	—6,8	—6,9	—7,9	—6,1
	—5,1	—4,4	—2,7	—4,0
Sverdlovsk	—2,2	—7,2	—8,6	—6,7
	—3,2	—5,7	—8,1	—5,2
	0,6	—3,4	—2,6	—2,2
Tbilisi	—8,7	—10,1	—9,8	—11,7
	—7,2	—8,1	—8,1	—10,0
	—3,7	—3,9	—6,3	—6,2
Khar'kov	—1,9	—6,9	—6,3	—8,3
	—2,4	—5,4	—4,8	—6,6
	—0,4	—2,7	—2,0	—3,6
Khabarovsk	—5,1	—7,9	—11,7	—7,2
	—4,4	—6,9	—10,6	—6,0
	—2,6	—4,9	—5,4	—4,7
Yakutsk	5,0	—5,5	—7,5	—2,2
	4,5	—5,0	—7,0	—2,2
	8,8	—2,7	—2,2	3,5

Point	Δt° Jan.	Δt° Apr.	Δt° July	Δt° Oct.
Upper Level Cloudiness				
Alma Ata	—19,6	—24,6	—24,5	—26,5
	—18,6	—23,6	—22,3	—25,5
	—16,8	—18,6	—19,7	—21,0
Ashkhabad	—18,0			—29,1
	—18,0			—28,6
	—15,3			—25,4
Kuybyshev		—21,9		—23,1
		—20,4		—20,8
		—18,4		—17,1
Leningrad	—25,9	—26,0	—32,8	—20,6
	—24,2	—24,5	—30,3	—18,6
	—22,7	—23,0	—27,3	—16,6
Novosibirsk		—31,6	—46,6	—21,0
		—29,6	—45,1	—20,3
		—28,1	—41,9	—18,3
Riga	—26,6	—28,8	—29,7	—26,5
	—24,4	—27,1	—27,9	—24,8
	—22,8	—25,3	—22,9	—22,0
Sverdlovsk	—16,5	—24,4	—31,0	—25,5
	—15,5	—22,8	—29,5	—23,5
	—13,5	—20,6	—24,5	—20,5
Khar'kov	—20,0			
	—17,8			
	—16,5			
Yakutsk		—20,7	—32,4	
		—20,2	—30,9	
		—18,2	—25,4	

Tr. Note: Commas indicate decimal points in this table.

4. Analysis of the Infrared Images of the Earth Obtained from the Weather Satellites

Let us now turn to the analysis of infrared pictures of the underlying surface and clouds obtained from the Nimbus-1 and Kosmos-122 satellites. In Figure 6, we present an IR-image of the cloudiness obtained from the Nimbus-1 satellite on 15 September 1964 at about 3 hrs. Moscow Time (258th loop) [11].

The infrared image envelopes a band of the earth about 1.5 thousand km wide. The orbit of the satellite passes from the Arctic Ocean to the Barents Sea, the Kola Peninsula, Finland, center of Western Eurpoe and Italy (see Figure 6).

From the analysis of the ground synoptic maps we can see that the weather in the region, over which the 258th loop of the Nimbus-1 satellite passes was determined by the cycloptic state over the north of Europe, Scandinavia, and the European territory of USSR, whereas the southern part of the territory was under the influence of the western periphery of a powerful anticyclone, located over the south of the European territory of USSR. The pressure in the center of this anticyclone amounted to more than 1,030 mb.

On the IR-picture our attention is drawn to the vortex character of the cloudiness. Three such vortexes can be counted, we will call the regions of which they are located A, B, C.

The regions where the vortexes are located on the photograph, obtained from the satellite coincide almost completely with the centers of cyclones on the ground synoptic map for 3 hrs., 15 September 1964.

The vortex cloudiness of region A represents a classic picture of a low cyclone, moving swiftly from the southwest to the northeast. Therefore, the outlines of the vortex on the IR-picture reproduce very precisely the direction of the cold and warm front, connected with the cyclone located over Finland and also with the occlusion front.

The cloudiness in the center of this cyclone is not high, is stratified with the base height at 300-600 m, and with the departure from the center of the cyclone to the south, along the warm front, the height of the cloudiness increases, and middle level clouds appear: altocumulus, and altostratus with the base height of 1,000-1,500 m. In region A (see Figure 6) dark sectors appear against the background of a clear white cloudiness area. In the region of the cyclone examined shower type rains are observed.

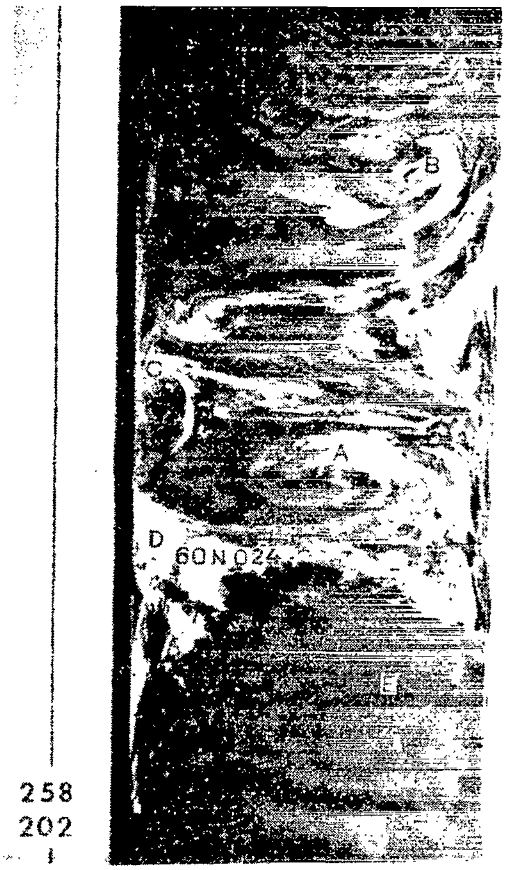

Figure 6a. Infrared Image of the Underlying Surface and Cloudiness Obtained from the Nimbus-1 Satellite on 15 September 1964 (Loop No. 258, 3 Hrs. Moscow Time).

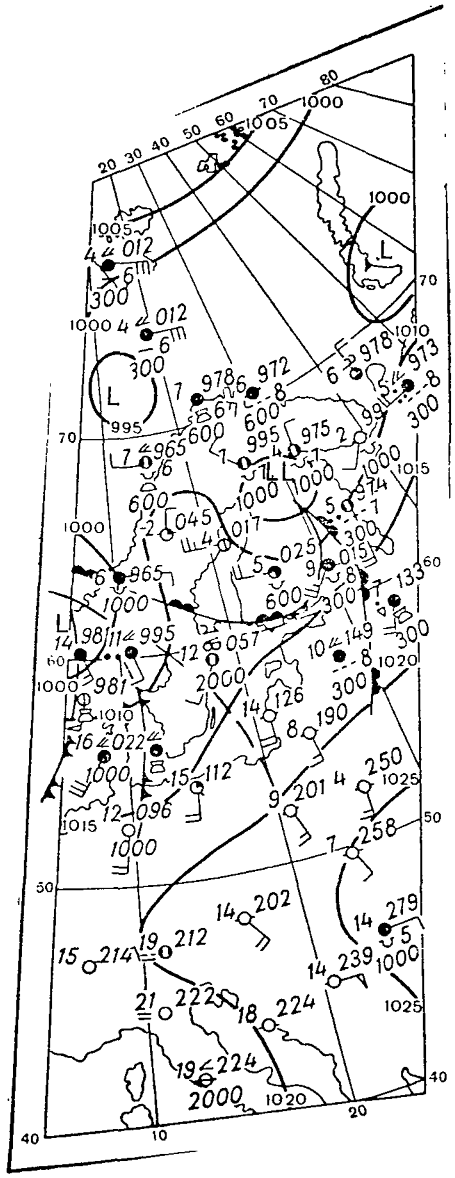

Figure 6b. The Synoptic Situation of the Region Under the Satellite.

The cloudiness region B is also connected with a distinctly expressed cyclonicity. The ground center of the cyclone is located in the Nar'yan-Mar region. This cyclone is high and not very mobile. The closed concentric isohypses are traced at all the altitude maps above Nar'yan-Mar, up to the 200 mb level.

Above the regions of the Arkhangel'skaya oblisk and Komi ASSR we observe /80
clouds of all three levels, since this is the transition zone between the two cyclones described (the Finnish cyclone which is the region of cloudiness A and the Nar'yan-Mar cyclone the region of cloudiness B). Here, we observe considerable breaks between the cloudiness, rain is marked by only a single station. Very large breaks in the clouds occur above the Barents Sea. Open water regions stand out well on the IR-picture by their darker tone.

On the picture we can also see well a part of the Gulf of Bothnia, not covered with clouds, and almost all of the Baltic Sea also.

The cloudiness region C is located over the northern part of Scandinavia and Barents Sea. Over the coast we observe lower level clouds of the cumulus forms with the base altitude of 600 m on the average. Above the sea, in addition to clouds of the lower level, we also note altocumulus clouds.

In addition to the three regions with the characteristic vortex cloudiness mentioned (A, B and C) in the left part of the picture there is a single large region with very dense cloudiness D. Caused by frontal divisions of the cyclone, located over the North Sea.

The field of vision of the IR-instrument included only a small part of /81
this cyclone and the clouds in region D are connected with the occlusion of the tropical front, the warm and cold branches of which in this region are erroded. The intensification of this front is probably caused by the radiation factors. The front is very well expressed on the ground synoptic map. In the frontal zone the meteorological stations mark shower type precipitation, thunderstorms, and solid cloudiness.

Along the front we observe middle level clouds (altostratus and altocumulus) with the base altitude of 1,000-1,500 m.

In the E region the weather is determined by the influence of the anticyclone and therefore the sky was cloudless over the entire Balkan Peninsula. On the map for 3 hrs. of the 15 September, a large number of stations noticed a haze. It is precisely because of this that in the region of E the terrestrial surface has a whitish tint.

The absence of clouds in E region is well supported by the radiation-balance measurement data. At Minsk station the value of the radiation balance was about 0.09 cal/cm^{2}min; at Riga station it was 0.10 cal/cm^{2}min; at Kovel station (west of Kiev) it is 0.07 cal/cm^{2}min; in the northern regions where cloudiness was observed, the radiation balance value decreased to 0.02 cal/cm^2 min at Umba station and 0.03 cal/cm^{2}min at Murmansk station.

In Figure 7a we present an IR-image of the terrestrial surface and the cloud cover, obtained on 15 September 1964 at 23 hrs. 49 min Moscow time. (Nimbus-1, 271st loop). On the north the boundary of the region included in the field of vision of the instrument passes at about 60°N, on the west from the Moscow region to the Black Sea coast of the Caucausus, along the 40°E to 10°N, and from the east from Omsk through the Kara Kums and to the Arabian Peninsula.

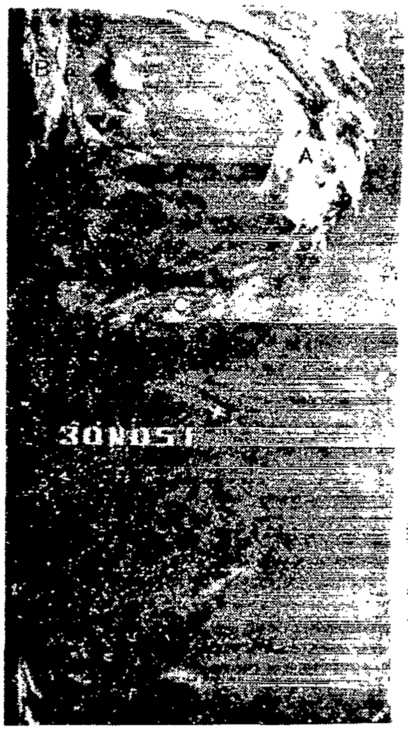

Figure 7a. Picture of the Underlying Surface in Cloudiness Obtained from the Nimbus-1 Satellite on 15 September 1964 (Loop No. 271, 23 Hrs. 49 Min. Moscow Time).

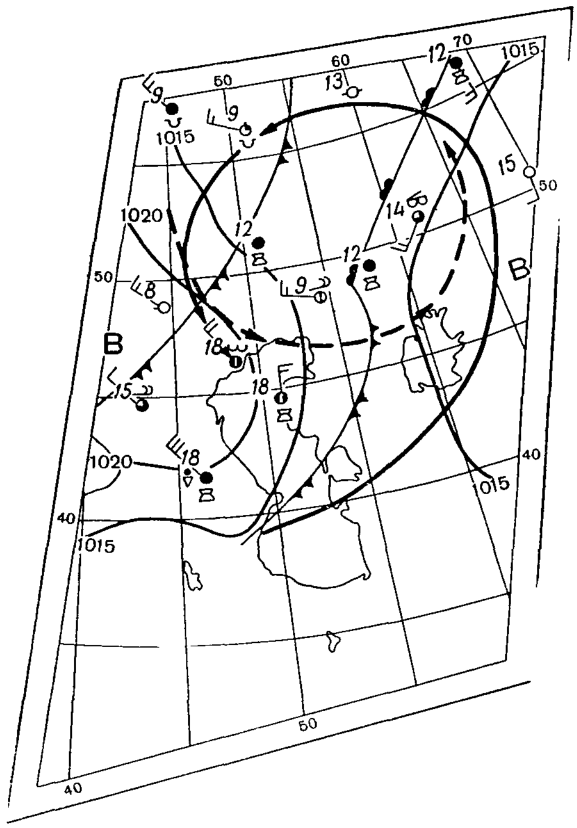

Figure 7b. Synoptic Situation of the Region Under the Satellite.

In the upper part of the IR-picture we can see a characteristic cloud vortex. In the remaining part of the picture we can trace a very uniform dark tone of the terrestrial surface. The cloudiness conditions are illustrated by both the ground synoptic map and the high altitude maps. On all the height pattern maps up to the map of the tropopause we can trace the cyclone, the center of which on the ground synoptic map is located in the Sverdlovsk region.

The brightest cloudiness region A presents the cloudiness of the cold front with waves caused by the cyclone near Sverdlovsk.

The center of the cyclone is delineated by a closed isobar of 1,010 mb. The clouds in this region are located only along the front, and we observe the /83 clouds of all the levels: stratocumulus with the base height of 600 m, middle level clouds (ridge type), and also cirrocumulus clouds.

The cloudiness in region B is caused by the influence of the vast cyclone occupying the entire northern and central parts of the European territory of USSR moving from the region of Finland and Leningrad oblasts. Over this region there is a strong northwestern wind.

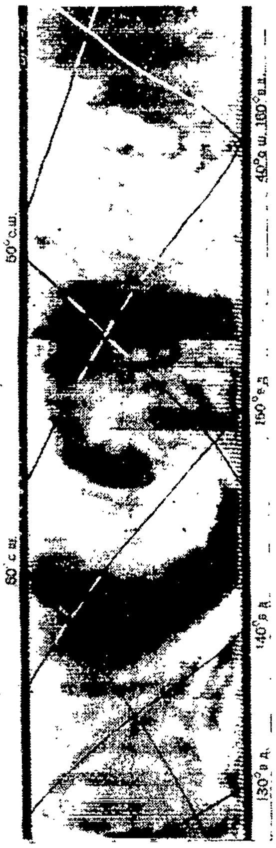

Figure 8a. Infrared Picture of the Cloudiness Obtained from the Kosmos-122 Satellite on 22 September 1966 (Loop No. 1,323, 15 Hrs. 03 Min. Moscow Time).

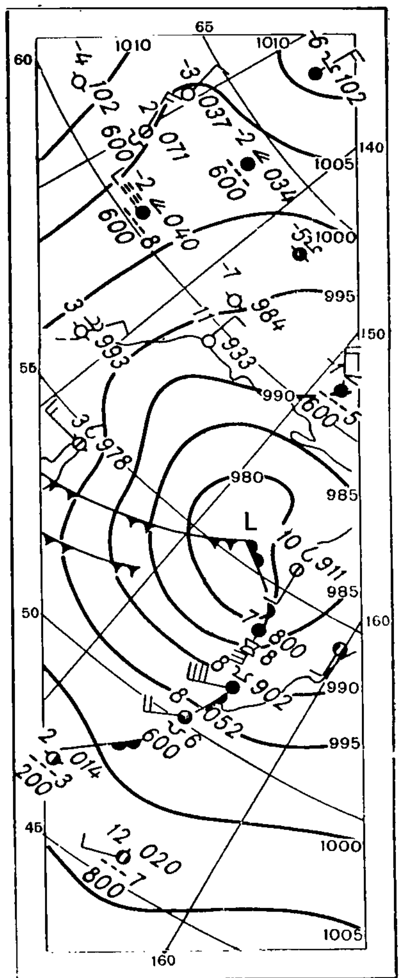

Figure 8b. Synoptic Situation in the Region Below the Satellite.

The synoptic analysis is supported well by the data of ground actinometric observations.

In Figure 8a we give the IR-image obtained from the meteorological satellite Kosmos-122 on 22 September 1966 at 15 hrs. 03 min. Moscow time, 1,323rd loop.

In the central part of the IR-image the cloudiness has a spirally form shape, the center of the vortex coinciding closely with the center of the high occluded cyclone, located on the ground weather map in the regions of the Sea of Okhotsk near Kamchatka (Figure 8b). /84

The right hand part of the vortex like cloudiness is oriented in the direction of the warm front, which on the ground map is plotted on the ground map according to the data of meteorological stations on the Kuril Islands. The photograph obtained from the satellite makes it possible to render more precise the position of the warm front above the ocean, where no meteorological observations have been made.

In Figure 9a we presented the infrared image of the territory of the earth along the trajectory of the Kosmos-122 satellite on 4 July 1966 at 12 hrs. 33 min., Moscow time (135th Loop) from the northern coast of Africa to Southern Urals and the measured field of radiation temperatures corresponding to the image. On the photographs we can see with sufficiently bright contrast the regions A and B in comparison with the main tone of the image. To these regions corresponded low radiation temperatures, which reach -32 and -35°C in region B.

Region C is characterized by a certain variegation of the image with a similar tone; to this region correspond the radiation temperature ranging from -5 to +20°C (Figure 9b).

In region D the outlines of the African coast stand out sharply by their darker tone, as do the islands of Crete and Cyprus in the Mediterranean Sea. To this region correspond the relatively constant radiation temperatures: 10-15° over the sea and 21-25° over the continent.

The synoptic situation (the map for 15 hrs) of the territory, represented on the IR-picture is characterized by the influence of a high stationary cyclone above the Caspian lowlands and the frontal zone connected with it (Figure 9c). The cloudiness in region A is connected with a warm front and in region B with a system of cold fronts of the same cyclone.

Possessing data on temperature and moisture of the air on the principal isobaric surfaces, taken from the synoptic map and the height pattern maps for individual regions of the territory to which the image pertains, we can calculate the radiation temperatures. The results of these calculations are given in Table 6.

Let us compare the results of calculations t_{rad} with the measurement by means of the satellite. The radiosonde data in the Kuybyshev regions indicate the presence of the middle level cloudiness, which can be also seen on the ground weather map. The mean radiation temperature, obtained according to the measurement data, amounts to -2°C. This coincides well with the calculated radiation temperatures equal to -1.5°C.

The solid lower cloudiness over the Black Sea has radiation temperatures ranging from -12.0 to -19.0°C the calculated temperature here is -17°C. Which also indicates the good coincidence of the results of calculations and satellite measurements.

Figure 9a. Infrared Image of the Underlying Surface and Cloudiness Obtained from the Kosmos-122 Satellite on 4 July 1966 (Loop No. 135, 12 Hrs., 33 Min. Moscow Time).

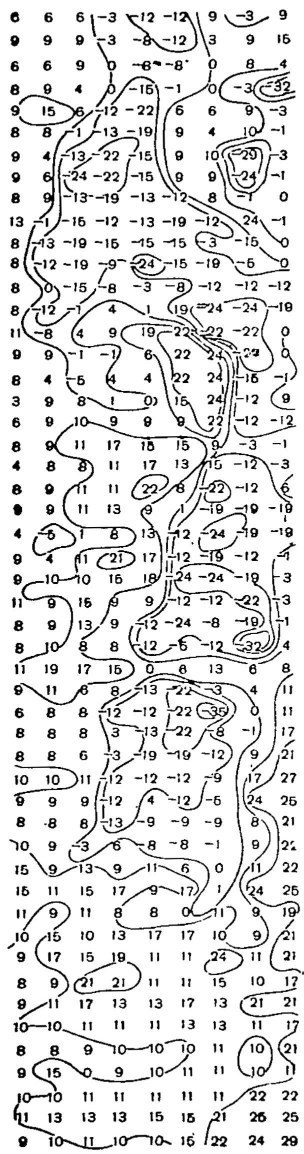

Figure 9b. The Measured Radiation Temperature Field.

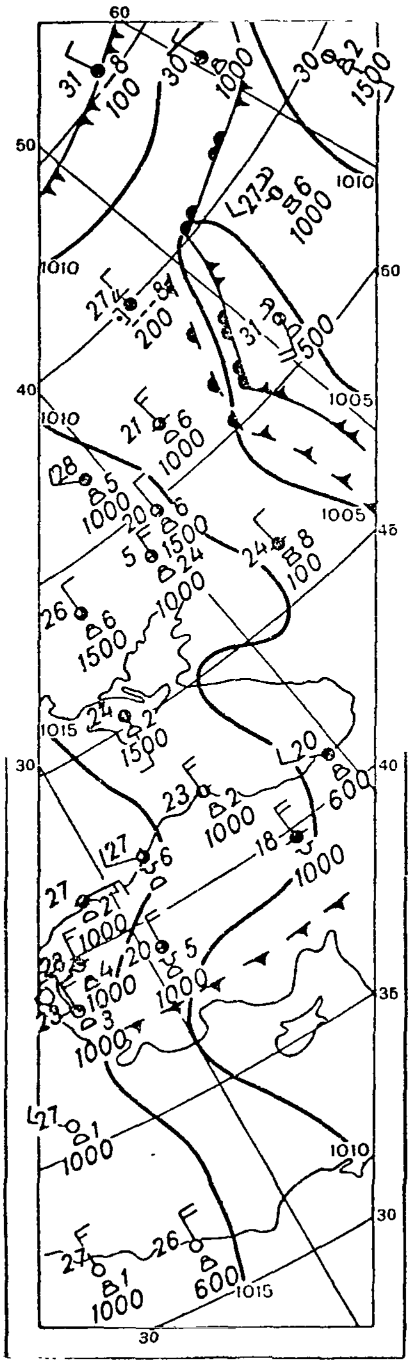

Figure 9c. The Synoptic Situation of the Region Under the Satellite.

The regions of the Mediterranean /86
Sea and African coast are characterized by weather with few clouds (0-1 points of cumulus clouds): the mean radiation temperatures, measured over the Mediterranean Sea amount to 13°C, t_{rad}, measured above the African regions amount to about 24°C.

From Table 6 we can see that the measurement data agreed quite well with the calculation results. The 135th Loop passes partly above the territory of the USSR, for some regions of which we possess probable values of the contrast of radiation temperatures of cloudiness against the background of the underlying surface.

The possible values of the contrast of radiation temperatures for the thick frontal cloudiness and vertical development clouds amounted to 30-40°, which makes it possible to interpret the regions A and B of the radiation field, as regions of high frontal cloudiness. Here the character of temperature change in the regions mentioned enables us to draw the conclusion that in region B we note frontal cloudiness of the cumulonimbus forms.

Let us compare the calculated most probable contrasts of the temperature ΔT°_{calc} for regions of Kuybyshev, Volgograd, Khar'kov and Odessa with the contrast of ΔT_{meas} in the measured radiation field of the 135th loop of the Kosmos-122 satellite on the 4th of July 1966 at 12 hrs 33 min Moscow time (Table 7).

As we can see from the table, the /8
probable values of radiation temperature contrasts with solid cloudiness are in sufficiently good agreement with the contrasts obtained as a result of measurement from satellites (Kuybyshev, Volgograd).

In the regions of Khar'kov and Odessa we note a more substantial difference in the values of the contrast, which enables us to assume the presence of cloudiness with breaks in these regions (in Khar'kov 6 points of lower level cloudiness, in Odessa 3-4 points of lower level cloudiness). This assumption is supported by the analysis of the synoptic situation on the ground weather map.

TABLE 6. COMPARISON OF THE MEASURED AND CALCULATED RADIATION TEMPERATURES.

Region	Cloudiness								t_{rad} °C, Measured from the Satellite
	Clear		Lower		Middle		Upper		
	J_{8-13}	t_{rad}	J_{8-13}	t_{rad}	J_{8-13}	t_{rad}	J_{8-13}	t_{rad}	
Kuybyshev Oblast	4393,7	20,9	1964,9	—20,6	2914,8	—1,5	3196,8	4,0	—2,0
Black Sea	3762,6	13,0	2119,4	—17,0	3011,7	0,5	3295,6	5,5	—12,0—19,0
Mediterranean Sea	4045,9	17,7	2390,1	—11,3	3166,9	4,0	3568,4	10,0	11,0—15,0
Africa	4716,8	26,0	2482,7	—9,5	3537,2	9,5	4040,4	17,0	21,0—29,0

Note: I_{8-13} is the intensity of the outgoing radiation (microwatts/cm^2 steradian) in the region of wavelengths of 8-13 μ; $t°_{rad}$ is calculated radiation temperature (°C).

Tr. Note: Commas indicate decimal points

TABLE 7. COMPARISON OF THE MEASURED AND CALCULATED VALUES OF RADIATION TEMPERATURE CONTRASTS.

Points	$\Delta T°_{meas}$	$\Delta T°_{calc}$ (cloudiness up to 10 points)	$\Delta T°_{calc}$ (partial cloudiness)
Kuybyshev	25,0	25,8 (middle)	
Volgograd	34,0	37,2 (lower)	
Khar'kov	19,0	27,2 "	17,0 (lower 6 points)
Odessa	12,0	28,6 "	12,2 (lower 4 points)

Tr. Note: Commas indicate decimal points

In Figures 10a and b we give the infrared image of the part of the surveyed band and the radiation field corresponding to the image (Loop 209, 9 July 1966). On the photograph regions A and C stand out with sufficient contrast against the dark background of the picture in the central part of B. In the radiation field two regions A and C correspond sufficiently low radiation temperatures (-27, -33°C) against the background of the principal field B, characterized by the positive values of temperature amounting to about 9°C.

Figure 10a. Infrared Picture of the Underlying Surface and Cloudiness Obtained from the Kosmos-122 Weather Satellite on 9 July 1966 (Loop No. 209, 12 hrs, 28 min. Moscow Time).

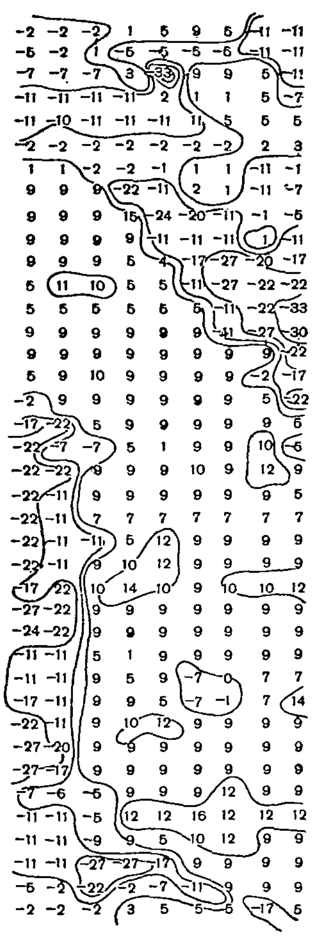

Figure 10b. The Measured Radiation-Temperature Field.

The synoptic situation (weather map for 15 hrs), corresponding to the territory portrayed on the picture, is determined by the influence of the cyclone the center of which is located near the points with coordinates of 70°N and 80°E and the frontal system connected with it. The cloudiness in region A represents the cold front cloudiness system. The central part of the territory (region B) is characterized by the influence of the anticyclone, we observe cloudless or little cloudy weather (Figure 10c). /88

In regions C we noted a considerable cloudiness, formed along the eastern periphery of the stationary anticyclone and consisting mainly of stratiform and stratocumulus and altocumulus clouds. We note individual massifs of cumulonimbus forms of cloudiness.

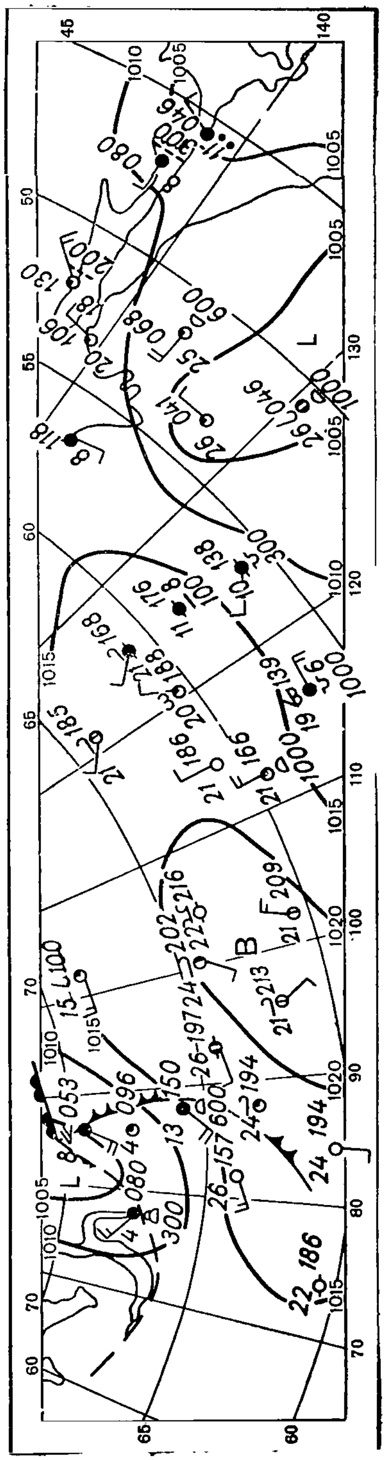

Figure 10c. Synoptic Situation of the Region Under the Satellite.

We can compare the probable values of the radiation temperature contrast and the measured values of the contrast only for the region of Yakutsk because of the absence of calculated data for other points. Actually, the temperature contrast observed for the cloudiness (excluding the frontal clouds) against the background of the underlying surface amounts to 8-11°. The probable value of the contrast for the cloudiness of the middle level in this region is equal to 9.3°C, which indicates a sufficiently good coincidence between the values examined. In the ground level synoptic map of the Yakutsk region we note solid cloudiness of the middle layer, which also supports the above-mentioned agreement.

The temperature contrast in the region A which reach the values of 30-35°, indicate the existence of frontal cloudiness in this region. In region C individual sectors have contrasts of radiation temperatures, reaching -36 and -42°, which indicates the presence of thick vertical development cloud massifs.

On the basis of the investigations performed by us we can make the following conclusions.

1. The infrared pictures obtained from the satellite yield a more complete /89
and whole picture of distribution of the cloudiness than the synoptic maps. The picture obtained enables us to refine the distribution of cloudiness over large areas of the terrestrial surface. However, in this case we should note that many details of the cloudiness structure, well visible on television pictures are smoothed out on infrared pictures (this indicates the necessity of raising the three-dimensional resolution of the infrared picture).

2. For refining certain positions in the interpretation of the satellite observations in a number of cases we can

use the radiation balance data.

3. The values of radiation temperature contrasts of the underlying surface and clouds according to the measurements from weather satellites agree well with analogous values of contrasts calculated according to the data of specific soundings of the atmosphere. This indicates that in the absence of the possibility of quantitative interpretation of infrared pictures or the climatical calculation data on the contrast may serve as a reliable orientation point for such interpretation.

4. The investigation performed on the possible deviations of the radiation contrast values from their mean values which may be obtained by us on the basis of the use of mean long-term values of temperatures of the underlying surface, altitude, and temperature of the upper cloud limit, the vertical distribution of the air temperature and moisture, showed that for interpretation of the infrared measurement data from satellites we can recommend the use of the most probable values of contrast between the radiation temperatures of the earth and cloudiness calculated by us earlier [4].

The possibility of the use of probable values of radiation contrast ΔT in the interpretation of infrared images, obtained from the satellite, is supported by the good agreement of these data with the results of the concrete satellite measurements.

REFERENCES

1. Kondrat'yev, K. Ya. and N. Ye. Ter-Markaryants: "On the Possibility of Detecting Cloudiness on the Night Side of the Earth According to the Data of Measurements of Outgoing Thermal Radiation in the Atmospheric Transparency Window," *Trudy GGO*, Issue 170, 1965.
2. Novosel'tsev, Ye. P.: "On the Degree of Blackness of Clouds of the Upper and Middle Layer," *Trudy GGO*, Issue 196, 1966.
3. Ter-Markaryants; N. Ye. and L. V. Murav'yeva: "On the Possibility of Tracing Cloudiness on the Shadowed Side of the Earth from Weather Satellites," *Trudy GGO*, Issue 196, 1966.
4. Zhvalev, V. F.; Kondrat'yev, K. Ya. and N. Ye. Ter-Markaryants: "On the Calculation of Spectral Values of Outgoing Radiation and Contrasts Between the Radiation Temperature of the Underlying Surface and Clouds in Connection with the Problem of Detecting Cloudiness from Satellites," *Trudy GGO*, Issue 203, 1967.
5. Guseva, L. N.: "On the Problem of Determination of Temperature of Soil Surface According to the Air Temperature," *Trudy GGO*, Issue 166, 1965.
6. Kondrat'yev, K. Ya.; Ye. P. Novosel'tsev and N. Ye. Ter-Markaryants: "On the Determination of Temperature of the Underlying Surface and Clouds from Weather Satellites," *Trudy GGO*, Issue 196, 1966.
7. Kondrat'yev, K. Ya.; O. A. Avaste; L. P. Federova and K. Ye. Yakushevskaya "*Pole Izlucheniya Zemli kak Planety* [Radiation Field of the Earth as a Planet]", Gidrometeyoizdat Press, Leningrad, 1967.

8. Novosel'tsev, Ye. P. and N. Ye. Ter-Markaryants: "On Reflection of the Longwave Radiation by the Water Surface," *Trudy GGO*, Issue 125, 1962.
9. Vetlov, I. P.: "Investigation of Cloudiness and Outgoing Radiation by Means of the Kosmos-122 Satellite," *Meteorologiya i Gidrologiya*, No. 1, 1967.
10. Hovis, W. A.: "Optimum Wavelength Intervals for Surface Temperature Radiometry," *Appl. Optics*, No. N5, 1966.
11. Nimbus I High Resolution Radiation Data Catalog and Users'Manual, Volume 1, Photofacsimile film strips. 15.I.1965. *Goddard Space Flight Center* Greenbelt, Md.

PROCEDURE FOR CALCULATING THE SHORTWAVE RADIATION FIELD DURING ANISOTROPIC REFLECTION FROM THE UNDERLYING SURFACE

K. S. Shifrin and V. Yu. Kolomiytsov

ABSTRACT: It is shown, that upon the consecutive evaluation of the diffusion of the first, second, and higher orders, the sensitivity of the function of the source to the reflection indicatrix, decreases. In order to evaluate from above the effect of the anisotropy of the reflection on the field of diffused radiation, it is sufficient to carry out the corresponding calculations taking into account only the double diffusion. The evaluations discovered the equality of the fields of diffused radiation above the arbitrary water surface and the Lambertian bottom with the direct radiation albedo. It has been shown that the contribution of the underlying surface to the diffused radiation decreases, if the role of multiple diffusion in the atmosphere increases (optical thickness grows), but this contribution grows, if we take into account not the single but the multiple diffusion with fixed parameters of the atmosphere. The radiation, absorbed by the layer of a turbid medium, is evaluated from above and from below by the values, obtained with an evaluation of only a single diffusion.

Introduction

The calculation of the shortwave radiation field in the atmosphere is usually carried out in the assumption that the underlying surface is Lambertian. However, we know well that, the actual surfaces deviate greatly from this theoretical model. This pertains not only to the marine surface but also to the dry land and clouds. /90

The method of calculation of the field with an anisotropic reflecting bottom was previously proposed by M. S. Malkevich [1]. In his work he examined the case of the weakly anisotropic bottom.

The purpose of the present work is to investigate the case of strongly anisotropic surfaces, close to the mirror ones, such for example as the principal surface of the terrestrial globe, namely the world ocean.

We shall show, that there is practically no necessity to consider the problem in its entirety,to seek the solution of the equation of transfer with the non-Lambertian bottom. It is sufficient to calculate carefully the reflected direct radiation according to the data on the brightness coefficient. As for the diffused radiation, it can be calculated very accurately considering the bottom Lambertian with a certain effective albedo.

Below we give the reasoning for the outgoing shortwave radiation (OSR) field having in view the analysis of the data of measurements from a satellite. In reality the system of calculation examined here may be used for calculating the field at any level in the atmosphere.

1. Contribution of the Reflection From the Underlying Surface to the Brightness in the Atmospheric Haze

Let us represent the brightness of the haze on the upper boundary of the atmosphere in the form of

$$I_D = I_D^0 + I_D^A.$$

Here, I_D^0 is caused only by the scattering in the atmosphere and does not depend on the albedo (the brightness of the haze when A = 0), I_D^A is the haze component dependent on the reflection of radiation at the lower boundary. Values I_D and I_D^A are functions of the optical thickness τ_0, albedo A, diffussion indicatrix $\kappa(\gamma)$, zenith distance of the sun i, and the selected direction θ, ϕ. Having fixed all of the variables, with the exception of τ_0 and A let us examine function /91

$$f(\tau_0,\ A) = \frac{I_D^A}{I_D} = \frac{I_D^A/I_D^0}{1 + I_D^A/I_D^0}, \tag{1}$$

characterizing the contribution of the underlying surface to the diffused radiation of the upper boundary of the atmosphere. When τ_0 is increased due to diffusion value I_D^0 grows monotonously, and I_D^A either decreases or grows (with small τ_0), but always slower than I_D^0, because the illuminance of the bottom causing it decreases. Therefore, I_D^A/I_D^0 and f are decreasing functions of τ_0, i.e., the contribution of the underlying surface to the diffused radiation decreases, if in the atmosphere of the planet the role of multiple diffusion increases (τ_0 grows). But on the other hand, this contribution increases upon conversion from single dispersion to multiple dispersion with the fixed parameters of the atmosphere. Indeed, if I_D^0 and $I_{D_k}^A$ are functions obtained when all the orders of diffusion down to the k-th included are taken into account, then upon the increase of index k both functions grow due to the increase of the number of diffusions, but in addition to this $I^A_{D_k}$ increases additionally through the increase of illuminance of the underlying surface. Consequently, upon the conversion from the single diffusion to multiple I^A_D grows faster than I^0_D. These reasonings may be easily checked quantitatively for the case of pure diffusion with a spherical indicatrix, using the exact values of the functions of the source, obtained by E. S. Kuznetsov and B. V. Ovchinski [2]. Having fixed the zenith distance of the sun and the direction of observation ($i = 30°$, $\theta = 0$), we carried out the calculations of functions f for selection of values of τ_0 and A (Table 1). For the same conditions we calculated function $f_1(\tau_0, A) = I^A_{D_1}/I_{D_1}$ (Table 2), i.e., we have found the contribution of the underlying surface to the brightness of the haze taking into account only the single diffusion. From the examination of the tables obtained we can draw a number of conclusions.

TABLE 1. CONTRIBUTION OF THE UNDERLYING SURFACE TO THE BRIGHTNESS OF THE HAZE AT THE UPPER BOUNDARY OF THE ATMOSPHERE (VALUES OF FUNCTION $f(\tau_0, A) = I^A_D/I_D$) WHEN $\lambda = \varkappa(\gamma) = 1$, $i = 30°$, $\theta = 0$

A	τ_0				
	0,2	0,3	0,4	0,5	0,6
0,1	0,115	0,104	0,0925	0,0870	0,0814
0,2	0,208	0,193	0,178	0,166	0,155
0,3	0,286	0,267	0,251	0,236	0,222
0,8	0,537	0,522	0,508	0,495	0,483

Tr. Note: Commas indicate decimal points.

1. Function $f_1(\tau_0, A)$, as well as $f(\tau_0, A)$, decreases with respect to τ_0 and increases with respect to A. The same may be said also of function $f_k(\tau_0 A)$. Inasmuch as $f(\tau_0, A)$ is a monotonously decreasing function of τ_0, it reaches its maximum value when $\tau_0 \to 0$, but f when $\tau_0 \ll 1$ coincides with f_1, consequently,

$$f_{\max}(\tau_0, A) = \lim_{\tau_0 \to 0} f_1(\tau_0, A), \quad (2)$$

function f_1 has the following appearance /92

$$f_1(\tau_0, A, i, \theta) = 1 - \frac{1 - e^{-\tau_0(\sec\theta + \sec i)}}{1 - e^{-\tau_0(\sec\theta + \sec i)}\,[1 - 2A\,(1 + \cos i \sec\theta) \cdot \psi_1(\tau_0, \theta)]}. \tag{3}$$

Here

$$\psi_1(\tau_0, \theta) = \int_0^{\tau_0} E_2(x)\, e^{\sec\theta \cdot x}\, dx, \quad E_2(x) = \int_1^{\infty} e^{-xy} \frac{dy}{y^2}. \tag{4}$$

TABLE 2. CONTRIBUTION OF THE UNDERLYING SURFACE TO THE BRIGHTNESS OF THE HAZE AT THE UPPER BOUNDARY OF THE ATMOSPHERE TAKING INTO ACCOUNT ONLY A SINGLE DISPERSION (VALUES OF FUNCTION $f_1(\tau_0, A) = I^A_{D_1}/I_{D_1}$), $\lambda = x(\gamma) = 1$, $i = 30°$, $\theta = 0$

A	τ_0 0,2	0,3	0,4	0,5	0,6
0,1	0,101	0,0859	0,0730	0,0629	0,0536
0,2	0,183	0,158	0,138	0,118	0,102
0,3	0,252	0,220	0,193	0,167	0,145
0,5	0,359	0,320	0,285	0,251	0,220
0,8	0,473	0,429	0,390	0,349	0,312
1	0,529	0,484	0,444	0,401	0,361

Tr. Note: Commas indicate decimal points.

Going on the limit (2), we obtain the maximum possible value of function $f(\tau_0, A)$ with the spherical diffusion indicatrix

$$f_{max}(A) = 1 - \frac{\sec\theta + \sec i}{\sec\theta + \sec i + 2A\,(1 + \cos i \sec\theta)}. \tag{5}$$

With $A = 0$ we obtain $f_{max} = 0$, from which it follows that in this case $f = 0$ with any value of τ_0 in accordance with its sense [see (1)]. When $A \neq 0$, in the particular case $i = \theta = 0$, we have from (5)

$$f_{max}(A) = \frac{2A}{1 + 2A}. \tag{6}$$

2. Function $f(\tau_0, A) \geq f_1(\tau_0, A)$ with any τ_0 and A, the inequality being the greater the larger is τ_0. Evidently, $f_k(\tau_0, A)$ increases monotonously with the growth of k and $f_k \to f$ when $k \to \infty$.

3. Function $f_k(\tau_0, A)$ grows with increase of k similarly for all the A. We have in view, that the relationship between functions f of the various orders is practically independent on the albedo, in particular that

$$f_1(\tau_0, A)/f(\tau_0, A) \approx \varphi(\tau_0).$$

Thus, we found that

$$f_k(\tau_0, A) = \frac{I^A_{D_k}/I^0_{D_k}}{1 + I^A_{D_k}/I^0_{D_k}} \tag{7}$$

is a decreasing function of τ_0 and increasing function of index k.

2. Evaluation of Absorption in the Atmosphere According to the Field of a Once Dispersed Radiation /93

The above-mentioned considerations enable us to give a simple evaluation of the amount of radiation absorbed in the terrestrial atmosphere.

Let us designate with $F_k^{\uparrow}$ and $F_k^{\downarrow}$ the semispherical flows of diffused radiation of the k-th order coming out through the upper and lower boundaries of the layer of the optical thickness τ_0, and with $F^{\uparrow}$ and $F^{\downarrow}$ the exact values of the flows ($k = \infty$). For the latter there is the following law of preservation of energy:

$$E_0 = E_{dr} + F_{ab} + F^{\uparrow} + F^{\downarrow}, \tag{8}$$

where E_0 is the spectral solar constant for the horizontal platform, F_{ab} is the radiation absorbed in the vertical column of the atmosphere of a unit cross-section in a unit of time, E_{dr} is the illuminance created by the direct solar radiation at the lower boundary of the atmosphere. For the sake of simplicity we consider that $A = 0$. Let us examine the solar radiation incident on the flat layer selected by us. Passing through the medium, direct radiation leaves a trace in the form of a singly dispersed radiation. This radiation of the first order is the only source of radiation of the higher orders. Therefore, if N_k is the full number of quanta in the medium after the k-th dispersion, then $N_k \leq N_1$. Actually, N_1 of singly dispersed quanta, engendered by direct radiation, cannot increase in number through subsequent dispersions, and may only decrease to real absorption. Hence, it follows that the total flow leaving through both boundaries of the medium cannot increase upon the increase of the order of dispersion, i.e.,

$$F_1'^{\uparrow} + F_1'^{\downarrow} \geqslant F_k'^{\downarrow} + F_k'^{\uparrow} \geqslant F^{\uparrow} + F^{\downarrow} \tag{9}$$

(The equality sign takes place during pure dispersion.) However, we know well that the function of source B_k (τ, θ, ϕ) grows monotonously with the increase of index k. In this case it is correct for any τ, θ, and ϕ and therefore the intensity of radiation in each point of the medium and at any angle increases upon the conversion to the radiation of the subsequent orders. In particular, for the flows going out of the medium we have

$$F^{\uparrow} + F^{\downarrow} > F_k^{\uparrow} + F_k^{\downarrow} > F_1^{\uparrow} + F_1^{\downarrow}. \tag{10}$$

The incompatibility of formulas (9) and (10) is explained by the fact that they pertain to different values. It is clear, that the total number of quanta during dispersion does not increase, but with the usual growth of the radiation field of the first order we exclude from examination those of the N_1 quanta, which have been subjected to a second collision, and leave only those, which pass through the medium without diffusion and absorption. Mathematically this is expressed by the factor $e^{-\tau \sec \theta}$ in the formula for the intensity. Going over to the dispersion of the second order, we add to the radiation field those quanta from the secondary dispersion, which were not subjected to the third collision and so forth, i.e., the function of the source grows, and consequently there is an inequality (10). If however, we consider that all the quanta located in the medium after the k-th dispersion go out through the boundary and their flow is equal to $F'^{\uparrow}_k + F'^{\downarrow}_k$, then upon conversion to the dispersion of the subsequent orders this flow will not increase, since the full number of the quanta will not increase, i.e., we obtain formula (9). Let us emphasize, that the law of preservation (8) is correct only for the true values of flows $F^{\uparrow}$ and $F^{\downarrow}$, knowing which we can calculate the absorption in the /94
atmosphere F_{ab}. If however we find $F_1'^{\uparrow} + F_1'^{\downarrow}$ and $F_1^{\uparrow} + F_1^{\downarrow}$, then because of the inequality of (9) and (10), we shall have:

$$F'_{ab1} \equiv E_0 - E_{dr} - (F_1'^{\uparrow} + F_1'^{\downarrow}) < F_{ab},$$

$$F_{ab1} \equiv E_0 = E_{dr} - (F_1^{\uparrow} + F_1^{\downarrow}) > F_{ab}.$$

Hence, the absorbed radiation may be evaluated from above and from below to the values, obtained taking into consideration only single dispersion

$$F'_{ab1} < F_{ab} < F_{ab1}. \tag{11}$$

In case of pure dispersion ($\lambda = 1$) the total flow to the boundaries of the entire singly dispersed radiation (not weakened through the departure of energy into the currents of the subsequent multiplicities) because of (9) coincides with the exact value of the flow, i.e., $F_1'^{\uparrow} + F_1'^{\downarrow} = F^{\uparrow} + F^{\downarrow}$, which upon substitution in (8) taking into account that $F_{ab} = 0$, yields

$$E_0 - E_{dr} = F_1'^{\uparrow} + F_1'^{\downarrow}. \tag{12}$$

Let us analyze this equation for the case when $x(\gamma) = 1$, $i = 0$. For the function of the source we have $B_1(\tau) = s/4 \cdot e^{-\tau}$. In order to find the intensity of the radiation of the first order leaving the medium $I_1'(\theta)$ without taking into account the weakening of the radiation, it is efficient simply to integrate the function of the source with respect to the entire medium

$$I_1'(\theta) = \sec\theta \int_0^{\tau_0} B_1(\tau)\, d\tau = \sec\theta \frac{S}{4}\left(1 - e^{-\tau_0}\right). \tag{13}$$

Let us remind the reader that the usual expression for the intensity has the appearance of $I_1(\theta) = \sec\theta \int_0^{\tau_0} B_1(\tau) e^{-\tau\sec\theta}\, d\tau$, i.e., we excluded the factor $e^{-\tau\sec\theta}$ in writing formula (13). Apparently value $I_1'(\theta)$ pertains simultaneously to both boundaries of the medium. For the total outgoing flow we have

$$\begin{aligned} F_1'^{\uparrow} + F_1'^{\downarrow} &= 2\int_{(2\pi)} I_1'(\theta)\cos\theta\, d\omega = 4\pi\frac{S}{4}\left(1 - e^{-\tau_0}\right) \times \\ &\times \int_0^{\frac{\pi}{2}} \sin\theta\, d\theta = \pi S\left(1 - e^{-\tau_0}\right). \end{aligned} \tag{14}$$

Since $i = 0$, then

$$E_0 = \pi S, \quad E_{dr} = \pi S e^{-\tau_0}, \quad E_0 - E_{dr} = \pi S\left(1 - e^{-\tau_0}\right).$$

Comparing this expression with formula (14) we see that equation (12) actually takes place.

§3. The Possibility of Using the Lambertian System in Calculating Diffused Radiation

Let us introduce into the examination the coefficient of reflection, determined as the ratio between the brightness of the reflected radiation I to the illuminance by the parallel flow of a horizontal platform E:

$$R(\theta, \bar{i}, \varphi) \equiv I(\theta, \varphi)/E(i). \tag{15}$$

Here i is the angle of incidence of the parallel beams of rays (the azimuth of the incident parallel beam ϕ_0 is assumed to be equal to zero), θ and ϕ are angular coordinates of the reflected ray. /95

Definition (15) assumes the isotropicity of the surface. Moreover, usually there is a symmetry of the reflected radiation with respect to the plane passing through the vertical and the incident ray, i.e.,

$$R(-\varphi) = R(\varphi), \quad 0 \leqslant \varphi \leqslant \pi. \tag{16}$$

Multiplying equation (15) from left to right by cosine θ and integrating with respect to the hemisphere, we obtain the relationship of the coefficient of reflection with the albedo of the surface

$$A(i) = \int_{(2\pi)} R(\theta, i, \varphi) \cos\theta \, d\omega = \int_0^{\pi} d\varphi \int_0^{\frac{\pi}{2}} R(\theta, i, \varphi) \sin 2\theta \, d\theta. \tag{17}$$

For the albedo of the surface, illuminated by a wide source with distribution of brightness $I(\theta, \phi)$, we have

$$A = \frac{\int_{(2\pi)} I(\theta, \varphi) A(\theta) \cos\theta \, d\omega}{\int_{(2\pi)} I(\theta, \varphi) \cos\theta \, d\omega}. \tag{18}$$

The last two expressions indicate that the albedo is determined not only by the reflecting properties of the surface, but by the conditions of the illumination. This circumstance was already noted in [3]. It complicates considerably the determination of the radiation field. Sometimes it is convenient to present the reflection coefficient in the following form

$$R(\theta, i, \varphi)=A(i)R'(\theta, i, \varphi), \tag{19}$$

$$\int R'(\theta), i, \varphi)\cos\theta\, d\omega=1. \tag{20}$$

In this recording the angular R' and energy A(i) parts of the reflection coefficient are divided, which enables us to compare directly the degree of unisotropy of the reflection of surfaces with their different albedos. The reduction to a unity enables us to call function R' (θ, i, ϕ) (by analogy with the diffusion indicatrix) the reflection indicatrix. We can easily see that in the case of isotropic reflection (Lambertian surface)

$$R=\frac{A}{\pi}, \quad R'=\frac{1}{\pi}=0.318\ldots \tag{21}$$

In the case of spherical indicatrix of diffusion the integral equation of radiation transfer has the following appearance

$$\begin{aligned} B(\tau)=\frac{\varkappa}{2}\int_0^{\tau_0} E_1|\tau-\tau'|B(\tau')d\tau'+\frac{\lambda S}{4}e^{-\tau\sec i}+ \\ +\frac{\lambda S}{4}\cos i\, e^{-\tau_0\sec i}\int_{(2\pi)} R(\theta, i, \varphi)\,e^{-(\tau_0-\tau)\sec\theta}d\omega+\frac{\lambda}{4\pi}\int_0^{\tau_0} B(\tau')\iint_{(2\pi)} R(\theta', \theta, \varphi)\times \\ \times e^{-[(\tau_0-\tau)\sec\theta'+(\tau_0-\tau')\sec\theta]}\,d\omega\, d\omega'\, d\tau'. \end{aligned} \tag{22}$$

Here πS is the spectral solar constant, λ is the probability of survival of the quantum, τ is the optical thickness, carried from the upper boundary of the atmosphere, R is the reflection coefficient introduced above, /96

$$E_1(x)=\int_1^{\infty} e^{-xy}\frac{dy}{y}.$$

Ye. S Kuznetsov [4] proposed a method for solving equation (22), but only with specific limitations imposed on the reflection coefficient. Moreover, this solution involves great difficulties and determines the radiation field only for the isotropic dispersion in the atmosphere. At the same time the dispersed radiation is determined fully by the function of source B, which in its turn depends mainly on the dispersing properties of the medium, and the coefficient of reflection is included in the equation for B only under the integral sign. Hence it is natural to assume, that the field of diffused radiation over the anisotropically reflecting surface and over the Lambertian surface with the same albedo differ little from one another, and if this is the case, then it is not necessary to solve equation (22) and an even more complicated equation with the random indicatrix and calculation of a part of the reflected radiation, which depends greatly on the reflection coefficient does not present any difficulty. M. S. Malkevich [1] gave a quantitative evaluation of the proposal made, having examined the equation for the function $f(\tau) = B_R(\tau) - B_A(\tau)$ where $B_R(\tau)$ is the function of the source at the spherical indicatrix of diffusion and anisotropic reflection from the underlying surface (the solution of equation (22)), and function $B_A(\tau)$ is given by the solution of the same equation upon replacement of R by A/π in its values for a great number of parameters are given in work [2]. It transpired, that if the reflection coefficient satisfies certain conditions, which are fulfilled for the majority of the underlying surfaces, then function $f(\tau)$ will be sufficiently small. This is a very substantial circumstance and enables us to reduce the problem to call for a determination of the dispersed radiation field in the atmosphere with anisotropic reflection to the corresponding problem with a Lambertian bottom, for which it is sufficient to find the albedo according to the prescribed coefficient of reflection, using the following formula:

$$A = \int\limits_{(2\pi)} R(\theta,\ i,\ \varphi)\cos\theta\, d\omega + \frac{\int\limits_0^{\tau_0} B_R(t) \int\limits_{(2\pi)} \left[\int\limits_0^{\frac{\pi}{2}} R(\theta,\theta',\varphi) e^{-t\sec\theta'} \sin\theta'\, d\theta' - R(\theta,\ i,\ \varphi) E_2(t) \right] \cos\theta\, d\omega\, dt}{0{,}5e^{-\tau_0 \sec i} \cos i + \int\limits_0^{\tau_0} B_R(t) E_2(t)\, dt}. \tag{23}$$

M. S. Malkevich showed that when $\tau_0 < 1$ the second component in (23) is small in comparison with the first, which represents the albedo of the direct radiation $A(i)$. From this it transpires that the albedo determining the value of the underlying surface in the dispersed radiation field in the atmosphere, depends mainly on the reflection of direct radiation. Having taken $A(i)$ as the first approximation, and calculated the corresponding function of the source $B_A(\tau)$ and substituted it in expression (23) instead of $B_R(\tau)$, we shall obtain the second approximation, and so forth.

The calculations by M. S. Malkevich for the case of the indicatrix of the dispersion of the $x(\gamma) = 1 + x_1 \cos\gamma$ yielded approximately the same values of function $f(\tau)$, as for the spherical indicatrix.

Thus, in work [1] the authors proposed the following system of calculation of the radiation field in the atmosphere with anisotropic reflection from the underlying surface. With the prescribed reflection coefficient R the albedo A is determined according to formula (23), then the integral equation is solved for the function of the source with a Lambertian underlying surface with the albedo value found, and finally, according to the function B obtained and the known coefficient of reflection we find the intensity value sought for any /97 known coefficient of reflection we find the intensity value sought for any point of the atmosphere and in any direction.

However, in determination of the radiation field above the surfaces with a sharply expressed anisotropy of reflection (water surface) such a system of calculation requires additional substantiation. In connection with this let us attempt to determine how does the effect of the anisotropy of reflection from the underlying surface change to dispersed radiation upon passage from the single to the multiple dispersion (with fixed parameters of the atmosphere). We remind the reader, that such a conversion is accompanied by the increase of the energy contribution of the reflection into the dispersed radiation. Today we are interested in something else: if B_R^k is a function of the case order with anisotropic reflection, and B_A^k is the function corresponding to it with the Lambertian bottom with the albedo (23), then how does their relationship change upon the increase of index k? Does it approach unity or go away from it? We calculated functions B_R^1/B_A^1 and B_R^2/B_A^2 for various values of parameters determining them and for surfaces with various optical properties (n and χ), the reflection from which obeys Frenel's formulas. It transpired that the second relationship is closer to unity than the first, i.e.,

$$\left|1-\frac{B_R^2}{B_A^2}\right| < \left|1-\frac{B_R^1}{B_A^1}\right| \tag{24}$$

and we can consider that in general

$$\left|1-\frac{B_R}{B_A}\right| < \left|1-\frac{B_R^1}{B_A^1}\right|. \tag{25}$$

This result is explained by the fact that upon conversion from the single dispersion to double to $B_R^i(\tau)$ terms are added in which the number of the integrations of function R' increases and integrals appear from the product of the reflection indicatrices, which results in the decrease of the sensitivity of the source function to the type of the reflection coefficient, this tendency being retained in the estimation of the subsequent orders of dispersion.

In this way, in order to evaluate from above the influence of anisotropy of reflection on the field of diffused radiation, it is sufficient to carry out the corresponding calculations taking into account only the single diffsion. Let us make use of this for the case of the smooth water surface, comparing the fields of singly diffused radiation with the mirror and isotropic reflection.

§4. Effect of Reflection Anisotropy on the Field of Diffused Radiation Above a Watery Surface

Let B_1 and I_1 be the function of the source and brightness of the haze of the first order on the upper boundary of the atmosphere in the case of mirror reflection B_1' and I_1' be the same value for the isotropic reflection. /98

Then

$$B_1(\tau,\ \theta,\ \varphi)=\frac{\lambda S}{4}e^{-\tau\sec i}\left\{\varkappa(\gamma^-)+r(i)e^{-2(\tau_0-\tau)\sec i}\varkappa(\gamma^+)\right\}, \tag{26}$$

$$I_1(\theta,\ \varphi)=\frac{\lambda S}{4}\sec\theta\left\{\frac{1-e^{-\tau_0(\sec i+\sec\theta)}}{\sec i+\sec\theta}\varkappa(\gamma^-)+\right.$$
$$\left.+r(i)e^{-2\tau_0\sec i}\frac{1-e^{-\tau_0(\sec\theta-\sec i)}}{\sec\theta-\sec i}\varkappa(\gamma^+)\right\}, \tag{27}$$

$$B_1'(\tau,\ \theta,\ \varphi)=\frac{\lambda S}{4}\left\{\varkappa(\gamma^-)e^{-\tau_0\sec i}+\right.$$
$$\left.+2A\cos i\,e^{-\tau_0\sec i}[E_2(\tau_0-\tau)+\chi_1\cos\theta\,E_3(\tau_0-\tau)]\right\}, \tag{28}$$

$$I_1'(\theta,\ \varphi)=\frac{\lambda S}{4}\sec\theta\left\{\frac{1-e^{-\tau_0(\sec i+\sec\theta)}}{\sec i+\sec\theta}\varkappa(\gamma^-)+\right.$$
$$\left.+2Ae^{-\tau_0(\sec i+\sec\theta)}\cos i\,[\psi_1(\tau_0,\ \theta)+\chi_1\cos\theta\,\psi_2(\tau_0,\ \theta)]\right\}. \tag{29}$$

In these formulas $\kappa(\gamma)$ is the diffusion indicatrix; $r(i)$ is the energy coefficient of Frenel's reflection for water.

$$\begin{aligned}\cos\gamma^-&=-\cos\theta\cos i+\sin\theta\sin i\cos\varphi,\\ \cos\gamma^+&=\cos\theta\cos i+\sin\theta\sin i\cos\varphi,\end{aligned} \tag{30}$$

$$E_n(x)=\int_1^\infty e^{-xy}\frac{dy}{y^n}, \tag{31}$$

$$\psi_1(\tau_0,\ \theta)=\int_0^{\tau_0}E_2(x)e^{\sec\theta x}\,dx,\quad \psi_2(\tau_0,\ \theta)=\int_0^{\tau_0}E_3(x)e^{\sec\theta x}dx, \tag{32}$$

χ_1 is the parameter of the composition of the indicatrix $\kappa(\gamma) = 1 + \chi_1 \cos\gamma$.

Let us note that formulas (27) and (29) have an identical component

$$I_1^0(\theta,\ \varphi)=\frac{\lambda S}{4}\sec\theta\,\frac{1-e^{-\tau_0(\sec i+\sec\theta)}}{\sec i+\sec\theta}\varkappa(\gamma^-), \tag{33}$$

which characterizes the radiation, caused by the diffusion of direct solar radiation on the path from the upper boundary of the atmosphere to the underlying surface. Inasmuch as in this case the haze of the first order does not present an independent interest for us, but is used only for evaluation of the effect of anisotropy of reflection on the field of diffused radiation above smooth water surface, it is sufficient to carry out the calculations only for several values of variables. In formulas (27) and (29) we assumed that

$\tau_0 = 0{,}3$, $i = 0, 30, 60°$, $\theta = 0, 30, 60°$, $\varphi = 0, 90°$ $r(i) = 0.02, 0.022, 0.06$ for $i = 0$ 30, and 60° respectively, $A = A(i) = r(i)$, $x_1 = 1.15$.

Calculations have shown that if we exclude the direction of the mirror ray $\theta = i$, $\phi = 0$, then the cases of mirror and Lambertian reflection are almost indistinguishable from one another, and even when $\theta = i$ this difference does not exceed 18%.

Moreover, the reflection from the real sea with waves is much closer to the isotropic than to the mirror reflection, and therefore upon passing from the mirror reflection to the reflection from the real sea, the field of diffused radiation of the first order will come much closer to the field above the isotropically reflecting surface with an albedo of $A(i) = \int\limits_{(2\pi)} R(\theta, i, \varphi)\cos\theta d\omega$ /99
and we can practically consider that $I_1(R) = I_1'(A(i))$ for all angles, including the direction of the mirror ray, and $I(R) = I'(A)$, proceeding from inequality (25). Let us remark, incidentially that the noticeable difference between the brightnesses of the haze with the mirror and isotropic reflections for $\theta = i$ has no significance whatever, if we are interested by a full radiation, departing from the upper boundary of the atmosphere, and the diffused radiation may be generally disregarded (of course only in the direction of the mirror ray). Consequently, in the case of the sea also we can pass over to the Lambertian surface with an albedo, determined according to formula (23).

Because of the small value of the water's albedo, the haze is caused mainly by the direct diffusion in the atmosphere, and consequently, is little sensitive to the change of albedo, on which depends approximately 1/20th of it. Therefore, in calculating the albedo according to formula (23) it is quite sufficient to limit ourselves to the first term, the more so, because owing to the smallness of the optical thickness of the atmosphere it is the principal one with any albedo of the underlying surface. In this way the field of diffused radiation above the sea with the reflection coefficient $R(\theta, i, \phi)$ is equivalent to the field above the Lambertian surface, the albedo of which is determined with $R(\theta, i, \phi)$ with the general formula (17).

REFERENCES

1. Malkevich, M. S.: "On the Influence of Non-Orthrotropicity of the Underlying Surface on the Diffused Light in the Atmosphere," *Izv. AN SSSR, Ser. Geofiz*, No. 3, 1960.

2. Kuznetsov, Ye. S. and B. V. Ovchinskiy: "Results of the Numerical Solution of the Integral Equation of the Theory of Diffusion of Light in the Atmosphere," *Trudy Geofiz., IN-Ta AN SSSR*, No. 4,(131), 1949.
3. Shifrin, K. S.: "On the Albedo Theory," *Trudy GGO*, Issue 39, 1953.
4. Kuznetsov, Ye. A.: "On the Problem of Estimation of Diffused Reflection of Light by the Terrestrial Surface in the Problem of Diffusion of Light in the Atmosphere," *Izv. AN SSSR, Ser. Geogr. i Geofiz.*, Vol. 9, No. 1, 1945.

PROBABILITY OF DETECTION OF CLOUDINESS AND UNDERLYING SURFACE BY THE IR-SYSTEM SIGNALS

G. P. Vimberg, V. I. Ivanov and V. V. Puchkov

ABSTRACT. The authors examined the possibilities of detection of cloudiness over various types of underlying surface, and also over various radiating surfaces against the background of the IR system's own noises.
It is shown that the IR system, installed on the Kosmos-122 satellite provides a sufficiently high probability of detection of cloudiness against the background of radiation of the principle types of underlying surfaces and the system's own noises. The probabilities of detection, calculated according to the experimental laws of distribution of the IR system video signal, are higher than the probabilities calculated from the condition of the normalcy of these laws.

We know [1, 2, 3], that the quantitative characteristic of the effectiveness of the use and the qualities of functioning of the technical means of observation (radar, infrared, television, etc.) is connected first of all with the evaluation of the probability of detection of objects in the zone of their action. /100

The solution of this problem requires statistical characteristics of the fluctuation interferences and useful signals (laws of distribution and their numerical characteristics at the input of the terminal link of the observation facility).

Applicably to the scanning IR-system of a weather satellite the abovementioned characteristics may be obtained on the basis of statistical processing of the records of video signals from various types of cloudiness, sectors of the background, and their combinations [4].

We shall assume, that the observer (the terminal link of the system) knows the laws of distribution of video signals from cloudiness $W(V/A_{cl})$, sectors of the background $W(V/A_b)$ and their numerical characteristics: mathematical expectations of voltages $\overline{V}_{cl}$, $\overline{V}_b$ and dispersion σ^2_{cl} and σ^2_b.

The law of distribution of fluctuation noises (of the IR-receiver, radio channel, and the radiation from the receiving systems' elements themselves) shall be considered normal with the mathematical expectation, equal to zero and dispersion σ_n^2.

Let us determine the problem of detection of cloudiness against the background of radiation of various types of underlying surface (sea, dry land, etc.). Since the laws of distribution $W(V/A_{cl})$ and $W(V/A_b)$ overlap, in the work of the terminal link, which makes the decision of the presence of a signal, pertaining to the class of cloudiness A_{cl} or background A_b, errors are possible, for example the spurious detection and omission of a signal [1].

The probability of these errors is determined with the following obvious relationships:

Probability of spurious detection

$$P_{s.d.} = \begin{cases} \int_{-\infty}^{V_0} W(V/A_b)\,dV, & \text{if} \quad V_{cl} < V_b \\ \int_{V_0}^{\infty} W(V/A_b)\,dV, & \text{if} \quad V_{cl} > V_b \end{cases} \tag{1}$$

The probability of omission of a signal /101

$$P_{om} = \begin{cases} \int_{-\infty}^{V_0} W(V/A_{cl})\,dV, & \text{if} \quad V_{cl} > V_b \\ \int_{V_0}^{\infty} W(V/A_{cl})\,dV, & \text{if} \quad V_{cl} < V_b \end{cases} \tag{2}$$

In these relationships V_0 is the threshold value of voltage, established by the observer.

Since the range of the values of the video signal voltages at the output of the IR system is limited and is measured in the $[0, V_{max}]$ range, in the calculation of probabilities of $P_{s.d.}$ and P_{om} on an electronic computer we may use the approximate formulas

$$P_{s.d.} \approx \begin{cases} \sum_{0}^{V_0} W(V/A_b)\,\Delta V = 1 - \sum_{V_{max}}^{V_0} W(V/A_b)\,\Delta V, & \text{when} \quad V_{cl} < V_b \\ \sum_{V_0}^{V_{max}} W(V/A_b)\,\Delta V = 1 - \sum_{0}^{V_0} W(V/A_b)\,\Delta V, & \text{when} \quad V_{cl} > V_b \end{cases} \tag{3}$$

$$P_{om} \approx \begin{cases} \sum\limits_{0}^{V_0} W(V/A_{cl})\Delta V = 1 - \sum\limits_{V_{max}}^{V_0} W(V/A_{cl})\Delta V, & \text{when} \quad V_{cl} > V_b \\ \sum\limits_{V_0}^{V_{max}} W(V/A_{cl})\Delta V = 1 - \sum\limits_{0}^{V_0} W(V/A_{cl})\Delta V, & V_{cl} < V_b \end{cases} \tag{4}$$

Value V_0 is found from the solution of equation

$$P_{s.d.} = \begin{cases} \sum\limits_{V_0}^{V_{max}} W(V/A_b)\Delta V = C = \text{const}, & \text{if} \quad V_{cl} > V_b \\ \sum\limits_{0}^{V_0} W(V/A_b)\Delta V = C = \text{const}, & \text{if} \quad V_{cl} < V_b \end{cases} \tag{5}$$

The probability of detection of cloudiness with a known V_0 is determined with the formula

$$P_{cl} = 1 - P_{om} = \begin{cases} \sum\limits_{V_{max}}^{V_0} W(V/A_{cl})\Delta V, & \text{if} \quad V_{cl} > V_b \\ \sum\limits_{0}^{V_0} W(V/A_{cl})\Delta V, & \text{if} \quad V_{cl} < V_b \end{cases} \tag{6}$$

The results of the calculations for certain characteristic combinations of cloudiness and background are given in Table 1.

As you can see from Table 1, in approximately 85% of the cases the probability of detection of various types of cloudiness against the background of radiation of the principal types of underlying surfaces is sufficiently close to a unity, which indicates the high noise resistance of the infrared system with respect to the background noises examined. /103

The physical explanation of the law of values of probabilities of detection for several combinations of cloudiness and background (for example in the combination of 1-1, 2-1, 3-5, 6-5, 1-6) lies in the small ratio between the signal from the cloudiness and the signal from the background, and the similar values of dispersions of these signals, as a result of which the laws of distribution of video signals for the above enumerated combinations overlap almost completely [4]. In evaluating the observability of various types of radiating surfaces against the background of the system's own noises the threshold voltage is determined according to the fixed probability of spurious detection $P_{s.d.} = c$ from the relationship:

$$P_{s.d.} = \frac{1}{\sqrt{2\pi}\sigma_n} \int_{V_0}^{\infty} e^{-\frac{V_n^2}{2\sigma_n^2}} dV_n = \frac{1}{2}\left[1 - \Phi\left(\frac{V_0}{\sqrt{2}\sigma_n}\right)\right] = C,$$

where $$\Phi(z) = \frac{2}{\sqrt{\pi}} \int_0^z e^{-t^2} dt$$

--is the probability integral,

$$V_0 = \sqrt{2}\sigma_n \arg \Phi(1 - 2c). \tag{7}$$

Where $\arg \Phi(y) = x$ is the function opposite of $y = \Phi(x)$. The probability of correct detection of the radiating surface against the background of the system's own noises in this case is calculated with the formula

$$P_{cl} \approx \sum_{V_0}^{V_{max}} W(V/A_{cl.b})\Delta V. \tag{8}$$

The results of calculations on the basis of formulas (7) and (8) are given in Table 2.

The above data indicate, that the scanning IR system of the meteorological satellite in 75% of the cases assures the reliable ($P_{det} \approx 1$) detection of the principal types of radiating surfaces against the background of the system's own noises. This indicates the high probability of detection of radiating surfaces by means of the system examined. The relatively small values of probability of detection of certain types of radiating surfaces (see radiating surfaces No. 8, 10, 17 in Table 2) against the background of the IR system's own noises are explained by the small value of the mathematical expectation of the voltage of video signal from these surfaces and its significant despersion, as the result of which the laws of distribution of video signals agree with the laws of noise distribution. Consequently, the higher is the radiating surface located, the lower is its radiation temperature, and the smaller is the probability of detection of this radiating surface against the background of the IR system's own noises. To eliminate this shortcoming, i.e., to increase the probability of detection of various radiating surfaces, especially with relatively low radiation temperatures, it is necessary to decrease the noises from the IR equipment and the radio telemetric channel, i.e. to raise the sensitivity of the system against the background of negative temperatures.

TABLE 1. PROBABILITY OF DETECTION OF CLOUDINESS AGAINST THE BACKGROUNDS OF VARIOUS TYPES OF RADIATING SURFACES

Ordinal No.	Radiating Surface	Object									
		Frontal Cloudiness	Solid Cloudiness of Stratiform Types	Solid Cloudiness of Cumuliform & Stratiform Types	Cumulus Cells	Solid Cloudiness in the Rear of the Cyclone	Cyclone	Cumulus Cloudiness with Breaks	Solid Cumulus Cloudiness	Frontal Cloudiness	$P_{s.d.}$
1.	Surface of the Pacific Ocean	0,005 0,186	0 0,650	0,204 0,663	0,660 0,814	0,835 0,910	0,228 0,615	0,670 0,780	0,205 0,540	0,880 0,998	10^{-3} 10^{-1}
2.	Mediterranean Sea	0,998 1,000	1,000 1,000	1,000 1,000	0,476 0,663	1,000 1,000	0,984 1,000	0,690 0,802	1,000 1,000	1,000 1,000	10^{-3} 10^{-1}
3.	Continent--Northern Part of Africa	1,000 1,000	1,000 1,000	1,000 1,000	0,332 0,722	1,000 1,000	0,980 1,000	0,700 0,867	1,000 1,000	1,000 1,000	10^{-3} 10^{-1}
4.	Continent--Central Part of South America	0,613 0,998	0,986 1,000	0,785 1,000	0,288 0,660	0,947 1,000	0,736 0,984	0,329 0,730	1,000 1,000	1,000 1,000	10^{-3} 10^{-1}
5.	Continent--Central Part of European Territory of USSR	0,100 0,980	0,100 0,780	0,037 0,663	0,952 1,000	0,745 0,900	0,137 0,493	0,563 0,790	1,00 1,00	0,573 0,997	10^{-3} 10^{-1}
6.	Continent--Northeastern Caucausus	0,186 0,400	0,844 0,900	0,245 0,340	0,902 1,000	0,807 0,928	0,614 0,704	0,449 0,781	1,000 1,000	1,000 1,000	10^{-3} 10^{-1}

Tr. Note: Commas indicate decimal points.

TABLE 2. PROBABILITY OF DETECTION OF VARIOUS TYPES OF RADIATING SURFACES AGAINST THE BACKGROUND OF THE IR SYSTEM'S OWN NOISES

Ordinal Number	Type of Radiating Surface	$P_d = 10^{-3}$	$P_d = 10^{-1}$
1.	Frontal Cloudiness Above the Pacific Ocean	1.000	1.000
2.	Solid Stratiform Cloudiness Above the Pacific Ocean	1.000	1.000
3.	Solid Cumuliform & Stratiform Cloudiness Above Bellingshausen Sea	1.000	1.000
4.	Surface of the Pacific Ocean Without Cloudiness	1.000	1.000
5.	Surface of the Pacific Ocean With Insignificant Cloudiness	0.990	1.000
6.	Wester Coast of South America (Dry Land)	1.000	1.000
7.	Central Part of South America (Dry Land)	1.000	1.000
8.	Thick Cumuliform Cloudiness Above So. America	0.115	0.722
9.	Cumuliform Cells Above the Atlantic Ocean	0.815	1.000
10.	Solid Cloudiness in the Read of the Cyclone Above the Atlantic Ocean	0.144	0.970
11.	Cyclone Over the Atlantic Ocean	0.998	1.000
12.	Cumuliform Cloudiness with Breaks Over South America	0.878	1.000
13.	Cumuliform Cloudiness with Breaks Over South America	0.100	0.830
14.	Continent (Northern Part of Africa)	1.000	1.000
15.	Thick Cumuliform Cloudiness Over Turkey	1.000	1.000
16.	Northeastern Caucausus	1.000	1.000
17.	Frontal Cloudiness Above the European Territory of the USSR	0.252	0.927
18.	Continent (Center of the European Territory of the USSR)	1.000	1.000
19.	Cyclone Over the West Siberian Lowlands	1.000	1.000
20.	Mediterranean Sea	1.000	1.000

On the curves in Figure 1 we give the relationship between the probability of detection of cloudiness of stratocumulus and cumulus forms against the background of the continents and the mathematical expectation of the video signal voltage. The laws of distribution of the voltages of video signals for these situations are shown in Figure 2, where with $W_1(V/A_{cl})$ we designate the law of distribution of the signal from the solid stratocumulus cloudiness, with $W_2(V/A_{cl})$, the distribution of the signal from the cumulus cloudiness with breaks, $W(V/A_b)$, distribution of the signal from the surface of dry land, and with $W(V_n)$, the density of distribution of the IR system's own noises.

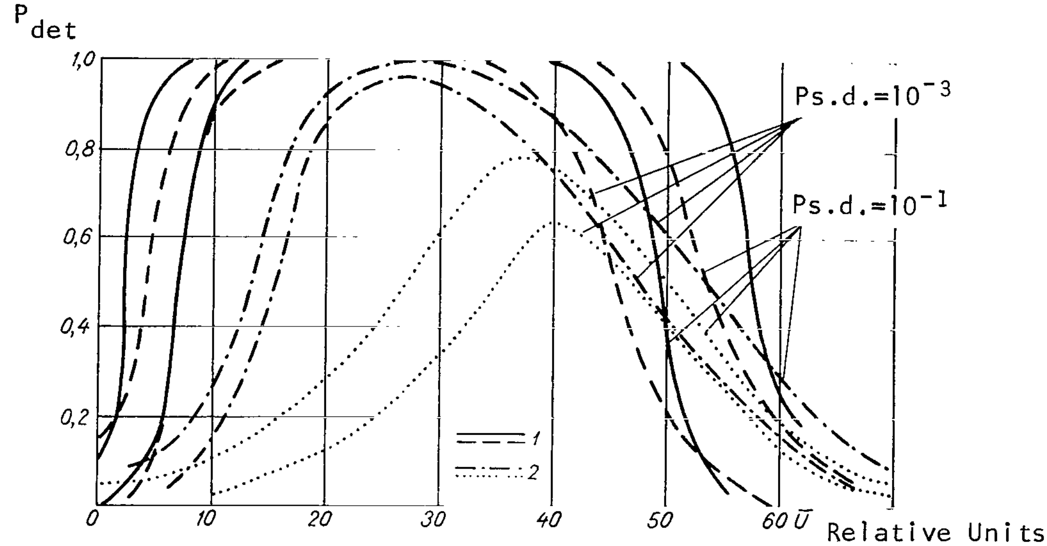

Figure 1. Dependence of the Probability of Detection of Solid Stratocumulus Cloudiness (1) and Cumulus Cloudiness (2) Against the Background of the Continent on the Level of the Video Signal.

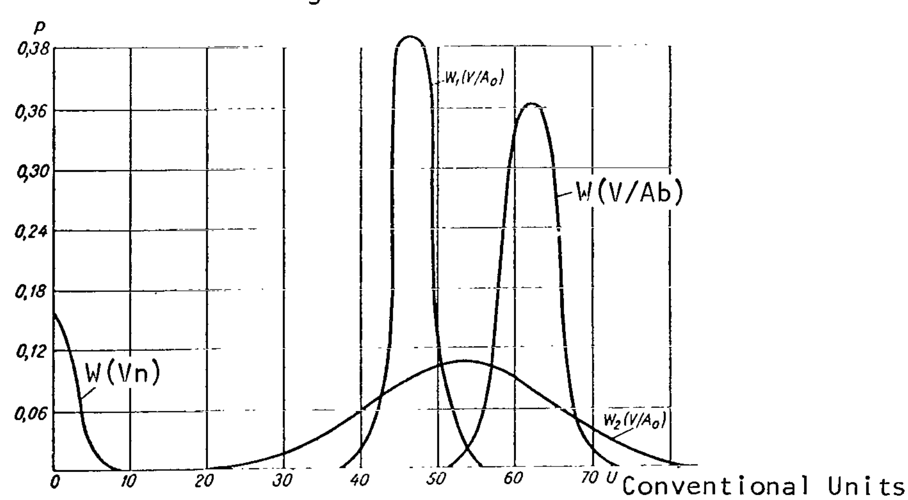

Figure 2. Laws of Distribution of Video Signals from Solid Stratocumulus Cloudiness, Cumulus Cloudiness with Breaks, and from the Surface of Dry Land.

The analysis of curves in Figure 1 shows that the practically reliable detection of the above-mentioned forms of cloudiness against the background of dry land is possible in the intervals between $25 \le \bar{V} \le 35$ and $10 \le \bar{V} \le 40$ relative units. The presence of the drop of curves in the left-hand part of the diagrams is explained by the influence of the system's own noises on the probability of detection of cloudiness. The decrease of the probability of detection when $\bar{V} \ge 35$ relative units and $\bar{V} \ge 40$ relative units, for Figure 1 irrespectively is caused by the effect of fluctuations of the background radiation. /106

In Figures 3 and 4 we present the curves of the probability of detection of cumuliform and cyclonic cloudiness against the background of the sea. The laws of distribution of video signals corresponding to them are given in Figure 5, where $W_1(V/A_{cl})$ is the law of distribution of the signal for the cyclonic cloudiness, $W_2(V/A_{cl})$ is the law for cloudiness of the cumuliform types and $W(V/A_b)$ is for the ocean surface.

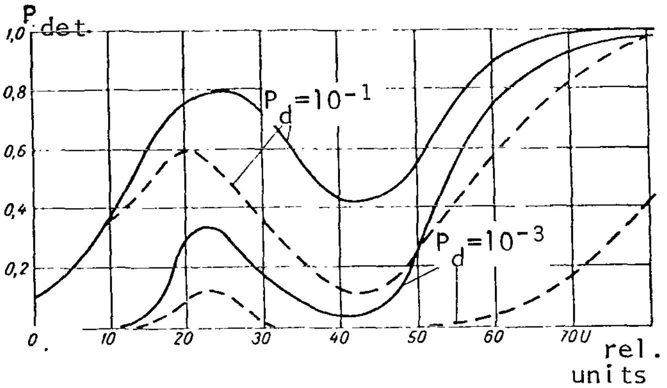

Figure 3. Dependence of the Probability of Detection of Cumuliform Cloudiness Against the Background of the Sea on the Video Signal Level.

The decrease of the probabilities of detection in the region of $\bar{V} < 10$ relative units is caused as it was in the previously examined cases, by the influence of the system's noises.

The minimum of probability of detection in the field of the video signal voltage of about 40 relative units is explained by the overlapping of the laws of distribution of cloudiness and backgrounds.

The dotted curves in Figures 1, 3 and 4 are obtained from the condition that the density of the probabilities of signals from cloudiness and backgrounds correspond to the normal laws with the same mathematical expectation $\bar{V}$ and the dispersion, as in the experimental laws of distribution.

The comparison of theoretical and experimental detection curves indicates, that the theoretical calculation produces results that are too low. /107

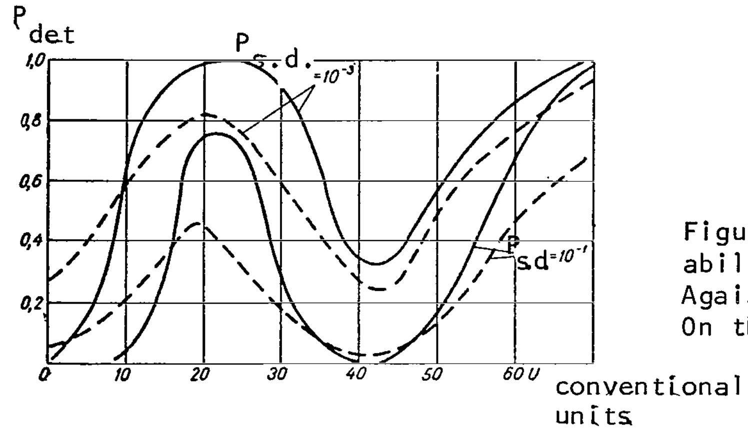

Figure 4. Dependence of the Probability of Detection of the Cyclone Against the Background of the Sea On the Video Signal Level.

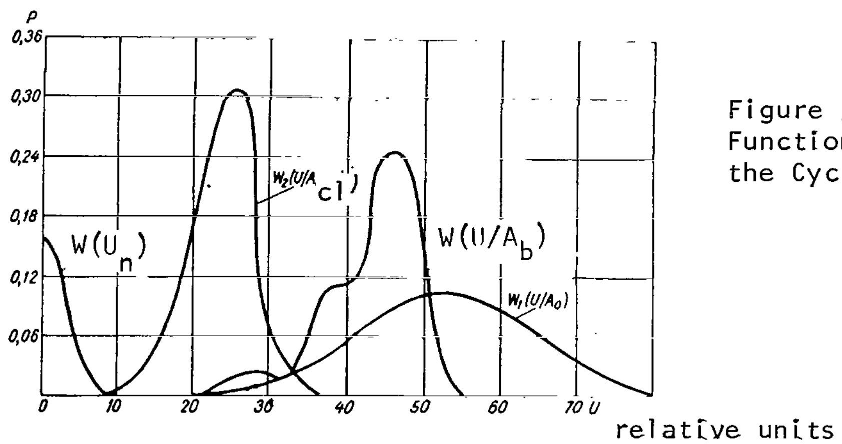

Figure 5. Autocorrelation Functions of Video Signals From the Cyclone.

REFERENCES

1. Dulevich, V. Ye. and A. A. Korostelev, *et al*, *"Fizicheskiye Osnovy Radiolokatsii* [Physical Principles of Radar]", *LVIKA*, im. *A. F. Mozhayskogo*, 1962.
2. Afanas'yev, A. A. and V. A. Gorbunov: *"Effektivnost' Obnaruzheniya Tseley Radiotekhnicheskimi Sredstvami Nablyudeniya*, [Effectiveness of Detection of Targets by Radio-Engineering Observation Facilities]", Voyenizdat Press, 1964.
3. Krasil'nikov, N. N.: "Calculation of Probability of Recognition of the Images Transmitted," *Tekhnika Kino i Televideniya*, No. 2, 1966.
4. Vimberg, G. P.; Yu. A. Dranishnikov; V. I. Ivanov and V. V. Puchkov: "Statistical Characteristics of Signals of the Scanning IR Equipment," See the present collection.

OUTGOING SHORTWAVE RADIATION FIELD ABOVE THE SEA

K. S. Shifrin and V. Yu. Kolomiytsov

ABSTRACT: The authors show, that the surface of an agitated sea is much closer to the Lambertian than to the mirror surface. The reflection in the maximum of the solar glitter (with the wind velocity of 10 m/sec.) exceeds the isotropic reflection by only a few times, whereas the decrease of the reflection upon the passage from the quiet water to waves amounts to four orders. The outgoing shortwave radiation field (OSR) above an agitated sea, as indicated by the calculations, is relatively little different from the field above the isotropically reflecting water surface, and the excess of intensity in the solar glitter does not exceed 3.5 times for all the elevations of the sun. The contribution of the diffused radiation in the OSR field above the sea is substantial in any direction and it cannot be disregarded even in the maximum of the glitter, where it is no smaller than 30%.

1. Introduction

In distinction from the smooth, watery surface, where the reflection is completely determined by the optical contents of the water, the reflection from a wavy watery surface depends substantially from the type of this surface. Considering that the surface of the sea represents a totality of areas statistically distributed according to the orientations and taking into account the reflection from each one of them according to the laws of geometrical optics, C. Cox and V. Munk [1] according to the photographs of the sun glitter from the airplane, obtain the function of distribution of the plain elements of the water surface according to the slopes. Yu. R. Mullamaa [2, 3] by means of this function examined the transformation of radiation at the boundary between the air and the sea, in particular calculated the coefficient of reflection from the sea with various velocities and directions of the wind. Using these data, G. V. Rosenberg and Yu. R. Mullamaa [4] investigated the radiation field, reflected from the sea. Disregarding the influence of the atmosphere they assumed that the outgoing shortwave radiation (OSR) field has the same structure and studied the possibilities of determination of the wind speed above the sea by observation from a satellite of the specific feature of the structure of this field, connected with the solar and lunar glitter. They base this possibility on the fact that in their opinion, the solar and lunar glitter are concentrated in a small region of angles. /108

To determine the wind velocity v G. V. Rosenberg and Yu. R. Mullamaa recommended the use of two parameters: displacement of the maximum of brightness of the glitter towards the horizon, growing rapidly with the increase of v and the transverse gradient of brightness. In Table 1 we present, according to the data of work [4], the values of θ_{max}, the angle of the maximum brightness of the glitter, in relation to v and the zenith distance of the sun i (for the mirror surface $\theta_{max} = i$).

TABLE 1

$i°$	v m/sec.				$i°$	v m/sec.			
	2	5	10	15		2	5	10	15
0	0	1,5	3,5	7	44	47	53	>90	>90
20	21	23	27	33	59	66	>90	>90	>90

Tr. Note: Commas indicate decimal points.

We shall see later, that these condsiderations on the structure of the OSR field above the sea, obtained without taking into consideration the influence of the atmosphere, require important corrections. We shall demonstrate, /109 that because of the smallness of the coefficient of reflection from the sea the relative role of dispersion in the atmosphere is quite significant. The atmosphere smooths out appreciably the anisotropy of the reflection. In the present work we shall take this influence into account. Let us note, that earlier, the problem examined was studied in work [5]. The principal purpose of our work, which was carried out in connection with the task of determination of the OSR fluxes according to the measurements from satellites, was the analysis of the influence of diffusion in the atmosphere and anisotropy of reflection on the OSR field.

2. Reflection from a Sea With Waves. Comparison with the Mirror and Isotropic Reflection

Let us examine the OSR field above the sea with a medium wind velocity (v = 10 m/sec), using the reflection coefficients $R(\theta, i, \phi)$, calculated in work [5]. The surface of the sea shall be considered isotropic, i.e., we shall not take into account the dependence of the reflection coefficient on the wind direction. To gain a concept on the anisotropy of the reflection from the real sea it is interesting to compare the isotropic mirror and real reflections from the sea. Let us examine first the mirror reflection. Here, we have

$$I_0^{dir}(\theta, i, \varphi) = \begin{cases} r(i) I_{dir}(i), & \text{if} \quad (\theta, \varphi) \in d\omega_0 \\ 0, & \text{if} \quad (\theta, \varphi) \notin d\omega_0 \end{cases} \tag{1}$$ [1]

[1]Symbol $\in$ signifies that θ and ϕ lie within a certain solid angle $d\omega_0$ around the direction $\theta = i$, $\phi = 0$.

Here $I_{dir}(i)$ and I_0^{dir} are the intensities of the direct and reflected radiation on the level of the underlying surface, r(i) is the Fresnel's energy coefficient for water.

On the other hand, according to the determination of the reflection coefficient

$$I_0^{dir}(\theta, i, \varphi) = R(\theta, i, \varphi) E_{dir}(i), \tag{2}$$

where $E_{dir}(i)$ is the illuminance by direct radiation. This illuminance is determined by the formula

$$E_{dir}(i) = I_{dir}(i) \cos i \, d\omega_0. \tag{3}$$

Substituting (3) in (2) and comparing with (1)

$$R(\theta, i, \varphi) = \begin{cases} \frac{1}{d\omega_0} \frac{r(i)}{\cos i}, & (\theta, \varphi) \in d\omega_0, \\ 0, & (\theta, \varphi) \notin d\omega_0 \end{cases} \tag{4}$$

Since the angular dimension of the sun $2\alpha = 32'$, then

$$d\omega_0 = 4\pi \sin^2 \frac{\alpha}{2} = \pi\alpha^2 = 6.81 \cdot 10^{-5} \text{ steradian.} \tag{5}$$

The value of Fresnel's energy coefficient for water (n = 1.34) and R coefficient are given in Table 2 (second and third lines).

TABLE 2.

$i°$	0	20	40	60	80
$r(i)$	0,02	0,02	0,025	0,06	0,35
$10^{-2} \cdot R(i,i,0)$ 1/ster	2,9	3,1	4,7	18	310
$A(i)$	0,027	0,028	0,034	0,064	0,22
$10^{2} \cdot R_v(i,i,0)$ 1/ster	3,4	3,6	7,0	40	1000

Tr. note: Commas indicate decimal points.

The comparison of these values with the values of the reflection coefficient from a wavy sea, given in [5], indicates, that in the presence of waves the brightness of the solar glitter in the maximum is four orders smaller than in the case of mirror reflection. The same circumstances may be formulated in a different way also: for the quiet sea all the reflected radiation is concentrated inside the solid angle $d\omega_0$ around the direction $\theta = i$, $\phi = 0$, then for the /110 wavy sea (v = 10 m/sec) in the solid angle only one ten thousandths of the reflected radiation is concentrated. Indeed, multiplying the left- and right members of the equation (2) by cosine θ and integrating with respect to the arbitrary solid angle $\omega \leq 2\pi$ we obtain

$$A_{\omega}=\int_{(\omega)} R(\theta,\ i,\ \varphi)\cos\theta\, d\omega, \tag{6}$$

where A_{ω} is the relationship of the energy reflected in the solid angle to $E_{dir}(i)$. The value

$$\frac{A_{\omega}}{A}=\frac{\int_{\omega} R(\theta,\ i,\ \varphi)\cos\theta\, d\omega}{\int_{(2\pi)} R(\theta,\ i,\ \varphi)\cos\theta\, d\omega} \tag{7}$$

signifies the share of the energy, reflected in the solid angle ω $\left(\frac{A_{\omega}}{A}\to 1,\right.$ when $\left.\omega\to 2\pi\right)$. Hence for the solid angle $d\omega_0$ around the direction ($\theta = i$, $\phi = 0$) we have

$$\frac{A_{d\omega_0}}{A}=\frac{1}{A(i)}R(i,\ i,\ 0)\cos i\, d\omega_0. \tag{8}$$

If you have a mirror reflection, then $A(i) = r(i)$, $R(i, i, 0)$ is expressed by the formula (4) and $A_{d\omega_0}/A = 1$, just as it should be.

For a wavy sea with the wind velocity of 10 m/sec., the magnitudes of value $R_v(i,i,0)$ and the direct radiation albedo $A(i) = \int_{(2\pi)} R(\theta, i, \varphi)\operatorname{cs}\theta d\omega$ is taken from work [5]. They are indicated in the 4th and 5th lines of Table 2.

Substituting all the values in formula (8) we obtain for all the i

$$\frac{A_{d\omega_0}}{A}\approx 10^{-4}, \tag{9}$$

i.e., the reflection from the wavy sea differs very much from the mirror reflection. This is also verified by the direct examination of function

(θ, i, ϕ). From the data of work [5] it follows, that the coefficient of reflection decreases smoothly and rather slowly upon the deivation from the direction, corresponding to the maximum reflection. Thus, for example, the region of angles for which the reflection coefficient decreases only two times with respect to the maximum value, amounts approximately to: from 0 to 45° with respect to θ and from -30 to +30° with respect to ϕ when i = 20° from 30 to 90° with respect to θ and from -15 to +15° with respect to ϕ when i = 40°. These regions of the angles form solid angles, equal to 0.30 and 0.45 steradian for i = 20° and for i = 40°, respectively, the last digit having to be increased at the expense of a part of the glitter located beyond the horizon (when i = 40° the reflection maximum lies near the horizon).

Let us take a circular cone with an opening of $2\theta_0$ and an axis directed along the mirror ray. Let us designate the solid angle at the apex of the cone with ω. Let us introduce the system of coordinates, connected with the axis of the cone. Then, for the directions, lying within ω, $0 \leq \theta \leq \theta_0$, $0 \leq \phi \leq 2\pi$; let γ be the angle between the arbitrary ray within the ω and the normal $\vec{n}$ to the surface at the point, where the apex of the cone is located, /111

$$\cos\gamma = \cos\theta\cos i + \sin\theta\sin i\cos\varphi. \tag{10}$$

With the new designations formula (7) will assume the following appearance

$$\frac{A_\omega}{A} = \frac{\overline{R}}{A}\int_0^{2\pi} d\varphi \int_0^{\theta_0} \cos\gamma\sin\theta\, d\theta = \frac{\overline{R}}{A}\pi\cos i\sin^2\theta_0. \tag{11}$$

Here $\overline{R}$ is the certain average value of the reflection coefficient for the solid angle ω. In the case of the isotropic reflection

$$\overline{R} = R = \frac{A}{\pi} \quad \text{and} \quad \left(\frac{A_\omega}{A}\right)_{is} = \cos i\sin^2\theta_0. \tag{12}$$

Let i = 20°, θ_0 = 20°, then according to formulas (11) and (12) we find

$$\frac{A_\omega}{A} \approx 0.35, \quad \left(\frac{A_\omega}{A}\right)_{is} = 0.11. \tag{13}$$

The evaluations performed indicate, that inside our cone the reflection from the wavy sea exceeds the isotropic reflection by only several times, whereas in passing from quiet water to waviness the reflection is decreased by four orders. This signifies, that the surface of the sea is much closer to the Lambertian than to the mirror type. In this wave the "solar glitter" occupies quite a large section of the angles (and not a small one as claimed in work [4]) it does not have a sharply expressed maximum, especially with wind velocities $v > 5$ m/sec, and low lying sun, when the maximum lies near the horizon or even goes beyond the horizon (see Table 1), and finally, when $v = 10$ m/sec., the brightness of the glitter with respect to the order of magnitude is comparable with the brightness of the isotropically reflecting sea with the same albedo. Let us note that the displacement of the maximum with the solar glitter towards the horizon is closely related with the increase of its angular dimensions. Indeed, upon the appearance of wind the maximum is deflected from the direction of the mirror ray towards greater angles, because the reflected radiation begins to receive a considerable contribution by the tilted platforms owing to the growth of the Fresnel's reflection coefficient with the increase of the angle of incidence. The same circumstance results in a blurring of the glitter, since the reflection, increasing with angles of $\theta > i$ and $\phi \approx 0$, decreases in the mirror direction rather slowly because, although the reflection from the horizontal areas is smaller, their number is greater than that of the tilted ones. Moreover, the purely geometrical factor increases the angular dimensions of the solar glitter. This follows from the well known fact upon the turn of the mirror by an angle α the reflected ray turns by an angle of 2α. Therefore, if the slopes of the areas of the water surface lie within the bounds of 0 to $\pm\alpha$, the reflected light occupies the region of angles

$$i - 2\alpha \leqslant \theta \leqslant i + 2\alpha.$$

3. System for Calculating the OSR Field /11

In work [6] we show that the diffused radiation field above the sea is equivalent to the field above the Lambertian surface with a direct radiation albedo

$$A = A(i) = \int_{(2\pi)} R(\theta, i, \varphi) \cos\theta \, d\omega. \tag{14}$$

Let us note at once, that for water in the shortwave region of the spectrum, we can disregard the dependence of the complex index of refraction on the wavelength, therefore the reflection coefficient $R(\theta, i, \phi)$ and albedo $A(i)$ are constant in the entire spectral range of $0.4\ \mu \leq \lambda \leq 2.5\ \mu$. Upon the change of the wind velocity, integral (14) will change less than function $R(\theta, i, \phi)$, moreover, as we have mentioned in work [6], the influence of the albedo on the dispersed radiation, because of its smallness, is insignificant. Therefore, with good substantiation we can consider, that upon the change of the wind velocity only the reflection of the direct radiation is changed, while the diffused radiation with all velocities is determined by the values of the albedo for $v = 10$ m/sec. (see Table 2). As for reflection of diffused radiation from the sea surface, inasmuch as it falls on the surface at a wide solid angle (from the half sphere), the anisotropy of its reflection will be much smaller than in direct radiation. Therefore, we shall consider that the diffused radiation is deflected isotropically with the albedo $A_p = 0.066$, equal to the albedo of the uniformly luminescent sky above the mirror-like reflecting water. Taking the above into account, for the spectral intensity of reflection on the upper boundary of the atmosphere I_{ab} we have

$$I_{ab}(\lambda, \theta, \varphi, i) = I_0^{dir}(\lambda, \theta, \varphi, i) + I_0^{H}(\lambda, \theta, i) + I_D(\lambda, \theta, \varphi, i). \tag{15}$$

Here

$$I_0^{dir}(\lambda, \theta, \varphi, i) = R(\theta, \varphi, i) E_{dir}(\lambda, i) T(\lambda, \theta) \Big|_0^{\infty} \tag{16}$$

the reflected direct radiation

$$I_0^{H}(\lambda, \theta, i) = \frac{0.066}{\pi} E_H(\lambda, i) T(\lambda, \theta) \Big|_0^{\infty} \tag{17}$$

is the reflected radiation of the sky,

$I_D(\lambda, \theta, \phi, i)$ is the brightness of the haze on the upper boundary. We add, that in formulas (16) and (17) the designations are: $E_H(\lambda, i)$ is the illuminance of the surface of the sea with diffused light,

$$E_{dir}(\lambda, i) = I_0(\lambda) T(\lambda, i) \Big|_0^{\infty} \cos i \tag{18}$$

is the flow of directed radiation through the horizontal area on the level of the underlying surface, $T(\lambda, \theta) \Big|_0^{\infty}$ are spectral functions of transmission in the direction of θ towards the zenith, $I_0(\lambda)$ are spectral values of a solar constant (see for example [7]).

We shall not give formulas for functions I_D and E_H, obtained for the standard radiation model of the atmosphere in works [8], [9], and will note only that both values are calculated when $A = A(i)$. Integrating with respect the spectrum the relationships (15)-(17), we find the OSR field on the upper boundary of the atmosphere above the sea: /113

$$I_{ab}(\theta, \varphi, i) = I_0^{dir}(\theta, \varphi, i) + I_0^{H}(\theta, i) + I_D(\theta, \varphi, i), \tag{19}$$

$$I_0^{dir}(\theta, \varphi, i) = R(\theta, \varphi, i)\int_{0,4}^{2,5} E_{dir}(\lambda, i)T(\lambda, \theta)\Big|_0^{\infty} d\lambda, \tag{20}$$

$$I_0^{H}(\theta, i) = \frac{0{,}066}{\pi}\int_{0,4}^{2,5} E_{H}(\lambda, i)T(\lambda, 0)\Big|_0^{\infty} d\lambda. \tag{21}$$

Let us stress once again, that on the coefficient of reflection, and consequently on the wind velocity depends only the reflected direct radiation, the calculation of which with known coefficients of reflection and the functions of transmission of the atmosphere is not difficult at all. The values of the integral brightness of the haze I_D, and also the functions I_0^H were obtained on the basis of the numerical calculations, performed by us in [9].

In Table 3 we give the values of the OSR field on the upper boundary of the atmosphere above the sea with v = 10 m/sec; the corresponding flows

$$F_{ab}(i) = \int_{(2\pi)} I_{ab}(\theta, \varphi, i)\cos\theta\, d\omega \tag{22}$$

and the albedo, adopted in the calculation of diffused radiation, are given in Table 4.

TABLE 3. INTEGRAL OSR FIELD ON THE UPPER BOUNDARY OF THE ATMOSPHERE ABOVE THE SEA $I_{ab}(\theta, i, \phi)$ cal/cm^2·min·ster.

φ	i = 20°, θ = 0	i = 20°, θ = 30	i = 20°, θ = 60	i = 40°, θ = 0	i = 40°, θ = 45	i = 40°, θ = 60
0	0,0389	0,0518	0,0349	0,0245	0,0689	0,0703
30		0,0442	0,0325		0,0389	0,0374
90		0,0272	0,0305		0,0258	0,0311
180		0,0266	0,0331		0,0287	0,0337

φ	i = 60°, θ = 0	i = 60°, θ = 45	i = 60°, θ = 75	i = 80°, θ = 0	i = 80°, θ = 45	i = 80°, θ = 75
0	0,0175	0,0651	0,282	0,0106	0,0303	0,466
30		0,0287	0,0745		0,0193	0,0989
90		0,0216	0,0402		0,0126	0,0276
180		0,0266	0,0508		0,0142	0,0348

Tr. note: Commas indicate decimal points.

TABLE 4.

i^o	20	40	60	80
$F F_{ab}$ cal/cm^2 min .	0,102	0,102	0,101	0,075
$A(i)$	0,028	0,034	0,064	0,22

Tr. Note: Commas indicate decimal points.

4. The Solar Glitter on the Upper Boundary of the Atmosphere. Comparison with the Lambertian Sea. /114

The calculations performed indicate the relatively slow angular variations of the intensity of the outgoing shortwave radiation and the absence of sharply expressed maxima, which agrees quite well with analysis of the coefficient of reflection of the sea (see S2).. Inasmuch as the anisotropy of the OSR field above the sea is called not only by the presence of the "solar glitter", but also by the diffusion in the atmosphere, to separate these factors it is sensible to carry out the comparison of the results obtained (Table 3) with the OSR field above the Lambertian Sea with the same albedo. More precisely, because the solar glitter is caused by the reflection of only direct radiation, the case of the Lambertian Sea will be obtained, by replacing $R(\theta,\phi,i)$ in formula (20) by $A(i)/\pi$,

$$I_0^{\prime\mathrm{dir}}(\theta, i) = \frac{A(i)}{\pi} \int_{0,4}^{2,5} E_{\mathrm{dir}}(\lambda, i) T(\lambda, \theta) \Big|_0^{\infty} d\lambda. \qquad (23)$$

Inasmuch as the other components of the field do not depend on the type of the coefficient of reflection, for the integral intensity of the outgoing radiation on the upper boundary of the atmosphere above the Lambertian Sea, we have

$$I'_{ab} = I_0^{\prime\mathrm{dir}} + I_0^{\mathrm{H}} + I_D. \qquad (24)$$

The comparison of intensities of I_{ab} and I'_{ab} makes it possible for us to judge on the contribution of the unisotropy of reflection in the OSR field. In Table 5 we gave the relationship of these values $F_i(\theta,\phi) = I_{ab}/I'_{ab}$, and also the mean value $\overline{f}_i$ and dispersion σ for each i.

TABLE 5. Comparison with the Lambertian Sea

$$f_i(\theta, \varphi) = \frac{I_{ab}(\theta, i, \varphi)}{I'_{ab}(\theta, i, \varphi)}$$

φ	$i=20°$, $\bar{f}=1{,}06$, $\sigma=0{,}27$			$i=40°$, $\bar{f}=0{,}961$, $\sigma=0{,}29$		
	θ			θ		
	0	30	60	0	45	60
0	1,30	1,79	0,980	0,851	2,24	1,96
30		1,53	0,913		1,26	1,04
90		0,901	0,838		0,806	0,852
180		0,806	0,846		0,822	0,862

φ	$i=60°$, $\bar{f}=0{,}915$, $\sigma=0{,}40$			$i=80°$, $\bar{f}=0{,}860$, $\sigma=0{,}35$		
	θ			θ		
	0	45	75	0	45	75
0	0,735	2,06	2,79	0,716	1,16	3,40
30		0,963	0,960		0,843	0,979
90		0,785	0,918		0,764	0,920
180		0,818	0,934		0,784	0,933

Tr. Note: Commas indicate decimal points.

From Table 5 we can see that the brightness field above the real sea differs relatively little from the field above the isotropically reflecting water surface, while the excess of the intensity in the solar glitter does not /115
exceed 3-3.5 times for all the i. The OSR flows for both cases practically coincide. The absence of a sharp change of the field upon the replacement of the isotropic reflection of the solar glitter is explained on the one hand by the rapid blurring of the glitter upon the passage from the quiet sea to the wavy sea, and on the other hand by the smallness of the albedo of the sea, which makes a substantial contribution to the diffused radiation, screening the direct radiation reflected. The latter circumstance is illustrated in Table 6, in which we give the relationship between the brightness (dependent only on the diffusion in the atmosphere) and the full intensity of the outgoing radiation. It is characteristic, that the contribution of the diffused radiation to the OSR field is substantial under any angles i, θ and ϕ and it cannot be disregarded even in the maximum of the glitter, where it is less than 30%. Hence it follows, that with the growth of the albedo of the underlying surface there will be an increase of the sensitivity of the OSR field towards the unisotropy of the reflection, inasmuch as the contribution of the diffused radiation will drop.

Upon the comparison of functions I_{ab} and I'_{ab} we are struck by the absence of the qualitative differences in their behavior with medium and large zenith distances of the sun and the presence of the maximum of function I_{ab} with small i (Figures 1 and 2). This is explained by the displacement of the maximum of the solar glitter to the horizon and its blurring. Actually, with

$i \geq 40°$ the maximum of the coefficient of reflection lies beyond the horizon, and therefore the intensity of the radiation increases monotonously with the increase of θ in the azimuth of the mirror ray ($\phi = 0$).

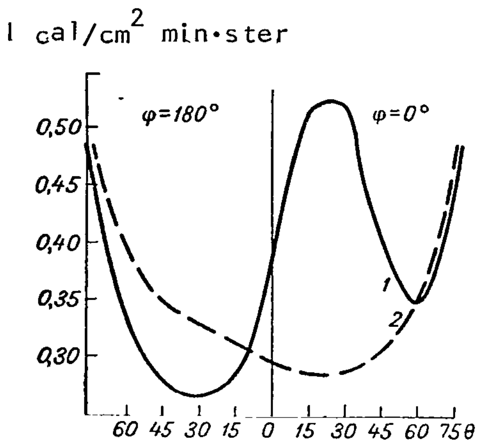

Figure 1. Brightness of the Outgoing Radiation (Zenith Distance of the Sun is 20°). 1, I_{ab}; 2, I'_{ab}.

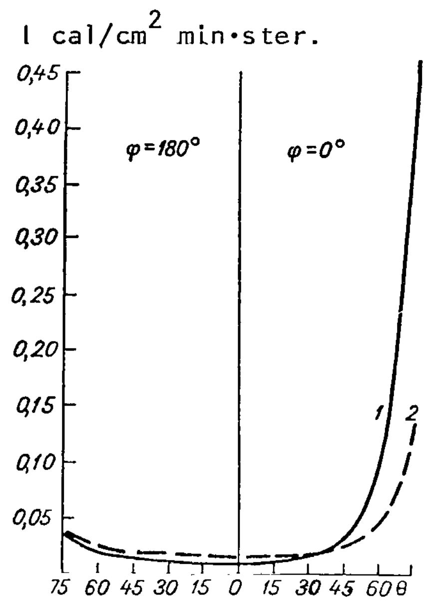

Figure 2. Brightness of the Outgoing Radiation (Zenith Distance of the Sun is 80°). The conventional designations are the same as in Figure 1.

Even for small zenith distances of the sun, when the glitter is located far from the horizon, and its maximum may be fixed, we do not observe a sharp drop in intensities. Thus, with $i = 20°$, the ratio between the maximum and the minimum brightnesses amounts to about 0.5, and that only with small θ (see Figure 1), with larger θ however, the glitter "does not have enough time" to reach the minimum because of the increasing role of the haze, therefore this ratio increases to 0.67. Let us note /116
that in the solar vertical the angular dimensions of the glitter (from minimum to minimum) amounts to 60°. It is necessary to bear in mind that inasmuch as the OSR flows above the Lambertian and the real sea practically coincide, the change in the brightness indicatrix with a fixed albedo results only in the redistribution of the intensity of the outgoing radiation according to the angles. This is reflected in the fact of intersection of the surfaces $I_{ab}(\theta,\phi)$ and $I'_{ab}(\theta,\phi)$ for any i.

TABLE 6. CONTRIBUTION OF THE DISPERSED RADIATION IN THE OSR FIELD ABOVE THE SEA. $I_r/I_{ab} = I_0^H + I_D/I_{ab}$, v = 10 m/sec.

φ	$i=20°$ θ 0	$i=20°$ θ 30	$i=20°$ θ 60	$i=40°$ θ 0	$i=40°$ θ 45	$i=40°$ θ 60
0	0,573	0,417	0,849	0,886	0,351	0,430
30		0,486	0,911		0,625	0,810
90		0,842	0,997		0,988	0,994
180		0,966	1,00		0,990	0,994

φ	$i=60°$ θ 0	$i=60°$ θ 45	$i=60°$ θ 75	$i=80°$ θ 0	$i=80°$ θ 45	$i=80°$ θ 75
0	0,989	0,395	0,346	1,00	0,733	0,290
30		0,833	0,993		0,984	1,00
90		1,00	1,00		1,00	1,00
180		1,00	1,00		1,00	1,00

Tr. Note: Commas indicate decimal points.

REFERENCES.

1. Cox, C. and C. Munk: "Slopes of the Sea Surface Deduced from Photographs of Sun Glitter," *Bull. Scripps, Inst. Oceanogr.*, Vol. 6, p. 401, 1956.
2. Mullamaa, Yu. R.: "Diffused Reflection and Transmission of Flight by the Uneven Surface of Two Isotropic Media," Investigation on the Physics of the Atmosphere. *IFA AN ESSR*, No. 3, 1962.
3. Mullamaa, Yu. R.: *"Atlas Opticheskikh Kharakteristik Vzvolonovannoy Poverkhnosti Morya"*, [Atlas of the Optical Characteristics of a Wavy Surface of the Sea], IFA AN ESSR, 1964.
4. Rosenberg, G. V. and Yu. R. Mullamaa: "On Certain Possibilities of Determination of Wind Velocities Above the Oceanic Surface According to Observations from a Satellite," *Kosmicheskiye Issledovaniya*, Vol. 2, 1964.
5. Avaste, O. A. and Yu. R. Mullamaa and K. S. Shifrin: "The OSR Field in the Nonorthotropic Underlying Surface," Investigations on the Physics of the Atmosphere, *IFA AN ESSR*, No. 6, 1964.
6. Shifrin, K. S. and V. Yu. Kolomiytsov: "Methods of Calculations of the Fields of Shortwave Radiation During Unisotropic Reflection from the Underlying Surface," See the present collection.
7. Shifrin, K. S. and N. P. Pyatovskaya: *"Tablitsy Naklonnoy Dal'nosti Vidimosti"*, [Tables of the Slant Range of a Visibility], Gidrometeyoizdat Press, Leningrad, 1959.
8. Shifrin, K. S.; I. N. Minin: "On the Theory of Nonhorizontal Visibility," *Trudy GGO*, Issue 68, 1957.
9. Shifrin, K. S.; V. Yu. Kolomiytsov and N. P. Pyatovskaya: "Determination of the OSR Flow by Means of Satellites," *Trudy GGO*, Issue 166, 1964.

CONTRIBUTION OF DIFFUSED REFLECTION BY THE WATER LAYER TO THE OUTGOING SHORTWAVE RADIATION FIELD

V. Yu. Kolomiytsov

ABSTRACT: The author proposes an approximate method of determination of the diffused radiation by the infinite thickness of water. It is based on the use of a great elongation of the diffusion indicatrix and complete internal reflection. It is calculated using the data on the albedo of the sea, and the radiation field in the atmosphere, caused by the diffusion in the water layer. The addition to the flows of outgoing shortwave radiation from this field amounts to 7-8%.

In work [6] we examined the structure of a beam of radiation, reflected from the wavy surface of the sea. Along with this, a certain contribution to the OSR field is also introduced by the radiation beam, emerging from the depth of the sea. In the terminology of work [1] in the first case they are speaking about the "external" and in the second about the "internal" reflection. In the present work we shall evaluate this second beam, originating through the diffusion of radiation on the turbidity elements. Let us note, first of all that in the spectral range interesting to us (0.3-4 μ) the water possesses a quite variable coefficient of absorption with respect to the spectrum, having a minimum of about 0.5 μ and growing rapidly towards greater and smaller wavelengths. Therefore, solar radiation passing through the water surface is absorbed in it completely in the ultraviolet and infrared regions of the spectrum and the diffused radiation field in its layer, and consequently the outgoing radiation, are concentrated only in the visible region of the spectrum. For the solution of the problem examined it is necessary to know the sea water diffusion indicatrix $\kappa(\gamma)$ and the parameter $\lambda = \rho/\alpha$, where ρ is the coefficient of diffusion, α is the coefficient of extinction (weakening) of the water. /117

The measurement of these values involves great difficulties. Most of the hydrooptical measurements of water constants are reduced to determination of the coefficient of extinction α either directly or through the values of the depth of disappearance of the Secchi disk. Little is contributed also by the theoretical calculations, pertaining to the optically empty water (i.e., to water devoid of finely suspended solids). Schematical measurements of indicatrices of diffusion of natural water were carried out by A. A. Gershun [2]. Different specimens of river and sea water yielded approximately the same angular variations of intensity of diffusion with a sharp increase in the region of small angles. However, the method used by A. A. Gershun made it possible to carry out measurements in the region of diffusion angles γ from 10 to 165°, which is insufficient for obtaining a standard diffusion indicatrix even for these angles, since the diffusion proceeds mainly in the direction of the incident beam, and no independent measurements of the diffusion coefficient ρ were performed. In the literature data are given on the diffusion indicatrices for γ from 0.5 to 145°, as well as values of parameter λ (for a number of water reservoirs). The diffusion forward exceeds the diffusion backwards by five orders into the first hemisphere about 97 to 98% of the light is diffused, and into the cone with an angle of 10° more than 50%. The values of coefficients ρ and α, measured at various points or in a single point, but at different times (after several days), differ by several times. In accordance with this $\lambda - \rho/\alpha$ also changes abruptly. Moreover, parameter λ has a clearly expressed spectral course, which also differs for various points. The matter stands somewhat better with the diffusion indicatrix: it is relatively stable, practically identical for fresh and salt water (the diffusion is determined by the suspended solids and not by the dissolved salts) and changes insignificanly with respect to the spectrum. However, the accuracy of the indicatrix values given is not high and the measurement error (without taking into account the method error) reaches 30%. As for the measurement of optical constants of oceanic waters, we have heard nothing about them. Thus, we do not possess any at all reliable experimental data averaged from a vast amount of material, on the required optical constants of the marine and especially oceanic waters. /118

Let us now turn to the theoretical side of the problem. For the plane-parallel nonuniform medium (λ and $\kappa(\gamma)$ depend on the optical depth) illuminated by a plane wave, the solution of the transfer equation represents an extremely complex problem. Therefore we shall consider the sea to be an infinite isotropic and uniform medium with a plane boundary. But even in this case, if we do not take into account the reflection of the diffused radiation from the water-air boundary back into the medium, the correct determination of the brightness coefficient (and consequently, of the outgoing radiation), as it had been noted in [3], is reduced to the numerical solution of the system $(n + 1)(n + 2)/2$ of integral equations, where $(n + 1)$ is the number of terms in the expansion of the diffusion indicatrix according to Legendre's polynomials. Evidently, this approach clearly does not vindicate itself because of the great elongation of the indicatrix.

We shall examine the approximate merit of solution of the transfer equation using the great elongation of the diffusion indicatrix.

Let us assume, that after refraction on the flat separation surface the solar rays enter the water layer at an angle of θ_0. We designate with πS the illuminance of the area on the upper boundary of the medium ($\tau = 0$)

perpendicular to the rays. We write the transfer equation in the form of a system of integral-differential equations for values $I_1(\tau,\theta,\phi)$ (downward radiation) and $I_2(\tau,\vartheta,\ \phi$ (upward radiation):

$$\cos\theta\,\frac{dI_1(\tau,\ \theta,\ \varphi)}{d\tau}=-I_1(\tau,\ \theta,\ \varphi)+\lambda\left\{\int_0^{2\pi}d\varphi'\int_0^{\frac{\pi}{2}}I_1(\tau,\ \theta',\ \varphi')\,\frac{x(\gamma^+)}{4\pi}\sin\theta'\,d\theta'+\right.$$
$$\left.+\int_0^{2\pi}d\varphi'\int_0^{\frac{\pi}{2}}I_2(\tau,\ \vartheta'\ \varphi')\,\frac{\varkappa(\gamma^-)}{4\pi}\sin\vartheta'\,d\vartheta'\right\}+\frac{\lambda S}{4}\varkappa(\gamma_1^+)\,e^{-\tau\sec\theta_0}, \tag{1}$$

$$-\cos\vartheta\,\frac{dI_2(\tau,\ \vartheta,\ \varphi)}{d\tau}=-I_2(\tau,\ \vartheta,\ \varphi)+$$
$$+\lambda\left\{\int_0^{2\pi}d\varphi'\int_0^{\frac{\pi}{2}}I_2(\tau,\ \vartheta',\ \varphi')\,\frac{\varkappa(\gamma^+)}{4\pi}\sin\vartheta'\,d\vartheta+\int_0^{2\pi}d\varphi'\int_0^{\frac{\pi}{2}}I_1(\tau,\ \theta',\ \varphi')\,\frac{\varkappa(\gamma^-)}{4\pi}\sin\theta'\,d\theta'\right\}+$$
$$+\frac{\lambda S}{4}\varkappa(\gamma_1^-)\,e^{-\tau\sec\theta_0}. \tag{2}$$

Here /119

$$\left.\begin{aligned}\cos\gamma^+&=\cos\theta\cos\theta'+\sin\theta\sin\theta'\cos(\varphi-\varphi')\\ \cos\gamma^-&=-\cos\theta\cos\vartheta'+\sin\theta\sin\vartheta'\cos(\varphi-\varphi')\\ \cos\gamma_1^+&=\cos\theta\cos\theta_0+\sin\theta\sin\theta_0\cos\varphi\end{aligned}\right\} \tag{3}$$

The boundary conditions have the following appearance:

$$\left.\begin{aligned}&I_1(0,\ \theta,\ \varphi)=R'(\theta)\,I_2(0,\ \vartheta,\ \varphi)|_{\vartheta=\theta}\\ &I_2(\infty,\ \vartheta,\ \varphi)=0,\ \theta,\ \vartheta<\frac{\pi}{2}\end{aligned}\right\} \tag{4}$$

where $R'(\theta)$ is Fresnel's energy coefficient for reflection in water from the water-air boundary.

The system of equations (1), (2) contains two types of integral terms. In the one integration is performed with respect to the region of small angles of diffusion including the zero angle (integrals, containing $x(\gamma^+)$, the others include large angles of dispersion (integrals with $x(\gamma^-)$). We shall consider that the diffusion indicatrix has a sharp maximum with the diffusion angle, equal to zero, which provides for a diffusion of 95-98% of the light into the front hemisphere, and a small constant value at all angles of diffusion, except for the region close to zero. Then we can carry out the intensity in the direction of the zero angle of diffusion beyond the sign of the integrals containing $x(\gamma^+)$, and in the integrals with large angles of diffusion we remove the constant value

$$x(\gamma^-) = x_0 = 2h \tag{5}$$

and for integral members of equation (1) we obtain

$$\left.\begin{aligned}
&\int_0^{2\pi} d\varphi' \int_0^{\frac{\pi}{2}} I_1(\tau,\theta',\varphi') \frac{x(\gamma^+)}{4\pi} \sin\theta' \, d\theta' = I_1(\tau,\theta,\varphi)(1-h) \\
&\int_0^{2\pi} d\varphi' \int_0^{\frac{\pi}{2}} I_2(\tau,\vartheta',\varphi') \frac{x(\gamma^-)}{4\pi} \sin\vartheta' \, d\vartheta' = h I_2(\tau)
\end{aligned}\right\} \tag{6}$$

Here $I_2(\tau)$ is the mean value of intensity I_2 at level τ. Value h characterizes the share of radiation, diffused into the rear hemisphere in a single act of diffusion and in our case does not exceed several hundred. The integral terms of equation (2) are converted to the analogous form.

Let us remind the reader, that we are interested in only the radiation going out into the atmosphere. But because of the full internal reflection radiation I_2, going at angles of $\vartheta > \arcsin\frac{1}{n} = 49^\circ$ $(n = 1{,}33)$, will not go outside. Therefore, it is sufficient for us to know the solution of equation (2) with $\vartheta < 49^\circ$. And this in its turn, signifies that angle γ^- included in it is not smaller than 90 - 49 = 41°. The latter circumstance is very favorable, inasmuch as it makes the assumption (5) much more precise. Moreover, it is easy to see that $\theta_0 < 49^\circ$ and $\gamma_1^- > 180 - 2 \cdot 49 = 82^\circ$, and therefore we may consider that $x(\gamma_1^-) = 2h$. Substituting expressions (6) in equations (1) and (2) and presenting each of the intensities in the form of the sum of two components, /120 one of which yields the solution of the problem examined in the assumption that single dispersion occurs with a real indicatrix, and multiple diffusion beginning with the second order, is reduced to the forward diffusion, we shall find having performed cumbersome but not complicated operations the solution of the problem on diffused reflection of light by a flat layer of an infinitely large optical thickness with a greatly elongated diffusion indicatrix:

$$I_2(0,\vartheta) = \frac{\lambda s h \cos\theta_0}{4} \left[\frac{2}{\cos\theta_0 (1-\lambda) + \cos\vartheta} + \lambda J \right], \tag{7}$$

where

$$J = \frac{2\cos\vartheta}{[\cos\vartheta + \cos\theta_0(1-\lambda+\lambda h)]\,[(1-\lambda)(\cos\vartheta+\cos\theta_0)+\lambda h\cos\theta_0]} \times$$

$$\times\left(1 - \frac{\pi h\lambda\cos\vartheta}{(\pi\cos\vartheta+2)(1-\lambda+\lambda h)}\right)+$$

$$+h\left(\frac{1}{\left[\cos\theta_0(1-\lambda)+\frac{2}{\pi}\right]\left[(1-\lambda)\left(\frac{\pi}{2}\cos\vartheta+1\right)+\lambda h\right]} - \right. \tag{8}$$

$$\left. - \frac{2\cos\theta_0}{[\cos\theta_0(1-\lambda)+\cos\vartheta]\,[(1-\lambda+\lambda h)\cos\theta_0+\cos\vartheta]}\right).$$

$I_2(0,\vartheta)$ is the radiation approaching from below to the water surface, while value s included in it characterizes the refracted solar radiation, going at an angle θ_0 to the normal. Let i be the zenith distance of the sun, $E\perp$ be the luminance of an area perpendicular to the rays, located in the air at the water surface level when the radiation passes through the air-water boundary $E\perp$ will change by $E'\perp = \pi s$, and i by θ_0.

From the law of conservation of energy it follows that

$$E'_{\perp}\cos\theta_0 = E_{\perp}\cos i\,(1 - R(i)], \tag{9}$$

where R(i) is the Fresnel's energy coefficient for reflection from water in air. Hence

$$s(i) = \frac{E'_{\perp}}{\pi} = \frac{E_{\perp}(i)}{\pi}\,\frac{\cos i}{\cos\theta}\,[1 - R(i)], \tag{10}$$

angles i and θ_0 are connected by the law of refraction

$$\sin i = n\sin\theta_0, \tag{11}$$

n is the refractive index of water,

$$E_{\perp}(i) = I_0(\lambda)\,e^{-\tau_0(\lambda)\sec i}, \tag{12}$$

$I_0(\lambda)$ is the solar constant, $\tau_0(\lambda)$ is the optical thickness of the atmosphere for the given wavelength. As we know, upon passage of light through the plane boundary between two medium there is the following relationship:

$$\frac{I_2(\theta_2)}{n_2^2} = \frac{I_1(\theta_1)}{n_1^2}[1 - R_1(\theta_1)] = \frac{I_1(\theta_1)}{n_1^2}[1 - R_2(\theta_2)]. \tag{13}$$

Here n_1 and n_2 are indices of refraction of media 1 and 2, $I_1(\theta_1)$ is the brightness of the light falling on the boundary, in medium 1, $I_2(\theta_2)$ is the brightness of the light passing into medium 2, $R_1(\theta_1)$ and $R_2(\theta_2)$ are Fresnel's coefficients for media 1 and 2.

Let us designate with I $(0,\theta)$ the radiation coming out of the water into the atmosphere at an angle θ to the normal (angle θ has nothing in common with the one used previously). Applying equation (13) to our problem we shall have /121

$$I(0, \theta) = \frac{I_2(0, \vartheta)}{n^2}[1 - R(\theta)], \tag{14}$$

where $n \sin \vartheta = \sin\theta$. Substituting in (14) the formulas (7), (10), and (12), we find the expression for the spectral intensity of the radiation leaving the sea

$$I_\lambda(0, \theta) = I_0(\lambda) e^{-\tau_0(\lambda)\cdot\sec i} \frac{[1 - R(\theta)][1 - R(i)]\cos i\,\lambda h}{4\pi n^2} \times$$
$$\times \left[\frac{2}{\cos\theta_0(1 - \lambda) + \cos\vartheta} + \lambda J\right]. \tag{15}$$

Here we should not confuse the wavelength λ with parameter λ, characterizing the relationship between the dispersion and absorption in the layer of water. Values λ and h are functions of the wavelength, knowing which we would be able to integrate the solution obtained, and obtain the integral outgoing radiation. However, as we have already mentioned, the required functions are unknown to us and we may found only on the approximate quantitative evaluations. Therefore, we consider that λ and h are constant, $\tau_0(\lambda) = \tau_0\ (0.55\ \mu) = 0.3$ and the spectral variations are connected only with the changes of the solar constant with respect to the spectrum. Taking into account, that the diffused radiation in the layer of water is concentrated in the visible region, and that $\int_{0,4}^{0,75} I_0(\lambda)d\lambda = 863\cdot 10^{-3}$ cal/cm^2 min, we obtain the integral value of the intensity of the radiation leaving the sea is 10^{-3} cal/cm^{2}min·ster

$$I(0) = 863\,\frac{[1 - R(\theta)][1 - R(i)]\cos i e^{-0,3\sec i}}{4\pi n^2}\lambda h\left[\frac{2}{\cos\theta_0(1 - \lambda) + \cos\vartheta} + \lambda J\right], \tag{16}$$

and finally, we find the contribution of the diffused radiation of the sea in the OSR field on the upper boundary of the atmosphere

$$I'(\theta) = 863\,\frac{[1-R(\theta)]\,[1-R(i)]\cos i\,e^{-0.3(\sec i+\sec\theta)}}{4\pi n^2}\times$$
$$\times\lambda h\left[\frac{2}{\cos\theta_0(1-\lambda)+\cos\vartheta}+\lambda J\right]. \tag{17}$$

The calculations of value I'(θ) are performed in the following way.

According to prescribed i and θ we find θ_0 and ϑ from the relationships $n \sin\vartheta = \sin\theta$, $n \sin\theta_0 = \sin i$, $n = 1.33$; Fresnel's energy coefficients R(θ) and R(i) for reflections from water are taken from tables. The substitution of the values of θ_0, ϑ and R, found, and also the prescribed values λ and h into the formulas (17) and (8) will yield the sought value of the intensity of the radiation coming out of the sea at the upper boundary of the atmosphere.

The solution obtained by us, as it should have been expected is very sensitive to the change in both optical parameters of water λ and h, which makes it impossible to use random, unreliable values of these parameters in numerical /122 calculations. We shall try to obtain reasonable figures by using additional information with respect to the albedo of the sea. Let us examine the reflection of radiation from the surface of the sea with a sun standing high, $i \approx 0$. Let E_d and E_s be the luminance of the surface of the sea by the direct and scattered radiation, E'_d and E'_s be the corresponding flows of reflected radiation, the albedo of direct and scattered radiation, as we know are equal to $A_d = E'_d/E_d \approx 0.02$ $(i \approx 0)$, $A_s = E'_s/E_s \approx 0.066$ (the albedo of the uniformly luminescent sky above a smooth water surface). Let us make use of the circumstance, that for the visible region $E_d/E_s \approx 3\text{-}7$ with $i < 60°$. Let us consider that, $E_s/E_d \approx 0.2$, with $i \approx 0$. For the total albedo we have:

$$A = \frac{E'_d + E'_s}{E_d + E_s} = \frac{E'_d}{E_d\left(1+\frac{E_s}{E_d}\right)} + \frac{E'_s}{E_d\left(1+\frac{E_s}{E_d}\right)} = \frac{1}{\left(1+\frac{E_s}{E_d}\right)}\left(\frac{E'_d}{E_d}+\frac{E'_s}{E_d}\right),$$

$$\frac{E'_p}{E_d} = \frac{A_s E_s}{E_d} \approx 0.2A_p\left(\text{since}\quad \frac{E_p}{E_d}\approx 0.2\right),$$

$$\frac{1}{1+\frac{E_s}{E_d}} = 1-\frac{E_s}{F_d}+\left(\frac{E_s}{E_d}\right)^2-\ldots = 1-0.2+0.04-\ldots = 0.84,$$

$$A \approx 0.84(A_d+0.2A_s) \approx 0.03.$$

If we take into account the waves on the sea, then with the mean wind velocity v = 10 m/sec $A_d \approx 0.03$ [4] and for the total albedo we have

$$A \approx 0.84(0.03 + 0.2 \cdot 0.066) \approx 0.036.$$

However, the experimental data collected in work by N.Ye. Ter-Markaryants [5], yield the albedo value of $A' \approx 0.056$ for $i = 0$. Therefore the difference $A' - A = 0.02$ which is missing should be provided by the radiation E_o outgoing from the sea. We can easily see, that the full albedo (observed value A') is expressed by the formula:

$$A' = \frac{E'_d + E'_s + E_o}{E_d + E_s} = A + \frac{E_o}{E_d + E_s} \approx A + \frac{E_o}{1{,}2E_d}.$$

from this $E_o/1.2\, E_\perp \approx 0.02$ and taking into account that $E_d = E_\perp$ when $i \approx 0$, we obtain

$$E_o \approx 0{,}025E_\perp. \tag{18}$$

From (18) and (15) now we can determine one of the parameters λ and h. As indicated by the calculations with formulas (15) and (16) the outgoing radiation may be considered isotropic (in our approximation). Therefore when $i \approx \approx 0$

$$E_o = \pi I_\lambda(0,\ 0)\big|_{i=0}. \tag{19}$$

Taking into account that

$$E_\perp(0) = I_0(\lambda)e^{-\tau_0(\lambda)} \tag{20}$$

and substituting formulas (19), (20) and (15) in expression (18), we obtain the following equation

$$f(\lambda) \equiv \lambda h\left[\frac{2}{2-\lambda} + \lambda\left\{\frac{2}{(2-\lambda+\lambda h)[2(1-\lambda)+\lambda h]}\left(1 - \frac{\pi h\lambda}{(\pi+2)(1-\lambda+\lambda h)}\right) + \right.\right.$$
$$\left.\left. + h\left(\frac{1}{\left(1-\lambda+\frac{2}{\pi}\right)\left[(1-\lambda)\left(\frac{\pi}{2}+1\right)+\lambda h\right]} - \frac{2}{(2-\lambda)(2-\lambda+\lambda h)}\right)\right\}\right] =$$
$$= 0{,}025\frac{4n^2}{[1-R(0)]^2} \approx 0{,}18. \tag{21}$$

We should note immediately, that in obtaining equations (18) and (21), pertaining to the spectral values, we use the data on the integral albedo. Moreover, owing to the considerable change with respect to the spectrum of the ration E_s/E_d, the relationship $E_s \approx 0.2\ E_d$ is rather arbitrary. To obtain more accurate expressions we should know the values of the spectral albedo, and also the values of the spectral luminance of the direct and scattered radiation.

From equation (21) we shall determine the value of parameter λ, considering value h to be known. We emphasize, that with any pair of values of λ and h, satisfying equation (21), the radiation going into the zenith with i = 0, will be the same:

$$I(0)|_{i=0} = 863\ \frac{[1-R(0)]^2 e^{-0,3}}{4\pi n^2} f(\lambda) \approx 5.0 \cdot \frac{\text{millicalories}}{\text{cm}^2\ \text{min}\cdot\text{ster}} \tag{22}$$

on the sea level and

$$I'(0)|_{i=0} = 863\ \frac{[1-R(0)]^2 e^{-0,6}}{4\pi n^2} f(\lambda) \approx 3.7 \cdot \frac{\text{millicalories}}{\text{cm}^2\ \text{min}\cdot\text{ster}} \tag{23}$$

on the upper boundary of the atmosphere.

As we have already noted the share of radiation dispersed by the elementary volume of water into the rear hemisphere, amounts to about 3%. Let us examine two very different values of h: /125

$$h_1 = 1.5 \cdot 10^{-2}, \quad h_2 = 5 \cdot 10^{-2}. \tag{24}$$

From equation (21) we find:

$$\lambda_1 = 0.936, \quad \lambda_2 = 0.807. \tag{25}$$

The radiation going out into the atmosphere at the sea level and on the upper boundary of the atmosphere, calculated according to formula (16), (17), and (8), practically coincides for both cases and its values are given in Table 1 and 2. Adding up I'(θ) with the previously obtained OSR field [6], we find the full OSR field above the sea I(θ, i, ϕ) and the corresponding flows F(i) (Table 3). In Table 4 we give the relationship I'(θ)/I(θ ,i, ϕ) in percent. We can see that the contribution of the diffused radiation of the sea to the OSR field in the upper boundary of the atmosphere is maximum with small zenith distances of the sun and small sighting angle θ outside of the solar glitter. /126

With large i and θ this contribution is negligibly small because of the screening action of the atmosphere, and also because of the increase of the reflection coefficient [see formula (17)].

TABLE 1. RADIATION LEAVING THE SEA I(θ) cal/cm² min·ster

i	θ 0	30	60	80
0	0,0050	0,0052	0,0054	0,0040
20	0,0047	0,0049	0,0051	0,0038
40	0,0037	0,0038	0,0040	0,0030
60	0,0021	0,0021	0,0022	0,0017

Tr. Note: Commas indicate decimal points.

TABLE 2. DIFFUSED RADIATION OF THE SEA ON THE UPPER BOUNDARY OF THE ATMOSPHERE I'(θ) cal/cm² min·ster.

i	θ 0	30	60	75
0	0,0037	0,0036	0,0030	0,0019
20	0,0034	0,0034	0,0028	0,0018
40	0,0028	0,0027	0,0022	0,0014
60	0,0015	0,0015	0,0012	0,0008

Tr. Note: Commas indicate decimal points.

In conclusion we shall note once again that the results obtained are approximate because of their assumptions made in the solution of the transfer equation, and also because of the necessity of using indirect experimental data data.

REFERENCES

1. Shifrin, K. S.: "On the Albedo Theory," *Trudy GGO*, Issue 39, 1953.
2. Kershun, A. A.: "On the Photometry of Turbid Media," *Trudy GOI*, Vo . XI, Issue 99, 1936.
3. Sobolev, V. V.: *"Perenos Luchistoy Energii v Atmosferakh Zvezd i Planet,"* [Transfer of Radiant Energy in the Atmospheres of Stars and Planets], Gostekhizdat Press, Moscow, 1956.
4. Avaste, O. A.; Yu. Mullamaa and K. S. Shifrin: "Investigations on the Physics of the Atmosphere," *IFA AN ESSR*, Vol. 6, 1964.
5. Ter-Markaryants, N. E.: "Albedo of the Sea," Author's abstract of the dissertation at the GGO, Leningrad, 1958.
6. Shifrin, K. S. and V. Yu. Kolomiytsov: "Field of the Outgoing Shortwave Radiation over the Sea,", See the present collection.

TABLE 3. THE OSR FIELD ABOVE THE SEA TAKING INTO CONSIDERATION THE DIFFUSION IN THE WATER LAYER $I(\theta)_i, \phi)$ cal/cm^2 min·ster

φ	0	15	30	45	60	75	0	15	30	45	60	75
	i=20°, F=0,115 cal/cm^2 min						i=40°, F=0,115 cal/cm^2 min					
0	0,0423	0,0554	0,0552	0,0431	0,0377	0,0473	0,0273	0,0360	0,0551	0,0713	0,0725	0,0686
15		0,0543	0,0530	0,0413	0,0369	0,0473		0,0354	0,0505	0,0601	0,0573	0,0577
30		0,0516	0,0476	0,0373	0,0353	0,0472		0,0333	0,0406	0,0413	0,0396	0,0489
45		0,0478	0,0413	0,0334	0,0340	0,0470		0,0311	0,0324	0,0314	0,0340	0,0472
60		0,0440	0,0362	0,0309	0,0334	0,0464		0,0293	0,0285	0,0286	0,0331	0,0467
75		0,0404	0,0326	0,0296	0,0333	0,0460		0,0281	0,0272	0,0281	0,0331	0,0463
90		0,0374	0,0306	0,0292	0,0333	0,0455		0,0275	0,0269	0,0282	0,0333	0,0459
105		0,0352	0,0297	0,0294	0,0338	0,0459		0,0272	0,0271	0,0288	0,0339	0,0463
120		0,0337	0,0292	0,0297	0,0344	0,0462		0,0271	0,0274	0,0294	0,0345	0,0467
135		0,0328	0,0294	0,0302	0,0350	0,0466		0,0272	0,0280	0,0300	0,0351	0,0470
150		0,0323	0,0295	0,0305	0,0353	0,0469		0,0274	0,0283	0,0304	0,0354	0,0473
165		0,0321	0,0297	0,0309	0,0356	0,0472		0,0275	0,0287	0,0308	0,0356	0,0476
180		0,0322	0,0300	0,0312	0,0359	0,0475		0,0277	0,0290	0,0311	0,0359	0,0479
	i=60°, F=0,110 cal/cm^2 min						i=80°, F=0,075 cal/cm^2 min					
0	0,0190	0,0203	0,0299	0,0665	0,155	0,283	0,0106	0,0116	0,0155	0,0303	0,107	0,466
15		0,0202	0,0274	0,0488	0,0792	0,115		0,0115	0,0148	0,0235	0,0431	0,118
30		0,0198	0,0234	0,0301	0,0404	0,0753		0,0114	0,0140	0,0193	0,0326	0,0989
45		0,0193	0,0213	0,0251	0,0344	0,0630		0,0112	0,0134	0,0174	0,0286	0,0811
60		0,0193	0,0206	0,0239	0,0323	0,0557		0,0111	0,0128	0,0158	0,0245	0,0634
75		0,0192	0,0204	0,0235	0,0303	0,0482		0,0110	0,0123	0,0142	0,0204	0,0464
90		0,0192	0,0204	0,0230	0,0282	0,0410		0,0109	0,0119	0,0126	0,0163	0,0276
105		0,0194	0,0209	0,0238	0,0292	0,0422		0,0109	0,0120	0,0129	0,0168	0,0288
120		0,0196	0,0214	0,0245	0,0303	0,0434		0,0109	0,0121	0,0132	0,0174	0,0300
135		0,0198	0,0219	0,0253	0,0313	0,0445		0,0110	0,0122	0,0134	0,0179	0,0312
150		0,0199	0,0224	0,0262	0,0330	0,0469		0,0110	0,0123	0,0137	0,0184	0,0324
165		0,0201	0,0228	0,0271	0,0347	0,0492		0,0110	0,0124	0,0140	0,0190	0,0336
180		0,0202	0,0233	0,0280	0,0365	0,0516		0,0110	0,0125	0,0142	0,0195	0,0348

Tr. Note: Commas indicate decimal points.

TABLE 4. CONTRIBUTION OF THE DIFFUSED RADIATION OF THE SEA TO THE OSR FIELD IN THE UPPER BOUNDARY OF THE ATMOSPHERE

$\frac{I'(\theta)}{I(\theta, i, \varphi)}$ %

φ	θ = 0	15	30	45	60	75
			$i = 20°$			
0	8,7	6,5	6,6	7,8	8,0	4,0
30		7,1	7,7	9,1	8,6	4,0
90		10,0	12,5	11,9	9,2	4,1
180		11,8	12,8	11,0	8,5	3,9
			$i = 40°$			
0	11,4	8,4	5,2	3,5	3,1	2,1
30		9,2	7,1	6,2	5,9	2,9
90		11,3	11,2	9,3	7,1	3,1
180		11,2	10,3	8,4	6,5	3,0
			$i = 60°$			
0	8,6	8,0	5,3	2,2	0,8	0,3
30		8,2	6,8	4,9	3,1	1,1
90		8,5	7,9	6,5	4,4	2,0
180		8,0	6,9	5,3	3,4	1,6

Tr. Note: Commas indicate decimal points.

RECONSTITUTION OF THE GROUND LEVEL PRESSURE FIELD
ACCORDING TO THE WEATHER SATELLITE DATA

O. S. Bogomolov

ABSTRACT. The author examines the possibilities of improvement of the method proposed by Sh. A. Musayelyan for reconstitution of the pressure field according to the data of meteorological satellites. He shows that the enlistment, along with the data on the amount of cloudiness, of information on its shape and height of the upper boundary, makes it possible to improve appreciably the accuracy of the solution of the above-mentioned problem.
An evaluation is made of the possibility of reconstitution of the ground-level pressure field and the geostrophic wind on the basis of information on the cloudiness field. The author notes a good qualitative agreement of the calculated and actual pressure fields. Above-mentioned procedure can be used for reconstitution of the pressure field and wind according to the satellite data above the regions, about which meteorological information is inadequate.

Modern weather satellites enable us to obtain information on the global distribution of the cloud cover. Already the first television pictures obtained from satellites enabled us to establish the high degree of organization of the cloud formations of various scales. The experience accumulated from comparison of these pictures with the data of the synoptic and aerological maps, supported the conclusion that the structure, quantity, shape, horizontal and vertical extent of the cloudiness are directly connected with the character and revolution of the pressure field, air masses, and atmospheric fronts. It is besides this relationship that is the basis of satellite nephanalysis, which found a very wide practical application in the evaluation of the synoptic situation, especially over the regions poorly covered with respect to meteorology. However, the qualitative methods require a great consumption of time and forces of highly qualified specialists, suffer from subjectivism, and are not subject to automation. At the same time the problem of automation of processing and analysis of satellite data is important in principle in connection with the specifics and the enormous volume of information, arriving from meteorological satellites. Therefore, the necessity arises to develop a numerical method of interpretation of this information. /127

Sh. A. Musayelyan [1] proposed a method for reconstitution of the vertical flows, functions of the flow and geopotential on the middle level of the atmosphere, according to the data on the general amount of cloudiness. It appears interesting, using the principal of the "correlation harmonics" which lies at the base of this method, to evaluate the possibility of reconstituting the field of the ground level pressure by means of information on cloudiness fields. The rationality of opposing this problem proceeds from the following physical concepts.

An important role in the formation of frontal cloud systems is played by the ordered vertical motions, caused by the convergence of the air flows under the effect of turbulent friction forces. Investigations [2] show that the vertical flows on the upper boundary of the friction layer retained their sign, at least within the bounds of the lower and the middle troposphere, where the principal mass of the clouds is located. On the other hand, we know, that the frictional vertical flows are directly connected with the geostrophic velocity vortex (ground level pressure Laplacian). It is precisely this that explains the well-known coordination of the fields of large-scale cloud systems and the Laplacian of the ground level pressure, which manifests itself in the fact that to the regions with a cyclonic curvature of the isobars (positive values of /128
the Laplacian) correspond the cloud massifs in the zones of ordered ascending motions.

Along with the ordered vertical flows in the formation of the cloudiness a certain role is also played by such processes as the horizontal and vertical turbulent exchange, thermal convection, cooling of the air mass through the heat exchange with the underlying surface. These processes result in the formation of the entire observed variety of cloud systems and in most cases reduce the coordination of the cloudiness fields and the ground pressure Laplacian. Therefore, the data on only the total volume of cloudiness do not always contain information on the intensity of pressure formations, and in some cases do not characterize even the sign of the pressure formations.

In this connection, in order to increase the successfulness of restitution of the pressure field according to the data on the cloudiness, it appears rational to separate those cloud massifs, which are closely connected with the pressure field (pressure Laplacian), and to filter off or decrease the influence of all the others. This problem may be solved, if along with the data on the quantity we use the information on the shape, and altitude of the upper boundary of the clouds. In this case, having in view the satellite data, the quantity and principal shapes (types), of cloudiness may be evaluated according to the television pictures, and the height of the upper boundary, according to the radiation measurements in the 8-12 μ channel [3].

The use of more complete information on the cloud cover enables us to construct a certain generalized characteristic of the cloudiness field, for example, in the form of

$$N = qnh,$$

where q is the weight coefficient, which takes into account the relationship between the shape of the cloudiness with the Laplacian of the ground level pressure; n, h are the amount and height of the upper boundary of the cloudiness, averaged with respect to area, the dimension of which is equal to the square of the step of the grid, adopted for the finite-difference concept of the Laplacian. We have separated three types (shapes) of cloudiness which may be identified according to the satellite data: the frontal, intramass, and cirrus. The weight coefficients for them were found statistically and transpired to be equal to 0.6; 0.3, and 0.1, respectively.

The introduction of the generalized characteristic N enables us to separate the cloud systems, connected with the pressure formations, and to obtain a more complete information on the pressure field. Indeed, cyclones and troughs are connected with frontal cloud systems developed vertically and covering substantial areas, whereas the intermass clouds have smaller horizontal dimensions (cumulus cloudiness) and a small vertical extent (stratus and stratocumulus cloudiness). The height of the upper boundary of the frontal clouds grows with the approach to the front line (trough access) and along the front line in the direction towards the center of the cyclone.

To evaluate the possibility of restitution of the ground level pressure field according to the data on the cloudiness field we selected a region with dimensions of 6,000 × 4,200 km, bounded by latitude circles of 35 and 75° N and meridians 0 and 60° E, which is covered well enough with meteorological data. For five periods of time in January 1967, separated in time by not less than four days from one another, according to radiosonde data and the maps of nephanalysis and synoptic maps we calculated the values of the generalized /129 characteristics of the cloudiness field N and the ground level pressure Laplacian Δp in the nodes of the square grid with a step of 300 km. For each line of the grid we performed the expansion of functions N(x) and Δp(x) into Fourier series:

$$N_j(x)=\frac{a^N_{0,j}}{2}+\sum_{m=1}^{10} a^N_{m,j}\cos\frac{\pi m x}{10}+b^N_{m,j}\sin\frac{\pi m x}{10}, \qquad (1)$$

$$\Delta p_j(x)=\frac{a^\Delta_{0,j}}{2}+\sum_{m=1}^{10} a^\Delta_{m,j}\cos\frac{\pi m x}{10}+b^\Delta_{m,j}\sin\frac{\pi m x}{10}, \qquad (2)$$

where j is the number of the line of the grid, x is the number of the node in the line, m is the number of the expansion coefficient.

In accordance with the method proposed by Sh. A. Musayelyan [1], we constructed the regression equation of the following type:

$$\begin{aligned} a^\Delta_m &= c_m a^N_m + s_m, \\ b^\Delta_m &= c'_m b^N_m + s'_m, \end{aligned} \qquad (3)$$

where a^{Δ}_{m}, b^{Δ}_{m}, a^{N}_{m}, b^{N}_{m} are Fourier's coefficients at the cosines and sines for the Laplacian and the generalized characteristic N, and N, a c_m, c'_m, s_m, s'_m are the coefficients of the linear relationship between them.

The restitution of the pressure field according to the data of the cloudiness field was performed in the following order. The initial field of the generalized characteristic of the cloudiness was presented in the form of Fourier's series (1) for each line of the grid. According to the obtained values of Fourier's coefficients by means of the regression equation (3) we converted the Laplacian field to Fourier's coefficients, and then calculated by means of formulas (2) the value of the Laplacian in the nodes of the grids. After this we solved Poisson's equation with respect to pressure with prescribed actual values of it on the boundaries of the region examined. The calculations according to this method were carried out for fifteen cases for December 1966, January and February of 1967, among which we included also the data, used for setting up regression equations (3).

The analysis of the results of the calculations shows that in all the cases there is a good qualitative agreement between the calculated and factual pressure fields. The coefficient of the multiple correlation between the restituted and actual field on the average for all the cases proved equal to 0.76. The mean absolute and root mean square errors of restitution amounted to 6 and 9 milibars respectively. However, in individual points the absolute value of the difference between the calculated and actual values of pressure reached 15 and even 25 milibars. Such differences were observed in cases, when the centers of the pressure formations on the restituted maps proved displaced with respect to the actual ones. This displacement was different for the pressure systems, which were found in various stages of development, and reached the maximum values, equal to 500-800 km, for the filling occluded cyclones.

To eliminate this shortcoming it appeared rational to enlist the data on the vortex structure of the cloudiness, obtained by means of television pictures from weather satellites. In work [4] it is shown, that this information enables us with a certain degree of accuracy to determine the position of the ground level centers and the stage of the development of the cyclones. /131.

As an example, in Figures 1 and 2 we present the resistituted and factual fields of the ground level pressure for 9 hours, 14 Feburary 1967.

The results obtained gives us ground to consider that the method presented may be used for restitution of ground pressure fields and geostrophic wind according to the weather satellite data on the cloudiness field over such poorly covered with meteorological inspection regions as for example the watery area of the oceans.

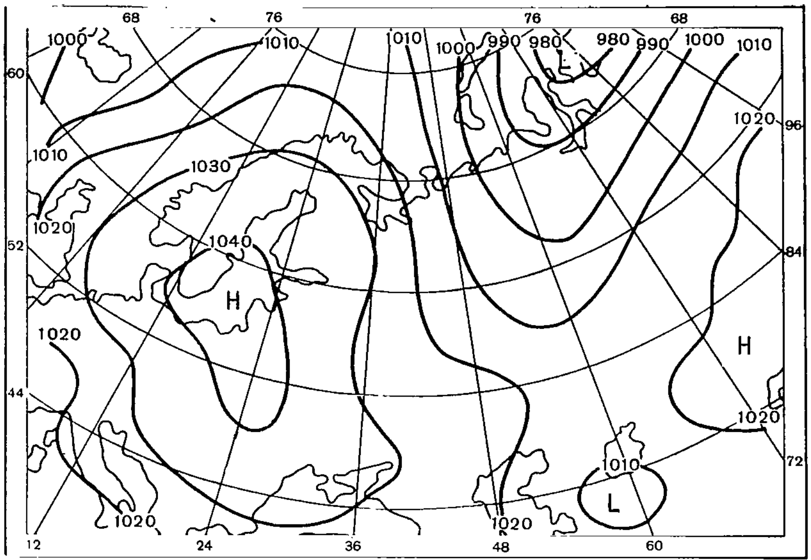

Figure 1. Factual Ground Level Pressure Field, 9 Hrs., 14 February 1967.

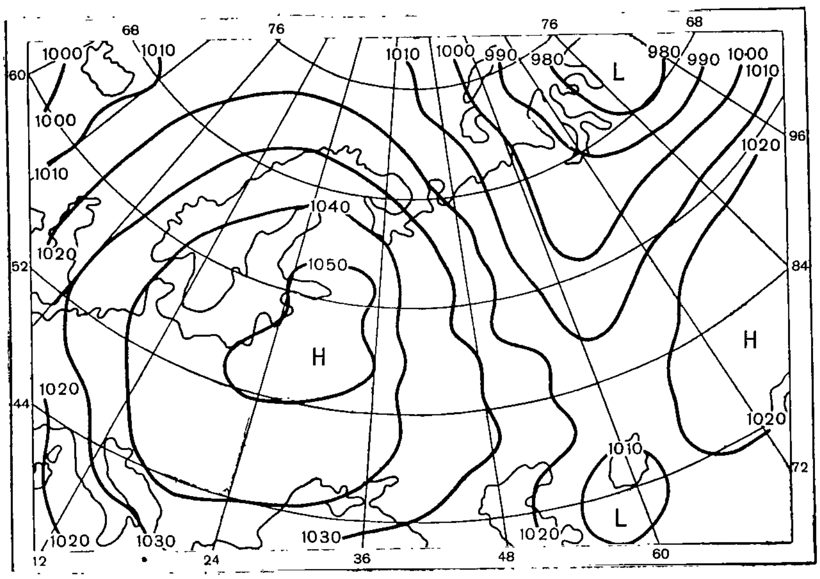

Figure 2. Restituted Ground Level Pressure Field, 9 Hrs., 14 February 1967.

REFERENCES

1. Musayelyan, Sh. A. and A. Z. Chkirda: "On the Numerical Interpretation of the Information on Cloudiness, Arriving From Weather Satellites," *Trudy GGO*, Issue 166, 1964.

2. Matveyev: L. T.: "Vertical Currents in the Boundary Layer of the Atmosphere and their Relationship with the Lower and Upper Boundaries of the Cloudiness," *Trudy VGMF SA*, Issue 11, 1955.
3. Boldyrev, V. G.: "On the Machine Plotting of Temperature Maps of the Terrestrial Surface and Altitude of the Upper Boundaries of Cloudiness According to the Weather Satellite Data," *Trudy MMTs*, Issue 11, 1966.
4. Minina, L. S.: *"Primeneniye Nablyudeniy Meteorologicheskikh Sputnikov za Oblachnym Pokrovom Zemli pri Analize Kart Pogody,"* [Utilization of Observations of Weather Satellites on the Cloud Cover of the Earth in the Analysis of Weather Maps], Gidrometeoizdat Press, Moscow, 1967.

ON THE DETERMINATION OF THE TEMPERATURE OF THE RADIATING SURFACE AND THE TOTAL MOISTURE CONTENT ACCORDING TO RADIATION MEASUREMENT ON A SATELLITE

B. D. Panin

ABSTRACT. The setting up and solution of the problem of determination of the temperature of the radiating surface taking into account the transformation of radiation by the atmosphere and the total moisture content according to the measurements of the thermal radiation on modern weather satellites in the 8-30, 8-18 and 6-6.5 μ reaions of the spectrum, and also in the 3-30 and 8-12 μ regions of the spectrum is analyzed. The solution of the problem is reduced to the solution of the system of two nonlinear algebraic equations with respect to the radiation energy at the temperature of the radiating surface and their special function corresponding to the total moisture content, according to the values of which then the temperature and moisture content are calculated. The author gives the results of the calculations, which are compared with the actual magnitudes of the values calculated.

The determination of the temperature of the radiating surface (underlying surface or the upper boundary of the clouds) according to the measurements of the thermal radiation on modern satellites is rendered complicated because of the difficulties of taking into account the transformation of radiation by the atmosphere. /132

Below, we examine the setting up and solution of the problem of determination of the temperature of the radiating surface on the basis of allowance for transformation of radiation by the atmosphere according to the measurements of the thermal radiation on modern weather satellites in 8-30, 8-12 and 6-6.5 μ sectors of the spectrum, and also in the 3-30 and 8-12 μ sectors of the spectrum.

For the outgoing thermal radiation in the 8-30 and 8-12 μ sectors of the spectrum assuming that the underlying surface in the clouds radiate as an absolutely black body, the transfer equations are written in the following form:

$$I^{\uparrow}_{8-30}=E_{8-30}(T_0)P_{8-30}(w_0,\ u_0,\ m_0)+\int\limits_{w_0,\ u_0,\ m_0}^{0} F_{8-30}(T)\,dP_{8-30}(w,\ u,\ m), \tag{1}$$

$$I^{\uparrow}_{8-12}=E_{8-12}(T_0)P_{8-12}(w_0,\ m_0)+\int\limits_{w_0,\ m_0}^{0} E_{8-12}(T)\,dP_{8-12}(w,\ m), \tag{2}$$

where $I^{\uparrow}_{8-30}$, $I^{\uparrow}_{8-12}$ is the outgoing radiation, $E_{8-30}(T_0)$, $E_{8-12}(T_0)$, $E_{8-30}(T)$ and $E_{8-12}(T)$ is the energy of the absolutely black radiation in the 8-30 and 8-12 μ sectors of the spectrum with the temperature T_0 of the radiation surface and the temperature T of the atmospheric air, respectively, P_{8-30}, P_{8-12} is the transmission function of the 8-30 and 8-12 μ sections of the spectrum, w_0, u_0, m_0, w, u, m are the general effective content of the water vapor, carbon-dioxide, ozone, and the effective content of these components above variable level respectively.

Let us examine the possibility of solving equations (1) and (2) with respect to radiation energy with the temperature of the radiating surface T_0 and the transmission function, corresponding to the full mass of absorbing components.

In this case we will have in mind that the variation of the content of carbon dioxide and ozone is considerably smaller than the variation of the water vapor. With sufficient grounds we can consider the vertical distributions of the carbon dioxide and ozone content to be known and invariable, or limit ourselves to allowing for planetary and seasonal variations.

According to the data in work [1] the dependence of the transmission function on the effectiveness of carbon-dioxide and water-vapor content in the 8-30 μ sector of the spectrum may be approximated by the empirical relationships of the following types /133

$$P_{8-30}(w,\ u)=0{,}79e^{-0{,}96\sqrt{w}}+0{,}21e^{-21{,}0w}-\left(0{,}224e^{-0{,}7w}+0{,}056e^{-3{,}0w}\right)\times \\ \times\left(1-0{,}58^{-0{,}042\sqrt{u}}-0{,}42e^{-0{,}5\sqrt{u}}\right), \qquad (3)$$

where w and u are the effective content of the water vapor and carbon dioxide respectively.

The variations of the general effective content of carbon dioxide in the atmosphere lies within the bounds of 110-150 cm.

For these values the second cofactor in the right member of relationship (3) is equal to 0.620 or 0.654 respectively (the mean value is 0.637). The value of the ozone on the outgoing radiation in the 8-30 μ sector of the spectrum is very small and we shall not take it into account.

In the 8-12 μ sector of the spectrum along with water vapor the influence of ozone is substantial.

According to the data of G. Yamomoto and others [3] the effect of the ozone may be taken into account assuming that it is linearly connected with the energy of the outgoing radiation in the 8-12 μ sector of the spectrum.

Following work [3] we shall evaluate the influence of ozone by introducing corrections into the values of the outgoing radiation energy and operate by the radiation temperature in the 8-12 μ sector of the spectrum taking into account the corrections for ozone.

Proceeding from the above, we shall consider, that the influence of carbon dioxide in the 8-30 μ sector of the spectrum may be taken into account through the constant coefficient in the (3) relationship and the influence in the 8-12 μ sector of the spectrum through the correction to the radiation temperature.

Taking this into account later we shall use the designations for the transmission functions in the 8-30 and 8-12 μ sectors of the spectrum, which indicate only the dependence on the unknown water vapor content, i.e., $P_{8-30}(w)$ and $P_{8-12}(w)$.

To solve the problem posed we shall use the model of the atmosphere, in which the temperature stratification is characterized with the values of the radiation temperature, corresponding to the radiation energy in the 8-12, 8-30 and 6.0-6.5 μ channels. We shall designate these values of radiation temperature with T^*_{8-12}, T^*_{8-30}, and $T^*_{6.5}$. For the transmission function in the 8-30 and 8-12 μ sectors of the spectrum at the levels to which T^*_{8-12}, T^*_{8-30} and $T^*_{6.5}$ pertain, we shall introduce the following designations

$$P_{8-30}(w^*_{8-12}),\ P_{8-30}(w^*_{8-30}),\ P_{8-30}(w^*_{6,5}),\ P_{8-12}(w^*_{8-12}),\ P_{8-12}(w^*_{8-30}),\ P_{8-12}(w^*_{6,5}).$$

In these designations w^*_{8-12}, w^*_{8-30}, and $w^*_{6.5}$ are values of the effective moisture content at the levels where $T = T^*_{8-12}$, $T = T^*_{8-30}$, and $T = T^*_{6.5}$.

In the model of the atmosphere examined all the levels are not fixed with respect to altitude and may sustain considerable fluctuations which are determined mainly by the variations in moisture.

For this model of the atmosphere equations (1) and (2) shall be rewritten in the following form:

$$I^{\uparrow}_{8-30} = E_{8-30}(T_0)P_{8-30}(w_0) + \frac{1}{2}\left[E_{8-30}(T_0) + E_{8-30}(T^*_{8-12})\right] \times$$
$$\times \left[P_{8-30}(w^*_{8-12}) - P_{8-30}(w_0)\right] + \frac{1}{2}\left[E_{8-30}(T^*_{8-12}) + E_{8-30}(T^*_{8-30})\right] \times \tag{4}$$

$$\times [P_{8-30}(w^*_{8-30}) - P_{8-30}(w^*_{8-12})] + \frac{1}{2}[E_{8-30}(T^*_{8-30}) + E_{8-30}(T^*_{6.5})] \times$$
$$\times [P_{8-30}(w^*_{6.5}) - P_{8-30}(w^*_{8-30})] + E_{8-30}(T^*_{6.5})[1 - P_{8-30}(w^*_{6.5})], \tag{4}$$

$$I^{\uparrow}_{8-12} = E_{8-12}(T_0) P_{8-12}(w_0) + \frac{1}{2}[E_{8-12}(T_0) + E_{8-12}(T^*_{8-12})] \times$$ /134
$$\times [P_{8-12}(w^*_{8-12}) - P_{8-12}(w_0)] + \frac{1}{2}[E_{8-12}(T^*_{8-12}) + E_{8-12}(T^*_{8-30})] \times$$
$$\times [P_{8-12}(w^*_{8-30}) - P_{8-12}(w^*_{8-12})] + \frac{1}{2}[E_{8-12}(T^*_{8-30}) + E_{8-12}(T^*_{6.5})] \times$$
$$\times [P_{8-12}(w^*_{6.5}) - P_{8-12}(w^*_{8-30})] + E_{8-12}(T^*_{6.5})[1 - P_{8-12}(w^*_{6.5})]. \tag{5}$$

In expressions (4) and (5) the radiation energy of the layers is presented in the form of a half sum of energy, corresponding to the values of the temperature at the boundary of the layers, with the exception of the last layer, which extends from the level with $T = T^*_{6.5}$ to the upper boundary of the atmosphere.

Within the bounds of the last layer it is assumed, that the temperature is an invariable with height and is equal to $T^*_{6.5}$, and at the upper boundary of this layer the transmission function in the 8-30 and 8-12 μ sectors of the spectrum is equal to one.

Let us solve the problem posed by means of equations (4) and (5). In order to solve equations (4) and (5) with respect to $E_{8-30}(T_0)$ and $P_{8-30}(w_0)$ or $E_{8-12}(T_0)$ and $P_{8-12}(w_0)$ it is necessary to decrease the number of the unknowns to two. Below we shall examine the method of reduction of the number of unknowns in the equations (4) and (5) to two, using certain linear empirical relationships.

The values of the radiation energy in the 8-12 and 8-30 μ sectors of the spectrum for T^*_{8-12}, T^*_{8-30}, and $T^*_{6.5}$ are known.

Above the $T = T^*_{6.5}$ level the constancy of the effective moisture content is fulfilled with a sufficient degree of accuracy, i.e., $w^*_{6.5}$ = const. [2], therefore at this level the values $P_{8-30}(w^*_{6.5})$ and $P_{8-12}(w^*_{6.5})$ may be also considered known.

The analysis of the results of the theoretical calculations of the outgoing radiation in the 8-12 and 8-30 (3-30) μ sectors of the spectrum, and also the measurements of the satellites and the vertical profiles of the effective moisture content corresponding to the place and time, indicate that the relationships of the transmission functions $P_{8-30}(w^*_{8-30})$ with $P_{8-30}(w_0)$, and $P_{8-12}(w^*_{8-12})$ with $P_{8-12}(w_0)$ is close to linear. These relations satisfy the empirical relationships:

$$P_{8-30}(w^*_{8-30}) = 0.2 + 1.4P_{8-30}(w_0), \tag{6}$$

$$P_{8-12}(w^*_{8-12}) = 0.5 + 0.5P_{8-12}(w_0). \tag{7}$$

The relationship between $P_{8-30}(w)$ and $P_{8-12}(w)$ is nonlinear. However, in spite of the nonlinearity of the relation as a whole, in the range of values $0.3 \leq P_{8-12}(w) \leq 0.92$ ($5.0 \geq w \geq 0.1$ grams/cm^2) this relationship is close to linear and it may be approximated by the relationship of the following type

$$P_{8-12}(w) = 0.3 + 1.25P_{8-30}(w). \tag{8}$$

The $5.0 \geq w \geq 0.1$ grams/cm^2 range of values encompasses practically all the possible values of w^*_{8-12} and the full effective mass of water vapor w_0 which may take place in the atmosphere.

Instances when $w > 5.0$ grams/cm^2 are relatively rare and may take place in the tropics and in the equatorial zone.

Proceeding from these considerations we shall use the relationship (8) for the expression $P_{8-12}(w_0)$ and $P_{8-12}(w^*_{8-12})$ through $P_{8-30}(w_0)$ in equations (4) and (5). /135

We should stress, that with $w_0 < 0.1$ grams/cm^2, when the relationship (8) is unsuitable, the contribution of the radiation of the atmosphere to the outgoing radiation is small, $T^*_{8-12} \approx T_0$ and the necessity for solving the problem practically disappears.

The evaluation of magnitudes of w^*_{8-30} shows that in the great majority of cases they lie within the bounds of $0.01 \leq w^*_{8-30} \leq 0.3$ grams/cm^2. For these values the relationship $P_{8-12}(w^*_{8-30})$ with $P_{8-30}(w_0)$ may be approximated by the linear function of the following appearance

$$P_{8-12}(w^*_{8-30}) = 0.9 + 0.1P_{8-30}(w_0). \tag{9}$$

Formulas (6-9) enable us to express all of the values of the transmission function in equations (4) and (5) with $P_{8-30}(w_0)$.

In order to transform equations (4) and (5) in such a way that in them, in addition to $P_{8-30}(w_0)$ only $E_{8-30}(T_0)$ would function alone, we shall use the linear relationship

$$E_{8-12}(T_0)=qE_{8-30}(T_0), \tag{10}$$

where q is a constant. The constancy of q is fulfilled well under the condition that the range of values of the temperature, for which we assume this condition, satisfies the inequalities

$$T_0-\Delta T\leqslant T_0\leqslant T_0+\Delta T, \quad \Delta T\leqslant 10^\circ,$$

The corresponding values of q may be selected according to the values of T^*_{8-12}.

Having substituted relationships (6-10) in equations (4) and (5), we shall obtain the system of two nonlinear equations with respect to $x = E_{8-30}(T_0)$ $y = P_{8-30}(w_0)$:

$$\left.\begin{aligned} I^{\uparrow}_{8-30}&=1{,}2xy+a_1y+b_1\\ I^{\uparrow}_{8-12}&=x(0{,}1+0{,}38y)+a_2y+b_2\end{aligned}\right\} \tag{11}$$

where

$$\left.\begin{aligned} a_1&=0{,}2E_{8-30}(T^*_{8-12})-0{,}7\left[E_{8-30}(T^*_{8-30})+E_{8-30}(T^*_{6,5})\right]\\ b_1&=0{,}1E_{8-30}(T^*_{8-12})+0{,}4E_{8-30}(T^*_{8-30})+0{,}5E_{8-30}(T^*_{6,5})\\ a_2&=-0{,}62E_{8-12}(T^*_{8-12})+0{,}8E_{8-12}(T^*_{8-30})\\ b_2&=0{,}33E_{8-12}(T^*_{8-12})+0{,}24E_{8-12}(T^*_{8-30})+0{,}03E_{8-12}(T^*_{6,5})\end{aligned}\right\} \tag{11'}$$

From the system of equations (11) we have

$$y=\frac{I^{\uparrow}_{8-30}-b_1}{1{,}2x+a_1}. \tag{12}$$

Taking into account (12) from (11) we obtain the quadratic equation with respect to x

$$0{,}12x^2 + Bx + C = 0, \tag{13}$$

where

$$\left.\begin{aligned} B &= 0{,}1a_1 + 0{,}38\left(I^{\uparrow}_{8-30} - b_1\right) + 1{,}2\left(b_2 - I^{\uparrow}_{8-12}\right) \\ C &= a_2\left(I^{\uparrow}_{8-30} - b_1\right) + a_1\left(b_2 - I^{\uparrow}_{8-12}\right) \end{aligned}\right\} \tag{14}$$

As indicated by calculations, the solution of the quadratic equation (13) corresponding to the minus sign (-) before the root, is always negative. Therefore, we shall use only the solution, corresponding to the plus sign (+) before the root, i.e., /136

$$x = \frac{-B + \sqrt{B^2 - 048C}}{0{,}24}. \tag{15}$$

Substituting x in (12), we obtain y, i.e. $P_{8-30}(w_0)$. Then we determine T_0 and w_0 according to the values of $E_{8-30}(T_0)$ and $P_{8-30}(w_0)$.

Below we have examined the solution of the problem for the cases when we use three types of initial data, i.e., T^*_{8-12}, T^*_{8-30}, and $T^*_{6.5}$.

We have investigated the possibility of simplifying the problem by means of using it for the solution of two types of initial data T^*_{8-12} and T^*_{8-30} or T^*_{8-12} and T^*_{8-30}. In this case we use the same calculation formulas (12), (14) and (15), but formulas (11') are presented in the following form:

$$\left.\begin{aligned} a_1 &= 0{,}2E_{8-30}\left(T^*_{8-12}\right) - 1{,}1E_{8-30}\left(T^*_{8-30}\right) \\ b_1 &= 0{,}1E_{8-30}\left(T^*_{8-12}\right) + 0{,}7E_{8-30}\left(T^*_{8-30}\right) \\ a_2 &= -0{,}62E_{8-12}\left(T^*_{8-12}\right) + 0{,}8E_{8-12}\left(T^*_{8-30}\right) \\ b_2 &= 0{,}33E_{8-12}\left(T^*_{8-12}\right) + 0{,}25E_{8-12}\left(T^*_{8-30}\right) \end{aligned}\right\} \tag{16}$$

Formulas (16) were obtained from formulas (11') on the basis of the analysis of radiations in the 8-30, and 6-6.5 μ sectors of the spectrum. The rationality of this simplification is substantiated by the results of the calculations, which were carried out on an electron computer according to the data of the Tiros-3 satellite (orbit No. 44) with the use of formulas (11') and (16).

The calculations show, that the use of formulas (16) has a small effect on the results of calculations of T_0 and w_0. The differences in the values of

T_0 and w_0, calculated by using formulas (11') and (16), as a rule do not exceed ±2° and ±0.5 grams/cm^2 respectively.

The calculations of T_0 and w_0 using formulas (16) were performed also according to the Kosmos-122 satellite (orbits No. 207 and 208). The evaluations carried out preliminarily indicated the differences in the spectral ranges of 8-30 and 3-30 μ have an insignificant effect on the values of the radiation temperature ($T^*_{8-30} \approx T^*_{3-30}$). Therefore, according to the Kosmos-122 satellite data all the calculations were performed with the same formulas (12)-(14),(16), i.e., the differences in the spectral characteristics of the equipment were not taken into account.

Certain results of the calculations according to the Tiros-III satellite (orbit No. 44) are given in Figure 1 and 2 and according to the Kosmos-122 satellite data (orbits No. 207 and 208) in Figure 3. In Figure 4 and 5 we give the synoptic maps for the periods close in time to the observations from the satellites.

It is difficult to carry out the evaluations of the results of calculations of T_0 and w_0 because we do not have the actual magnitudes of these values during the time of observation from the satellites. The comparison of the results of calculations of T_0 with the temperature of the ground level air according to the data of observations at the stations in the North African region, where little cloudy and unclouded weather were observed indicates, that in the majority of the cases the calculated values of T_0 exceed the actual values of /139 the temperature at the level of the cyclometric booth by 20-25°. On the average the difference between the temperature at the booth level and the temperature of the underlying surface during daylight hours under a cloudless sky for continental regions also lie within these limits [4]. This gives us grounds to assume, that for cloudless conditions the calculated values of T_0 reflect the principal features of the actual distribution of the temperature of the underlying surface.

In the regions with solid thick frontal cloudiness the T_0 values obtained differ little from the values of the radiation temperature in the 8-12 μ sector of the spectrum (T^*_{8-12}), which also corresponds to the existing concepts.

It is practically impossible to interpret the results of calculation of /140 T_0 in regions with cirrus or nonsolid cloudiness of the middle and lower levels. In these regions the calculated values of T_0 exceed T^*_{8-12}, but as a rule they are below the temperature at the booth level.

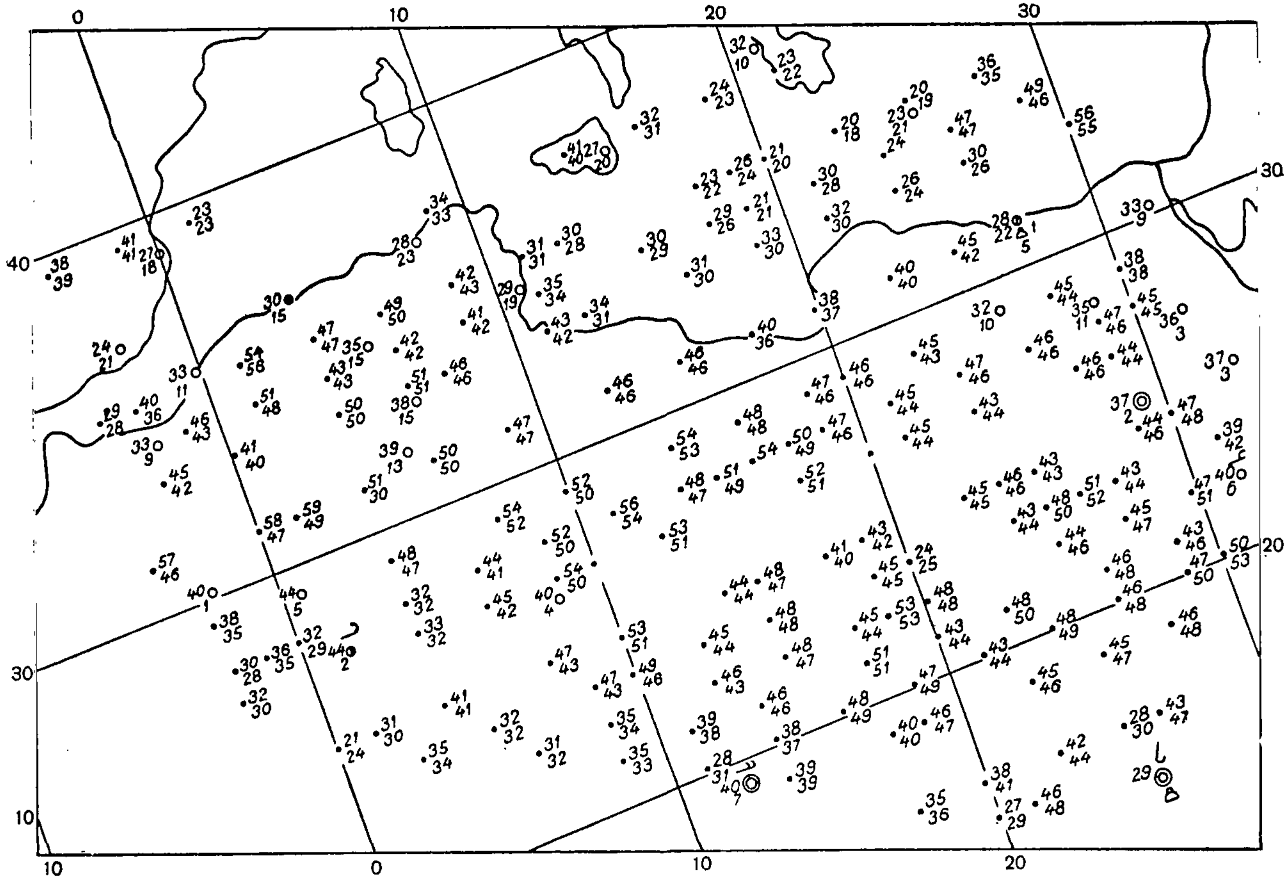

Figure 1. Results of Calculations of T_0 According to the Tiros-III Satellite 15 July 1961, Orbit No. 44, Greenwich Time 10 Hrs. 42 Min.--10 Hrs. 55 Min. (To the right above and below we mark the values of T_0, calculated using the formulas (11') and (16) respectively).

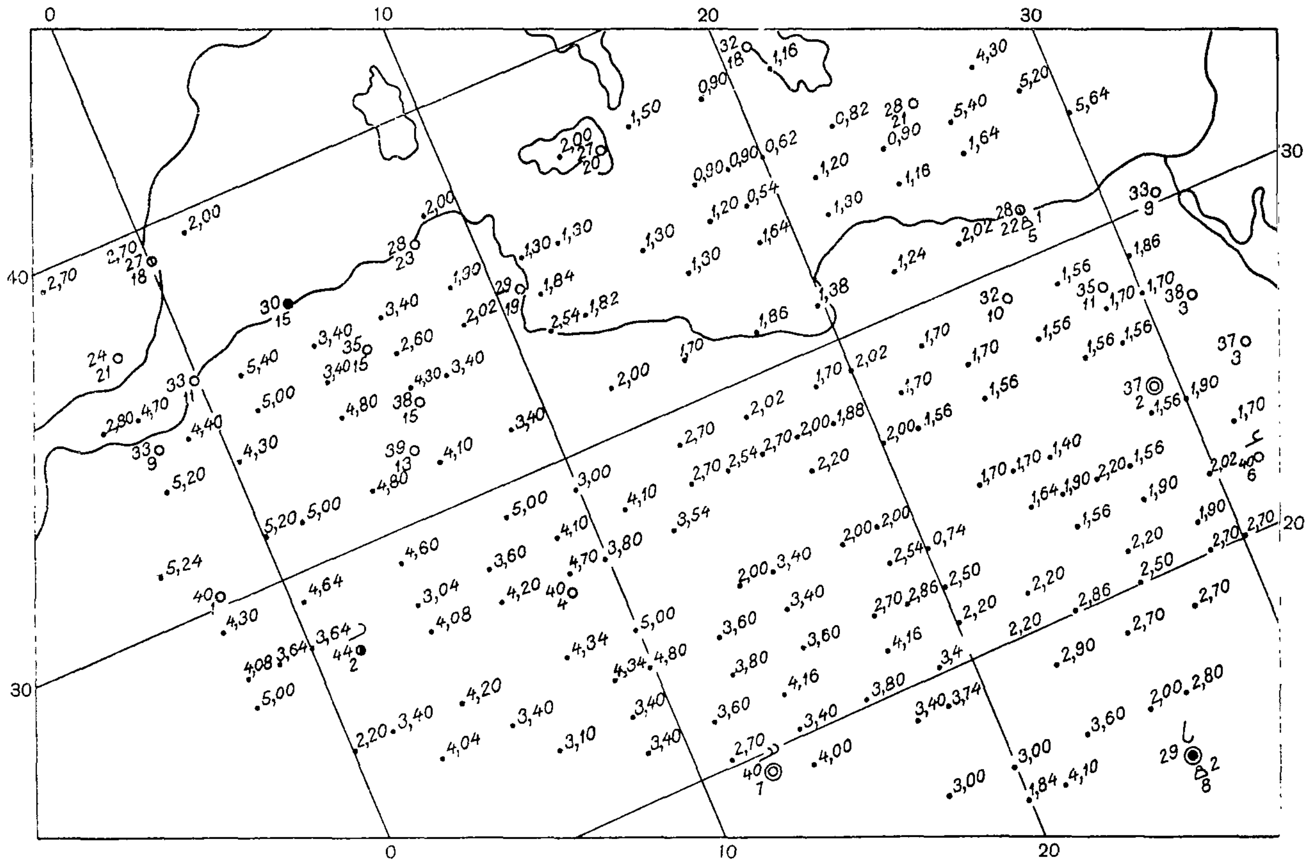

Figure 2. Results of Calculations of w_0 grams/cm^2 According to the Data of Tiros-III Satellite 15 July 1961, Orbit No. 44, 10 Hrs. 42 Min.--10 Hrs. 55 Min. Greenwich Time.

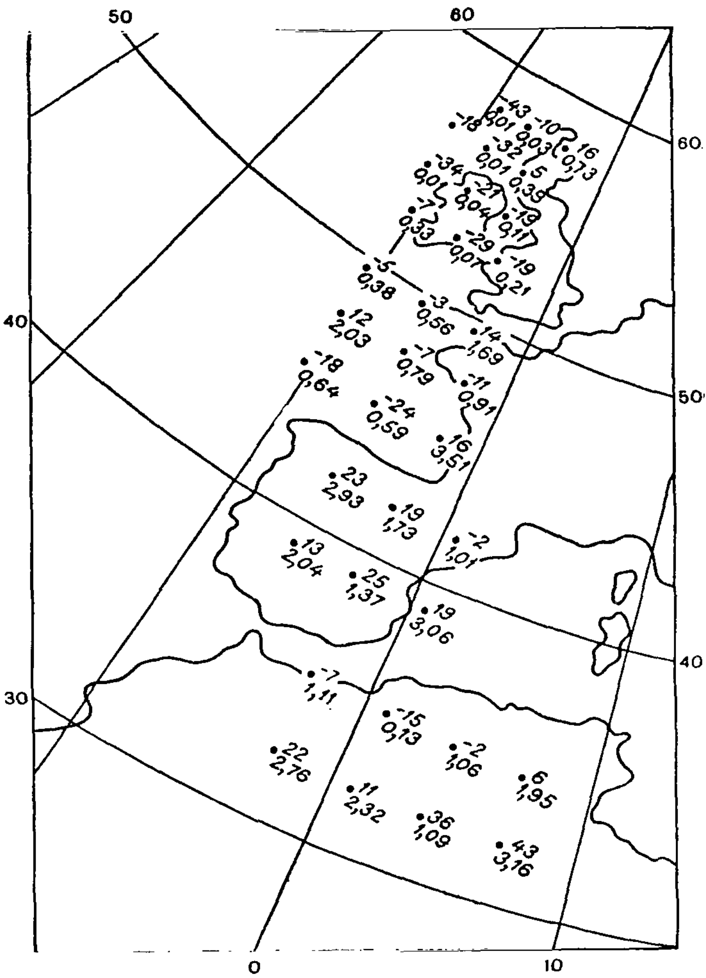

Figure 3. Results of Calculations of T_0°C (Marked Above to the Right) and w_0 grams/ /cm^2 (To the Right Below), According to the Kosmos-122 Satellite Data, Orbit No. 207 and 208, 9 Hrs. 15 Min.--10 Hrs. 57 Min. Greenwich Time.

The evaluation of the results of calculation of w_0 was made using the data of 20 radiosonde observations. The values of the total effective moisture content in the regions with cloudless weather, calculated according to the radiation measurements from a satellite and according to the radiosonde data, in points located near the regions observed by the satellites, when the difference in observation time did not exceed 3 hrs., differ on the average by not more than 0.43 grams/cm^2 (the mean absolute error).

Naturally the above-mentioned evaluations, especially with respect to calculations of w_0 do not pretend to be strict and may be examined as tentative.

The substantiated reasonings on the effectiveness of the method examined for determining the temperature of the radiating surface and the total moisture content may be stated only after a comprehensive checking by means of comparison of the results of calculations with the actual data.

However, the results obtained enable us to consider, that the approach presented may be used in automation of the processing of information from modern weather satellites.

In conclusion we note that the attempts to solve the problem examined more strictly without limitations, connected with the use of linear relationships for the radiation energy and the transmission function did not bring about an /141
Moreover the calculation formulas are becoming much more complicated.

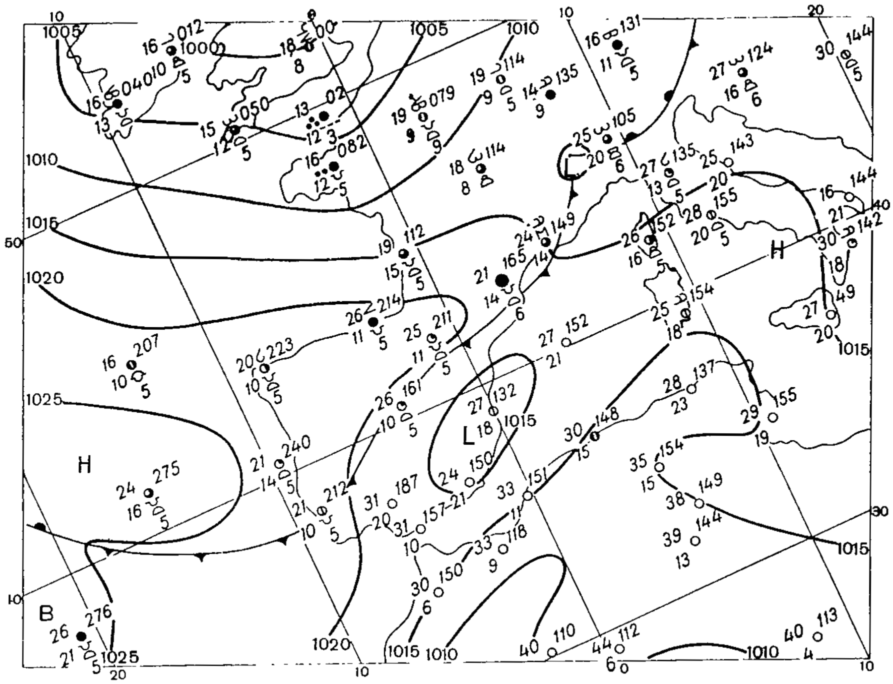

Figure 4. Weather Map for 12 Hours Greenwich Time, 15 July 1961.

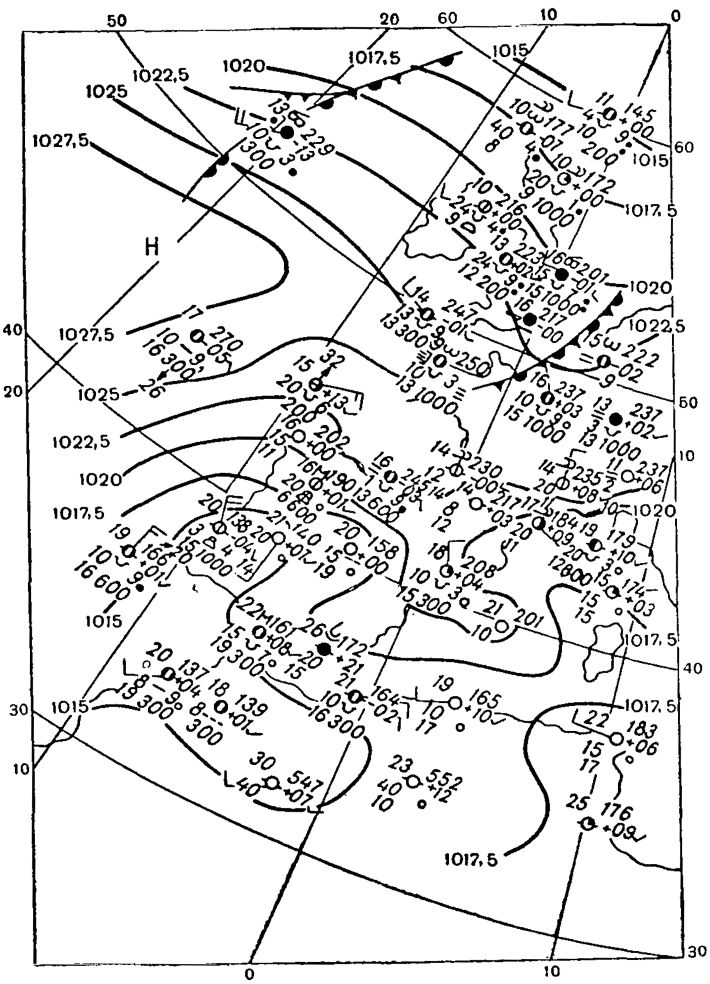

Figure 5. Weather Map for 9 Hours Moscow Time, 9 July 1966.

REFERENCES

1. Kondratiev, K. Y. and H. J. Niilisk: "The New Radiation Chart," *Geofisica pura e Applikata*, Milan, Vol. 49, 1961.
2. Panin, B. D.: "On the Determination of Moisture Content of the Atmosphere According to the Outgoing Radiation of the Earth's Atmosphere System in the 6-6.5 Sector of the Spectrum," *Izv. AN SSSR, Physics of the Atmosphere and the Ocean*, Vol. 3, No. 2, 1967.
3. Yamomoto, G.; D. Q. Wark and J. H. Lienesch: "Methods of Estimating Infra-red Flux and Surface Temperature from Meteorological Satellites," *Journ. of Atm. Sci. Am. Met. Soc.*, Vol. 19, 1962.
4. Guseva, L. N.: "On the Problem of Determination of the Temperature of a Soil Surface According to the Air Temperature," *Trudy GGO*, Issue 196, 1966.

EFFECT OF ANISOTROPY OF THE REFLECTION FROM THE UNDERLYING SURFACE ON DETERMINATION OF THE FLOW OF OUTGOING SHORTWAVE RADIATION ACCORDING TO MEASUREMENTS FROM A SATELLITE

K. S. Shifrin and V. Yu. Kolomiytsev

ABSTRACT. The authors have calculated the outgoing shortwave radiation (OSR) fields over snow and agitated seas. The authors obtained the formulas characterizing the increase in the sensitivity of the OSR field to the type of reflection indicatrix B with the growth of the albedo. The OSR flows are practically independent of the type of B. The authors give a quantitative evaluation of the applicability of the Lambertian system of conversion from the brightness to the flow for the surface with arbitrary B and Albedo A. They show that the greater is A the more rigid the requirements are presented to value B. With the exception of small regions of angles, the Lambertian system is applicable to the watery underlying surface and is not applicable to the snow surface.

Introduction

Calculations performed in works [1, 2], enable us to turn to the analysis of our principal problem, namely the development of a system of conversion from brightness, measured from a satellite to the flow of shortwave radiation going into the outer space. This flow is indispensible for calculating the radiation balance of the atmosphere and further for evaluating the heating of the atmosphere through absorption of solar radiation. /142

Let us assume that a lowest limit of the radiation heating, which is still worthwhile taking into account, has the following value

$$\frac{dT}{dt} = 0.5 \quad \text{degrees/24 hrs.} \tag{1}$$

Considering the atmosphere to be homogeneous with parameters $c_p = 0.24$ cal/gram/degree $\rho H = 10^3$ gram/cm^2, it is easy to find the amount of heat, which is absorbed by the column of the atmosphere of a unit cross-section in a unit of time in measuring the temperature per 0.5°/24 hrs. through radiation heating

$$\frac{\Delta Q}{\Delta t} = c_p \rho \frac{dT}{dt} H \approx 0.08 \quad \text{cal/min.} \tag{2}$$

Apparently the flow value obtained yields an absolute error permissible in the determination of the radiation balance.

Since the transfer of radiant energy through the arbitrary element of volume occurs in the vertical direction (within the framework of the plane-stratified model of the atmosphere), this radiation, absorbed by the vertical column, is determined by the flows of energy on the upper and lower boundaries F_1 and F_2

$$\frac{\Delta Q}{\Delta t} = (F_1 - F_2) \quad \text{cal/cm}^2 \cdot \text{min.} \tag{3}$$

As we know, $F_1 = S_0 \cos i - F^{\uparrow}$, $F_2 = E(1 - A)$. Here, S_0 is solar constant. $F^{\uparrow}$ is the flow leaving the upper boundary for the outer space, E is the total radiation near the surface of the earth, A is the albedo of the underlying surface. From formulas (2) and (3) it follows that it is sufficient to determine the flows of the OSR (Outgoing Shortwave Radiation) with an accuracy of /143

$$\Delta F^{\uparrow} \approx 0.04 \quad \text{cal/cm}^2 \cdot \text{min.} \tag{4}$$

The fact that the absolute and not the relative error is essential in the determination of the flows, simplifies considerably the problem of finding the above-mentioned system of conversion with small albedos of the underlying surface, and to the contrary, complicates it with large A. Moreover, inasmuch as the value of the OSR flows above the sea is little greater than 0.1 cal/cm^2·min. [2] and consequently it is sufficient to determine them with the accuracy of the order of 40%, for the cloudless sea the values of the flows may be fixed at certain mean magnitudes. But this, of course, does not signify that we do not need any measurements of the outgoing radiation above the cloudless sea, since the OSR field carries information on the characteristics of the surface of the sea and the atmosphere and may serve for their determination. Moreover, inasmuch as in operative processing of information arriving from satellites, it is much more convenient to have a single algorithm for all the underlying surfaces, it is sensible to check the applicability of the Lambertian system of conversion from brightness to the flow [3] for the case of cloudless atmosphere above the sea. As we have already noted, the anisotropy of the reflection from the underlying surface affects the OSR field the stronger, the greater is the albedo of the surface. Let us turn to the quantitative side of this problem, carrying out a comparison of the radiation fields above the sea and snow.

§1. Deviation from the Lambertian Nature of the OSR Field Over Snow and the Sea

Let us examine the OSR field over snow with a reflection coefficient taken from work [4]:

$$R_c(\theta, i, \varphi)=\frac{1}{\pi}\{2{,}4(1-\cos\theta-\cos i+\cos\theta\cos i)(1+\cos\varphi)+ \\ +0{,}6\cos i-0{,}06\cos\theta\cos i\}. \tag{5}$$

Here we do not exclude the effect of diffused radiation, therefore function $R_c(\theta, i, \phi)$ determines the reflection of total radiation. The intensity of the radiation reflected from the surface on the upper boundary of the atmosphere is expressed with the formula

$$I_0(\theta, i, \varphi)=R_c(\theta, i, \varphi)\psi(i, \theta), \tag{6}$$

where

$$\psi(i, \theta)=\int\limits_{0,4}^{2,5} E[\lambda, i, A_c(i)]\, T(\lambda, \theta)\Big|_0^{\infty} d\lambda, \tag{7}$$

E is the total illuminance, T is the transmission function of the atmosphere, $A_c(i)$ is the albedo of the snow, obtained easily from the expression for the reflection coefficient:

$$A_c(i)=\int\limits_0^{\pi} d\varphi \int\limits_0^{\frac{\pi}{2}} R_c[\theta, i, \varphi)\sin 2\theta\, d\theta=0{,}8-0{,}24\cos i. \tag{8}$$

Adding up the reflected radiation with the brightness of the haze, we obtain the OSR field over the snow on the upper boundary of the atmosphere:

$$I(\theta, i, \varphi)=I_0(\theta, i, \varphi)+I_D[\theta, i, \varphi, A_c(i)]. \tag{9}$$

In the same way as in the case of the sea [1] it isn't hard to find the OSR field above the Lambertian snow surface I', for which it is sufficient to replace in formula (6) $R_c(\theta, i, \phi)$ by $A_c(i)/\pi$. Let us write down the magnitudes of the mean values and dispersion functions f = I/I' for the sea ($\bar{f}_m, \sigma_m$) and snow (f_c, σ_c) underlying surfaces (Table 1). We see, that the deviations from the Lambertian state is quite large and approximately of the same order for both cases, although the anisotropy of the reflection from the wave covered sea is expressed more sharply. This is explained by the fact that upon conversion from the sea surface to the snow the albedo grows considerably and the contribution of the diffused radiation to the outgoing radiation decreases appreciably. The latter results in an increase of the sensitivity of the outgoing radiation intensity to the type of the reflection coefficient, which /144 compensates the decrease of the anisotropy of reflection upon conversion from the sea to the snow and the results in an approximately similar deviation from the Lambertian state. We note, that the absolute changes of intensity upon conversion from the real reflection to the isotropic in the case of snow will be noticed more. Indeed,

$$\frac{I}{I'}=f, \quad \Delta I=I'-I=I'(1-f),$$

but value I' is several times greater for snow than for the sea, and values $\bar{f}_u$ and $\bar{f}_c$ are approximately equal. As for the OSR flows, upon the replacement of the real reflection with isotropic reflection they change negligibly little. These flows coincide on the level of the underlying surface (surfaces with equal albedo and different reflection laws are compared) and the equality between them on the upper boundary of the atmosphere is disrupted only through the change of the absorption of reflected radiation upon the redistribution of it over the angles. Therefore, in calculating the flows of outgoing radiation with any underlying surface, we can always consider that the reflection occurs isotropically. Our problem however, is much more complicated. We had to determine the OSR flow according to a separate value of the intensity, which depends to a great extent on the reflection coefficient.

TABLE 1. MEAN VALUES AND DISPERSION OF THE RELATIVE DEVIATION OF THE OSR FIELD FROM THE FIELD WITH ISOTROPIC REFLECTION FOR THE SEA AND SNOW.

$i°$	$\bar{f}_M$	σ_M	$\bar{f}_c$	σ_c
20	1,1	0,27	0,97	0,07
40	0,96	0,29	0,94	0,22
60	0,92	0,40	0,87	0,36
80	0,86	0,35	0,79	0,40

Tr. Note: Commas indicate decimal points.

§2. Effect of the Reflection Anisotropy on the Outgoing Radiation With Different Albedos

Let us examine the problem of the sensitivity of the OSR field to anisotropy of reflection in relation to the albedo of the underlying surface. For this purpose it is convenient to divide the reflection coefficient R into the energy (albedo of direct radiation A) and angular (reflection R' indicatrix) parts: /145

$$R(\theta, i, \varphi)=A(i)R'(\theta, i, \varphi). \tag{10}$$

For the coefficient and the indicatrix of the reflection as we know, the following standardization conditions are fulfilled:

$$\int\limits_{(2\pi)} R(\theta,\ i,\ \varphi)\cos\theta\, d\omega = A(i), \quad \int\limits_{(2\pi)} R'(\theta,\ i,\ \varphi)\cos\theta,\ d\omega = 1. \tag{11}$$

In the case of isotropic reflection values R and R' have a simple form:

$$R_{is} = \frac{A}{\pi}, \quad R'_{is} = \frac{1}{\pi} = 0{,}318\,\frac{1}{\text{ster.}} \tag{12}$$

The radiation intensity on the upper boundary of the atmosphere may be presented in the form of

$$I = I_0 + I_p, \tag{13}$$

where I_p is the contribution of the diffused radiation in the OSR field. However upon the change of the reflection coefficient through the value of R' (with a fixed albedo) there is a change in only the reflected direct radiation I_0:

$$I_0(\theta,\ \varphi,\ i) = R(\theta,\ i,\ \varphi)\, I_1(i,\ \theta) = A(i)\, R'(\theta,\ i,\ \varphi)\, I_1(i,\ \theta), \tag{14}$$

where

$$I_1(i,\ \theta) = \int\limits_{0,4}^{2,5} E(\lambda,\ i)\, T(\lambda,\ \theta) \Big|_0^\infty d\lambda \tag{15}$$

is the direct radiation at the level of the underlying surface. Therefore,

$$\Delta I(\theta,\ i,\ \varphi) = \Delta I_0(\theta,\ i,\ \varphi) = A(i)\, \Delta R'(\theta,\ i,\ \varphi)\, I_1(i,\ \theta). \tag{16}$$

From this we can see, that the sensitivity of the outgoing radiation intensity to the type of the reflection indicatrix increases linearly with the increase of

$$A\left(\frac{dI}{dR} = AI_1\right)$$

Inasmuch as the albedo may change more than by one order (for example in conversion from water to snow) and inasmuch as we are interested precisely by the absolute errors, caused by the approximate estimation of the reflection anisotropy (the absolute errors of the currents sought is fixed for the system of conversion), then, if for the two surfaces $A_2/A_1 = \alpha > 1$, the reflection indicatrix for the first surface may be prescribed with an absolute error α times greater than for the second:

$$\frac{\Delta R_1'}{\Delta R_2'} = \frac{A_2}{A_1}\bigg|_{\Delta I = \mathrm{const}}. \tag{17}$$

With the growth of the albedo there is also an increase of the relative change of intensity of the outgoing radiation when the reflection indicatrix increment value ΔR' is fixed. Actually, let us examine the expression

$$\frac{I(R'+\Delta R') - I(R')}{I(R')} = \frac{\Delta I}{I} = \frac{\Delta I_0}{I_0 + I_p}. \tag{18}$$

Using formulas (14) and (16), we converted to the form

$$\frac{\Delta I}{I} = \frac{\Delta R'}{R'} \frac{1}{\left(1 + \frac{I_p}{I_0}\right)}. \tag{19}$$

Inasmuch as the contribution of diffused radiation to the outgoing radia- /146
tion decreases with the growth of the albedo, the ratio I_p/I_0 increases and value ΔI/I increases.

§3. Applicability of the Lambertian System of Conversion

Let us examine the question of applicability of the Lambertian system of conversion from brightness to flows [3] in the case of anisotropic reflection from the underlying surface. Let us find the relationship between the deviation from the isotropic reflection and the corresponding change of the flow of the outgoing radiation, obtained according to the Lambertian system. More precisely, according to the prescribed value of the radiation intensity I(i, θ, ϕ) we look for the deviation ΔR'(θ, i, ϕ) of the reflection indicatrix from the Lambertian (with a fixed albedo A), causing error ΔF in the determination of the Lambertian system of hemispheric flow F. Let us remind the reader that the flow of outgoing radiation from the upper boundary is practically independent on the type of brightness indicatrix, and is determined by the height of the sun and the albedo, therefore, here we are speaking about the errors introduced by the conversion system. For value I in the case of anisotropic reflection from formulas (13) and (14) we have

$$I(\theta, i, \varphi, A, R') = AR'(\theta, i, \varphi) I_1(i, \theta) + I_p(\theta, i, \varphi, A). \tag{20}$$

From here, according to the prescribed value of I (the value measured on the satellite) and the known functions R', and I_1 and I_p we can find A and then the looked-for flow F(i, A). If, however, we consider the reflection from the given surface to be isotropic (R' = 1/π), i.e., we apply the Lambertian system, then with the same value of I we obtain a different albedo A' and accordingly an incorrect value of the flow F(i, A'). Considering the diffused radiation to be the linear function of the albedo and using equation (20), we can easily find the looked-for dependence of the value $\Delta R'$ on I and ΔF. It is more convenient, however, to correlate function $\Delta R'$ with values of ΔF and A, so as to obtain directly the permissible deviations from the isotropic reflection for the surface with the prescribed albedo. Let I be the intensity of the outgoing radiation over the Lambertian surface with albedo A, F(I) is the current obtained according to the Lambertian system and coinciding with its true value. With deviation from the isotropic reflection by the value of $\Delta R' = |1/\pi - R'|$ the intensity I will change according to formula (16): $\Delta I = A\Delta R' I_1$; and although the OSR flow remains the same, the application of the Lambertian system will results in an error $\Delta F = dF/dI \times \Delta I$. From here we at once find the looked-for relationship between the values $\Delta R'$, ΔF and A:

$$\Delta I = \frac{dI}{dF}\Delta F = A\,\Delta R' I_1, \quad \frac{dI}{dF} = \frac{dI}{dA}\Big/\frac{dF}{dA} \tag{21}$$

and

$$\Delta R'(A, \Delta F, i, \theta, \varphi) = \frac{\Delta F}{A}\Phi(i, \theta, \varphi), \tag{22}$$

where

$$\Phi(i, \theta, \varphi) = \frac{\left(\frac{dI}{dA}\right)_{i, \theta, \varphi}}{\left(\frac{dF}{dA}\right)_i I_1(i, \theta)}. \tag{23}$$

Using the OSR field values calculated by us [3], we have found function Φ. It was found that dependence upon angle ϕ is practically absent, and the changes with respect to θ are noticeable only at large angles; the final values of function $\Phi(i, \theta)$ are summarized in Table 2. In this way, prescribing to ourselves error ΔF in the determination of the flow and albedo A, we at once find the deviation from the isotropic reflection, with which we may still use the Lambertian system to obtain the correct values of the OSR flow (within the bounds of error ΔF). Formula (22) has a clear physical sense: the greater the albedo, the stronger is the influence of the underlying surface on the outgoing radiation, and consequently, the smaller are the changes in the reflection indicatrix which lead to the same errors in the determination of the flow; the direct proportionality between $\Delta R'$ and ΔF signifies the simple fact that the greater the deviation from the isotropic reflection, the rougher is the determination of the flow according to the Lambertian system; and finally, the increase of function $\Phi(i, \theta)$ upon the increase of i and θ is connected with the decrease of the contribution of the underlying surface to the outgoing radiation at lower altitudes of the sun. Therefore it is not difficult to evaluate the correctness of the Lambertian system for the wave covered marine surface, and also to carry out a comparison with the case of reflection from /147 the snow surface. Let ΔF = 0.04 cal/cm^2·min., according to formula (4). Then in the case of the sea, using the value of the direct radiation albedo [5], we obtain for all i and $\theta \leq 60°$,

$$\Delta R' \approx 0.60, \quad \frac{\Delta R'}{R'_{is}} = \pi \Delta R' \approx 190\%. \tag{24}$$

TABLE 2. FUNCTION $\Phi(i,\theta)$ STER.$^{-1}$ (cal/cm^2 min.)$^{-1}$.

$i°$	$\theta°$		$i°$	$\theta°$	
	0—60	75		0—60	75
20	0,42	0,54	60	0,94	1,2
40	0,54	0,64	80	4,1	4,9

Tr. Note: Commas indicate decimal points.

We can see that the permissible deviations from the Lambertian nature are quite large. The regions of angles, for which $\Delta R' > 0.60$ and which should be excluded when the Lambertian conversion system is used, are given in Table 3. The values of the corresponding solid angles in fractions of the hemispherical angle 2π given there also, show that the Lambertian system yields correct values of flows in more than 90% of the cases.

TABLE 3. REGIONS OF NON-APPLICABILITY OF THE LAMBERTIAN SYSTEM IN THE CASE OF THE SEA.

$i°$	$\Delta\varphi$	$\theta°$	$\frac{\omega}{2\pi}$	$i°$	$\Delta\varphi$	$\theta°$	$\frac{\omega}{2\pi}$
0	0—180	0—15	0,034	60	0—15	40—90	0,064
20	0—45	15—40	0,050	80	0—10	60—90	0,028
40	0—25	30—90	0,12				

Tr. Note: Commas indicate decimal points.

Let us examine analogous relationships for the OSR field over snow. Again, assuming that ΔF = 0.04 cal/cm^2 min., we obtain with formula (22) the permissible deviations from the isotropic reflection (Table 4). Here, the requirements to the reflection indicatrix are considerably more rigid than in the case of the sea, and the regions of inapplicability of the Lambertian system are quite large and amount, as indicated by the elementary estimation, to 16, 38, 49 and 23% of the hemispherical angle 2π for i, equal to 20, 40, 60, and 80° respectively. The error ΔF for all the angles exceeds considerably the limit of 0.04 cal/cm^2 min. established by us. /148

TABLE 4. PERMISSIBLE DEVIATIONS FROM THE ISOTROPIC REFLECTION FOR THE SNOW SURFACE

$$\Delta R' = \frac{\Delta F}{A} \Phi(i, \theta) \left[\frac{1}{\text{ster}}\right], \quad \Delta F = 0{,}04 \ \text{cal/cm}\cdot\text{min}$$

$i°$	A	$\Delta R'$ $\theta = 0$–$60°$	$\Delta R'$ $\theta = 75°$	$i°$	A	$\Delta R'$ $\theta = 0$–$60°$	$\Delta R'$ $\theta = 75°$
20	0,58	0,029	0,037	60	0,68	0,055	0,071
40	0,62	0,035	0,041	80	0,76	0,22	0,26

Tr. Note: Commas indicate decimal points.

In this way, also the anisotropy of the reflection is considerably higher for the sea than for the snow, the absolute deviations of the OSR field from the corresponding values with isotropic reflection on the average are considerably higher in the case of snow, and although it looks strange at first glance, the Lambertian system of conversion from brightness to the flows may be applied with much greater substantiation to the sea than to the snow. This is explained, as we had already mentioned, by the increase of the sensitivity of the outgoing radiation field to reflection anisotropy upon the increase of the albedo.

§4. The Role of the Clouds, Conclusion

In connection with the above the correct estimation of the reflection from clouds should be extremely important. Unfortunately the systematic data on brightness indicatrices of the clouds are absent. These indicatrices depend on both the face structure of the cloud (we know that the clouds with an "icy" summit have a strong mirror effect), and also in the form of their surface. Stratiform clouds usually have a slightly undulating almost flat surface, whereas for the cumuliform clouds the presence of individual pillars, ridges, and breaks, is characteristic. Therefore the cumulus clouds indicatrixes may be very greatly (because of the shading, etc.) differ from the theoretical calculations, usually carried out for flat layers.

Let us return to the stratiform clouds and estimate the minimum error in the flow, which will be caused by the reflection anistropy.

From formula (22) we have

$$\Delta F = \frac{A}{\Phi(i, \theta)} \Delta R'. \tag{25}$$

For evaluation of ΔR' let us turn to the calculation by Ye. M. Feygel'son ([6] Chapter 6). In her designations, value R' will be

$$R' = \frac{R}{A} = \frac{I(\theta, i, \varphi)}{\int\limits_{(2\pi)} I(\theta, i, \varphi) \cos\theta \, d\omega}. \tag{26}$$

Let us note, that the data in Table 6, 11 in [6] are 100% too high. This has no significance for calculation of R' according to (26), but we should take it into account in comparing with other calculations, The calculations /149
with formulas (25) and (26) yielded the following values of error ΔF in cal/ /cm^2·min., for the cases selected by us;

ΔF = 0.074 with θ = 0 and ΔF = 0.027 with θ = 45°, φ = 0 (i = 30°),

ΔF = 0.03 with θ = 0 and ΔF = 0.001 with θ = 45°, φ = 0 (i = 50°).

The first value of ΔF is greater than the permissible error of 0.04, the others lie within the required limits..

In the light of the obtained results we should revise the problem on the determination of the OSR field over the clouds, which was calculated in the assumptiom of the isotropic reflection. Actually, inasmuch as the albedo of clouds reaches great values, the permissible deviations from the Lambertian nature will be approximately the same as for the surface of the snow also (see Table 4), and also there is no basis for attributing the "snow" reflection coefficient to the clouds (5), nevertheless, we may expect that the regions of inapplicability of the Lambertian system in the case of clouds will be noticed, since it will not be possible to disregard them, especially if we shall require an accuracy greater than 0.04 cal/cm^2·min. Therefore, first of all it is necessary to determine experimentally the reflection indicatrix (both integral and spectral) in relation to the albedo and the type of cloudiness, and the thicker the clouds the more precise should be the measurements. The accumulation of sufficient material will enable us after its statistical processing, to obtain the standard reflection indicatrix in the clouds and construct the corresponding system of the transfer from brightness to the flow assuring the minimum error. Similarly, having available to us the experimental data on the reflection indicatrixes and the albedo of the real underlying surfaces, we can plot a non-Lambertian system for the entire terrestrial globe, which would enable us to determine the OSR flows with greater accuracy than it is given by the Lambertian model.

REFERENCES

1. Shifrin, K. S. and V. Yu. Kolomiytsev: "The OSR Field Above the Sea," See the present collection.
2. Kolomiytsev, V. Yu.: "Contribution of the Diffused Reflection by the Water Layer to the Outgoing Shortwave Radiation Field," See the present collection.
3. Shifrin, K. S.; V. Yu. Kolomiytsev and N. P. Pyatovskaya: "Determination of the OSR Flow by Means of Satellites," *Trudy GGO*, Issue 166, 1964.

4. Malkevich, M. S.: "On the Effect of Nonorthotropicity of the Underlying Surface on the Diffused Light in the Atmosphere," *Izv. AN SSSR, Geographical Series*, No. 3, 1960.
5. Avaste, O. A.; Yu. R. Mullamaa and K. S. Shifrin: "The OSR Field with an Nonorthotropic Underlying Surface," *Investigations on the Physics of the Atmosphere, IFA AN ESSR*, No. 6, 1964.
6. Feygel'son, Ye. M.: *"Radiatcionnyye Protsessy v Sloistoobraznykh Oblakakh"* [Radiation Processes in Stratiform Clouds], Nauka Press, 1964.

DETERMINATION OF WIND VELOCITY AND WAVES ON THE SEA BY MEASURING THE SOLAR GLITTER PARAMETERS FROM SATELLITES

K. S. Shifrin and V. Yu. Kolomiytsev

ABSTRACT. It is shown that it is possible to obtain not more than three gradations of wind velocity above the oceanic surface in the 0 to 15 m/sec. range. The measurement of wind direction and also velocities greater than 15 m/sec. is impossible by this method. It is necessary to have on the satellite a system, making it possible to measure the radiation, coming from the given point in two (or several) prescribed directions. It is required to develop a reliable method, with which it is possible to separate the cases of cloudless atmosphere in the measurements of the solar glitter from a satellite. Aircraft measurements should be made of the solar glitter at various wind velocities and sun elevations.

§1. Introduction

To determine the wind velocity in the water level layer G. V. Rosenberg and Yu. R. Mullamaa [1] proposed, as we have already noted in work [2], to use two parameters: the displacement of the maximum of brightness of the solar glitter towards the horizon, which grows rapidly with the increase of the wind velocity v and the lateral brightness gradient $dI/d\phi$. The dependence of these parameters from the wind direction is very small, and cannot serve for determining the latter. The values of angle θ_{max} given in [2], corresponding to the maximum of brightness of the glitter, indicates that the position of the maximum may be recorded only with small i, inasmuch as upon the increase of the zenith distance of the sun, the glitter rapidly approaches the horizon and even goes beyond the horizon. The same circumstance makes it impossible to draw any kind of information on the water level layer according to the measurements of the outgoing radiation with a low sun, especially if we take into account the screening effect of the atmosphere. Therefore, it is reasonable to examine the reflection of the sea only with $i \leq 60°$. As for the lateral brightness gradient, we know that this determination is connected with the necessity of absolute measurements, which renders the problem much more complicated: the measurement of the logarithmic gradient $d \log I/d\phi$ however, is not advisable because of its small sensitivity to wind velocity [1]. /150

In the present article we shall examine the solar glitter, taking into account the diffusion in the atmosphere and find, how the outgoing radiation field changes above the sea on the upper boundary of the atmosphere upon the change of the wind velocity. This will enable us to evaluate the possibility of determining the wind velocity and the waves on the sea according to the measurements of the solar glitter parameters from the satellites.

§2. Sensitivity of the OSR Brightness Field to Wind and Waves on the Sea

The diffusion of radiation in the atmosphere has a parasitic influence. In order to decrease this effect it is necessary to carry out the measurements with greater wavelengths. Therefore we have performed calculations for the following three sectors of the spectrum:

$\lambda = 0.76\ \mu$ (0.74-0.79 μ , transparency window), /151

$\lambda = 1.31\ \mu$ (1.25-1.38 μ, the water vapor absorption band), and

$\lambda = 1.68\ \mu$ (1.67-1.70 μ, transparency window).

The further advance into the IR-region is hardly sensible, inasmuch as the sensitivity to the reflecting properties of the water surface will not increase, and the amount of energy, coming to the receiver, will rapidly diminish. For the intensity of the radiation on the upper boundary of the atmosphere we have

$$I_v(\lambda, \theta, \varphi, i) = I_{0v}(\lambda, \theta, \varphi, i) + I_S(\lambda, \theta, i) + I_D(\lambda, \theta, \varphi, i), \qquad (1)$$

where: I_{0V} is the reflected direct radiation, I_S is the reflected radiation of the sky, I_D is the brightness of the haze.

Let us stress, that on the wind velocity depends only the first component, the calculation of which with a known reflection coefficient $R_V(\theta, i, \phi)$ is not difficult. Let us write formula (1) more briefly

$$I_v(\lambda, \theta, \varphi, i) = I_{0v}(\lambda, \theta, \varphi, i) + I_p(\lambda, \theta, \varphi, i). \qquad (1')$$

The outgoing radiation field component independent of v was calculated in work [6] according to the system developed by us [3], and the coefficients of reflection were taken from works [4, 5, 6]. The calculated values I_V in M cal/cm^2 min·ster. (integral in the above-mentioned spectral intensity ranges) for i = 0, 20, 60° and v = 2, 5, 10, 15 m/sec., are given in Table 1.

We can see, that the brightness fields change appreciably upon conversion from one wind velocity to another, especially with small v, dI_V/dv being maximum in the region of angles, directly adjacent to the direction of the mirror ray ($\theta = i$, $\phi = 0$). Therefore, the measurement of the absolute value of the intensity for this direction may serve for determining the velocity.

Upon the increase of the wavelengths the drop between the maximum and the minimum values of the radiation field $[I_{max}/I_{min}]$ increases in the sectors of the spectrum outside of the absorption bands.

In Table 2 we give the ratio between the full intensity of radiation to its part independent on v (I_v/I_p), from which immediately follows the decrease of the contribution of the diffused radiation to the brightness of the glitter with the growth of the wavelength and the blurring of the glitter (decrease in the maximum with increase along the edges) upon the increase of the wind velocity. The latter indicates the small sensitivity of the radiation field to the wind velocity with large v.

Let us examine the lateral brightness gradient of the glitter on the upper boundary of the atmosphere. In Table 3 we give the values of $dI/d\phi$ for four i (0, 20, 44 and 60°), four v (2, 5, 15 m/sec.) and three λ (0.76; 1.31; 1.68 μ) with $\theta \approx i$ and $\phi = 0$.

The first thing that strikes the eye is the sharp decrease of the gradient with the increase of the velocity (as it is without the allowance for the atmosphere [1]), which once more indicates the small effectiveness of the optical method of determination of velocity when its values are great. Moreover, the smaller wavelengths are more advantageous for measurement [$dI/d\phi$ is maximum with $\lambda = 0.76\ \mu$). This is explained by the fact, that the gradient is determined by the difference of absolute values of the intensities of the /154 reflected direct radiation (since the brightness of the haxe changes much slower than the brightness of the glitter), while upon the decrease of λ this difference grows through the increase of the solar constant faster than it decreases through the diffusion in the atmosphere. The value of the brightness gradient for all the shortwave region (0.4-4 μ) exceed by more than one order the corresponding values for $\lambda = 0.76\ \mu$ ($\Delta\lambda = 0.05\ \mu$). Thus, for $dI/d\phi$ the millicalories/cm^2 min·ster·degree.with $i = 20°$ and $i = 60°$ we have: (See Table 4).

In this way, in order to determine v according to the lateral gradient of the solar glitter we can use the integral measurements in the entire shortwave region of the spectrum. However, in order to find the velocity with the accuracy of about 3 m/sec., it is necessary to carry out measurements of the absolute values of the intensities with a relative error of about 4% in the band between 10 and 250 millicalories/cm^2 min·ster.

In the measurements in individual spectral ranges the same accuracy is needed as with smaller values of the signal.

TABLE 1. THE SPECTRAL FIELD OF THE OUTGOING RADIATION OVER THE SEA ON THE UPPER BOUNDARY OF THE ATMOSPHERE WITH DIFFERENT WIND VELOCITIES

$I_v(\lambda, i, \theta, \varphi)\left[\frac{\text{MILLICALORIES}}{\text{cm}^2\ \text{min}\cdot\text{ster}}\right]$

v m/sec	θ°	λ μ			λ = 0,76 μ			λ = 1,31 μ			λ = 1,68 μ		
		0,76	1,31	1,68	φ = 0	φ = 30	φ = 90	φ = 0	φ = 30	φ = 90	φ = 0	φ = 30	φ = 90
		$i = 0°$			$i = 20°$								
2	0	9,64	1,44	1,03	1,45			0,213			0,110		
	23	1,20	0,175	0,076	9,02	4,15	0,881	1,21	0,558	0,125	0,974	0,419	0,043
	60	1,10	0,152	0,052	1,06	1,06	1,08	0,151	0,151	0,150	0,052	0,051	0,051
5	0	4,98	0,759	0,508	2,08			0,305			0,182		
	23	2,01	0,286	0,168	4,82	3,22	1,08	0,646	0,432	0,152	0,494	0,312	0,066
	60	1,10	0,152	0,052	1,19	1,10	1,08	0,165	0,155	0,150	0,068	0,056	0,051
10	0	3,07	0,479	0,296	1,89			0,277			0,160		
	23	2,23	0,317	0,193	2,98	2,41	1,24	0,393	0,324	0,174	0,285	0,220	0,085
	60	1,11	0,153	0,053	1,62	1,24	1,08	0,214	0,171	0,151	0,122	0,073	0,051
15	0	2,39	0,379	0,219	2,29			0,334			0,205		
	23	2,13	0,303	0,181	2,29	2,00	1,27	0,307	0,269	0,177	0,206	0,174	0,087
	60	1,15	0,158	0,058	1,95	1,40	1,11	0,250	0,188	0,153	0,162	0,093	0,054
					$i = 60°$								
2	0				0,637			0,079			0,030		
	60				17,7	1,60	0,982	1,71	0,219	0,129	2,27	0,076	0,049
	78				14,3	6,86	2,25	1,41	0,762	0,262	1,35	0,400	0,150
5	0				0,697			0,079			0,030		
	60				9,35	1,62	0,982	0,933	0,221	0,129	1,11	0,079	0,049
	78				19,5	6,86	2,25	1,80	0,762	0,262	2,32	0,400	0,150
10	0				0,659			0,081			0,032		
	60				5,91	1,69	0,982	0,585	0,227	0,129	0,631	0,089	0,049
	78				19,3	6,86	2,25	1,78	0,762	0,262	2,28	0,401	0,150
15	0				0,692			0,085			0,037		
	60				4,68	1,76	0,982	0,501	0,234	0,129	0,460	0,098	0,049
	78				18,0	6,88	2,25	1,68	0,764	0,262	2,04	0,404	0,150

Tr. Note: Commas indicate decimal points.

TABLE 2. CONTRIBUTION OF THE DIFFUSED RADIATION IN THE FIELD OF THE OUTGOING RADIATION ON THE UPPER BOUNDARY OF THE ATMOSPHERE

$$\left(\frac{I_v(\lambda, i, \theta, \varphi)}{I_p(\lambda, i, \theta, \varphi)}\right)$$

λ μ	θ°	v m/sec															
		2	5	10	15	2	5	10	15	2	5	10	15	2	5	10	15
						$\varphi=0°$				$\varphi=30°$				$\varphi=90°$			
		$i=0°$				$i=20°$											
0,76	0	10,6	5,48	3,38	2,63	1,74	2,50	2,27	2,75	1,74	2,50	2,26	2,75	1,74	2,50	2,27	2,75
	23	1,35	2,26	2,50	2,39	11,6	6,22	3,85	2,95	5,30	4,11	3,07	2,55	1,06	1,29	1,48	1,52
	60	1,00	1,00	1,01	1,04	1,00	1,12	1,53	1,84	1,00	1,04	1,17	1,32	1,00	1,00	1,00	1,03
1,31	0	8,94	4,71	2,98	2,35	1,73	2,48	2,25	2,72	1,73	2,48	2,25	2,72	1,73	2,48	2,25	2,72
	23	1,32	2,15	2,38	2,28	12,7	6,27	3,87	2,98	5,31	4,11	3,08	2,56	1,05	1,28	1,46	1,49
	60	1,00	1,00	1,01	1,04	1,00	1,09	1,42	1,66	1,00	1,03	1,13	1,24	1,00	1,00	1,00	1,02
1,68	0	19,4	9,58	5,58	4,13	2,72	4,51	3,97	5,08	2,72	4,51	3,97	5,08	2,72	4,51	3,97	5,08
	23	1,86	4,09	4,70	4,41	29,2	14,8	8,53	6,16	12,4	9,23	6,50	5,14	1,14	1,74	2,23	3,31
	60	1,00	1,00	1,02	1,13	1,01	1,31	2,37	3,15	1,00	1,10	1,43	1,83	1,00	1,00	1,01	1,06
						$i=60°$											
0,76	0					1,00	1,00	1,03	1,09	1,00	1,00	1,03	1,09	1,00	1,00	1,03	1,09
	60					8,76	4,63	2,92	2,32	1,00	1,01	1,06	1,10	1,00	1,00	1,00	1,00
	78					1,40	1,91	1,89	1,79	1,00	1,00	1,00	1,00	1,00	1,00	1,00	1,00
1,31	0					1,00	1,00	1,03	1,08	1,00	1,00	1,03	1,08	1,00	1,00	1,03	1,08
	60					6,73	3,67	2,30	1,97	1,00	1,01	1,04	1,07	1,00	1,00	1,00	1,00
	78					1,27	1,62	1,60	1,51	1,00	1,00	1,00	1,00	1,00	1,00	1,00	1,00
1,68	0					1,00	1,00	1,09	1,23	1,00	1,00	1,09	1,23	1,00	1,00	1,09	1,23
	60					25,0	12,2	6,95	5,07	1,00	1,03	1,16	1,29	1,00	1,00	1,00	1,00
	78					2,33	4,01	3,94	3,52	1,00	1,00	1,00	1,01	1,00	1,00	1,00	1,00

Tr. Note: Commas indicate decimal points.

TABLE 3. THE LATERAL GRADIENT OF THE SOLAR GLITTER ON THE UPPER BOUNDARY OF THE ATMOSPHERE.

millicalories/cm^2 min·ster.·deg.

λ_μ	v m/sec 2	5	10	15	v m/sec 2	5	10	15
	$i=0°$				$i=20°$			
0,76	0,26	0,11	0,05	0,02	0,16	0,053	0,019	0,010
1,31	0,04	0,02	0,01	0,01	0,022	0,007	0,002	0,001
1,68	0,03	0,01	0,01	0,002	0,018	0,006	0,002	0,001
	$i=44°$				$i=60°$			
0,76		0,16	0,086		0,54	0,26	0,14	0,097
1,31		0,018	0,009		0,050	0,026	0,019	0,009
1,68		0,020	0,010		0,073	0,034	0,018	0,012

Tr. note: Commas indicate decimal points.

TABLE 4.

$i°$	v m/sec 2	5	10	15	$i°$	v m/sec 2	5	10	15
20	2,4	0,75	0,4	0,17	60	6,9	3,3	1,8	1,3

Tr. Note: Commas indicate decimal points.

Let us return to the examination of relative values and their relationship with the wind velocity. Let f(v) represent the ratio between the brightness of the glitter in the direction of the mirror ray ($\theta \approx i$, $\phi = 0$) to the intensity of the radiation under the same zenith angle in the plane perpendicular to the solar vertical, i.e.,

$$f(v)=\frac{I_v(\theta\approx i,\ \varphi=0)}{I_v(\theta\approx i,\ \varphi=90°)}. \tag{2}$$

Here, again we find rapid decrease of function f(v) with small velocities /155 and a slow decrease with large velocities through the blurring of the glitter (Table 5).

Function f(v) reaches the maximum values when $\lambda = 1.68\ \mu$ through deep minima, caused by a small contribution of the haze (Table 2). Prescribing the same error $\Delta v = 3$ m/sec. we find that the relative values of the intensities should be measured with an error of about 6-7% for $\lambda = 0.76\ \mu$ in the signal range of 0.5-20 millicalories/cm^2 min·ster. Measurements with $\lambda = 1.68\ \mu$ may be carried out with a somewhat lower accuracy (about 10%), but with considerably smaller values of energy 0.03-2 millicalories/cm^2 min·ster.

In general upon the expansion of the spectral ranges and upon the conversion to smaller wavelengths, function f(v) will decrease and accordingly the required accuracy of the measurements will increase, but the values of the signals will grow and the ratio between the maximum intensity and the minimum will decrease. Thus, the measurements for the entire shortwave region (0.4-4μ) will require the accuracy of 5% in the energy range of 10-250 mcal/cm^{2}min^{2}ster. indicated, the drop of the intensities however, will decrease from 70 to 40 (for λ = 1.68 μ and λ = 0.76 μ respectively) to 25.

TABLE 5. RELATIVE VALUE OF THE MAXIMUM OF THE SOLAR GLITTER ON THE UPPER BOUNDARY OF THE ATMOSPHERE WITH DIFFERENT WIND VELOCITIES

λ μ	v m/sec											
	2	5	10	15	2	5	10	15	2	5	10	15
	$i=0°$				$i=20°$				$i=60°$			
0,76	10	5,1	2,8	1,9	10	4,5	2,4	1,8	18	9,5	6,0	4,8
1,31	11	5,7	3,3	2,2	9,7	4,3	2,3	1,7	13	7,2	4,5	3,9
1,68	24	12	5,2	2,8	22	7,5	3,4	2,4	46	23	13	9,4
	$f(v)=\frac{I_v(\theta=0)}{I_v(\theta=47°)}$				$f(v)=\frac{I_v(\theta=i,\ \varphi=0)}{I_v(\theta=i,\ \varphi=90°)}$							

Tr. Note: Commas indicate decimal points.

It is clear, that the selection of the optimum spectral range depends on the specific characteristics of the equipment.

From the data examined, we can see, that it is practically impossible to measure the wind velocity according to the lateral gradient of the glitter $dI/d\phi$, since this requires both absolute measurements, and a high accuracy of these measurements.

As a real method we can consider the determination of the relative variation of the brightness in the glitter (the measurement of function f(v)).

§3. The Difficulties and Prospects of the Method

On the basis of the calculations performed we can say even today that by the "solar glitter" method it would be hardly possible to obtain more than three gradations of velocity in the 0-15 m/sec range, and it will not be possible at all to determine the direction of the wind. The main shortcoming is /156
connected however, with the fact that this method does not permit us to carry out the measurements in the region of greater velocities, precisely when the data on the wind and waves are needed the most.

The measurement of large wind velocities by the solar glitter method is impossible inasmuch as even with v = 10 m/sec. it is greatly blurred and little sensitive to v. Naturally, we can hope that the albedo of the sea will change owing to the appearance of foam, however, the dependence of the albedo on the velocity with very large v's may be determined only experimentally. But even in the velocity range examined by us it is necessary to carry out additional investigations on determining the non-ambiguity of the relationship between the characteristics of the waves and the wind velocity, and also to find the relationship between the spectrum of the waves and Kocks and Munks function of distribution of planes along the inclines.

The latter will make it possible for us to determine the characteristics of the waves according to the measurements of the solar glitter. Moreover, it is important to determine how much the Kochs and Munk's function is typical for the entire world ocean. And the most important factor is that to obtain the final deductions and reliable quantitative relationships it is necessary to carry out measurements of the solar glitter from airplanes above the oceanic surface during various wind velocities and heights of the sun.

In conclusion we shall note two difficulties of the use of this method on satellites, which in our opinion are of a principial nature.

1. To determine the wind velocities in a given point, it is necessary to measure the radiation issuing from it at various angles. Thus, in order to obtain the value of function f(v) we should measure the brightnesses in two directions, located on the conical surface $\theta = i$ and separated by 90° over the azimuth, and whether in measurements from an airplane for the successive production of these signals it is sufficient merely to turn the vertical plane, passing through the axis of the instrument by 90°, this turn on a satellite would separate the points cited by a substantial distance. For example, when the satellite is at a height of h = 500 km above the surface of the earth, this distance will amount to about 1,000 km for $\theta = i = 60°$. Therefore, the signal ratio $\frac{I_v(\theta=i,\ \varphi=0)}{I_v(\theta=i,\ \varphi=90°)}$ in general is not at all equal to function f(v), unambiguously connected with the wind velocity, and we cannot say anything either about the first ($\phi = 0$), or of the second point ($\phi = 90°$) and cannot even talk about a certain mean velocity over a large territory, inasmuch as both signals are quite independent and carry no information on the regions being sighted (the measurements are made simply of the ratio between the intensities at different angles in different points). Hence, it follows that it is necessary to have a definite tracking system from a satellite for a given region, which assures its being viewed at prescribed angles.

2. The complete or partial filling of the field of vision of the instrument with clouds makes it impossible to use this method. Therefore, in measuring the solar glitter, we should be confident that the signal obtained pertains to a cloudless atmosphere and consequently, it is necessary to develop a method which would enable us to discard cases with cloudiness during the routine processing of information. Moreover, it is necessary to find a relationship between the wind velocity and the probability of inclusion of cloudiness in the instrument's field of vision for various values of the latter.

These data will determine the possibilities of the method and also the optimum value of the field of vision.

REFERENCES

/157

1. Rosenberg, G. V. and Yu. R. Mullamaa: "On Certain Possibilities of Determining Wind Velocity over the Oceanic Surface According to Satellite Observations," *Kosmicheskiye Issledovaniya*, Vol. 2, 1964.
2. Shifrin, K. S. and V. Yu. Kolomiytsev: "The OSR Field Above the Sea," See the present collection.
3. Shifrin, K. S.; V. Yu. Kolomiytsev and N. P. Pyatovskaya: "Determination of the OSR Flow by Means of Satellites," *Trudy GGO*, Issue 166, 1964.
4. Mullamaa, Yu. R.: "Diffused Reflection and Transmission of Light by an Uneven Surface of Two Isotropic Media," *Investigations on the Physics of the Atmosphere. IFA AN ESSR*, No. 3, 1962.
5. Mullamaa, Yu. R.: *"Atlas Opticheskikh Kharakteristik Vzvolnovannoy Poverkhnosti Morya,"* [Atlas of Optical Characteristics of a Wave Covered Surface of the Sea], IFA AN ESSR, 1964.
6. Avaste, O. A.; Yu. R. Mullamaa and K. S. Shifrin: "The OSR Field With an Nonorthotropic Underlying Surface," *Investigations on the Physics of the Atmosphere. IFA AN ESSR*, No. 6, 1964.

ON THE PROBLEM OF AVERAGING IN MEASURING HYDROMETEOROLOGICAL FIELDS

N. N. Verenchikov

ABSTRACT. In the article the author examines certain problems connected with the averaging in the measurement of hydrometeorological fields. He derives an equation for determining the root-mean-square error with which the value of the hydrometeorological element averaged within the limits of a certain range, may be assumed equal to the true element at the moment of time sought. Using the example of the temperature field of the surface in the Gulf Stream region it is shown how the representativity of the averaged measurements changes with the change in the averaging range. Using this work, it is possible to calculate the variability of the averaged values of the hydrometeorological element, i.e., such characteristics for example as the radius of the representative measurements, the error in the interpolation of the element according to its discrete averaged measurements, the required distance between the points of measurement with a prescribed maximum error of the measurement result interpolation, etc.

The variability of many hydrometeorological elements is extremely great, /158 and because of this the practical applicability of the results of individual measurements is substantially limited. In particular, the temperature of the water surface, for example in the Gulf Stream region, is so variable, that at the distances of more than 3 km and after a time period of more than 1.5 hrs. the measurements already lose their value, i.e., the mean value of the temperature characterizes it more precisely than the above-mentioned measurement. The situation is a little better but is in general quite similar with the representativity of the discrete measurements, between which interpolation of the values of the hydrometeorological element is possible. Thus, the interpolation of temperature of the water surface in the Gulf Stream region for the same reason is sensible only in case the distance between the measurement points does not exceed 7 km and the time period 4 hours.

The above-mentioned representativity of the results of measurements for an entire series of problems is quite insufficient. In connection with this the equation arises whether it is possible to characterize the true fields of the hydrometeorological element in particular the water surface temperature field, with some other field, which would transmit the principal features of the temperature field but would have a considerably lesser variability in time and space. Evidently, such a field may be the hydrometeorological element field, obtained as the result of measurements performed with the averaging within the bounds of a certain interval θ.

The averaging within the bounds of the prescribed range may be carried out technically by various ways and primarily by using an integrating device. In radiometric equipment of the infrared and centimeter range the averaging of the earth's surface temperature during measurements occurs through the finite dimensions of the instrument's resolution element.

It is necessary to note, that in any equipment because of its inertia, the measurement results are always smoothed out to a certain extent. As it has been shown in work [1] this smoothing out with the corresponding error may be equated with averaging.

The idea that the data on the averaged value of a meteorological element for a number of problems are more convenient than the true values, was expressed in many works [2, 3, 4]. In works [3, 4] on the basis of a series of experimental observations the optimum averaging range was determined for measurement of certain meteorological elements. In [2] the author examined the optimum properties of averages of meteorological fields in time and space. /159
This work makes it possible to determine the optimum averaging range of any hydrometeorological element, if we know its structural function. We should note, that this is important to know not only the optimum averaging range but also the effect yielded by the averaging, i.e., how the variability decreases and the representativity of the results of measurements carried out with various averaging ranges increases proportionally. None of the above mentioned works makes it possible to obtain this value. The variability of the hydrometeorological element is characterized by its structural function. Therefore, having established the relationship of the structural function of the values of the hydrometeorological elements averaged within the limits of certain range θ with its structural function, we shall solve our problem in the general form.

Let us assume, that beginning with a certain initial moment t = 0 the hydrometeorological parameter is averaged for a period of time (interval) θ. Later, at any moment of time t (the physical sense of t may be anything: time, distance r, vertical coordinate, etc.) the value of the hydrometeorological parameter is assumed equal to this mean value. Following [2], we shall find the root-mean-square error of this assumption:

$$\psi^2(\theta, t) = \overline{\left[f(t) - \frac{1}{\theta}\int_0^\theta f(\tau)\,d\tau\right]^2} =$$
$$= \frac{1}{\theta^2}\int_0^\theta d\tau \int_0^\theta \left[\overline{f(t)} - \overline{f(\tau)}\right]\left[\overline{f(t)} - \overline{f(\tau_1)}\right] d\tau_1. \tag{1}$$

Let us transform the expression (1) under the integral, using the identity:

$$2[\varphi(A)-\varphi(B)].[\varphi(C)-\varphi(D)]=[\varphi(A)-\varphi(D)]^2+[\varphi(B)-\varphi(C)]^2- \\ -[\varphi(A)\varphi(A)-\varphi(C)]^2-[\varphi(B)-\varphi(D)]^2, \tag{2}$$

where A, B, C, D are points in a fourth-dimensional space x, y, z, t. Then we obtain:

$$\psi^2(\theta,\ t)=\frac{1}{2\theta^2}\int_0^\theta d\tau\int_0^\theta [B(t-\tau_1)+B(\tau-t)-B(\tau-\tau_1)]\,d\tau_1= \\ =\frac{1}{\theta}\int_0^\theta B(t-\tau_1)\,d\tau_1-\frac{1}{2\theta^2}\int_0^\theta d\tau\int_0^\theta B(\tau-\tau_1)\,d\tau_1, \tag{3}$$

where B(t) is the structural function, depending on coordinate t.

If

$$B(t)=2\sigma^2\left(1-e^{-\alpha|t|}\right), \tag{4}$$

then

$$\psi^2(\theta,\ t)=2\sigma^2\left[\frac{1}{2}-\frac{1}{\alpha\theta}e^{-\alpha(t-0)}+\frac{1}{\alpha\theta}e^{-\alpha t}+\frac{1}{\alpha^2\theta^2}\left(\alpha\theta+e^{-\alpha\theta}-1\right).\right. \tag{5}$$

Having opened the indeterminancy, we can find that with $\theta = 0$ /160

$$\psi^2(\theta,\ t)=2\sigma^2\left(1-e^{-\alpha t}\right)=B(t). \tag{6}$$

With $t = \theta$

$$\psi^2(\theta,\ t)=\psi^2(\theta)=2\sigma^2\left[\frac{1}{2}+\frac{1}{\alpha\theta}e^{-\alpha\theta}+\frac{1}{\alpha^2\theta^2}\left(\alpha^{-\alpha\theta}-1\right)\right]. \tag{7}$$

Here $\psi^2(\theta)$ determines the square of the root-mean-square deviation of the hydrometeorological element from its main value within the limits of the interval θ or the dispersion of the hydrometeorological element in this interval.

It is not hard to see, that with $\theta \to \infty$

$$\psi^2(\theta)\to D=\sigma^2. \tag{8}$$

In Figure 1 we present the result of the calculation of $\psi_2(r,\ \theta)$ (equivalent to $\psi^2(t,\ \theta)$ with various r and θ and $\alpha = 0.1$ km^{-1}

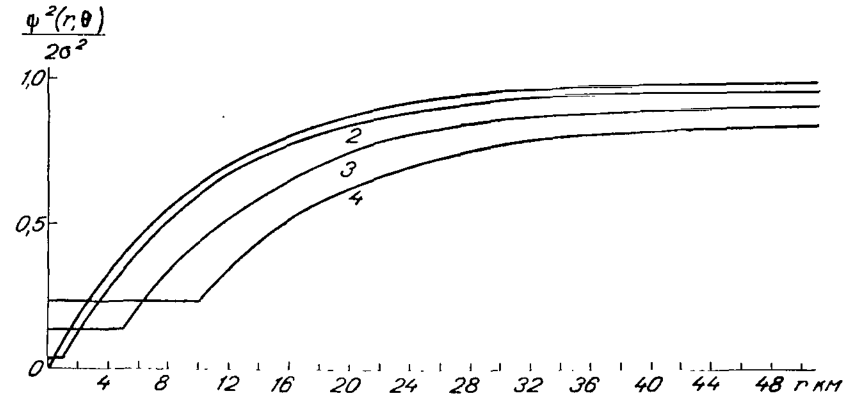

Figure 1. The Standardized (Divided by the Double Dispersion) Square of the Root-Mean-Square Deviation of the True Value of the Hydrometeorological Element in Point r from its Value, Averaged Within the Bounds of the θ Interval.

$\alpha=0{,}1$ км$^{-1}$, $\theta=1$ км, 2) $\alpha=0{,}1$ км$^{-1}$, $\theta=0$; 3) $\alpha=0{,}1$ км$^{-1}$, $\theta=5$ км; 4) $\alpha=0{,}1$ км$^{-1}$, $\theta=10$ км.

Now we shall assume that at point t we are interested not in the true value of the hydrometeorological parameter, but in the value, averaged within the bounds of the same interval θ (to moment t corresponds the beginning of the averaging interval). Equating this value to the averaged value referred to the initial time moment, we assume the root-mean-square error, equal to

$$B(t,\ \theta)=\overline{\left[\frac{1}{\theta}\int_0^\theta f(t+\tau)\,d\tau-\frac{1}{\theta}\int_0^\theta f(t)\,d\tau\right]^2}. \tag{9}$$

Proceeding from the determination of the structural function [5], it is not hard to see, that B(t, θ) is nothing other than the structural function, dependant on coordinate t and averaging interval θ. It may be represented as the structural function, calculated according to continuous measurements, performed by the instrument, having an integrating device with an averaging interval equal to θ. Or, this is such a structural function, which may be calculated upon determining the non-averaged values of the hydrometeorological element, if /161
this is averaged with a certain sliding step θ.

By analogy with (1)-(3) we present expression (9) in the form of

$$B(t,\ \theta)=\frac{1}{\theta^2}\overline{\left[\int_0^\theta f(t+\tau)\,d\tau-\int_0^\theta f(\tau)\,d\tau\right]\left[\int_0^\theta f(t+\tau_1)\,d\tau_1-\int_0^\theta f(\tau_1)\,d\tau_1\right]}=$$

$$=\frac{1}{\theta^2}\int_0^\theta d\tau\int_0^\theta \{B\,[(t+\tau)-\tau_1]-B(\tau-\tau_1)\}\,d\tau_1. \tag{10}$$

If the structural function of the hydrometeorological element has the appearance of

$$B(t) = \beta |t|^n, \tag{11}$$

then expression (10) is reduced to the form of:

$$\begin{aligned} B(t, \theta) &= \frac{\beta}{\theta^2 (n+1)(n+2)} [-2t^{n+2} + (t+\theta)^{n+2} + (t-\theta)^{n+2} - 2\theta^{n+2}] \\ &\qquad \text{when} \quad t \geqslant \theta, \\ B(t, \theta) &= \frac{\beta}{\theta^2 (n+1)(n+2)} [-2t^{n+2} + (t+\theta)^{n+2} + (\theta-t)^{n+2} - 2\theta^{n+2}] \\ &\qquad \text{when} \quad t \leqslant \theta. \end{aligned} \tag{12}$$

If the structural function has the appearance of

$$B(t) = 2\sigma^2 [1 - k(t)] = 2\sigma^2 [1 - e^{-\alpha |t|}], \tag{13}$$

where k(t) is the standardized correlation function, dependant on coordinate t, then

$$\left.\begin{aligned} B(t, \theta) &= \frac{2\sigma^2}{\alpha^2 \theta^2} [2e^{-\alpha t} - e^{-\alpha (t+\theta)} - e^{-\alpha (t-\theta)} + 2\alpha\theta - 2 + 2e^{-\alpha\theta}] \\ &\qquad \text{when} \quad t \geqslant \theta, \\ B(t, \theta) &= \frac{2\sigma^2}{\alpha^2 \theta^2} [2e^{-\alpha t} - e^{-\alpha (t+\theta)} - e^{-\alpha (\theta-t)} + 2\alpha t - 2 + 2e^{-\alpha\theta}] \\ &\qquad \text{when} \quad t \leqslant \theta. \end{aligned}\right\} \tag{14}$$

If the structural function has the appearance of

$$B(t) = 2\sigma^2 [1 - k(t)] = 2\sigma^2 [1 - e^{-\alpha |t|} \cos \beta |t|], \tag{15}$$

then

$$\begin{aligned} B(t, \theta) = \frac{2\sigma^2}{\theta^2 (\alpha^2 + \beta^2)} \Big\{ & 2\alpha\theta - 2\frac{\alpha^2 - \beta^2}{\alpha^2 + \beta^2} + 2e^{-\alpha\theta} \Big[\frac{\alpha^2 - \beta^2}{\alpha^2 + \beta^2} \cos \beta\theta - \\ & - \frac{2\alpha\beta}{\alpha^2 + \beta^2} \sin \beta\theta \Big] + 2e^{-\alpha t} \Big[\frac{\alpha^2 - \beta^2}{\alpha^2 + \beta^2} \cos \beta t - 2\frac{\alpha\beta}{\alpha^2 + \beta^2} \sin \beta t \Big] - \\ & - e^{-\alpha (t+\theta)} \Big[\frac{\alpha^2 - \beta^2}{\alpha^2 + \beta^2} \cos \beta (t+\theta) - \frac{2\alpha\beta}{\alpha^2 + \beta^2} \sin \beta (t+\theta) \Big] - \\ & - e^{-\alpha (t-\theta)} \Big[\frac{\alpha^2 - \beta^2}{\alpha^2 + \beta^2} \cos \beta (t-\theta) - \frac{2\alpha\beta}{\alpha^2 + \beta^2} \sin \beta (t-\theta) \Big] \Big\}, \\ & \qquad \text{when} \quad t \geqslant \theta, \end{aligned} \tag{16}$$

$$B(t,\ \theta)=\frac{2\sigma^2}{\theta^2(\alpha^2+\beta^2)}\Big\{2\alpha\theta-2\frac{\alpha^2-\beta^2}{\alpha^2+\beta^2}+2e^{-\alpha\theta}\Big[\frac{\alpha^2-\beta^2}{\alpha^2+\beta^2}\cos\beta\theta-$$ /162

$$-\frac{2\alpha\beta}{\alpha^2+\beta^2}\sin\beta\theta\Big]+2e^{-\alpha t}\Big[\frac{\alpha^2-\beta^2}{\alpha^2+\beta^2}\cos\beta t-\frac{2\alpha\beta}{\alpha^2+\beta^2}\sin\beta t\Big]-$$

$$-e^{-\alpha(t+\theta)}\Big[\frac{\alpha^2-\beta^2}{\alpha^2+\beta^2}\cos\beta(t+\theta)-\frac{2\alpha\beta}{\alpha^2+\beta^2}\sin\beta(t+\theta)\Big]-$$

$$-e^{-\alpha(\theta-t)}\Big[\frac{\alpha^2-\beta^2}{\alpha^2+\beta^2}\cos\beta(\theta-t)-\frac{2\alpha\beta}{\alpha^2+\beta^2}\sin\beta(\theta-t)\Big]-2\alpha(\theta-t)\Big\}$$

$$\text{when}\quad t\leqslant\theta \tag{17}$$

[1]

In Figure 2 we give the result of calculation of B(r, θ) of the form (14) with various r, α and θ. From the diagram, we can see that function B(r, θ) approaches the non-averaged functions the more the smaller is the averaging interval, and with the prescribed averaging interval, the smaller is the coefficient α.

When r or t → ∞ the structural function B(r, θ) or B(t, θ), having the form of (14), is equal to

$$B(t,\ \theta)=2D_\theta=\frac{2\sigma^2}{\alpha^2\theta^2}\left[2\alpha\theta+2e^{-\alpha\theta}-2\right]. \tag{18}$$

Here D_θ is the dispersion of the values of the hydrometeorological element averaged within the bounds of the interval θ. From Figure 2 we can see that with the increase of the averaging range the dispersion of the averaged values /163 D_θ decreases. With θ → ∞ it tends towards zero.

In Figure 3 we present the standardized structure of functions of the values of the hydrometeorological element of type (14) averaged within the limits of the interval, calculated according to the relationship:

[1] When

$$t\leqslant\theta\qquad B(t,\ \theta)=\frac{2\sigma^2}{\theta^2}\Big\{\int_0^\theta d\tau\int_0^\tau e^{-\alpha(\tau-\tau_1)}\cos\beta(\tau-\tau_1)\,d\tau+\int_\tau^\theta e^{-\alpha(\tau_1-\tau)}\times$$

$$\times\cos\beta(\tau_1-\tau)\,d\tau_1-\int_0^t d\tau_1\int_0^\theta e^{-\alpha(t+\tau-\tau_1)}\cos\beta(t+\tau-\tau_1)\,d\tau-$$

$$-\int_t^\theta d\tau_1\Big[\int_0^{\tau_1-t}e^{-\alpha(\tau_1-t-\tau)}\cos\beta(\tau_1-t-\tau)\,d\tau+\int_{\tau_1-t}^\theta e^{-\alpha(t+\tau-\tau_1)}\cos\beta(t+\tau-\tau_1)\,d\tau_1\Big]\Big\}.$$

$$\left.\begin{aligned}
\beta(t,\ \theta) &= \frac{B(t,\ \theta)}{2D_\theta} = \frac{2e^{-\alpha t} - e^{-\alpha(t+\theta)} - e^{-\alpha(t-\theta)} + 2\alpha\theta + 2e^{-\alpha\theta} - 2}{2\alpha\theta + 2e^{-\alpha\theta} - 2} \\
&\qquad \text{when} \quad t \geqslant \theta, \\
\beta(t,\ \theta) &= \frac{B(t,\ \theta)}{2D_\theta} = \frac{2e^{-\alpha t} - e^{-\alpha(t+\theta)} - e^{-\alpha(\theta-t)} + 2\alpha t + 2e^{-\alpha\theta} - 2}{2\alpha\theta + 2e^{-\alpha\theta} - 2} \\
&\qquad \text{when} \quad t \leqslant \theta.
\end{aligned}\right\} \tag{19}$$

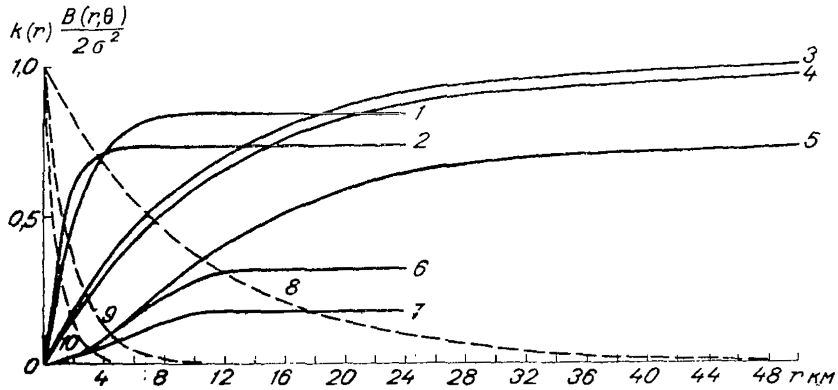

Figure 2. The Standardized Correlation Function k(r) and the Semi-Standardized (Divided by the Double Dispersion) Structural Function B(r, θ) of the Values of the Hydrometeorological Elements Averaged Within the Limits of the Interval θ.

1) $\alpha=0{,}5$ км$^{-1}$, $\theta=1$ км; 2) $\alpha=1$ км$^{-1}$, $\theta=1$ км; 3) $\alpha=0{,}1$ км$^{-1}$, $\theta=0$; 4) $\alpha=0{,}1$ км$^{-1}$, $\theta=1$ км; 5) $\alpha=0{,}1$ км$^{-1}$, $\theta=10$ км; 6) $\alpha=0{,}5$ км$^{-1}$, $\theta=10$ км; 7) $\alpha=1$ км$^{-1}$, $\theta=10$ км 8) $\alpha=0{,}1$ км$^{-1}$; 9) $\alpha=0{,}5$ км$^{-1}$; 10) $\alpha=1$ км$^{-1}$.

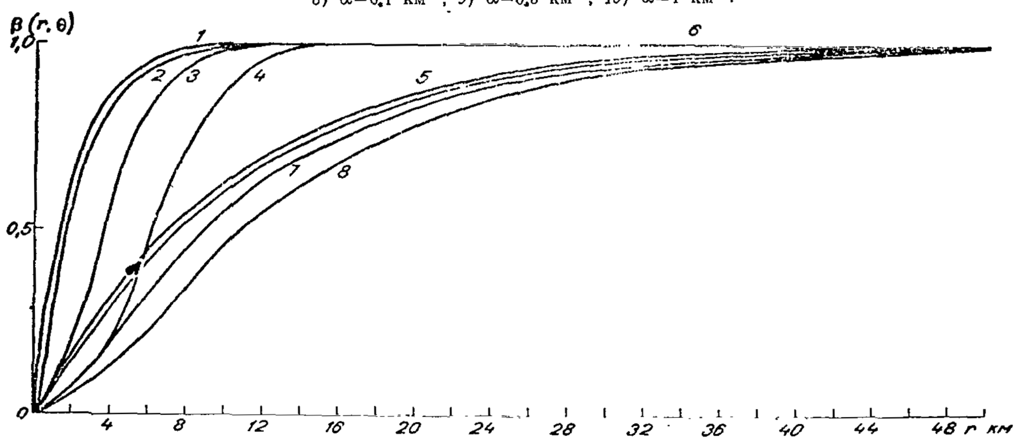

Figure 3. The Standardized Structural Function of the Hydrometeorological Element Values Averaged Within the Bounds of Interval θ.

$\alpha=0{,}5$ км$^{-1}$, $\theta=0$; 2) $\alpha=0{,}5$ км$^{-1}$, $\theta=1$ км; 3) $\alpha=0{,}5$ км$^{-1}$, $\theta=5$ км; 4) $\alpha=0{,}5$ км$^{-1}$, $\theta=10$ км; 5) $\alpha=0{,}5$ км$^{-1}$, $\theta=0$; 6) $\alpha=0{,}1$ км$^{-1}$, $\theta=1$ км; 7) $\alpha=0{,}1$ км$^{-1}$, $\theta=5$ км; 8) $\alpha=0{,}1$ км$^{-1}$. $\theta=10$ км.

As we can see from this Figure 3, the standardized structural function of the averaged values of the hydrometeorological element upon the increase of the averaging range shifts towards the greater values of r.

Apparently, the distance between the points of measurements with a prescribed accuracy of interpolation of the hydrometeorological elements within the interval between the points, and also the representativity radius for various measurements will be the greater, the more is the structural function shifted towards the region of greater r or t and the less is the dispersion of the elements. Consequently, upon the increase of the averaging range the representativity of the measurement results increases both through the shift of the standardized structural functions towards greater r and also through the decrease of dispersion D_θ.

The illusion is created that with the increase of the averaging range θ not only does the representativity of the measurement results increase, but so does the accuracy of information on the elements field. In reality, only the accuracy of the concept of the averaged field increases. From Figures 1 and 2 we can see that with increase of θ dispersion D_θ decreases, but there is an increase of the dispersion of the hydrometeorological elements in the θ interval, i.e., ψ_θ^2. The total remains practically constant. Thus, upon averaging of the hydrometeorological element the accuracy with which we know its true value at any point of the field, does not change, and only the representativity /164 of the averaged values measured increases.

As an example, let us examine the temperature field of the water surface in the Gulf Stream region.

The structural function of the water surface temperature in the Gulf Stream region (May 1963, $\lambda = 60°$, $\phi = 40°$) may be approximated with the expression (see Figure 4)

$$B(r) = 2K(0) - 2K(r) = 2\sigma^2 [1 - k(r)] = = 1,1 \left(1 - e^{-0,175r} \cos 0,225r\right), \quad (20)$$

where K(r) and k(r) are the correlation function and the standardized correlation function, dependent on coordinate r (in kilometers).

If we prescribed the maximum permissible error $\alpha = \Delta T_{max}$, then the value of the temperature, measured at a certain point, in accordance with the relationship

$$\Delta T_{max} = 3\sqrt{B(R_p)} = 3\sqrt{2\sigma^2\beta(R_p)} = 3,1\sqrt{1 - e^{-0,175R_p} \cos 0,225R} \quad (21)$$

may be extended to the distance R_p, equal to 250 m with $\Delta T_{max} = 0.5°C$, 600 m with $\Delta T_{max} = 1°C$, 1,300 m with $\Delta T_{max} = 1.5°C$ and 2,600 m with $\Delta T_{max} = 2°C$. The R_p distance may be determined as the radius of the measurement representativity.

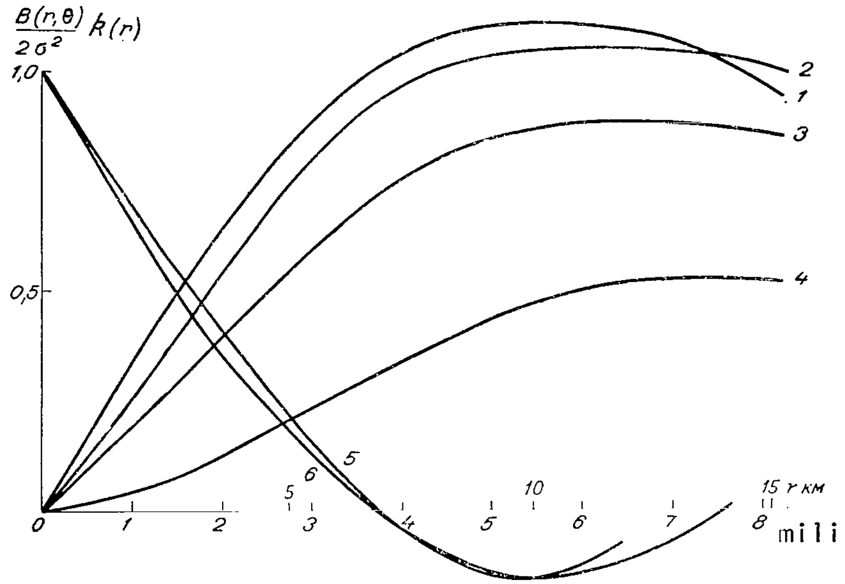

Figure 4. Standardized Three-dimensional Correlation Function k(r) and the Semi-standardized (Divided by the Double Dispersion) Structural Function B(r, θ) of the Water Surface Temperature Averaged Within the Bounds of the θ Range, in the Region of the Gulf Stream.

$m(x) = 20.2°C$, $D = 0.531$ deg^2 $\sigma = 0.728$ deg.
$\theta = 0$, 2) $\theta = 1$ км, 3) $\theta = 5$ км, 4) $\theta = 10$ км, 5) $k(r) = e^{-0.325r} \cos 0.418\, r$ mili 6) $k(r) = e^{-0.175r} \cos 0.225r$ км.

If the measurements are performed at equidistant intervals R, and the temperature value T(r) in the intervals between the measurements are interpolated by means of relationship [6] /165

$$T(r) = aT(0) + bT(R), \tag{22}$$

where

$$a = \frac{K(0)K(r) - K(R)K(R-r)}{K^2(0) - K^2(R)},$$

$$b = \frac{K(0)K(R-r) - K(R)K(r)}{K^2(0) - K^2(R)},$$

Then the mean square of the error in the middle of the interval will be equal to

$$\varepsilon_{max}^2 = K(0) - 2\frac{K(R/2)}{K(0) + K(R)} \tag{23}$$

or taking into account the known relationship

$$B(r) = 2K(0) - 2K(r) = 2[D - K(r)] = 2\sigma^2[1 - k(r)] \tag{24}$$

$$\varepsilon_{max}^2 = D - \frac{[2D - B(R/2)]^2}{4D - B(R)}. \tag{25}$$

Then the maximum error of the interpolated values of the temperature will be

$$\Delta T_{max} = 3\sqrt{\varepsilon_{max}^2}. \tag{26}$$

From expressions (20), (23), (25) and (26) it is not hard to find, that in order that the errors of the interpolated temperature values would exceed 0.5; 1; 1.5 and 2° the distance between the measurement points R should not exceed 700, 2,100, 5,000 and 9,500 m, respectively.

In actual practice the same distance is determined, if we use the conventional, linear interpolation frequently used in synoptic practical work

$$T(r) = T(0) + \frac{r}{R}[T(R) - T(0)]. \tag{27}$$

The error of such interpolation in the middle of the interval is determined by the relationship

$$\varepsilon_{max}^2 = 1{,}5K(0) - 2K\left(\frac{R}{2}\right) + 0{,}5K(R) \tag{28}$$

or taking into account (24)

$$\varepsilon_{max}^2 = B\left(\frac{R}{2}\right) - 0{,}25B(R). \tag{29}$$

If the measurements are performed with a certain averaging interval θ, then by analogy with (21) and (26)

$$\Delta T^{\theta}_{\max} = 3\sqrt{B(R_p\theta)} = 3\sqrt{2D_{\theta}\beta(R_p\theta)} \tag{30}$$

$$\Delta T^{\theta}_{\max} = 3\sqrt{\varepsilon^{2\theta}_{\max}}. \tag{31}$$

Here

$$\varepsilon^{2\theta}_{\max} = D_{\theta} - \frac{\left[2D_{\theta} - B\left(\frac{R}{2},\, \theta\right)\right]^2}{4D_{\theta} - B(R,\, \theta)} \tag{32}$$

With linear interpolation of the (22) type and /166

$$\varepsilon^{2\theta}_{\max} = B(R/2,\, \theta) - 0{,}25B(R,\, \theta)$$

according to the linear interpolation of the (27) type.

The concrete values of R and R_p with different maximum errors of extrapolation and interpolation of results of measurement of the water surface temperatures in the Gulf Stream region, performed with a different averaging interval θ, are given in Table 1.

TABLE 1

$\Delta T_{\max}$ °C	R_p км				R км			
	θ км				θ км			
	0	1	5	10	0	1	5	10
0,5	0,25	0,3	0,4	1,5	0,7	0,9	1,2	5,5
1,0	0,6	0,75	1,0	3,5	2,1	3,1	4,3	11,0
1,5	1,3	1,6	2,3	5,7	5,0	6,5	8,6	—
2,0	2,6	2,9	3,9	9,2	9,5	11,0	11,0	—

Tr. Note: Commas indicate decimal points.

From this table we can see, that the greater is the averaging range with which the measurements are performed, the greater is the distance and the longer is the time period to which the measurement results could be extended and consequently the greater is the range (spatial and time) that could be selected between the measurements. This results not only in a reduction of the number of measurements, in surveying the temperature field, but also to the increase of the period for which the map, plotted according to the measurement results, is applicable.

In conclusion, we should note that the present work supplements works [2, 3, 4].

Using the above-mentioned works we can determine the optimum averaging range of the hydrometeorological element measured, and by means of the present work we can calculate the variability of the average values of the hydrometeorological element, for example, such characteristics as the radius of the representative measurements, the error in interpolation of the element according to its discrete average measurements, the required distance between the measurement points with the prescribed maximum measurement result interpolation error, etc.

REFERENCES

1. Kagan, R. L.: "On the Estimation of the Time Lag of an Instrument in Meteorological Measurements," *Izv. AN SSSR, Geophysical Series*, No. 2, 1964.
2. Yudin, N. I.: "Certain Problems of the Theory of Meteorological Fields," *Trudy GGO*, Issue 19 (81), 1950.
3. Andreyev, I. D.: "Selection of the Optimum Wind Velocity Averaging Range", *Trudy GGO*, Issue 83, 1958.
4. Chiow Ming Yui: "Optimum Averaging Periods in Measuring Meteorological Fields," *Izv. AN SSSR, Physics of the Atmosphere and the Ocean*, Vol. 2, No. 5, 1966.
5. Gandin, L. S.: *"Ob"yektivnyy Analiz Meteorologicheskikh Poley* [Objective Analysis of Meteorological Fields]" Gidrometeoizdat Press, Leningrad 1963.
6. Belyayev, B. N.: "Selection of the Discreteness Range and Evaluation of the Loss of Information Upon the Replacement of Continuous Measurements of Hydrological Elements with Discrete Measurements," *Journal Okeanologiya*, Issue 3, 1964.

CERTAIN REGULARITIES IN THE VERTICAL DISTRIBUTION OF THE ASCENDING LONGWAVE RADIATION

Ye. P. Barashkova

ABSTRACT. The analysis of the result of actinometric sounding brings us to the conclusion that the vertical distribution of the flow of ascending longwave radiation depends mainly on the distribution of the temperature. As the calculations have shown the moisture content w_z has a substantial effect on the value of the ascending longwave radiation flow u_z only upon the change within the limits of $0 \leqslant w_z \leqslant 0.5$ grams/cm^2, i.e., in the ground layer of the atmosphere. In the general case the flow of ascending longwave radiation u_z may be expressed through the soil temperature T_0 and the difference between the temperatures of the soil and air $T_0 - T_z$ in the form of a formula.

Information on the principal regularities of the vertical distribution of longwave radiation is necessary not only to obtain a concept of the three-dimensional structure of the radiation field, but also for solving such problems as interpretation of radiation measurements from satellites, and evaluation of the contribution of the radiant heat influx to the total energy of the atmosphere. /167

The actinometric radiosondes created during the last decade enable us to carry out a systematic investigation of the vertical distribution of longwave radiation at night up to considerable altitudes. On the territory of the Soviet Union for the first time the regular actinometric soundings was organized by the Central Aerological Observatory in 1963, in the following eight points: Vladivostok, Tashkent, Sverdlovsk, Dolgoprudnyy, Rostov on the Done, Kiev, Minsk, Murmansk. In the sounding the actinometric probe designed by G. N. Kostyanoy was used.

G. N. Kostyanoy's actinometric radiosonde [1] consists of a RKZ-1A radiosonde with an electric switch and radiometer which is the sensor of the flows and balance of longwave radiation. The receiving surfaces of the radiometer made of aluminum foil are blackened with a mixture of carbon black, shellac, and BF-2. The receiving surfaces are protected from the action of the external medium by polyethylene filters, which have a convex shape because of the excess pressure inside the instrument. The information on the temperature of the receiving surfaces is transmitted to the earth. The connection between the temperature of the receiving surface T_B and the radiation flow incident on it Q is established by the method of calculation on the basis of the equation of thermal balance of the receiving surface. In this case information values of the coefficients of absorption, heat conductivity, specific heat, and others, included in the thermal balance equation, were borrowed from literature sources and their mean values were used in the calculations. However, since the parameters of the radiometers used may not coincide with these mean characteristics, the values of the fluxes obtained as the result of these calculations will differ from their true magnitude.

A certain idea on the possible limits of deviations of the values obtained from the actual values are given by the following evaluations. Let us assume, that all the coefficients of the thermal balance equation assume their minimum values. In this case the deviation of the ascending flow from that calculated with mean values of coefficients with temperature t = 40°C reaches /168
0.08 cal/cm^{2}min., which amounts to about 14% of the size of the flow. With maximum values of the coefficients at the same temperatures t = 40°C this deviation reaches 0.04 cal/cm^{2}min., and the relative correction amounts to 7%. With the temperature t = -60°C the deviation from the minimum values of the coefficients amounts to 0.04 cal/cm^{2}min., with the maximum -0.026 cal/cm^{2}min ., the relative deviations in this case amount to 20 and 13%, respectively.

Simultaneously with the temperature of the receiving surfaces of the radiometer the actinometric radiosonde transmits information on pressure, temperature, and moisture of the air. Therefore, the results of actinometric sounding make it possible not only to form a definite conclusion on the character of the vertical distribution of longwave flows, but also to analyze their relationship with the temperature and moisture of the air.

In the present work we shall limit ourselves to the examination of sounding results, obtained under a cloudless sky.

The ascending flow of thermal radiation u at level z, in the assumption that the underlying surface radiates as a black body, can be written in the following form:

$$u(w_z) = B_0 P(w_z) + \int_0^{w_z} B\, dP(w_z - \mu). \qquad (1)$$

Here $B_0 = \sigma T_0^4$ is the radiation of the black body at the temperature of the underlying surface T_0, P is the transmission function, $B = \sigma T_\xi^4$ is the radiation of the black body at the air temperature T_ξ at the level ξ; $w_z = \int_0^z \rho(\xi) f(\xi)\, d\xi$ is the effective absorbing mass in which $\rho(\xi)$ is the density of the absorbing substance $f(\xi) = \frac{\sqrt{p_\xi}}{\sqrt{p_0}}$ is the correction for pressure,

$\mu = \int_0^{\xi} \rho(\xi) f(\xi) d\xi$ is the integration variable.

The first component in formula (1) determines the part of the underlying surfaces on radiation, reaching the level examined, the second component characterizes the radiation of the layer of the atmosphere located between the terrestrial surface and the level examined.

Proceeding from formula (1), the vertical distribution of the ascending longwave current u_z will be determined by the distribution of temperature T_z and the effective absorbing mass w_z. The absolute value u_z to a great extent will be determined by the temperature of the underlying surface T_0.

According to the data of the actinometric sounding the relationship between the ascending current and the longwave radiation u_z with the temperature of the underlying surface T_0 is traced through the entire extent of the troposphere, and at all the altitudes we observe a linear correlation of u_z and σT_0^4. Although the correlation coefficient r between u_z and σT_0^4 decreases somewhat with altitude, within the bounds of the troposphere it remains everywhere greater than 0.8. In Table 1 we give the values of the correlation coefficient σT_0^4 and u_z at various levels of z. In the calculation of these correlation coefficients we use data for all the eight points.

TABLE 1. RELATIONSHIP BETWEEN u_z WITH σT_0^4

z km.	No. of Cases	r	u_z
1—1,5	112	0,959	$u = 0,969\sigma T_0^4 + 0,018$
2—2,5	115	0,943	$u = 0,820\sigma T_0^4 + 0,018$
3—3,5	115	0,930	$u = 0,840\sigma T_0^4 + 0,016$
4—4,5	111	0,910	$u = 0,780\sigma T_0^4 + 0,052$
6—6,5	111	0,896	$u = 0,660\sigma T_0^4 + 0,064$
8—8,5	107	0,890	$u = 0,560\sigma T_0^4 + 0,064$
10—10,5	109	0,846	$u = 0,420\sigma T_0^4 + 0,098$

Tr. Note: Commas indicate decimal points.

In order to determine the degree of relationship between the ascending current of longwave radiation and the air temperature t_z and the effective content of the water vapor in the atmospheric layer w_z we calculated the corresponding correlation relationships [2], presented in Table 2. Along with u_z we introduced into the examination also the value of relationship $u_z / \sigma T_0^4$. The lowest correlation relationships are noted between u_z and w_z, the highest between u_z and t_z; $u_z/\sigma T_0^4$ and Δt. As the illustration in Figures 1 and 2 we present graphically the corresponding relationships according to the actinometric sounding data. /169

TABLE 2. CORRELATION RELATIONSHIPS OF THE ASCENDING LONGWAVE CURRENT u_z AND RELATIONSHIPS OF $u_z/\sigma T_0^4$ WITH THE AIR TEMPERATURE t_z, THE EFFECTIVE WATER VAPOR CONTENT w_z, AND THE TEMPERATURE DIFFERENCE BETWEEN THE SOIL AND THE AIR $\Delta t = t_0 - t_z$.

Point	Elements Correlated					
	u_z; w_z	u_z; t_z	u_z; Δt	$\frac{u_z}{\sigma T_0^4}$; w_z	$\frac{u_z}{\sigma T_0^4}$; t_z	$\frac{u_z}{\sigma T_0^4}$; Δt_z
Murmansk . . .	0,538	0,847	0,675	0,525	0,755	0,913
Minsk	0,643	0,927	0,577	0,589	0,826	0,976
Sverdlovsk . .	0,452	0,916	0,558	0,673	0,804	0,987
Kiev	0,444	0,936	0,661	0,710	0,849	0,972
Vladivostok	0,486	0,915	0,547	0,610	0,734	0,801
Tashkent . . .	0,372	0,961	0,872	0,892	0,948	0,982

Tr. Note: Commas indicate decimal points.

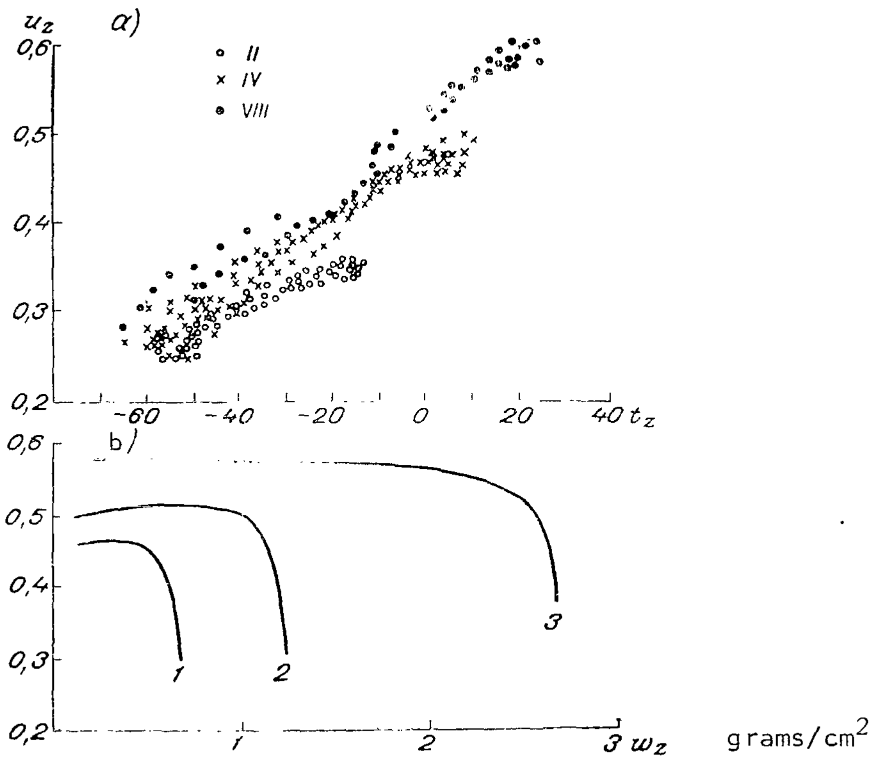

Figure 1. Dependence of the Current of Ascending Longwave Radiation u_z on the Temperature (a) and Water Vapor Content (b). 1, 4 November; 2, 2 October; 3, 12 August.

From Figure 1 it follows that the current of the ascending longwave radiation at level z is an increasing function of temperature t_z. However, the quantitative relationships between u_z and t_z vary substantially from month to month, so that various values of u_z correspond to the same values of t_z during different months. One of the causes of these variations of u_z with t = const may be the difference in the temperature t_0 of the underlying surface.

The peculiar variations of u_z with the variations of w_z, presented in Figure 1b are explained by the fact that the decrease of the temperature has a more substantial influence on value u_z than do the variations of w_z, which at altitudes of more than 2-3 km are very insignificant. Because of this, the quantitative relationships between u_z and w_z also vary substantially in relation to t_0 and t_z. /170

In Figure 2 we present the relationship of the ratio $u_z/\sigma T_0^4$ and the difference between the soil and air temperature Δt and with the effective moisture content at constant Δt values.

From the diagram we can see that the variation of the difference Δt has a substantial influence on the value of ratio $u_z/\sigma T_0^4$, whereas the variation of w_z has practically no effect on its value.

The main dependence of $u_z/\sigma T_0^4$ on the Δt, portrayed in Figure 2a, may be represented by the exponential function

$$\frac{u_z}{\sigma T_0^4} = 10^{-a\,\Delta t}. \quad (2)$$

The analogous relationship between the ratio $u_z/\sigma T_0^4$ and Δt is observed /172 in other points as well, and the value of coefficient a changing insignificanly from point to point. In Table 3 we give the mean dependences of $u_z/\sigma T_0^4$ on Δt, obtained on the basis of observations at different points, and the values of coefficient a corresponding to them. From formula (2) it follows that the vertical distribution of the ascending longwave radiation is mainly determined by the behavior of the difference between the soil and air temperatures, and since in every individual case the soil temperature is constant, in the final count it is determined by the behavior of the air temperature t_z. This is indicated also by the direct comparison of the profiles of u_z and t_z, performed in Figure 3, from which it follows, that the variation of the temperature and the ascending longwave flow with altitude is marked by similar features.

/171

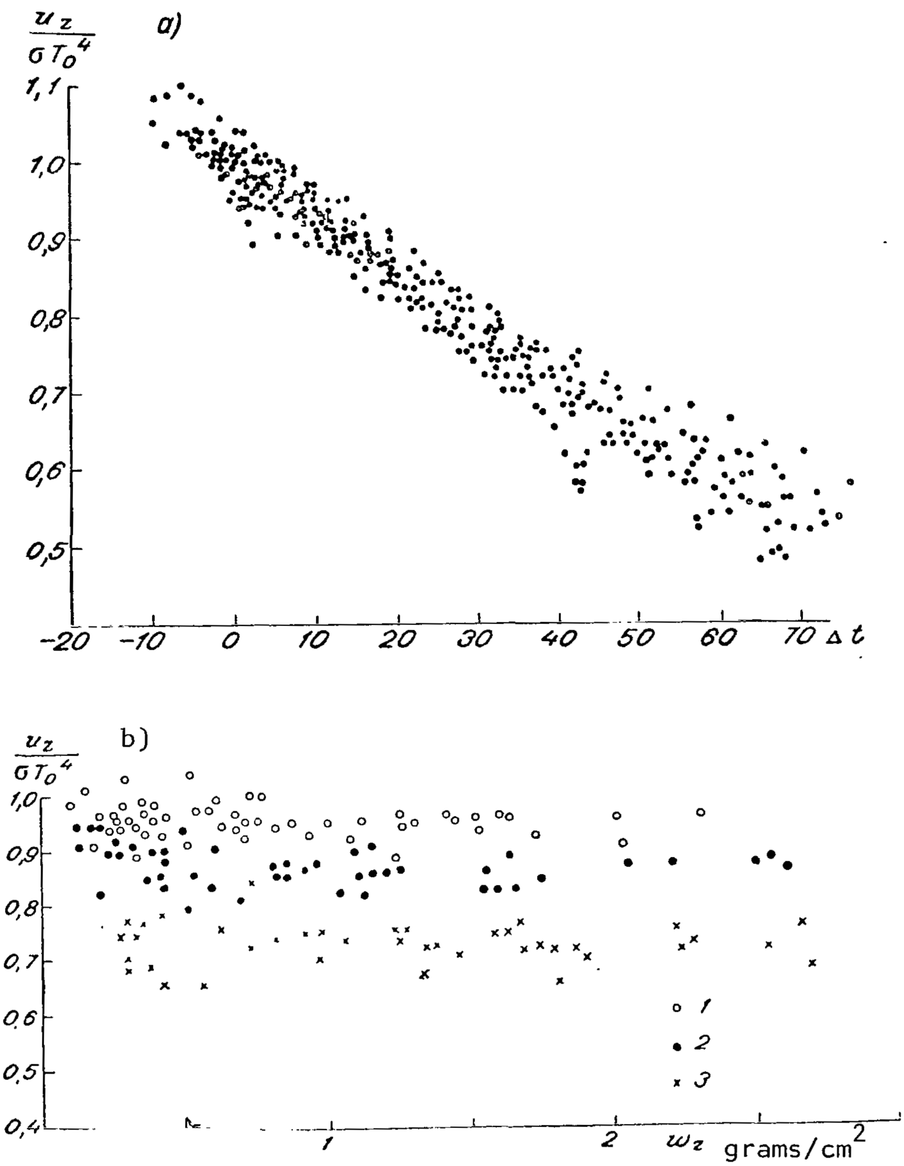

Figure 2. Dependence of Ratio $u_z/\sigma T_0^4$ on the Difference Between the Temperature of the Soil and the Air (a) on the Water Vapor Content in the Atmospheric Layer at Δt = const (b) at Minsk Station. 1) $\Delta t = 10{,}0°$; 2) $\Delta t = 20{,}0°$; 3) $\Delta t = 40°$.

According to the character of relationship of u_z and z the range of altitudes between 0 and 30 km may be divided into three zones. /173

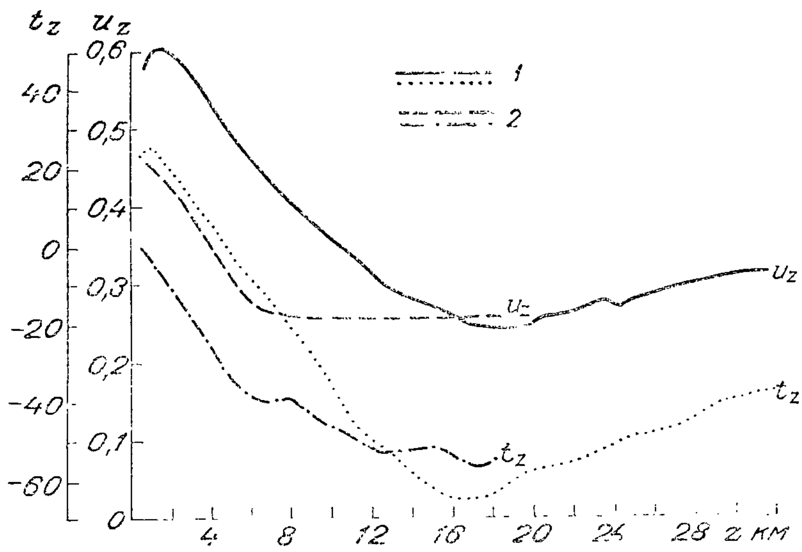

Figure 3. Vertical Profiles of the Ascending Longwave Radiation and Air Temperature on 27 August (1) and 6 November (2).

TABLE 3. DEPENDENCE OF $u_z/\sigma T_0^4$ ON Δt.

Point	$\Delta t°$											
	−10	0	10	20	30	40	50	60	70	80	90	a
Minsk	1,10	1,00	0,93	0,86	0,78	0,72	0,65	0,58	0,53	—	—	0,0039
Tashkent	—	1,01	0,94	0,86	0,79	0,72	0,66	0,59	0,54	0,48	0,43	0,0037
Vladivostok	1,10	1,00	0,94	0,86	0,77	0,69	0,64	0,58	0,52	0,46	—	0,0040
Dolgoprudnyy	1,09	1,00	0,92	0,85	0,77	0,72	0,65	0,60	0,54	—	—	0,0038
Kiev	—	1,00	0,91	0,85	0,76	0,71	0,64	0,58	0,53	0,50	—	0,0039
Vysokaya Dubrava	1,12	1,03	0,90	0,85	0,76	0,70	0,68	0,57	0,53	—	—	0,0039
Murmansk	—	1,05	0,97	0,90	0,82	0,74	0,67	—	—	—	—	

Tr. Note: Commas indicate decimal points.

1. The ground level zone is distinguished by the wide variety of relationship between the variations of u_z and the altitude. In this zone we observe both the decrease of u_z with altitude $(\gamma = -\frac{\Delta u_z}{\Delta z} > 0)$, and the increase ($\gamma < 0$) and the independence on the altitude ($\gamma = 0$), and the combination of all these types of variations of u_z with altitude. The altitude of this zone varies in time and space from several meters to 4.5 km. The γ gradients vary from -0.05 to 0.05 cal/cm^{2}min. per 1 km.

2. The second zone is characterized by the decrease of u_z with altitude. This zone extends to the tropopause level. In each individual case the decrease occurs with a gradient constant for the entire altitude of the zone,

but from case to case the gradient changes in relatively wide ranges. On the basis of the material available to us we obtained for the second zone $0.009 \leq \gamma < 0.026$ cal/cm min per 1 km. Upon passage through the troposphere the value of the ascending longwave radiation decreases by 30-50%.

3. In the third zone located beyond the boundaries of the troposphere, the ascending longwave flow remains practically constant, in this zone the gradients do not leave the limits of $-0.005 \leq \gamma \leq +0.005$.

In Table 4 we give the mean profiles of u_z/u_0, obtained at various points.

TABLE 4. MEAN VALUES OF u_z/u_0.

z KM	Kiev	Minsk	Tashkent	Vladivostok	Sverdlovsk
	Summer			Winter	
0	1,00	1,00	1,00	1,00	1,00
0,5	1,02	1,04	—	1,08	—
1	0,95	0,99	1,04	1,10	1,05
2	0,91	0,95	1,00	1,07	1,08
3	0,86	0,91	0,95	1,04	1,07
4	0,81	0,86	0,88	1,01	1,03
5	0,77	0,81	0,83	0,98	0,98
6	0,73	0,76	0,77	0,95	0,91
7	0,69	0,72	0,72	0,91	0,85
8	0,66	0,68	0,68	0,87	0,80
9	0,62	0,64	0,64	0,83	0,75
10	0,58	0,59	0,61	0,78	0,70
11	0,55	0,55	0,58	0,75	0,68
12	0,52	0,52	0,55	0,74	0,68
13	0,51	0,52	0,53	0,71	0,68
14	0,51	0,52	0,53	0,73	0,68
15	0,52	0,51	0,51	0,73	0,69
16	0,52	0,51	0,50	0,73	0,69
17	0,53	0,51	0,50	0,72	0,70
18	0,53	0,52	0,50	0,72	0,70
19	0,53	0,52	0,50	0,72	0,70
20	0,53	0,52	0,51	0,72	0,70
21	0,53	0,52	0,51	0,72	0,71
22	0,53	0,52	0,52	0,72	0,72
23	0,53	—	0,53	0,72	0,72
24	0,53	—	0,54	0,72	0,72
25	0,53	—	0,55	—	—
26	0,54	—	—	—	—

Tr. Note: Commas indicate decimal points.

The conclusion that the vertical profile of the longwave radiation is determined only by the distribution of the temperature, at first glance appears unexpected, since the ascending current of longwave radiation (1) depends also on the distribution of the absorbing mass. However, owing to the fact that the components of the ascending longwave radiation flow $u_z^1 = B_0P(w_z)$ and /174

$u_z^2 = \int BdP\,(w_z - \mu)$ upon a change of w_z change in various directions, the effect of w_z on u_z smoothes out somewhat.

The existing methods do not enable us to measure the individual components of the ascending radiation, therefore, in order to evaluate the influence of the meteorological factors on individual components and obtain a concept on their role in the formation of the flow of ascending longwave radiation, we carried out the corresponding calculations.

In the calculations we used the following assumptions.

1. The temperature decreases linearly from the underlying surface to the tropopause $T_z = T_0 - \gamma z$, located at the altitude of $z = 10$ km.

2. The underlying surface is absolutely black.

3. The absorbing substance is water vapor, the distribution of which with altitude is described by the following formula

$$\rho_z = \rho_0 e^{-\beta z}, \quad \rho_0 = \frac{217 \cdot 10^{-6}}{T} q_0,$$

where q_0 is the water vapor pressure in millibars.

With the assumptions made on the basis of their approximate method of calculation, proposed by K. Ya. Kondrat'yev [3], the ascending longwave flow may be written in the following form

$$u(w_z) = \sum_{j=1}^{4} u_j(w_z) = \sum_{j=1}^{4} p_j B(w_z) + \\ + \frac{\gamma}{\beta} 4\sigma T^3_{(0,\,z)} \sum_{j=1}^{4} e^{k_j(w_\infty - w_z)} \{Ei(-k_j w_\infty) - Ei[-k_j(w_\infty - w_z)]\}. \tag{3}$$

The radiation of the underlying surface, which reached level z

$$u^{(1)}(w_z) = \sum_{j=1}^{4} p_j B_0 e^{-k_j w_z}, \tag{4}$$

the atmospheric radiation

$$u^{(2)}(w_z) = u(w_z) - u^{(1)}(w_z). \tag{5}$$

Here j is the number of the spectral sample ($j = 1, 2, 3, 4$); $p_j = B_j/B = 1/4$;

$B = \sigma T_0^4$; k_j is the coefficient of absorption of water vapor for this spectral samples (with allowance for the diffusion of radiation $k_1 = 0.166$, $k_2 = 2.60$, $k_3 = 36.2$, and $k_4 = 189$ $cm^2/gram$); w_∞, w_z are the effective content of water vapor in the entire atmosphere and in the layer of the atmosphere from the underlying surface to the level examined; Ei is the integral exponential function;

$$\gamma = 6 \cdot 10^{-5} \text{ deg/cm}; \quad \beta = 4.5 \cdot 10^{-6} \text{ 1/cm};$$

$$\sigma = 8.14 \cdot 10^{-11} \text{ cal/cm}^2\text{min. deg}^4.$$

The calculations were performed for five cases with various values of T_0 and q_0. The initial data, used in the calculations are given in Table 5. /175

TABLE 5. INITIAL DATA USED IN THE CALCULATIONS.

Ordinal Number	T_0	q_0	$\rho_0 \cdot 10^6$	w_∞
1	232,1	0,14	0,13	0,025
2	368,9	2,30	1,86	0,356
3	296,3	12,00	8,80	1,688
4	300,0	19,00	13,88	2,662
5	303,0	30,00	21,48	4,120

Tr. Note: Commas indicate decimal points.

Here T_0 is the temperature of the underlying surface in degrees Kelvin, q is the air moisture in millibars at the altitude of 1.5 m, ρ_0 is in grams/cm^3, w_∞ is in grams/cm^2.

The results of the calculations are given in Table 6. On the basis of these results we can draw the following conclusions.

1. Value $u_z^{(1)}$ is a decreasing function of w_z and the dependence of $u_z^{(1)}$ on w_z may be presented in the following form

$$u_z^{(1)} = \sigma T_0^4 (1 - 0{,}76 w_z^{0{,}114}), \tag{6}$$

where $\sigma T_0^4 = u_0^{(1)}$ is the radiation at the underlying surface level, w_z is the effective absorbing mass in the layer between 0 to level z. On Figure 4a with various symbols we have marked the data from Table 6, corresponding to various cases; the solid line corresponds to formula (6).

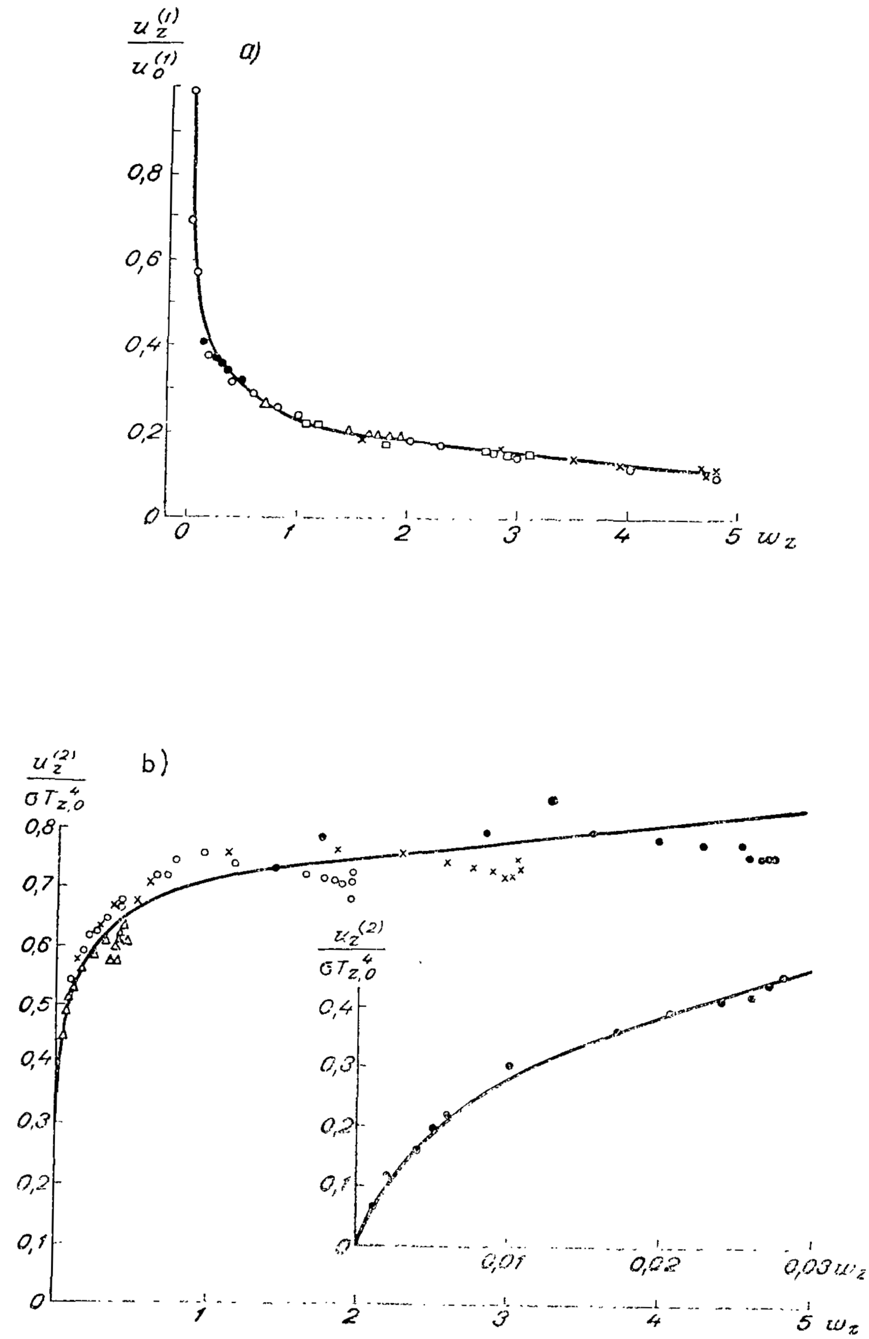

Figure 4. Dependence of $u_z^{(2)}/\sigma T_0^4$ (a) and $u_z^2/\sigma T_{0,z}^4$ (b) on the Water Vapor Content.

TABLE 6. ASCENDING CURRENT u_z AND ITS COMPONENTS $u_z^{(1)}$ AND $u_z^{(2)}$ AT VARIOUS LEVELS IN THE TROPOSPHERE.

z	t_z	w_z	u_z	$u_z^{(1)}$	$u_z^{(2)}$	$\frac{u^2}{\sigma T^4_{(0,z)}}$	$\frac{u_z}{u_0}$
			Case 1				
0,0	—40,9	0,000	0,236	0,236	0,000	0,000	1,000
0,1	—41,5	0,001	0,236	0,221	0,015	0,064	1,000
0,2	—42,1	0,002	0,236	0,208	0,026	0,111	1,000
0,3	—42,7	0,004	0,236	0,199	0,037	0,159	1,000
0,4	—43,3	0,005	0,236	0,191	0,045	0,195	1,000
0,5	—43,9	0,006	0,236	0,184	0,050	0,218	1,000
1,0	—46,9	0,010	0,236	0,166	0,070	0,312	1,000
2,0	—52,9	0,016	0,232	0,151	0,081	0,380	0,984
3,0	—58,9	0,020	0,230	0,145	0,085	0,421	0,975
4,0	—64,9	0,022	0,229	0,142	0,087	0,455	0,970
5,0	—70,9	0,023	0,228	0,141	0,087	0,481	0,967
6,0	—76,9	0,024	0,228	0,140	0,088	0,514	0,967
7,0	—82,9	0,024	0,228	0,139	0,089	0,550	0,967
8,0	—88,9	0,025	0,227	0,139	0,089	0,543	0,962
9,0	—94,9	0,025	0,227	0,139	0,089	0,575	0,962
10,0	—100,9	0,025	0,227	0,138	0,089	0,659	0,962
			Case 2				
0,0	—4,2	0,000	0,425	0,425	0,000	0,000	1,000
0,1	—4,8	0,018	0,424	0,266	0,158	0,373	0,998
0,2	—5,4	0,036	0,422	0,232	0,190	0,453	0,994
0,3	—6,0	0,052	0,420	0,214	0,206	0,484	0,988
0,4	—6,6	0,068	0,419	0,203	0,216	0,517	0,986
0,5	—7,2	0,083	0,417	0,196	0,221	0,531	0,982
1,0	—10,2	0,145	0,409	0,177	0,232	0,571	0,962
2,0	—16,2	0,231	0,395	0,161	0,234	0,603	0,930
3,0	—22,2	0,282	0,381	0,152	0,229	0,623	0,898
4,0	—28,2	0,313	0,371	0,148	0,223	0,629	0,873
5,0	—34,2	0,332	0,364	0,145	0,219	0,648	0,853
6,0	—40,2	0,342	0,360	0,144	0,216	0,671	0,848
7,0	—46,2	0,349	0,359	0,143	0,216	0,703	0,846
8,0	—52,2	0,353	0,358	0,143	0,215	0,735	0,842
9,0	—58,2	0,355	0,359	0,142	0,216	0,777	0,842
10,0	—64,2	0,356	0,357	0,142	0,215	0,812	0,841
			Case 3				
0,0	23,3	0,000	0,627	0,627	0,000	0,000	1,000
0,1	22,7	0,086	0,625	0,287	0,338	0,541	0,997
0,2	22,1	0,168	0,622	0,254	0,368	0,592	0,992
0,3	21,5	0,247	0,619	0,233	0,386	0,622	0,988
0,4	20,9	0,322	0,616	0,216	0,400	0,648	0,982
0,5	20,3	0,394	0,613	0,203	0,410	0,667	0,978
1,0	17,3	0,685	0,599	0,166	0,433	0,718	0,955
2,0	11,3	1,094	0,569	0,140	0,429	0,742	0,918
3,0	5,3	1,338	0,543	0,135	0,408	0,735	0,866
4,0	—0,7	1,483	0,520	0,126	0,394	0,742	0,829
5,0	—6,7	1,570	0,502	1,123	0,379	0,741	0,800
6,0	—12,7	1,622	0,490	0,122	0,368	0,753	0,781
7,0	—18,7	1,652	0,482	0,121	0,361	0,770	0,768
8,0	—24,7	1,671	0,481	0,121	0,360	0,803	0,766
9,0	—30,7	1,682	0,481	0,120	0,361	0,843	0,766
10,0	—36,7	1,688	0,480	0,120	0,360	0,882	0,765

Tr. Note: Commas indicate decimal points.

TABLE 6. (Concluded)

z	t_z	w_z	u_z	$u_z^{(1)}$	$u_z^{(2)}$	$\frac{u^2}{\sigma T^4_{(0,z)}}$	$\frac{u_z}{u_0}$
			Case 4				
0,0	27,0	0,000	0,659	0,659	0,000	0,000	1,000
0,1	26,4	0,135	0,657	0,278	0,379	0,576	0,997
0,2	25,8	0,265	0,654	0,240	0,414	0,633	0,992
0,3	25,2	0,389	0,651	0,214	0,436	0,668	0,988
0,4	24,6	0,508	0,645	0,210	0,435	0,670	0,980
0,5	24,0	0,621	0,642	0,181	0,461	0,714	0,974
1,0	21,0	1,081	0,627	0,148	0,479	0,756	0,952
2,0	15,0	1,725	0,594	0,126	0,468	0,770	0,901
3,0	9,0	2,109	0,560	0,117	0,443	0,757	0,850
4,0	3,0	2,338	0,540	0,112	0,428	0,765	0,820
5,0	—3,0	2,475	0,516	0,110	0,406	0,755	0,783
6,0	—9,0	2,557	0,497	0,108	0,389	0,755	0,754
7,0	—15,0	2,606	0,494	0,107	0,387	0,685	0,750
8,0	—21,0	2,634	0,493	0,107	0,386	0,818	0,748
9,0	—27,0	2,652	0,493	0,106	0,387	0,856	0,748
10,0	—33,0	2,662	0,492	0,106	0,386	0,893	0,746
			Case 5				
0,0	30,0	0,000	0,686	0,686	0,000	0,000	1,000
0,1	29,4	0,210	0,684	0,265	0,118	0,612	0,995
0,2	28,8	0,411	0,680	0,221	0,459	0,673	0,990
0,3	28,2	0,603	0,676	0,191	0,485	0,715	0,984
0,4	27,6	0,786	0,672	0,173	0,499	0,739	0,978
0,5	27,0	0,962	0,668	0,160	0,508	0,755	0,972
1,0	24,0	1,672	0,650	0,132	0,518	0,786	0,946
2,0	18,0	2,670	0,615	0,110	0,505	0,796	0,895
3,0	12,0	3,262	0,582	0,100	0,482	0,793	0,847
4,0	6,0	3,616	0,557	0,094	0,463	0,793	0,810
5,0	0,0	3,828	0,530	0,091	0,439	0,784	0,772
6,0	—6,0	4,003	0,525	0,088	0,437	0,814	0,764
7,0	—12,0	4,032	0,498	0,088	0,410	0,794	0,725
8,0	—18,0	4,077	0,498	0,087	0,411	0,833	0,725
9,0	—24,0	4,104	0,497	0,087	0,410	0,870	0,724
10,0	—30,0	4,120	0,497	0,086	0,409	0,904	0,724

Tr. Note: Commas indicate decimal points.

2. Value u_z^2 is the increasing function of w_z and its dependence on w_z may be approximately represented by the formula

$$u_z^{(2)} = 0{,}70\sigma T^4_{(0,\,z)} w_z^{0{,}114}, \tag{7}$$

where $T_{(0,z)} = \frac{T_0 + T_z}{2}$.

In Figure 4b, where we give the dependence of $u_z^2/\sigma T_0^4$ on w_z, the solid lines correspond to formula (7). Proceeding from formulas (6) and (7) for u_z we get

$$u_z = u_z^{(1)} + u_z^{(2)} = \sigma T_0^4 (1 - 0.76 w_z^{0.114}) + 0.70 \sigma T_{(0,z)}^4 w_z^{0.114}. \tag{8}$$

In this way the effect of w_z on the total flow u_z is appreciably smaller than on its individual components u_z^1 and u_z^2.

On the basis of formula (8) a relative variation of the ascending long-wave current with altitude may be written in the following forms:

$$\frac{u_z}{u_0} = \frac{u_z}{\sigma T_0^4} = 1 - 0.76 w_z^{0.114} + 0.70 \left(\frac{T_{0,z}}{T_0}\right)^4 w_z^{0.114}. \tag{9}$$

The u_z/u_0 ratio varies with altitude because of the variation of T_z and w_z. To evaluate the role of these factors we could use the derivatives /178

$$\frac{d\left(\frac{u_z}{u_0}\right)}{dz} = \frac{\partial\left(\frac{u_z}{u_0}\right)}{\partial w_z} \frac{dw_z}{dz} + \frac{\partial\left(\frac{u_z}{u_0}\right)}{\partial T_z} \frac{dT_z}{dz},$$

$$\frac{\partial\left(\frac{u_z}{u_0}\right)}{\partial w_z} = 0.086 \left(1 - 0.93 \frac{T_{0,z}^4}{T_0^4}\right) w_z^{-0.886},$$

$$\frac{\partial\left(\frac{u_z}{u_0}\right)}{\partial T_z} = 2.8 w_z^{0.114} \frac{T_{0,z}^3}{T_0^4}.$$

Replacing dz with a finite increment Δz = 100 m and dw_z and dT_z by the increments of these values in the 100 m thick layer, we obtain for case 5 the following values $\frac{\partial\left(\frac{u_z}{u_0}\right)}{\partial w_z} \Delta w_z$ and $\frac{\partial\left(\frac{u_z}{u_0}\right)}{\partial T_z} \Delta T_z$ at various altitudes:

/179

z км	$A=\frac{\partial\left(\frac{u_z}{u_0}\right)}{\partial w_z}\Delta w_z$	$B=\frac{\partial\left(\frac{u_z}{u_0}\right)}{\partial T_z}\Delta T_z$	$\frac{A}{B}$
0,0— 0,1	0,00540	0,00464	1,164
0,1— 0,2	0,00307	0,00500	0,614
0,2— 0,3	0,00212	0,00524	0,404
0,3— 0,4	0,00164	0,00540	0,304
0,4— 1,5	0,00139	0,00548	0,253
1,0— 2,0	0,00051	0,00625	0,081
2,0— 3,0	0,00032	0,00582	0,054
3,0— 4,0	0,00020	0,00568	0,036
4,0— 5,0	0,00014	0,00554	0,024
5,0— 6,0	0,00012	0,00539	0,022
6,0— 7,0	0,00008	0,00539	0,014
7,0— 8,0	0,00004	0,00520	0,007
8,0— 9,0	0,00002	0,00502	0,005
9,0—10,0	0,00002	0,00482	0,004

Tr. Note: Commas indicate decimal points.

In this way, the variation of the water vapor content and temperature play a similar role in the variation of the u_z/u_0 ratio with altitude only in the lowest layers of the atmosphere. Beginning with the altitude of 1 km the changes in the u_z/u_0 ratio under the effect of water vapor amount to several percent of the change of u_z/u_0 under the effect of temperature.

In equation (9) the $T_{0,z}/T$ ratio may be presented as $T_{0,z}/T_0 = 1 - T_0 - T_z/2T_0$ and then the use of $u_z u_0$ ratio may be examined as a function of the $T_0 - T_z$ difference. The immediate comparison of u_z/u_0 with the difference $T_0 - T_z$ is given in Figure 5. In this diagram we can see clearly the influence of moisture: two cases with lower moisture content with the constant $\Delta T = T_0 - T_z$ correspond the greater values of u_z/u_0. In every individual case the dependence of u_z/u_0 on Δt may be presented by the formula of the type of formula (2).

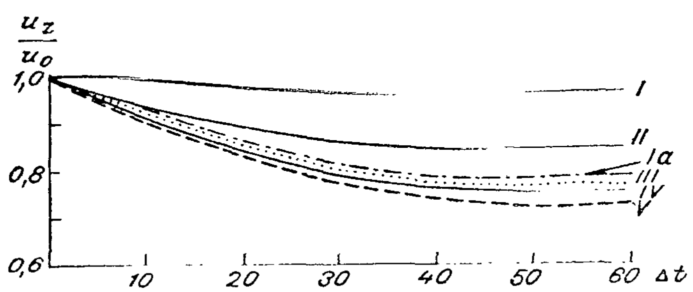

Figure 5. Relationship of the Relative Variation of the Ascending Longwave Current With the Difference Between the Soil and the Air Temperatures.

The value of coefficient a for everyone of the five examined cases is given in the following table: /180

TABLE 7.

Case	w_∞	a (H_2O)	a ($H_2O + CO_2$)
1	0,025	0,0005	0,0030
2	0,357	0,0023	0,0031
3	1,688	0,0033	0,0033
4	2,662	0,0035	0,0035
5	4,120	0,0037	0,0037

Tr. Note: Commas indicate decimal points.

The value of coefficient a increases with the increase of the moisture content in the atmosphere, but substantial variations of a are noted only with small values of w_∞.

The results given above were obtained in the assumption that the absorbing substance in the atmosphere is water vapor. The question arises, which additional influence on the vertical distribution of the ascending longwave radiation may be caused by carbon dioxide and ozone. The transfer of longwave radiation in the atmosphere is affected by ozone in the region of 9.0 - 10.3 μ. This sector of the spectrum accounts for an average of 0.067 of the radiation of the black body. According to K. Ya. Kondrat'yev and Niylisk evaluations [4] in passing through the troposphere the radiation in the 9.0-10.3 μ range varies by 0.006-0.008 cal/cm^2 min, i.e., the relative influence of ozone on the integral flow is insignificant.

Carbon dioxide has a considerably greater influence on the transfer of longwave radiation. In Table 8 we give the results of calculations of the flow of the ascending longwave radiation taking into account the water vapor and carbon dioxide. In the calculation the volume content of CO_2 is assumed to be constant with altitude and equal to 0.03%. The greatest influence on the value of the flows is exercised by CO_2 when the values of moistures are low, the variations of the individual components u_z^1 and u_z^2 being more substantial than that of the complete current u_z, since the variations in u^1 and u^2 under the influence of CO_2 have different signs. In the first case, which corresponds to the minimum water vapor content, under the effect of CO_2 value u^1 decreases by 56-57%, and the radiation of the atmosphere increases by 47--120%, the sum $u_z' + u_z^2 = u_z$ changes by 4-16%. In the third case the discrepancy between the values of u_z does not exceed 5%.

TABLE 8. COMPARISON OF THE ASCENDING LONGWAVE CURRENT, CALCULATED ONLY WITH THE ALLOWANCE FOR WATER VAPOR (H_2O) AND WITH ALLOWANCE FOR WATER VAPOR AND CARBON DIOXIDE ($H_2O + CO_2$) /181

$\Delta u_z = u_{z_{H_2O+CO_2}} - u_{z_{H_2O}}$

z KM	u_z H_2O	u_z H_2O+CO_2	Δu_z	$\frac{\Delta u_z}{u_{z(H_2O)}}$ %	u_z^1 H_2O	u_z^1 H_2O+CO_2	Δu_z^1	$\frac{\Delta u_z^1}{u^1_{z(H_2O)}}$	u_z^2 H_2O	u_z^2 H_2O+CO_2	Δu_z^2	$\frac{\Delta u_z^2}{u_z^2}$
*						Case 1						
0	0,236	0,236	0,0	0,0	0,236	0,236	0,00	0,0	0,000	0,000	0,000	0,0
1	0,236	0,226	—0,010	4,1	0,166	0,072	—0,094	56,6	0,070	0,154	0,084	121
2	0,232	0,214	—0,017	7,5	0,151	0,063	—0,089	58,6	0,081	0,152	0,071	88
3	0,230	0,205	—0,025	10,7	0,145	0,061	—0,085	58,4	0,084	0,144	0,060	71
4	0,229	0,198	—0,031	13,3	0,142	0,060	—0,082	57,8	0,087	0,138	0,052	60
5	0,228	0,192	—0,035	15,5	0,141	0,060	—0,081	57,5	0,087	0,133	0,045	52
6	0,228	0,191	—0,039	17,0	0,140	0,060	—0,080	57,5	0,088	0,132	0,044	50
7	0,228	0,190	—0,037	16,3	0,139	0,059	—0,080	57,2	0,088	0,131	0,043	48
8	0,228	0,190	—0,038	16,4	0,139	0,059	—0,080	57,0	0,089	0,131	0,042	47
9	0,227	0,190	—0,038	14,7	0,139	0,059	—0,080	57,0	0,089	0,131	0,042	47
10	0,227	0,190	—0,037	16,4	0,139	0,059	—0,080	57,0	0,089	0,131	0,042	47
						Case 3						
0	0,627	0,627	0,000	0,0	0,627	0,627	0,000	0,0	0,000	0,000	0,000	0,0
1	0,599	0,594	—0,005	0,8	0,166	0,140	—0,026	15,8	0,432	0,454	0,021	4,9
2	0,569	0,562	—0,007	1,2	0,140	0,131	—0,009	6,5	0,429	0,431	0,002	0,5
3	0,543	0,533	—0,010	1,9	0,135	0,126	—0,009	6,8	0,409	0,407	—0,001	0,3
4	0,520	0,507	—0,014	2,6	0,126	0,122	—0,003	2,6	0,395	0,384	—0,010	2,6
5	0,502	0,485	—0,017	3,4	0,123	0,121	—0,003	2,1	0,379	0,364	—0,014	3,8
6	0,490	0,470	—0,020	4,1	0,122	0,120	—0,002	1,8	0,368	0,350	—0,018	4,8
7	9,482	0,459	—0,023	4,8	0,121	0,119	—0,002	1,8	0,361	0,340	—0,021	5,8
8	0,481	0,459	—0,021	4,4	0,121	0,119	—0,002	1,8	0,360	0,341	—0,019	5,3
9	0,480	0,459	—0,022	4,2	0,121	0,119	—0,002	1,6	0,360	0,341	—0,019	5,2
10	0,480	0,459	—0,021	4,4	0,120	0,118	—0,002	1,6	0,360	0,341	—0,019	5,3

Tr. note: Commas indicate decimal points.

When we take into account the absorption by carbon dioxide the value of the coefficient in formula (2) for case 1 changes from 0.0005 to 0.0030, in this way values u_z/u_0 with Δt = const for all the five cases approach one another (Figure 5, Curve I a). In this case the values of a are sufficiently close to those obtained on the basis of experimental data (Table 3). Upon the change of w_∞ from 0.4 to 4 grams/cm^2 the maximum difference in the values of u_z/u_0, noted at the greatest values of Δt = 60, i.e., at high altitudes, does not exceed 10%. In this way, if we do not take into account the influence of moisture on the value of coefficient a, and use its mean value, then the deviations in the u_z/u_0 ratio from that corresponding to the mean value of the coefficient will not exceed 5%. Consequently, formula (2) may be used for evaluation of the ascending longwave radiation flow at various points with a single constant value of coefficient a. /182

The correctness of this conclusion is substantiated by the comparison of the values of the ascending longwave radiation measured and calculated with formula (2) when a = 0.0036. The results of the comparison are given in Table 9, where we give the recurrence of the ratio u_z^f/u_z calculated according to the formula of u_z^f and measured values of u_z.

TABLE 9. RECURRENCE (%) OF THE RATIO u_z^f/u_z AT VARIOUS ALTITUDES (ACCORDING TO THE DATA FOR SIX POINTS), u_z^f IS THE ASCENDING LONGWAVE FLOW CALCULATED ACCORDING TO THE FORMULA; u_z IS THE ONE MEASURED BY THE RADIOSONDE

z KM	No. of Cases	Limits of Ratio $\frac{u_z^f}{u_z}$										
		<0,90	0,90 – 0,94	0,95 – 0,99	1,00	1,01 – 1,05	1,06 – 1,10	<1,10	<1	>1	0,95 – 1,05	0,90 – 1,10
0,0 — 1,0	149	0,67	2,01	7,38	4,03	59,06	22,15	4,70	10,06	85,91	70,47	94,63
1,01 — 2,0	108	0,00	0,92	29,63	12,04	47,22	7,41	2,78	30,55	57,41	88,89	97,22
2,01 — 3,0	103	0,00	7,77	34,95	15,53	35,92	3,88	1,94	42,72	41,74	86,40	98,05
3,01 — 4,0	100	0,00	6,00	35,00	13,00	29,00	13,00	4,00	41,00	46,00	77,00	96,00
4,01 — 5,0	99	2,02	8,08	38,38	7,07	35,35	8,08	1,01	48,94	44,44	80,80	96,96
5,01 — 6,0	85	2,35	14,12	29,41	9,41	32,94	10,59	1,18	45,88	44,71	72,76	96,47
6,01 — 7,0	95	2,10	4,21	34,74	4,21	38,94	10,53	5,26	41,05	54,73	77,89	92,63
7,01 — 8,0	68	1,47	5,88	32,35	5,88	26,47	14,71	13,24	39,70	54,42	64,70	85,29
8,01 — 9,0	90	3,33	6,67	27,78	8,89	23,33	20,00	10,00	37,78	53,33	60,00	86,67
9,01 — 10,0	69	4,35	7,25	27,54	5,80	26,09	13,04	15,94	39,14	55,07	59,43	79,72
0,0 — 10,0	1259	1,36	5,25	23,82	8,82	32,87	15,81	12,07	30,43	60,75	65,51	86,57

Tr. Note: Commas indicate decimal points.

TABLE 10. RECURRENCE OF u_z^d/u_z AT VARIOUS ALTITUDES (ACCORDING TO THE DATA FOR SIX POINTS)

z KM	No. of Cases	Limits of Ratio $\frac{u_z^d}{u_z}$										
		<0,90	0,90–0,94	0,95–0,99	1,00	1,01–1,05	1,06–1,10	>1,10	<1	>1	0,95–1,05	0,90–1,10
0,0 — 1,0	29	0,0	0,00	6,91	6,89	51,72	24,14	10,34	6,90	86,20	65,52	89,66
1,01— 2,0	74	0,0	0,00	18,92	12,16	59,46	9,46	0,00	18,92	68,92	90,54	100,00
2,01— 3,0	86	0,0	1,16	22,09	15,12	54,65	5,82	1,16	23,25	60,47	91,86	98,84
3,01— 4,0	87	0,0	0,00	19,54	16,09	50,57	11,49	2,31	19,54	62,06	86,20	97,69
4,01— 5,0	87	0,0	1,16	22,98	10,34	51,72	12,64	1,16	24,14	64,36	85,04	98,84
5,01— 6,0	62	0,0	1,62	12,90	14,51	41,93	22,58	6,46	14,52	64,51	69,34	93,54
6,01— 7,0	87	0,0	1,15	3,45	5,75	50,57	27,59	11,49	4,60	78,16	59,77	88,51
7,01— 8,0	60	0,0	0,00	0,00	0,00	31,67	21,67	46,66	0,00	100,00	0,00	53,34
8,01— 9,0	75	0,0	0,00	2,56	1,28	19,23	26,92	50,01	2,56	96,16	23,07	49,99
9,01—10,0	38	0,0	0,00	0,00	0,00	7,89	15,79	76,32	0,00	100,00	7,89	23,68
0,0 —10,0	810	0,0	0,73	10,48	7,65	37,79	16,17	27,01	11,21	80,97	55,92	72,82

Tr. Note: Commas indicate decimal points.

In the calculations as the temperature of the underlying surface we took the temperature of the soil on the meteorological platform, measured at the moment of launching of the radiosonde, and the radiating capacity of the underlying surface was assumed to be equal to a unity. At the same time we carried out the comparison of the measured values of u_z with the calculated ones according to the radiation diagram of Shekhter [5]. The results of this comparison are given in Table 10. In the calculation according to Shekhter's diagram we use data on the temperature and moisture of the air, obtained simultaneously with the radiation flows by the actinometric radiosonde. /183

From Table 10 we can see that in most of the cases Shekhter's diagram yields higher values of the ascending longwave currents than the actinometric radiosonde. The difference between the measured and calculated values increases with the increase of the altitude, and whereas at the altitudes of up to 5 km the relationship $u_z^d/u_z > 1$ in only 60-70% of all the cases, and more than 90% of all the cases, this ratio fluctuates between 0.90 and 1.10, at altitudes of more than 7 km all the values of $u_z^d/u_z > 1$, in 50-76% of the cases the ratio $u_z^d/u_z > 1.10$.

The values of the ascending longwave current obtained from formula (2) are found to correspond in the best way with the measurement results. The u_z^f/u_z ratio has narrower limits of variations and the variations of the height is reflected to a lower extent on the distribution of values of u_z^f/u_z. Up to an altitude of 7 km the u_z^f/u_z ratio within the limits between 0.80 and 1.10 is noted in more than 90% of all the cases, with the further increase of the altitude the number of cases in this range decreases, but even on the altitude of 10 km it still amounts to 80% of all the cases. This indicates that the calculations according to formula (2) assure the coincidence with the measured values with an accuracy of up to 10%, i.e., the calculation error lies within the limits of the measurement accuracy.

The idea of the distortion of the vertical profile of ascending longwave motion produced as the result of the calculations, is given in Figure 6, in which we give the profiles of the ascending current obtained by various methods: as the result of measurements, with formula (2), and with Shekhter diagram.

In the majority of cases the vertical distribution obtained with formula (2) is closer to the one obtained on the basis of the actinometric soundings. In this way, formula (2) reflects sufficiently well the principal of regularities of the vertical distribution of the flow of ascending longwave radiation.

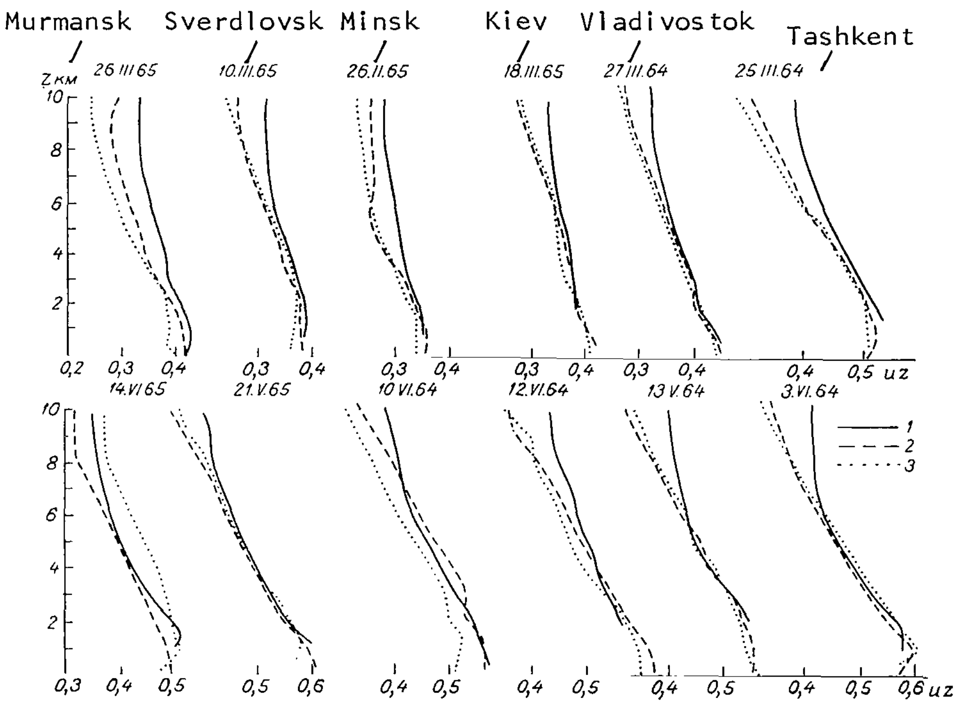

Figure 6. Comparison of the Vertical Profiles of the Ascending Longwave Radiation Flow. 1, Calculated with Shekhter Diagram; 2, According to Formula (2); 3, Measured.

From Table 6 it follows also, that already beginning with the significant altitudes the radiations of the atmosphere give the principal contribution to the current of the ascending longwave radiation. The contribution of the atmospheric radiation increases with the increase of moisture content, and an especially rapid growth is noted upon the change of w_z from 0 to 0.02 grams/ /cm^2.

Below we give the dependence of ratio u_z^1/u_z and u_z^2/u_z ratios on the "effective" content of water vapor in the w_z layer of the atmosphere. /184

w_z grams/cm^2	0,0	0,02	0,2	1,0	2,0	3,0	4,0
u_z^1/u_z	1,00	0,31	0,28	0,24	0,22	0,19	0,17
u_z^2/u_z	0.0	0,69	0,72	0,76	0,78	0,81	0,83

In this way, when $w_z > 0.2$ the contribution of the atmosphere is 2-5 times greater than the contribution of the underlying surface to the flow of the ascending longwave radiation.

REFERENCES

1. Kostyanoy, G. N.: "The Actinometric Radiosonde," *Meteorologiya i Gidrologiya*, No. 7, 1963.
2. Dlin, A. M.: *Matematicheskaya Statistika v Tekhnike*, [Mathematical Statistics in Technology]," Moscow, 1958.
3. Kondrat'yev, K. Ya.: *Luchistyy Teploobmen v Atmosfere*, [Radiant Heat Exchange in the Atmosphere]," Gidrometeoizdat Press, Leningrad, 1956.
4. Kondrat'yev, K. Ya. and Kh. Yu. Niylisk: "On the Problem of Thermal Radiation of the 9.6 μ Band of Absorption by Ozone in the Atmosphere," *Problemy Fiziki Atmosfery* [Problems of the Physics of the Atmosphere], Collection No. 2, Publication of the LGU, 1963.
5. Shekhter, F. N.: "On the Calculation of Radiant Flows of Heat in the Atmosphere," *Trudy GGO*, Issue 22 (84), 1950.

SPECTRAL BRIGHTNESS OF CLOUDS AND LANDSCAPE OBJECTS IN THE VISIBLE AND NEAR INFRARED SECTORS OF THE SPECTRUM

L. I. Chapurskiy, V. V. Klemin, N. I. Andreyeva and M. V. Startseva

ABSTRACT. Nadir measurements of the spectral brightness of five types of cloudiness and six types of underlying surface were made with elevations of the sun from 0-50°. The instrument was calibrated in absolute unital brightness. The equipment made it possible to control the stability of its characteristics in time.
From the point of view of reflecting properties of natural formations the authors explain the spectral variations of their brightness.
All the results of the measurements and calculations are represented in the form of graphs and tables.

Information on the spectral brightness of the principal types of cloudiness and objects of the landscape, obtained as the result of direct measurements under various conditions of lighting and sighting, is necessary for solving a number of applied and theoretical problems. Such data may be obtained by means of airplane spectral equipment, calibrated in absolute units of brightness, and which makes it possible to control the stability of its characteristics in time. The data given in the present article were obtained as the result of investigations which are the continuation of measurements performed earlier in the visible and near infrared sectors of the spectrum [1]. /185

1. Equipment and Procedure of the Measurements

The visible channel was created in the airplane infrared spectrometer [2] by installation of a second output slot. As the radiation receiver, in addition to the lead sulfide photoelectric resistor, a photoelectronic multiplier FEU-27 was used. The spectral resolution at the wavelengths of 0.4, 0.7, and 2.5 μ , amounted to 0.003, 0.01 and 0.05 μ respectively. The angles of the field of vision are equal to 0.5 × 5°. The spectrum scanning time is about 1 second. In the spectrometer after each measuring cycle the radiation of the comparison map is automatically recorded, as the result of which we control the spectral sensitivity in time. The instrument was installed inside an IL-18 airplane. The sighting was performed vertically down through a mirror head installed on a window baffle.

Before and after each flight through the mirror head the brightness of a white screen installed inside a hollow sphere which screen completely overlapped the aperture of the spectrometer, was recorded. The screen was illuminated by the light of the lamp, reflected from the internal walls of the sphere. The spectral brightness of the screen was measured under laboratory conditions by comparing it with the brightness of a ribbom filament lamp calibrated in the State Astronomical Institute named after Shternberg. In this way it became possible to present the measurement result in absolute spectral brightness units. In Table 1 we give the minimum brightnesses and errors in determination of the brightness of cloudiness at certain wavelengths, registered by the instrument.

/186

TABLE 1

Wavelength, μ	0,4	0,5	0,6	0,7
Minimum recordable brightness watts·cm^{-2}·ster^{-1}·μ^{-1}	$1,8 \cdot 10^{-5}$	$9,0 \cdot 10^{-6}$	$8,8 \cdot 10^{-5}$	$1,4 \cdot 10^{-5}$
Relative error in determination cloud brightness, %	60	30	30	60
Wavelength, μ	**1,0**	**1,5**	**2,0**	**2,5**
Minimum recordable brightness watts·cm^{-2}·ster^{-1}·μ^{-1}	$7,4 \cdot 10^{-5}$	$3,0 \cdot 10^{-5}$	$2,1 \cdot 10^{-5}$	$3,6 \cdot 10^{-5}$
Relative error in determination cloud brightness, %	40	30	25	60

Tr. Note: Commas indicate decimal points.

In May-June 1966 a series of flights was carried out within the limits from the Kara Sea to the regions of the Caspian Sea and from the Ukraine to Western Ural. Mostly the flights were performed along the route at altitudes close to the ceiling for the given type of the airplane, therefore in carrying out the investigations the principal attention was concentrated on obtaining the greatest possible amount of data pertaining to various objects. At the same time with the measurements detailed records were kept in the journals on the characteristics of the clouds and landscape objects investigated, and also on the state of their illumination. Observations were carried out along the optical axis of the spectrometer. Since the tying-in of the measurements was performed visually, the signals were recorded from sufficiently elongated formations. Proceeding from the reflective properties of the objects, and a also from their microphysical characteristics, eleven types of cloudiness and underlying surface were separated, which are given in Table 2.

TABLE 2.

Ordinal Number	Type of Cloudiness and Background
1.	Dense Cirrus Clouds
2.	Alto-cumulus and Alto-stratus Clouds
3.	Stratus, Strato-cumulus and Cumulus Clouds in Good Weather
4.	Thick Cumulus Clouds
5.	Translucent Cirrus Clouds with Clouds of the Lower and Middle Levels
6.	Old Ice Covered with Snow
7.	Denuded Soil (Deserts and semi-Deserts, Plowed Fields, Sandy Coastlines)
8.	Green Meadows and Planted Fields
9.	Forests and Brush
10.	Tundra with Remnants (10-20%) of Snow
11.	Watery Surfaces

During processing the data were systematized according to six gradations of the height of the sun, the boundaries of which were determined by equal values of the cosine of the senate angle (see Table 3). As it follows from the table the greatest number of measurements pertains to clouds of the lower and middle levels with the altitudes of the sun of 42-55°. Relatively few measurements were carried out on cirrus clouds because frequently it is impossible to reach their upper edge. /187

The measurements of the brightness signal amplitudes on the oscillograms were carried out manually. Further processing of the data was performed on the M-20 computer. The problem, composed on the "ALGOL-60" language, provided for the calculation and delivery for printing of the following data:

1. Absolute values of the spectral brightness of specific formation recorded in individual measurements;

2. Medium and extreme values of spectral brightness of eleven types of objects at various heights of the sun;

3. For certain wavelengths of recurrence (according to seven gradations between the extremum values) of brightnesses of specific types of objects under various lighting conditions;

4. Values of brightness of the clouds and background in the spectral radius, the boundaries of which are determined by the water absorption bands, and also by the optical properties of the atmosphere and landscape objects.

2. Measurement Results

In Figures 1-4 and in Table 3 we give certain materials obtained after carrying out the present investigations. As the result of the analysis of the experimental data the following has been established.

1. The highest absolute values of brightness both in the visible and in the infrared sectors of the spectrum were obtained from thick cumulus clouds, in the second place with respect to brightness are the clouds of the middle layer. The clouds of the upper layer, having a crystalline structure, have a relatively great brightness in the visible and near infrared sectors of the psectrum up to 1.2-1.3 μ. However, in infrared rays with wavelengths of more than 1.5 μ these clouds, in comparison with the liquid droplet clouds appear darker because of the lower reflecting capabilities of the ice particles. In this case the brightness contrasts are from 20-70%. Consequently, the data on the distribution of brightness in the visible and near infrared sectors of the spectrum enable us to evaluate the type of the cloudiness observed.

2. The reflection minima of the crystalline clouds were shifted, as it is the case for snow, to the region of longer waves. They are centered near 1.21, 1.50, and 2.00 μ, which corresponds to the location of the maxima of absorption by ice, whereas in liquid droplet clouds they are found near 1.19; 1.45; and 1.94 μ. According to the location of the reflection minima we can determine the phase of the cloud elements, and consequently we can distinguish the cloud types. The depth of the minima on the average depends on the height of the upper boundary of the cloudiness. In some cases this property may be used for evaluating the height of the reflecting surface.

3. On the basis of the anaylsis of dependences of the spectral brightness of clouds on illumination conditions it has been established that their mean brightness changes slower, than the sign of the elevation of the sun, and in the infrared part of the spectrum the cloud brightness depends less on the elevation of the sun, than in the visible and the near infrared range up to 1-1.2 μ. This specific feature may be explained by the fact, that with the increase of the height of the sun the angle of dispersion of the light decreases. In this case the amount of energy dispersed upwards, increases. Moreover, upon the increase of the zenith angle of the sun the number of events of dispersion of the higher orders increases. The last two factors cause a certain increase of the cloud albedo with the approach of the luminary to the horizon. /189

The greater stability of brightness in the infrared region of the spectrum upon the change of the lumination conditions, in addition to the above-mentioned factors, is affected by the great transparency of the atmosphere for radiations with wavelengths of more than 1 μ.

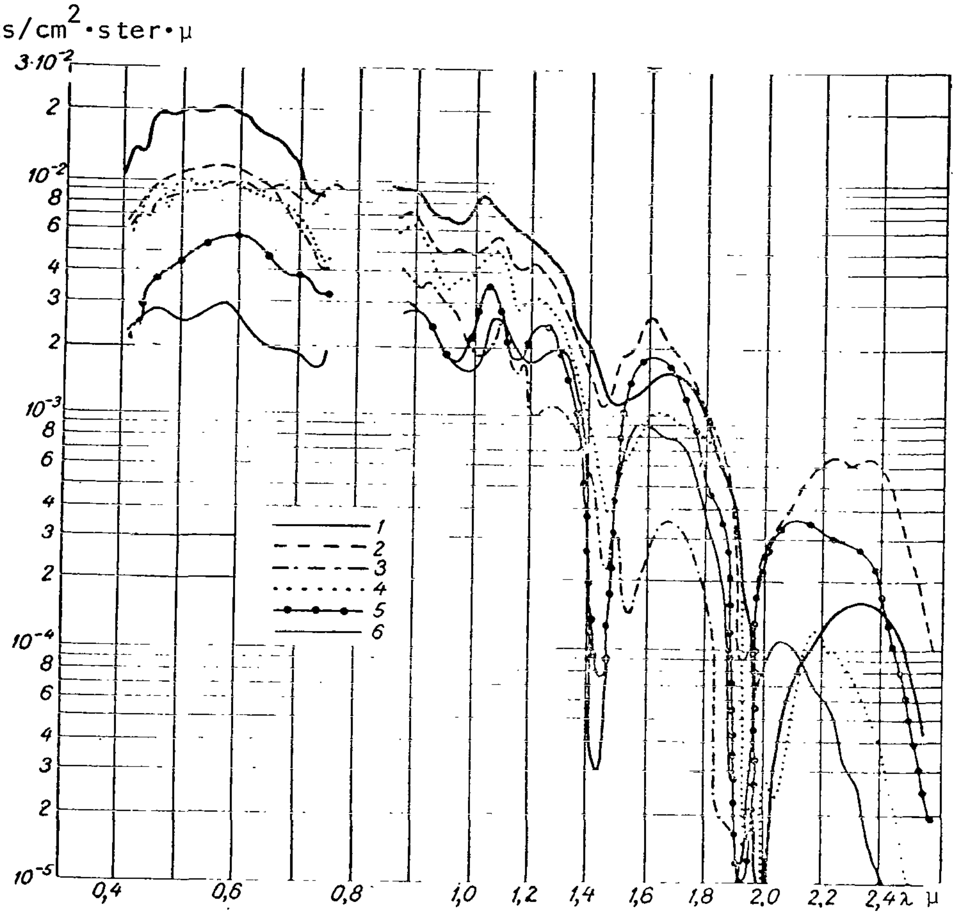

Figure 1. Mean Spectral Brightnesses of Objects at Various Elevations of the Sun: 1, Cirrus Clouds, $H_\odot$ = 40°; 2, Cumulus Clouds $H_\odot$ = 30°; 3, Old Ice with Snow, $H_\odot$ = 26-29°; 4, Multilevel Cloudiness, $H_\odot$ = 36-42°; 5, Deserts and Semi-deserts, $H_\odot$ = 34-36°; 6, Tundras with Snow Remnants (10-20%), H⊙ = 43-46°.

4. The brightness of various sectors of cumulus, stratocumulus and alto-cumulus clouds in the infrared sector of the spectrum varies by more than two orders, whereas in the visible band it varies by not more than one and a half order. This is caused by the considerable contribution of the diffused radiation in the visible range of the spectrum, and also by the relatively small transparency of the clouds to infrared radiation.

TABLE 3. MEAN BRIGHTNESS OF CLOUDS AND LANDSCAPE OBJECTS IN MEGAWATTS/cm^2 STER, RECORDED IN MAY-JUNE 1966 ON THE EUROPEAN TERRITORY OF USSR IN VARIOUS SPECTRAL RANGES AT VARIOUS ELEVATIONS OF THE SUN.

Type of Cloudiness	No. of Measurements	Spectral Ranges, μ						
		0,40—0,71	0,55—0,74	1,08—1,24	1,28—1,57	1,67—2,14	0,87—1,33	1,33—2,56
1	2	3	4	5	6	7	8	9
			I. Solar Elevation 42—55°					
1	12/9	3,52	1,92	0,91	0,67	0,35	2,45	0,792
2	65/107	3,62	2,10	0,886	0,745	0,620	2,30	1,13
3	77/124	3,9	2,23	0,667	0,58	0,446	1,71	0,882
4	18/20	5,03	2,57	1,34	1,20	0,95	3,97	1,89
5	9/9	2,64	1,56	0,512	0,488	0,418	1,46	1,476
6	21/33	5,52	3,25	0,412	0,160	0,0089	1,33	0,074
7	24/37	0,924	0,5730	0,508	0,432	0,326	1,37	0,959
8	18/20	0,972	0,509	0,471	0,406	0,311	1,38	0,540
9	42/66	0,767	0,411	0,381	0,288	0,198	1,04	0,340
10	19/32	0,827	0,458	0,357	0,318	0,222	0,939	0,349
			II. Solar Elevation 32—42°					
1	15/15	5,40	2,9	1,25	0,72	0,397	3,25	0,816
2	24/61	2,88	1,67	0,779	0,686	0,550	2,19	1,06
3	15/34	2,54	1,45	0,456	0,417	0,374	1,32	0,696
4	3/0	4,24	2,11	—	—	—	—	—
5	12/6	2,94	1,63	0,634	0,376	0,214	1,79	0,417
7	21/42	1,52	0,93	0,420	0,368	0,379	1,09	0,658
			III. Solar Elevation 21° 40′—32°					
2	12/6	1,52	0,785	0,625	0,537	0,393	1,70	0,833
3	3/36	1,60	0,646	0,466	0,412	0,415	1,29	0,746
4	3/3	2,75	1,50	0,828	0,699	0,542	2,22	1,18
6	24/24	3,23	1,90	0,285	0,167	0,066	0,914	0,142
7	15/9	0,676	0,322	0,228	0,248	0,167	0,745	0,334
10	3/3	0,353	0,291	0,353	0,291	0,256	1,07	0,394
11	6/0	0,694	0,307	—	—	—	—	—
			IV. Solar Elevation 12° 31′—21° 40′					
2	15/39	1,14	0,67	0,304	0,279	0,256	0,864	0,448
3	6/6	1,08	0,55	0,347	0,344	0,367	0,952	0,746
7	6/6	1,2	0,68	0,180	0,148	0,193	0,520	0,854
9	3/9	0,191	0,091	0,190	0,161	0,092	0,582	0,193
10	0/12	—	—	0,216	0,197	0,135	0,574	0,230
11	6/0	0,29	0,14	—	—	—	—	—
			V. Solar Elevation 4°—12° 30′					
3	12/15	0,58	0,32	0,344	0,37	0,40	0,03	0,799
9	15/18	0,25	0,13	—	—	—	—	—
11	6/0	0,21	0,103	—	—	—	—	—
			VI. Solar Elevation —2°, —4°					
2	3/0	0,21	0,12	—	—	—	—	—
7	3/0	0,129	0,081	—	—	—	—	—

In column 2 in the numerator we give the number of measurements in the visible channel, in the denominator the number of measurements in the infrared channel.
Tr. Note: Commas indicate decimal points.

5. From the analysis of the character of distribution of recurrences of various gradations of spectral brightness of clouds in the middle and lower levels (for which we obtained the greatest number of cases) it has been estab- /190 lished that the latest recurrence is possessed by brightnesses, which are somewhat greater than the medium values.

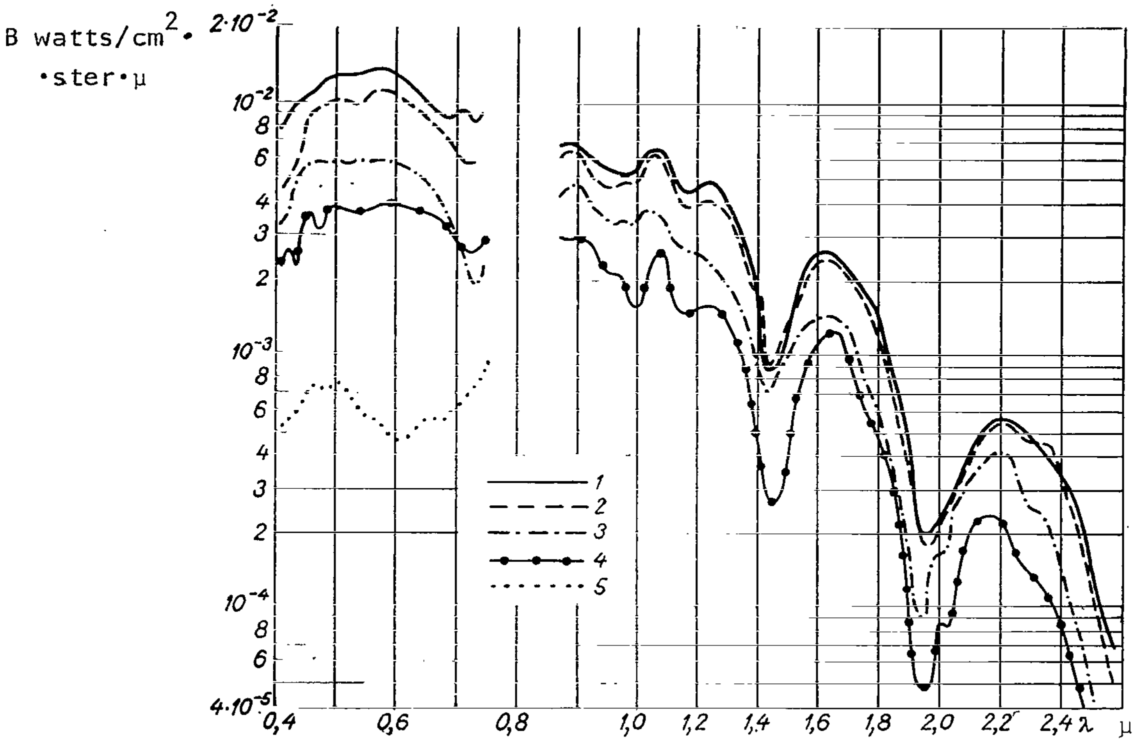

Figure 2. Mean Spectral Brightnesses of Clouds of the Middle Level at Different Elevations of the Sun.

1) $H_{\odot} = 42 \div 55°$, 2) $H_{\odot} = 32 \div 42°$, 3) $H_{\odot} = 21{,}7 \div 32{,}0°$, 4) $H_{\odot} = 12{,}5 \div 21{,}7°$, 5) $H_{\odot} = 1 \div 2°$.

6. In works [1 and 3] it is shown that in the 1.4 to 2.5 μ sector of the spectrum the brightness of the clouds is considerably greater than that of the snow, however, in this band we often encounter difficulties in detection of clouds against the background of denuded soils and vegetation covers. The measurements performed showed that the spectral brightness of old ice with snow recorded in the southeastern part of the Kara Sea, in the visible band is commensurable with the brightness of clouds of the upper and middle levels and exceeds the mean brightness of clouds of the lower levels. In the infrared sector of the spectrum the brightness of the ice rapidly decreases and at wavelengths of more than 1 μ the illumination conditions being equal, becomes 1-2 orders below the brightness of any type of cloudiness. In the spectral distribution of ice brightness curves near 1.1, 1.4, and 1.9 μ, we find two

minima, connected with the absorption bands of the water vapors contained in the atmosphere and with ice reflection minima.

7. In landscape objects, combined under the term "denuded soil" in the 0.6-0.9 μ spectral range the brightness is practically unchanged with the wavelength. This is caused by the fact that upon the passage from the visible /191 band to the infrared the reflective capacity of these objects increases, which compensates the decrease of energy with the wavelength in the solar spectrum. The measurements showed that the greatest contrast between the clouds and the desert landscapes are observed in the violet and blue parts of the spectrum. The three-dimensional variability of brightness of individual types of denuded soil, such as desert, sectors of sandy coast, and plowed fields is not large. However, in general, their brightness may vary by two orders.

B watts/cm^2·ster·μ

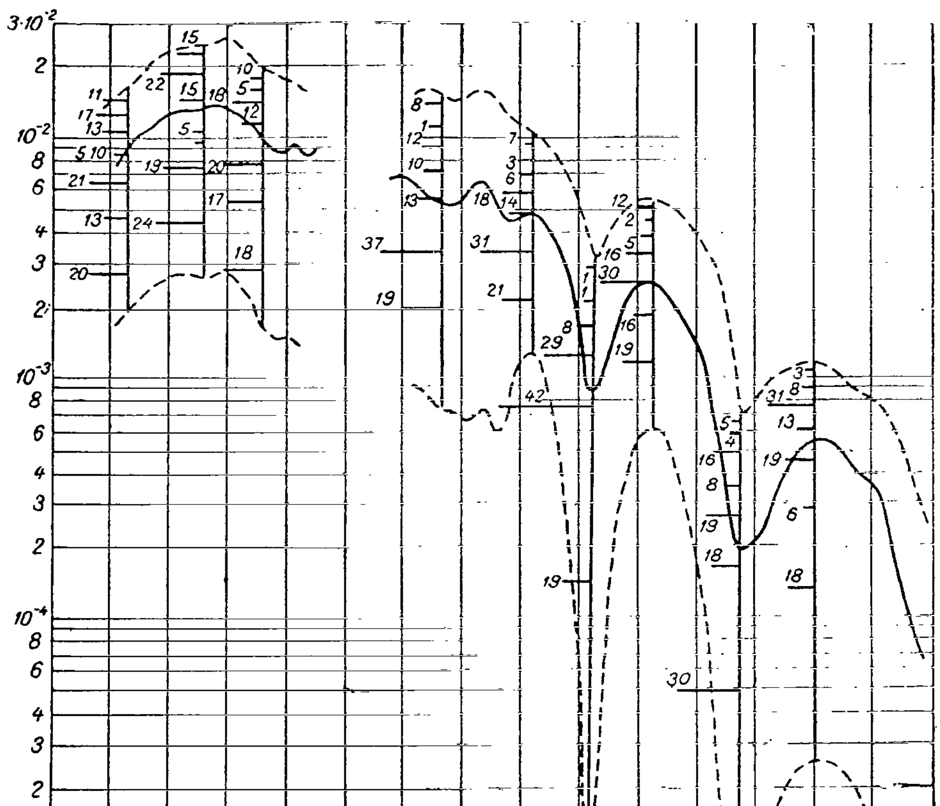

Figure 3. Mean Maximum Values and Recurrences (%) or Various Gradations of Spectral Brightness of the Cloudiness in the Second Level with the Sun Elevations of 42-45°.

8. The spectral brightness of the meadows and green fields and also the tundra landscape increases somewhat in the 0.7-0.9 μ sector of the spectrum, through the sharp increase of their reflective capacity. In the infrared region, beginning with 1.6 μ , the brightness coefficients of these objects decrease with the wavelengths, in connections which only the near 2.3μ the values of the brightness contrast between the clouds and green landscapes approach the values, observed in the visible sector of the spectrum. The analogous variations of the spectral brightness is observed for forests massifs also, however the values of forest brightness are less than the brightness of meadows and green fields. Through the growth of the albedo of vegetation landscapes, with the increase of the zenith angle of the sun, their brightness decreases slower with the decrease of the elevation of the sun, than the cosine of the zenith angle. /192

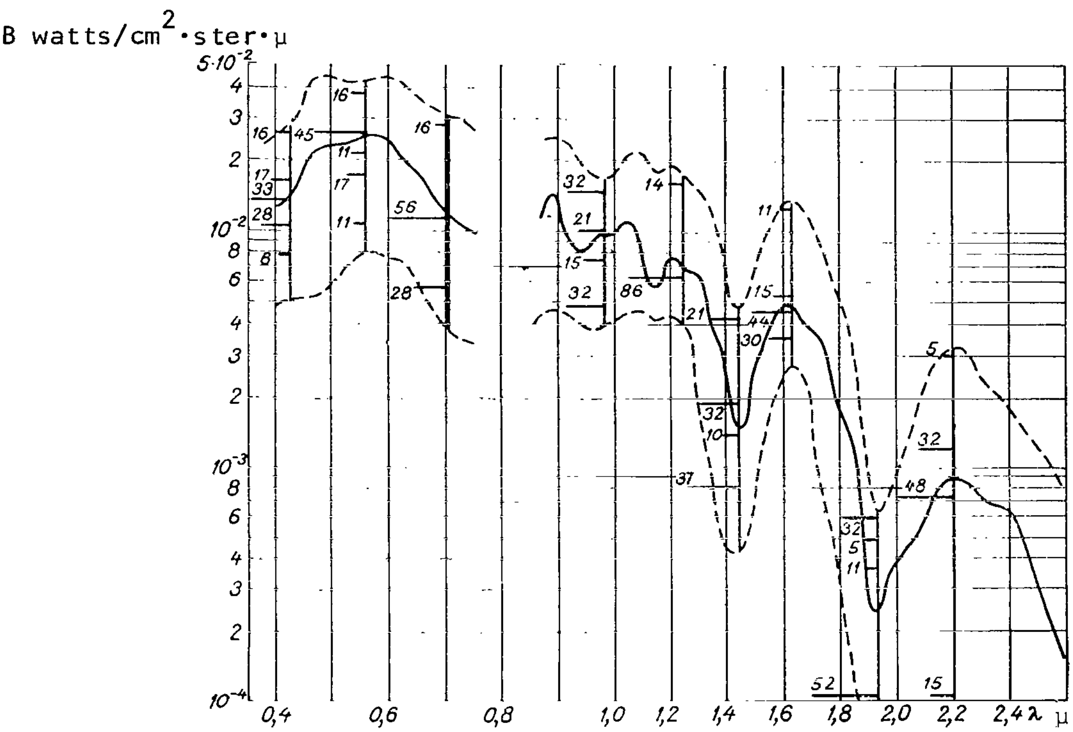

Figure 4. Mean and Extremal Values and Recurrences (%) of Various Gradations of the Spectral Brightness of Thick Cumulus Cloudiness with Sun Elevations of 42-45°.

3. Comparison of Experimental Data with the Theoretical Calculation Data

The experiment performed enabled us to check the theoretical systems of the calculation of spectral brightness of cloudiness in the visible band of the spectrum, developed at the IFA AN SSSR and at the GGO.

The spectral brightness of the cloud-atmosphere system observed from the satellite is determined by the relationship

$$B(z_{\odot}, \theta, \varphi, \tau_{cl}) = I_0(\lambda)[B_{rel}(z_{\odot}, \theta, \varphi, \tau_{cl}) T_{\lambda}(z_{\odot}, \tau_{atm}) \times \times T_{\lambda}(\theta, \tau_{atm}) + D(z_{\odot}, \theta, \varphi, \tau_{cl}, \tau_{atm})], \tag{1}$$

where

$$B_{rel}(z_{\odot}, \theta, \varphi, \tau_{cl}) = kB_{rel}(z^{\circ}_{\odot}, \theta^{\circ}, \varphi^{\circ}, \tau^{\circ}_{cl});$$

$$B_{rel}(z^{\circ}_{\odot}, \theta^{\circ}, \varphi^{\circ}, \tau^{\circ}_{cl}) = \frac{\cos z^{\circ}_{\odot} \cdot A}{\sum\limits_{\theta=0}^{\pi/2} \sum\limits_{\varphi=0}^{2\pi} K \sin\theta \cos\theta \, \Delta\varphi \, \Delta\theta};$$

$$B_{abs}(z_{\odot}, \theta, \varphi, \tau_{cl}) = I_0 B_{rel}(z_{\odot}, \theta, \varphi, \tau_{cl});$$

$I_0(\lambda)$ is the intensity of the solar light in the upper boundary of the atmosphere at the wavelength of λ, $T_{\lambda}(z_{\odot}, \tau_{atm})$ and $T_{\lambda}(\theta, \tau_{atm})$ are the spectral functions of transmissions of the atmosphere from its upper boundary to the clouds, and from the clouds to the receiver, $D(z_{\odot}, \theta, \phi, \tau_{cl}, \tau_{atm})$ is the relative brightness of the air haze, τ_{cl} and τ_{atm} are the optical thicknesses of clouds and atmosphere respectively. k is the cloud diffusion indicatrix, $z_{\odot}$ is the zenith distance of the sun, θ is the sighting angle, ϕ is the sighting azimuth, A is the albedo of the clouds. /193

The $B_{rel}(z^{\circ}_{\odot}, \theta^{\circ}, \phi^{\circ}, \tau^{\circ}_{cl})$ value was calculated for the conditions: $z^{\circ}_{\odot} = 30^{\circ}$ $\theta^{\circ} = 0^{\circ}$, $\tau^{\circ}_{cl} = 10$. The value of the cloud albedo for $\tau^{\circ}_{cl} = 10$ when the calculation of the mean brightness was assumed equal to 50% according to [4], and with the calculation of the maximum brightness, to 75%. The values of k are taken from Table II.6.11 of work [4], and the values of T_{λ} and D were taken from work [5].

The calculations were carried out for clouds of the upper level (A = 75%, $\tau_{cl} = 50$, the altitude of the upper boundary is 10 km), of the middle level (A = 75%, $\tau_{cl} = 50$, height of the upper boundary is 3 km), and thin clouds of the lower level (A = 50%, $\tau_{cl} = 10$, height of the upper boundary is 0.55 km). It was assumed, that in the existence of cloudiness in the upper level, the brightness of the super cloud layer of air haze is equal to zero; in the presence of cloudiness in the second level $D = D^{\infty}_{3\ km}$, and for cloudiness of the lower level $D = D^{\infty}_{0.55\ km}$. The optical thickness of the atmosphere τ_0 was assumed equal to 0.3, which corresponds to the horizontal visibility of 20 km beyond the clouds.

TABLE 4. COMPARISON OF THE MEASURED AND CALCULATED VALUES OF ABSOLUTE SPECTRAL BRIGHTNESS OF CLOUDINESS B mwt/cm^2·ster·μ (FIRST LINES ARE THE MEAN VALUES, SECOND LINES ARE THE MAXIMUM VALUES).

	Elevation of the Sun, degrees							
	50		40		25		5	
Wavelength μ	$B_{calc.}$	$B_{meas.}$	$B_{calc.}$	$B_{meas.}$	$B_{calc.}$	$B_{meas.}$	$B_{calc.}$	$B_{meas.}$
0,45	26,6	16	21,2	18	5,4	5,6	1,8	—
	39,8	30	31,8	24,2	8,2	6,2	2,6	—
0,55	23,4	17	20,2	20	5,0	5,0	1,6	—
	35,2	31	28,8	21,5	7,4	5,7	2,4	—
0,65	18,8	13	16,4	16	4,0	3,0	1,4	—
	28,2	31	23	17	6,0	4,0	2,1	—
	Cloudiness of the Middle Level							
0,45	18,2	11	14,6	8	4,0	5,5	0,7	1,2
	27,2	22	22	19	4,8	6,7	0,8	—
0,55	18,8	12	16	11	4,0	5,8	1,0	1,4
	28,2	24	24	21	5,2	6,3	1,2	—
0,65	16,6	10	15	9	3,8	4,3	1,0	1,4
	24,8	21	22,6	17	4,6	4,7	1,2	—
	Cloudiness of the Lower Level							
0,45	12,2	13	9,2	7,2	4,0	6,3	0,7	0,8
	18,2	16,5	13,8	12	4,2	7,7	0,8	0,9
0,55	13,8	14	10,8	10	4,1	6,7	0,8	0,7
	20	19	16,2	14,8	4,4	7,5	1,0	0,9
0,65	15,4	11	12,2	7	4,2	(5)	1,0	0,6
	23,2	17,2	18,4	11,1	4,6	2,3	1,4	0,7

Tr. Note: Commas indicate decimal points.

The calculated mean and maximum brightness values of the clouds in the upper and middle levels at sun elevations of 40 and 50° in all the visible sector of the spectrum proved higher than the corresponding measured mean values. This is explained by the fact that in the majority of the cases the flights were carried out above the intramass thin clouds, the optical thickness of which probably was not high, and consequently their albedo with the sun elevations mentioned proved less than 75%. It is quite possible also, /194 that among a limited series of observations there were no data on the cloudiness of the upper level with an albedo equal to 75%.

We know that the albedo of clouds increases with the decrease of the elevation of the sun, this relationship being the more pronounced, the smaller is the optical thickness of the clouds [4]. At the same time the albedo of clouds is less dependent on their optical thickness at low elevations of the sun, than at large elevations. The wide range of variations of the albedo of clouds illuminated by the sun, located high above the horizon (the albedo of clouds in this case according to the data of works [6, 7] changes from 30 to 75%), causes considerable fluctuations of the absolute brightness of the cloud cover. With a limited series of observations, this may result in the fact that the value of the mean absolute brightness obtained to the basis of this series, may prove substantially different from the true mean value. At the same time with low elevations of the sun the scattering of the albedo values (and consequently, also the absolute brightness values) is not great, and the mean of the measured values of absolute brightness should be close to the true values even with a small series of observations. From the experimental data, given in Table 4, we can see that the difference between the maximum and mean values of absolute brightness, refer to the mean value, with elevations of the sun of 40-50°, amounts to 30-100 %, whereas for 25-5° elevations of the sun it amounts to only 10-30%. This may explain the good agreement of the measured and calculated values of the absolute spectral brightness of the cloud-atmosphere system with 25-5° elevations of the sun.

We should note, that with 25-5° elevations of the sun, the calculated maximum values of the clouds of the lower and middle levels proved smaller than those obtained experimentally. Apparently this is explained by the higher contents of the aerosol than it was assumed in the calculations, and consequently, by the higher brightness of the air haze. With higher elevations of the sun the share of the brightness of the air haze in the clouds-atmosphere system is insignificant, and the total flow of radiation is determined first of all by the reflective capacity of the clouds. With small elevations of the sun, the contribution of the air haze brightness is comparable with or exceeds the flow of radiation reflected by the clouds. Therefore with 25 and 5° elevations of the sun the actual brightness of the cloud-atmosphere system proved higher than that calculated theoretically. The fact that in the shortwave sector of the spectrum we observed a greater difference between the calculated and measured values than in the longwave factor speaks in favor of the assumption of the high aerosol content.

4. Comparison of the Results of Spectrometric and Pyronometric Measurements

Simultaneously with the measurements of the ascending spectral flows in the narrow solid angle of vision in the nadir on the IL-18 aircraft by means of pyronometers measurements were made of the flows of shortwave radiation, incident on the unit area from the lower and upper hemisphere. The sensors /195
were installed in the upper and lower parts of the airplanes' fuselage. The signals were recorded on an instrument of the EPP-09M-1 type. The sensitivity of the pyronometers was periodically checked in the laboratory.

Moreover, immediately before the flights and after them the reasings were compared with the control pair of pyronometers.

The processing of the measurement results was performed according to the usual procedure [8]. For comparison with the results of the spectrometric measurements the data on pyronometers, obtained over fields of 8-10 points cloudiness with the corresponding elevation of the sun were used. The conversion of the readings of the spectrometer to the pyronometer data was performed in the assumption of the orthotropic reflection by the clouds, i.e., the calculation of the ascending flow $E^{\uparrow}_{sp}$ was carried out by means of the formula

$$E^{\uparrow}_{sp} = \pi \left[\sum_{\lambda=0.40}^{\lambda=0.74} B_{\lambda}\,\Delta\lambda + \sum_{\lambda=0.86}^{\lambda=2.56} B_{\lambda}\,\Delta\lambda + \frac{B_{0.74} - B_{0.87}}{2}(0.87 - 0.74) \right], \qquad (2)$$

where B_{λ} is the spectral brightness of the clouds, measured at the sighting angle θ, equal to 0° (watts/cm^2·ster·μ), $\Delta\lambda$ is the "spectral resolution" of the measurements (μ).

Taking into account the fact that the time constant of the instruments differ substantially, for the comparison, spectrometric data were used which were averaged for the corresponding time intervals. Since pyronometers are sensitive to radiation with wavelengths of 0.3-3.0 μ and the spectrometer operates in the 0.4 to 2.5 μ range, the values obtained as the result of calculations according to formula (2), should be 5-10% less than those obtained by measurements by means of pyronometers, with identical accuracy of calibration of both types of instruments.

We succeeded in checking the correspondence of the absolute calibration of the equipment during synchronous measurements performed inside clouds, where the radiation flows in all directions are identical. The verification showed, that no substantial discrepancies in the readings of the two types of instruments are observed. Thus, in the flight on 21 May inside thick altostratus clouds, converting to cirrus clouds, the ascending and descending flows according to the pyronometers were equal to 0.621 and 0.813 cal/cm^2·min, and the ascending flow according to the spectrometer is equal to 0.602 cal//cm^2·min. On the 19th of June during the flight along the upper edge of cirro-stratus clouds, turning to altostratus, in one case we obtained values of 0.53, 1.54 and 0.47 cal/cm^2·min, respectively and in the other to 0.720, 1.43 and 0.620 cal/cm^2·min. /196

In Figure 5 we compared the values of the ascending shortwave radiation flows over fields of clouds of the lower and middle level measured synchronously by means of a spectrometer and pyronometer. The data on the spectrometers are taken from Table 3 and an averaging was performed for the same conditions of 68 individual measurements with the pyronometer. The quantity of solar radiation reflected by the cloudiness, calculated according to the readings on the spectrometer, proved less than the quantity of radiation, measured by the pyronometer; in this case the differences in the readings are inversely proportional to the value of the radiation flow reflected by the cloudiness. Thus, this difference referred to the readings of the pyronometer, amounts to 30-35% with $E^{\uparrow}_{pyr} < 0.6$ cal/cm^2·min. and 15-25% with $0.6 < E^{\uparrow}_{pyr} < 0.7$ cal/cm^2·min. Inasmuch as the amount of radiation reflected by the cloudiness depends primarily on the elevation of the sun, the large differences between the readings of these instruments are observed with very small elevations of the sun. This is caused by the fact that with the small elevations of the sun the cloud diffusion indicatrix stretches in the direction of the mirror reflected ray and consequently, the diffusion of light by the clouds differs substantially from the orthotropic [4], the brightness in the nadir proving smaller than the mean brightness B*, calculated according to formula $B^* = 1/\pi\, E^{\uparrow}_{pyr}$. Hence it follows, that the brightness coefficient $k = \frac{\pi \int_{\lambda_1}^{\lambda_2} B_{\lambda} d\lambda}{I_0 \cos z_{\odot}}$ proves too low as compared with the albedo, calculated according to formula $A = E^{\uparrow}_{pyr}/I_0 \cos z_{\odot}$ (here I_0 is the intensity of solar radiation in the wavelength range between 0.3 and 3 μ, coming to the upper boundary of the atmosphere) therefore, in calculation of the cloud albedo according to the measurements from the satellite it is necessary to take into account the cloud diffusion indicatrix. The assumption of the orthotropic reflection of the solar radiation by the cloud cover results in low albedo values. In particular, this is one of the causes of low values of cloud albedo, calculated in work [9] according to the data of measurements from the Tiros-IV satellite.

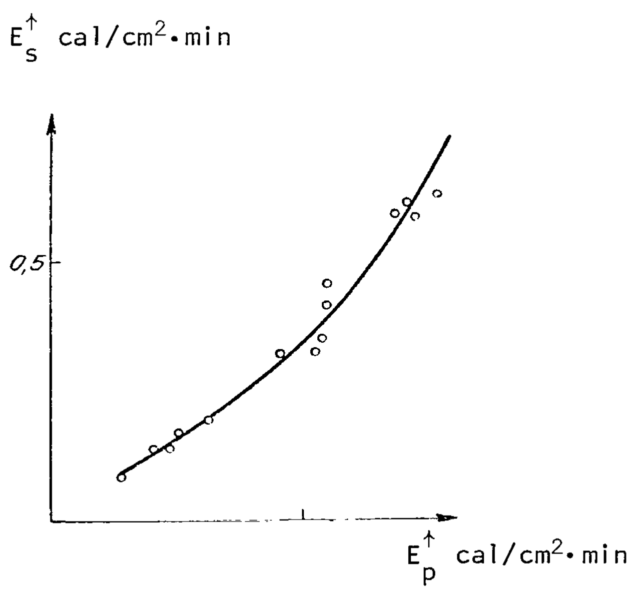

Figure 5. Comparison of the Flows of Solar Radiation Reflected by Cloudiness Performed by Means of the $E^{\uparrow}_{p}$ Pyronometer and $E^{\uparrow}_{s}$ Spectrometer.

Similar comparison of the results of measurement of the ascending currents, obtained by means of various equipment, are interesting from the point of view of development of correct methods of the use of results of pyronometric measurements, obtained during flights in the last few years, with the evaluations of the values of signals picked up by narrow angle instruments.

In conclusion we should note that the materials given in the article may be used in the interpretation of the data obtained from satellites.

REFFRENCES

1. Chapurskiy, L. I.: "Experimental Investigations of Spectral Brightness Characteristics of Clouds, Atmosphere, and Underlying Surface in the 0.3-2.5 μ Wavelength Range," *Trudy GGO*, Issue 196, 1966.
2. Chapurskiy, L. I.: "The Airplace Infrared Spectrometer," *Inform. sb. NIOLVIKA im. A. F. Mozhayskogo*, No. 71, *LVIKA*, Leningrad, 1964.
3. Chapurskiy, L. I.: "On the Selection of the Optimum Spectral Range for Detecting Cloudiness," *Trudy NTK "Ispol'zovaniye Informatsii Meteorologicheskikh Iskusstvennykh Sputnikov Zemli"* [Works of the NTK "Utilization of Information From the Weather Satellites], Part II. Publication of the LVIKA Im. A. F. Mozhayskogo, Leningrad, 1966.
4. Feygel'son, Ye. M.: *"Radiatsionnyye Protsessy v Sloistoobraznykh Oblakakh"* [Radiation Processes in Stratiform Clouds], Nauka Press, 1964.
5. Shifrin, K. S. and N. P. Pyatovskaya: *"Tablitsy Naklonnoy Dal'nosti Vidimosti i Yarkosti Dnevnogo Neba."* [Tables of Oblique Visibility Range and Brightness of Daylight Sky], Gidrometeoizdat Press, Leningrad, 1959.
6. Fritz, S.: "Measurements of the Albedo of Clouds," *Bull. Amer. Met. Soc.*, Vol. 31, No. 1, 1950.
7. Fritz, S. and T. H. Macheonald: "Measurements of Adsorption of Solar Radiation of Clouds," *Bull. Amer. Met. Soc.*, Vol. 32, No. 6, 1951.
8. Kastrov, V. G.: "Investigation of Certain Errors in Determination of Solar Radiation Absorption in the Atmosphere by Means of Pyronometers," *Trudy TsAO*, Issue 32, 1959.
9. Fritz, S.; P. Rao Krishna and M. Weinstein: "Satellite Measurements of Reflected Solar Energy and the Energy Received at the Ground," *Journal of the Atmospheric Sciences*, Vol. 21, No. 2, 1964.

EXPERIMENTAL INVESTIGATION OF LIGHT DIFFUSION BY CLOUD PARTICLES. I. SIMULATION OF WATER DROPLETS

O. I. Kasatkina

ABSTRACT. In order to investigate the light diffusion indicatrices by the cloud particles a method is proposed for simulating the water droplets. The models represent suspensions of glass globules in an immersion fluid. The optical characteristics of the models have been examined in detail and compared with those of the water droplets. The methods for obtaining these models are examined and the possible degrees of polydisperseness of the suspensions obtained are evaluated.

In the entire question of diffusion of light by small particles, the most difficult and as yet unsolved problem is the determination of diffusion indicatrices, the knowledge of which is especially indispensible for solving the problems of geophysics, such as the optical phenomena in clouds and fogs, visibility in fogs, cloud formation kinetics, transfer of radiation in the atmosphere, and etc. Further, for the interpretation of optical measurements performed on satellites, in particular for determining the upper boundary of the clouds, distinction between the clouds of various levels, and between clouds and snow we should know the regularities of the behavior of radiation, reflected and emanated by clouds, and these regularities to a great extent are determined by the indicatrix of diffusion of light by cloud particles and the atmosphere above the clouds. As mentioned by us earlier [1] it doesn't appear possible to obtain these indicatrices by the calculation methods, and the most rational is apparently the experimental method, which is the subject of the examination in our present work. /198

The experimental investigation of light diffusion indicatrices by cloud particles is rendered difficult by the fact that under laboratory conditions it is not possible to isolate a droplet suspended in air during the time required for measurement, or to obtain a monodispersive system of droplets (fog). In this connection, we decided to resort to a method of simulating the water droplets with particles, the optical and geometric characteristics of which would not differ from those of water droplets. Then the problem of investigation of light diffusion by water droplets is broken down into two: the study of the characteristics of the models and the measurements of diffusion indicatrices by the simulated water droplets.

Let us examine the first problem in more detail.

1. *Selection of optical glasses and fluids.* As the models we have used glass globues suspended in a viscous immersion fluid. In the selection of glass and fluid first of all the main requirement should be met $m_{gl}/m_f = m_w$ in the 0.35-1.0 μ region of the spectrum. The second requirement is that the fluid should be sufficiently viscous to make the globules settle down during a time exceeding the experiment time.

Let us make the evaluation for the mean index of refraction of water $m_w = 1.33$. It is obvious, that in order to obtain $m_{gl}/m_f = 1.33$ we need glass with a large refractive index.

From the optical glass catalog we selected STF1 ($m_D = 2.0360$) and TF6 ($m_D = 1.9300$). We do not limit ourselves to one type of glass, since in order to cover the entire range of m_λ for water, one glass-fluid pair is insufficient. /199

Knowing m_{gl}, we determine the suitable fluids: $m_{f1} = 2.0360/\ 1.3300 = 1.5300$, $m_{f2} = 1.9300/1.3300 = 1.4510$.

In selecting the fluids with such refractive indices it is necessary to take into account the requirements for viscosity. Let us evaluate approximately the required viscosity of the liquid.

Let us prescribe the maximum time of settling of the particles in the fluid. It is clear, that this time should be two to three times greater than the time required for measuring the indicatrix, which does not exceed 10 hrs. Let us calculate the required viscosity of the fluid, using Stokes formula

$$v = \frac{2}{9} \cdot \frac{(\sigma - \sigma') r^2 g}{\eta}, \tag{1}$$

where v is the settling rate of the globule in the fluid (cm/sec.), σ is the density of the substance of the globule (grams/cm^3), σ' is the density of the fluid (gram/cm^3), r is the radius of the sphere (cm), η is the fluid viscosity (poise), g = 981 cm/sec^2, which is the acceleration of gravity.

The time, during which the particle will leave the beam of light t = vs, where s is the width of the light beam.

We have: s = 1.8 cm and t = 30 hours,

$$\eta = \frac{2t(\sigma - \sigma')r^2 g}{9S}. \qquad (2)$$

Substituting the numerical data to formula (2) we obtain for r = 5 μ and for TF6 glass η = 15 poises.

Thus, the fluid should possess a viscosity of about 15 poises, preferably at room temperature.

From a large number of existing immersion fluids with the above-mentioned refractive index we choose glycerin and cedar oil.

In Table 1 we give the principal characteristics of these fluids.

TABLE 1.

Fluids	m_D	η poises at 20°C	σ grams/cm^3	Degree of Transparency in the Visible Region of the Spectrum
Cedar Oil	1,5160	9,9	0,92	Transparent, slightly yellow colored
Glycerin	1,4570	14,9	1,26	Transparent, colorless

Tr. Note: Commas indicate decimal points.

Thus, we finally select the following pairs: STF1 glass and cedar oil and TF6 glass and glycerin.

2. *Spectral characteristics of the glasses and fluids selected.* Among the principal spectral characteristics of the optical medium are the curves of the spectral transmission in the region of the spectrum in which we are /200 interested and the spectral dispersion. The spectral transmission of glasses was measured by us on a SF-4 spectrophotometer (Figure 1). The transmission spectra of both glasses investigated proved similar, without noticeable absorption lines, which is a very important factor when these glasses are used as models for water droplets, which is transparent in the visible region of the spectrum.

In Tables 2 and 3 we give the values of the refractive indices of glasses STF1 and TF6 and fluids (glycerin and cedar oil) in relation to the wavelength and also the relative indices of refraction of STF1 glass in the cedar oil (model I) and TF6 in glycerin (model II).

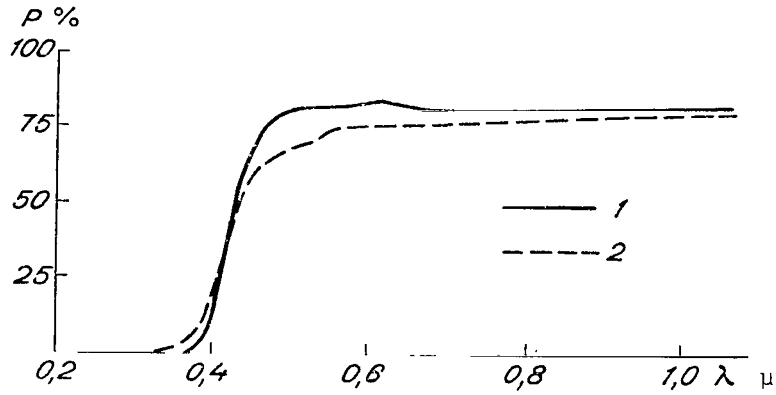

Figure 1. Curve of Spectral Transmission of STF1 (1) and TF6 (2) Glasses.

TABLE 2

λ mμ	STF1	Cedar Oil	Model I
460	2,094	1,3723	1,5258
500	2,070	1,3600	1,5220
560	2,045	1,3474	1,5176
600	2,033	1,3415	1,5154
660	2,019	1,3346	1,5125
700	2,012	1,3311	1,5115
760	2,004	1,3271	1,5100
800	2,000	1,3254	1,5089
860	1,995	1,3233	1,5076
900	1,992	1,3220	1,5068
940	1,989	1,3207	1,5060
$m_F - m_c$	0,0580	0,0103	

TABLE 3

λ mμ	TF6	Glycerin	Model II
360	2,025	1,4664	1,3810
400	1,995	1,4641	1,3625
460	1,965	1,4616	1,3444
500	1,952	1,4600	1,3370
560	1,936	1,4580	1,3280
600	1,930	1,4567	1,3250
660	1,921	1,4552	1,3210
700	1,917	1,4544	1,3180
760	1,912	1,4532	1,3164
800	1,910	1,4527	1,3148
860	1,907	1,4520	1,3134
900	1,905	1,4514	1,3125
940	1,904	1,4510	1,3122
1000	1,903	—	—
$m_F - m_c$	0,0343	0,005	

Tr. Note: Commas indicate decimal points.

Curves in Figure 2 represent the curves of dispersion of water (1) of Model I (2) and Model II (3). From the analysis of the curves we can see, that the entire range of measurement of water in the visible sector of the spectrum may be performed with Model I using the 440-592 region of the spectrum, and with model II in the 544-800 region. As we can see, the presence of two models enables us to carry out measurements for several monochromatic sectors of wavelengths, i.e., to carry out a spectral investigation of the light dif- /201
fusion by water droplets, which is of an undoubted scientific interest.

3. *On preparation of the glass balls and sizing them, preparation of suspensions.* In order to obtain spherical glass particles we are using the method applied at the Chair of Colloidal Chemistry at the Leningrad State

University. The diagram of the installation is given in Figure 3. In a glass mill the glass is reduced to a powder. Thereupon this powder is preliminarily separated into fractions by means of standard sieves. The latter make it possible to separate the following fractions: 3-30, 31-53, 54-60, 61-75, 76-90, 91-100, 100-120 μ. From this powder the globules are obtained by fusing the fragments in the flame of an acetylene burner.

The output of the installation is determined by the following figures: 50 grams of powder pass through the flame during 40 minutes, the yield is 40%; 95% of all the particles fused are spheres.

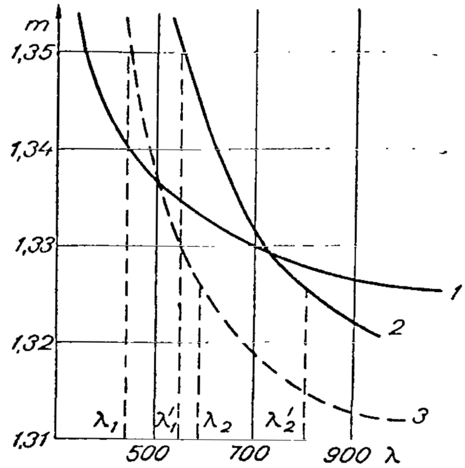

Figure 2. Water Dispersion Curves (1), Model I (2) and Model II (3).

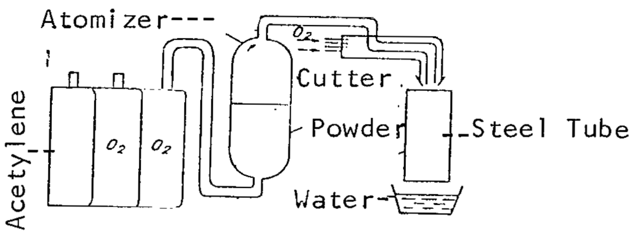

Figure 3. Diagram of the Apparatus for Production of Steel Globules.

The final separation of the globules into sufficiently fine fractions is performed by setting down the globules in a column of fluid. For this purpose the state Geophysical Institute Fractiometer is used which consists of a glass cylindrical vessel 150 cm high and 10 cm in diameter. Below the vessel turns into a rubber tube with several clamps. By opening the clamps, at the required periods of time, from the beginning of settling of the globules, we can obtain various size fractions of the globules.

Let us evaluate the possibilities of obtaining monodispersive specimens of globules by settling them down from a polydispersive powder. The degree of monodispersness is determined by the value $\Delta r/\bar{r}$, where $\bar{r}$ is the mean radius of the globules, Δr is the deviation of the radius from the mean value.

In Table 4 we give certain calculation data according to which we can judge the possible degree of monodispersness of the specimen obtained. The calculations were performed for three fluids of different viscosity and for three regions of dimensions of the globules with relative deviations $\Delta r/\bar{r}$ (10% and 3%).

For the extreme sizes of each of the ranges of sizes examined according to formula (2) we calculated the settling time of the globules in the 150 cm column of liquid. Their difference, naturally yields the time during which the given fraction of the globules with the prescribed width $\Delta r/\bar{r}$ will be separated. /202

TABLE 4

$\frac{\Delta r}{\bar{r}}$	r μ		Water η = 0.01 poises	Linseed Oil η = = 0.3 poises	Glycerin η = 8.3 poises
10%	5	t Δt	1,35 hr. 13 min	4 hr. 30min	1000 hr. 200 hr.
	50	t Δt	48 sec 8 sec	24 min 4 min	110 hr. 18 hr.
	100	t Δt	12,1 sec. 2,1 sec.	6 min. 1,1 min.	28 hr. 4,7 hr.
3%	5	t Δt	1,35 hr. 5 min.	4 hr. 10 min.	— —
	50	t Δt	48 sec. 3 sec.	24 min. 2 min.	— —
	100	t Δt	12,1 sec. 0,4 sec.	5 min. 15 sec.	28 hr. 1 hr.

Tr. Note: Commas indicate decimal points.

As we can see from Table 4, the 5-5.5 μ fraction is conveniently separated when the globules are settled down in water or linseed oil, since the time required for it is sufficiently large so that it would be possible to measure it and sufficiently small from the point of view of the length of the experiment performed. Glycerin proved too viscous for this purpose, since it requires too much time, although for small $\Delta r/\bar{r}$ it possibly will prove suitable.

For the average values of the balls (50 μ) and large values (100 μ) the most suitable is linseed oil.

The table data indicate also that in this way we can separate very narrow fractions with $\Delta r/\bar{r}$ = 3%.

In order to avoid errors, connected with convective currents in the fluid, through imparting of various initial velocities through the particles, etc., we should perform the above-mentioned process of sedimentation several times, consecutively narrowing down the fractions.

Let us perform a certain approximate evaluation of the amount of particles in the given range of sizes, which may be obtained from the given quantity of polydispersive powder.

Let us assume that the distribution of globules in the sample is subject to the γ distribution law of the type:

$$\frac{dn}{dr} = f(r) = Ar^2e^{-\beta r}. \tag{3}$$

The parameter A is determined from the conditions of standardization [4]:

$$\int_0^\infty Ar^2e^{-\beta r}\,dr = A\,\frac{\Gamma(3)}{\beta^3} = N,$$

where N is the number of particles in 1 cm^3.

Hence /203

$$A = \frac{N\beta^3}{1}$$

and

$$f(r) = \frac{N\beta^3}{2}\,r^2e^{-\beta r}. \tag{4}$$

Let us prescribe to ourselves a certain mass of the entire sample M, i.e.,

$$\frac{N\beta^3}{2}\cdot\frac{4}{3}\,\pi r^3\sigma\int_0^\infty r^2e^{-\beta r}\,dr = M, \tag{5}$$

where σ is the specific gravity of the substance of the globules.

We note that

$$\int_0^\infty r^5e^{-\beta r}\,dr = \frac{\Gamma(5+1)}{\beta^{(5+1)}} = \frac{120}{\beta^6}.$$

Then after simplification

$$\frac{240\,N\sigma}{\beta^3} = M$$

and finally

$$N = \frac{N\beta^3}{240\sigma}. \tag{6}$$

Let us make the calculations for the three distributions, characterized by value r_m (from [4] $r_m = 2/\beta$), for M = 200 grams.

Let us now determine for each distribution taken the number of particles dN, which are in the $\bar{r} \pm dr$ size range. Let us prescribe the relative width of the $\Delta r/\bar{r}$ range, equal to 10%,

$$dN = \frac{N\beta^3}{2}\,r^2e^{-\beta r}\,dr. \tag{7}$$

TABLE 5.

r_m μ	β	N
100	200	$1\cdot10^6$
50	400	$8\cdot10^6$
25	800	$6{,}4\cdot10^7$

The calculations, performed with formula (7) are given in Table 6. The data in Table 6 should be compared with the number of particles required for the measurements, suspended in the measurement cell [5].

The number of particles in the diffusion volume is limited by the size of the multiple diffusion, which obscures the true picture of the diffusion. The extent of multiplicity of diffusion in a turbid medium is characterized by the multiplicity parameter τ [6], which is determined by the geometrical parameter of the diffusion volume

$$\tau = \frac{r^2R}{l^3}, \tag{8}$$

where R is the maximum dimension of the diffusion volume, r is the radius of the particle, l is the distance between the particles.

When τ << 1 the multiple diffusion may be not taken into account. Let us prescribe to ourselves the value τ = 0.01. If we prescribe the cubicle shape of the diffusing volume, then the number of particles in the volume is /204

$$N = \frac{R^3}{l^3} = \frac{R^2\tau}{r^2}. \tag{9}$$

TABLE 6

r	Δr	dN: $r_m=100$ μ, $N=10^6$	dN: $r_m=50$ μ, $N=8\cdot10^6$	dN: $r_m=25$ μ, $N=6{,}4\cdot10^7$
5	0,5	45	$2{,}6\cdot10^3$	$1{,}2\cdot10^5$
10	1,0	320	$1{,}7\cdot10^4$	$7{,}4\cdot10^5$
20	2,0	$2\cdot10^3$	$9{,}2\cdot10^4$	$2{,}6\cdot10^6$
50	5,0	$2\cdot10^4$	$4{,}4\cdot10^5$	$2{,}4\cdot10^6$
100	10,0	$6{,}4\cdot10^4$	$4{,}0\cdot10^5$	$6{,}6\cdot10^5$
200	20,0	$5{,}6\cdot10^4$	$8{,}0\cdot10^4$	$1{,}0\cdot10^3$
400	40,0	$5{,}1\cdot10^4$	$3{,}2\cdot10^2$	$1{,}4\cdot10^{-3}$

Tr. Note: Commas indicate decimal points.

In Table 7 we give the values of N, calculated with formula (9) for various particle sizes and for R = 1.8 cm.

TABLE 7

r μ	5	6	10	50	100
N	$8{,}9\cdot10^4$	$7{,}2\cdot10^4$	$3{,}7\cdot10^4$	910	220

From the comparison of Table 6 and 7 we can see that from one sample of powder roughly separated into fractions (M ≐ 200 grams) we can obtain sufficient amount of particles in any range of sizes.

As indicated by the evaluations given above, it is practically possible to obtain models of the system of cloud particles of any degree of polydisperseness up to $\Delta r/r$, equal to 1-2%; this is only a problem of time.

In conclusion, we may say, that the simulation method is not at all limited to spherical particles, and in this probably, lies its principal advantage. Indeed, by placing into the fluid particles of different shapes and consistency, we may model any particles encountered in the atmosphere, for which no other methods exist for investigating their diffusing properties. In particular, the suspension of crystals of a substance isomorphic to ice in a suitable fluid will simulate well the particles in icy clouds, this is a subject for a special examination.

REFERENCES

1. Kasatkina, O. I. and K. S. Shifrin: "On the Problem of the Indicatrix of Diffusion of Light by a System of Globular Particles," *Trudy GGO*, Issue 170, 1965.
2. Bokiy G. B.: *"Imersionnyy Metod"* [The Immersion Method], MDU Press, Moscow, 1948.
3. Ioffe, B. V.: *"Rukovodstvo po Refraktometrii Dlya Khimikov"* [Instructions on Refractometry for Chemists], LGU Press, Leningrad, 1956.
4. Shifrin, K. S.: "On Calculation of the Microstructure," *Trudy GGO*, Issue 109, 1961.
5. Golikova, O. I.: "A Cell for Nephalometric Measurements with High Angular Resolution in the 5-175° Angle Region," *Trudy GGO*, Issue 152, 1964.
6. Shifrin, K. S.: *"Rasseyaniye Sveta v Mutnoy Srede"* [Diffusion of Light in a Turbid Medium], Gostekhizdat Press, Leningrad, 1951.

EXPERIMENTAL INVESTIGATION OF DIFFUSION OF LIGHT BY CLOUD PARTICLES. II. MEASUREMENT OF INDICATRICES OF DIFFUSION OF LIGHT BY WATER DROPLET MODELS

O. I. Kasatkina

ABSTRACT: The indicatrices of light diffusion by models of cloud particles should be measured in a wide range of angles of diffusion with high angle resolution. A description is made of the nephalometric apparatus making it possible to measure the indicatrices of light diffusion by the quasi-monodispersive suspension (the suspension of glass globules in a fluid) within a sufficiently small spread of particles with respect to size Δr with high accuracy. The possible errors and the ways to decrease them are examined.

Let us formulate the demands, which should be met by the measurement apparatus, enabling us to measure the indicatrices of diffusion of quasimonodispersed suspension (suspension of glass globules in a fluid) [1] with any sufficiently small dispersion of particles with respect to size Δr with a high accuracy. /205

1. The apparatus should have enough light power, because the diffusive capacity of small particles is low ($K_r \approx r^6$), especially at angles close to 90°.

2. The particles diffusing the light should be illuminated by a parallel beam of light with a small angle of divergence δ, so that the averaging of the indicatrices with respect to particle size would not be confused with averaging with respect to the angle. For particles in the size region of 2-100 μ the permissible angle δ may be prescribed with the value of 0.2°, then the change in the intensity of the light diffused by the particles, caused by such nonparallel state of the illuminating beam, does not exceed 10%.

3. Inasmuch as the indicatrices of diffusion of light by the droplets of the size range examined have a sharply expressed oscillating character, the measuring apparatus should have a high angular resolution of not less than 0.2°.

4. From the requirements for a high resolution issues the requirement for continuous recording of the diffused light, i.e., the recording part of the apparatus should have at its output an instrument continuously recording the signal.

5. Inasmuch as the degree of polydispersness of the system of diffusing particles $\Delta\rho$ depends on both Δr, and $\Delta\lambda$, there should be a high monochromatization of the light, desirably in several bands of the spectrum.

6. Considering all the structure of the problem posed, which interest us, there is a necessary condition of the smallness of the diffusing volume with a linear dimension of d in comparison with the distance to the receiver R. For a 5% accuracy of the measurements, this condition is determined by the ratio $R/d \geq 40$.

7. The indicatrices should be measured in a wide band of diffusion angles.

8. The multiple diffusion of light on the particles should be excluded as much as possible.

In the present work we describe the photo-electric nephalometric apparatus developed at the GGO, satisfying all the requirements enumerated. The simplified diagram of the apparatus presented in Figure 1, has been worked out /206 by us on the basis of the instrument of Plaza *et al* [2].

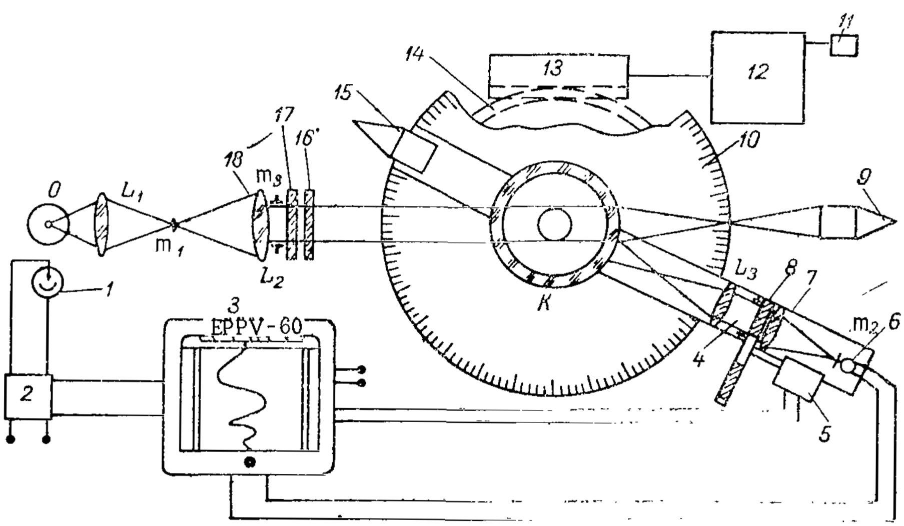

Figure 1. Simplified Diagram of the Measuring Apparatus. 1, Photo-electric Cell; 2, Capacitor; 3, EPPV-60; 4, Beam; 5, Motor; 6, Photomultiplier; 7, lens; 8, Neutral Light Filters; 9, Light Trap; 10, Disc; 11, Motor; 12, Gear Box; 13, Worm Gears; 14, Worm Wheel Gear; 15, Absolutely Black Body; 16, Poloroid; 17, Light Filter; 18, Lens.

The illuminator consisting of a source of light O (mercury lamp SVDSh-100), capacitor L_1(f = 30 mm, d = 11 mm), and the objective achromatic lens L_2(f = 220 mm, d = 20 mm), creates a parallel beam of light with a divergence angle $\delta = 0.1°$. Determined by the size of the diaphragm D_2(d = 0.1 mm). Diaphragm D_3 forms a beam of rectangular section 8×18 mm^2. Leaving the objective lens the parallel light beam formed passes through light filters, which admit the spectral lines of mercury: 0.365; 0.405;0.436; 0.546; 0.578 μ. The width of every spectral line indicated does not exceed 0.01 μ and $\Delta\lambda/\lambda$ 2%. In addition to these lines in the visible region of the spectrum we use two lines in the near infrared region: 1.014 and 1.129 μ. To separate them we use the combinations of filters: ZS-6 with FS-7 and ZS-6 with IKS-2 respectively. The width of the lines here is considerably greater (0.3 μ) and $\Delta\lambda/\lambda \approx 20\%$. After passing through the specimen investigated the direct light enters a light trap with a reflection $r = 0.007\%$. The light diffused by the specimen is collected by means of the achromatic objective lens L_3(f = 220 mm, d = 20 mm) in the plane of the diaphragm D_2 placed directly in front of the photomultiplier, and is measured by the latter against the background of a black body, the degree of blackness of which $\eta = 0.999$. The diameter of the diaphragm determines the angle of divergence of the diffused light beam, which with d = 1.5 mm amounts to 0.2°. The light diffused in any other direction $\beta \lessgtr \beta_0 \pm 0.2°$ does not enter the receiver and will not be recorded, i.e., in this way we determine the high angular resolution of the apparatus.

The receiving device (lens, diaphragm, and photomultiplier,) are rigidly connected on one end of a general iron rod, on the other end of which the black body is fixed. The rod, connected to the goniometric disk, rotates about /207
the axis passing through the center of the specimen examined. The disk is put into motion by means of a worm gear pair through a synchronous motor SD-54 with the reducing gear. The factory-made reducing gear from the IKS-12 spectrometer set, used by us, provides eight rotation speeds, and in our case one revolution of the reducing gear rod corresponds to three degrees of the disk. For eight stages of the reducing gears we have the following scanning speeds:

Number of the Stage . . .	1	2	3	4	5	6	7	8
Speed, degrees/min. . .	0,085	0,17	0,34	0,68	1,36	2,72	5,46	10,92

The outside dimensions of all the parts of the apparatus are selected in such a way that it would be possible to measure the diffusion indicatrices in a wide band of angles of diffusion (8°-172°), and also in order to carry out the condition of the smallness of the volume producing the diffusion. The double cylindrical cell, used by us for the measurements, has been described by us earlier in work [3].

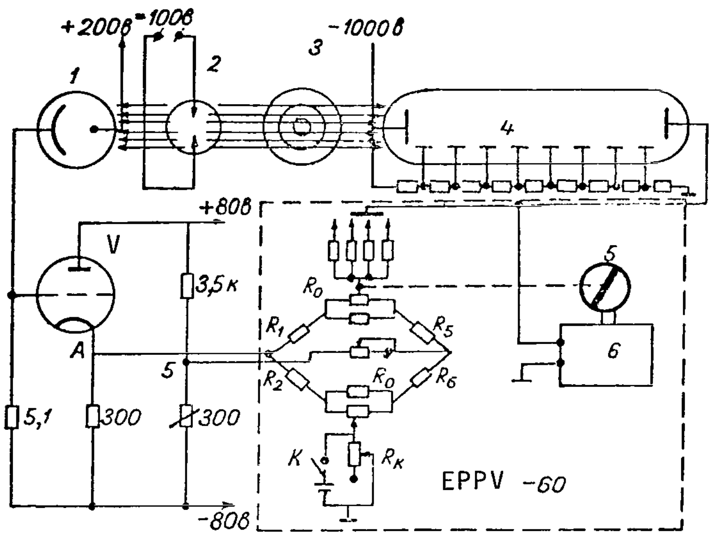

Figure 2. Electrical Measuring Circuit Diagram of the Apparatus. 1, Photo-electric Cell; 2, Mercury Lamp; 3, Cell; 4, Photomultiplier; 5, Motor; 6, Capacitor.

For a continuous recording of the indicatrix at the output of the apparatus there is an electronic automatically recording EPPV-60 potentiometer which enables us to record the signal directly from the photo-electric multiplier, without preliminary amplification.

The recording is made by an ink pen, the time constant of the apparatus is 8 sec. in the entire scale, which with the scanning speeds selected provides for recording of the indicatices with the required angular resolution. The electrical measuring system of the apparatus is presented in Figure 2. To exclude the fluctuations of the light flow from the mercury lamp we use an attachment to the potentiometer previously described by us in work [4], which has been somewhat improved at the present time.

The essence of this device consists of the fact that the potentiometer records the ratio between the measurement light flow and a certain initial light flow dependent upon the total light flux of the lamp. This is attained /20
by the fact that the feed to the rheochord of the potentiometer is formed by a voltage, proportional to the illuminance of the compensation photo-electric cell. This voltage is read off the points A and B in the cathodic repeater circuit, into the circuit of the grid of which the photo-electric cell is connected.

The test of the compensation circuit yielded good results: the deviations of the signal on the diagram tape with substantial fluctuations of the light flux of the lamp (up to 50%) do not exceed 1-3 mm, which amounts to 1-2% in the middle of the scale. To decode the records on the potentiometer tape the angles are marked every 3° and 0.6°. The accuracy of reading of the angles on the diagram amounts to not less than 0.01°.

To maintain an approximately constant measurement accuracy in recording the diffusion indicatrices it is necessary to have a little changing level of illumination of the photo-electric multiplier photocathode. Inasmuch as the drops in the intensity of light diffused by the spherical particles of the size range examined at different angles reach 10^3-10^4 times, we use a special device for the automatic introduction of calibrated neutral light filters into the diffused beam [5].

In order to select the most efficient light receiver and evaluate the possible errors in measurments, we performed an approximate energy calculation of the apparatus. For this purpose we have calculated for seven spectral bands and two particle sizes the following (minimum) values: spectral density of the luminous flux of the incident beam J_0, density of the luminous flux J_p, diffused by one particle, density of the luminous flux $J_{\Sigma p}$, diffused by particles located in the diffusing volume [1], the flux of diffused radiation Φ', falling on the photomultiplier; these values are given in Table 1.

TABLE 1

λ μ	J_0 watt /cm ^{2}	J_p watt/cm^2		$J_{\Sigma p}$ watt/cm^2		Φ' watts	
		$r=6$ μ	$r=100$ μ	$r=6$ μ	$r=100$ μ	$r=6$ μ	$r=100$ μ
0,365	$1,30\cdot10^{-2}$	$7,1\cdot10^{-15}$	$1,1\cdot10^{-13}$	$5,2\cdot10^{-10}$	$2,5\cdot10^{-11}$	$1,7\cdot10^{-9}$	$7,8\cdot10^{-11}$
0,405	$0,54\cdot10^{-2}$	$3,0\cdot10^{-15}$	$4,6\cdot10^{-14}$	$2,2\cdot10^{-10}$	$1,0\cdot10^{-11}$	$0,7\cdot10^{-9}$	$3,2\cdot10^{-11}$
0,436	$0,92\cdot10^{-2}$	$5,1\cdot10^{-15}$	$7,8\cdot10^{-14}$	$3,7\cdot10^{-10}$	$1,7\cdot10^{-11}$	$1,2\cdot10^{-9}$	$5,5\cdot10^{-11}$
0,546	$1,20\cdot10^{-2}$	$6,8\cdot10^{-15}$	$10,2\cdot10^{-14}$	$4,8\cdot10^{-10}$	$2,3\cdot10^{-11}$	$1,6\cdot10^{-9}$	$7,2\cdot10^{-11}$
0,577	$1,00\cdot10^{-2}$	$5,5\cdot10^{-15}$	$8,5\cdot10^{-14}$	$4,0\cdot10^{-10}$	$1,9\cdot10^{-11}$	$1,3\cdot10^{-9}$	$6,0\cdot10^{-11}$
1,014	$0,44\cdot10^{-2}$	$2,4\cdot10^{-15}$	$3,7\cdot10^{-14}$	$1,8\cdot10^{-10}$	$0,8\cdot10^{-11}$	$0,6\cdot10^{-9}$	$2,6\cdot10^{-11}$
1,129	$0,17\cdot10^{-2}$	$0,96\cdot10^{-15}$	$1,4\cdot10^{-14}$	$0,7\cdot10^{-10}$	$0,3\cdot10^{-11}$	$0,2\cdot10^{-9}$	$1,0\cdot10^{-11}$

Tr. note: Commas indicate decimal points.

Inasmuch as there is no data in the literature on the spectral distribution of radiation energy of the SVDSh-type mercury lamps in the calculations we used a similar distribution of the ultraviolet normal (high pressure capillary type mercury lamp), the light characteristics of which were close to those of the SVDSh-100 lamp [6].

In Table 2 we give the calculations of the size of current I produced on the photomultiplier, the values of the ratio between the voltage of the signal and the voltage of the noise ϕ and the value of the threshold sensitivity Φ_n for two types of photomultipliers: FEU-22 and FEU-17. We borrowed the energy spectral sensitivity γ_λ of the photomultipliers from work [7].

As we can see from the evaluations performed by us, in general,(with the exception of λ = 1.129 μ) the fluxes measured exceed very much the threshold fluxes for both types of the FEU (photoelectric multipliers) and the value of the ratio between the signal and noise is very high, especially for FEU-17. /209

The potentiometer used by us has the following measurement limits with respect to current:

I Channel $0\text{-}4 \cdot 10^{-10}$ amps with R_{in} = 1,000 megohms,

II Channel $0\text{-}2.6 \cdot 10^{-9}$ amps with R_{in} = 150 megohms,

III Channel $0\text{-}2.6 \cdot 10^{-8}$ amps with R_{in} = 15 megohms,

IV Channel $0\text{-}4 \cdot 10^{-7}$ amps with R_{in} = 1 megohm.

TABLE 2

λ μ	$T\lambda$ milli-amps/watts	I amp $r=6$ μ	I amp $r=100$ μ	φ	Φ_n watts
		FEU -22			
0,365	1,80	$3,2 \cdot 10^{-7}$	$1,4 \cdot 10^{-8}$	170	$1,3 \cdot 10^{-13}$
0,405	1,00	$0,7 \cdot 10^{-7}$	$3,2 \cdot 10^{-9}$	73	$2,4 \cdot 10^{-13}$
0,436	0,70	$0,8 \cdot 10^{-7}$	$3,9 \cdot 10^{-9}$	80	$3,4 \cdot 10^{-13}$
0,546	0,85	$1,3 \cdot 10^{-7}$	$6,1 \cdot 10^{-9}$	100	$2,8 \cdot 10^{-13}$
0,577	1,00	$1,3 \cdot 10^{-7}$	$6,0 \cdot 10^{-9}$	100	$2,4 \cdot 10^{-13}$
1,014	0,72	$0,4 \cdot 10^{-7}$	$1,9 \cdot 10^{-9}$	50	$3,3 \cdot 10^{-13}$
1,129	0,25	$5,0 \cdot 10^{-9}$	$2,5 \cdot 10^{-10}$	8	$9,6 \cdot 10^{-12}$
		FEU -17			
0,365	90,0	$1,5 \cdot 10^{-5}$	$7,0 \cdot 10^{-7}$	1500	$2,6 \cdot 10^{-15}$
0,405	82,0	$0,6 \cdot 10^{-5}$	$2,6 \cdot 10^{-7}$	770	$3,0 \cdot 10^{-15}$
0,436	83,0	$1,0 \cdot 10^{-5}$	$4,5 \cdot 10^{-7}$	1000	$3,0 \cdot 10^{-15}$
0,546	60,0	$1,0 \cdot 10^{-5}$	$4,3 \cdot 10^{-7}$	1000	$4,0 \cdot 10^{-15}$
0,577	50,0	$0,6 \cdot 10^{-5}$	$3,0 \cdot 10^{-7}$	860	$4,8 \cdot 10^{-15}$
1,014	0			—	—

Tr. Note: Commas indicate decimal points.

We can see that the current produced at the photo-electric multiplier for all the ranges of the spectrum may be measured by the potentiometer with the specification accuracy of 1% (for the entire scale of the instrument).

Inasmuch as the fluid filling the cell also possesses a certain diffusing property, the measurements are performed twice: first we record the indicatrix of the light diffusion by the fluid, and then by the fluid with the suspended balls; the result is obtained after subtraction of the first indicatrix from the second. The double cylindrical cell used by us enables us to replace the object of investigation very rapidly and conveniently: into the large cell we place a small cell filled in one case by a pure immersion fluid, and in the other case by a fluid with a suspension of the spheres.

The testing recordings performed showed that the currents produced in the photomultiplier when the indicatrices of diffusion by the pure fluid are recorded, also lie within the limits of the possibilities of the potentiometer.

Let us evaluate the possible errors of the measurement apparatus and enumerate the measures taken for decreasing them.

a. In order to decrease the errors connected with the use of the photomultiplier, we have thoroughly selected a photoelectric multiplier with the minimum dark current, with high sensitivity, and stability. To feed the FEU we used the stabilized VS-9 rectifier, with a stabilization accuracy of the output voltage of ±0.5%. The constant illumination level of the FEU cathode provides a high linearity of the outlet current (up to 1%), and a relatively /210
large light spot, projected onto the cathode (4.5 mm in diameter) , excludes the influence of nonuniform sensitivity of the photo-electric cathode with respect to the area. Moreover, before the measurements the photo-electric multiplier and the potentiometer are heated through for 1-2 hours, until the recording of any constant signal becomes sufficiently stable.

b. The compensation circuit excludes the effect of nonstability of the light flux of the mercury lamp with an accuracy of up to 1-2%.

c. The optical part of the apparatus is thoroughly adjusted, the initial rading angle ($\beta = 0°$) is strictly fixed, when the direct beam falls immediately on the photo-electric multiplier. The accuracy of reading of the angle of diffusion according to the makrs on the tape during the revolution of the photo-electric multiplier in one direction is sufficiently high. (0.01°), and the checking of the angle of resolution yielded in three cases the following values for angle γ: 10.5'; 11.0' and 11.6', i.e., in the required limits.

d. When the apparatus was designed and built measures were taken for eliminating the parasitic highlights from the light scattered in the apparatus. For this we used the suitably calculated systems of blends and darkenings of the internal walls. Moreover, the measurements on the instrument are performed a darkened room, so that the errors from the highlights does not exceed 1%.

e. Inasmuch as we are interested by the absolute values of the diffusion indicatrices, it is necessary to standardize the relative measurement data, which can be done with a certain accuracy. To standardize the measured indicatrices, we use a suspension of particles, for which there are tabulated values of functions Mi. Then it is sufficient to record a small sector of the control suspension indicatrix, in order to determine the scale of the records in absolute values.

However, we should bear in mind that the measurement data are proportional to the concentration of the light-diffusing particles, and the measurements of the control system and the system investigated may be incomparable because of the different concentration of the particles. Let us evaluate approximately the error arising from the inexact determination of the concentrations of the controls and the investigated specimens.

In Table 3 we give the following values for four particle sizes: the number of particles in the diffusing volume N, the weight concentration of particles in the diffusing volume c, the total mass of particles P in the diffusing volume, and the total mass of particles M in the entire volume of the cell. The diffusing volume is equal to 2.03 cm^3.

TABLE 3

Value	r μ			
	5	10	50	100
N	$8{,}9\cdot10^4$	$3{,}7\cdot10^4$	910	220
c г/см³	$1{,}6\cdot10^{-4}$	$3{,}2\cdot10^{-4}$	$1{,}6\cdot10^{-3}$	$3{,}2\cdot10^{-3}$
P г	$8{,}2\cdot10^{-4}$	$6{,}5\cdot10^{-4}$	$3{,}2\cdot10^{-3}$	$6{,}5\cdot10^{-3}$
M г	$1{,}04\cdot10^{-3}$	$2{,}0\cdot10^{-3}$	$10{,}4\cdot10^{-3}$	$2{,}0\cdot10^{-2}$

Tr. Note: Commas indicate decimal points.

The masses of the substance of such values, as are indicated in Table 3, may be weighed with an accuracy of up to 0.1 mg, so that for particles with r = 10 μ the relative weighing error will be about 5%. This error may be decreased if we weigh on a balance a specimen exceeding the required specimen by 10 times and diluted in a ten-fold volume of fluid. Then 1/10 of the suspension prepared will contain the required quantity of the diffusing particles, weighed with an accuracy of up to 0.5%.

The error in the determination of the diffusion function i with respect to the control specimen is determined as /211

$$\frac{\Delta i}{i}=\frac{\Delta N_1}{N_1}+\frac{\Delta N_2}{N_2}+\frac{\Delta i_к}{i_к}, \quad (1)$$

where i_k is the exact value of the diffusion function for the control specimen, calculated with formulas Mi, N_1 is the number of particles in the suspension examined, N_2 is the number of particles in the control suspension.

Taking into account the above-mentioned evaluations we obtain

$$\frac{\Delta i}{i}=\frac{\Delta i_к}{i_к}+1\%. \quad (2)$$

Summarizing the above, we can evaluate the total error of the apparatus described as 5-8%.

REFERENCES

1. Kasatkina, O. I.: "Experimental Investigation of Light Diffusion by Cloud Particles, I. Simulation of Water Droplets," See the present collection.
2. Plaza, J.: L. Norris and R. S. J. Stein: *Polimer Sci.*, Vol. 24, p. 455, 1957.
3. Golikova, O. I.: "Cell for Nephalometric Measurements with a High Angular Resolution in the Region of 5° to 175° Angles," *Trudy GGO*, Issue 152, 1964. Order No. 289, duplicates of literature p. 20, *Mitro'anova gr 3*.
4. Kasatkina (Golikova) O. I. and L. B. Krasil'shchikov: "Elimination of the Effect of Light Source Inconstancy in Objective Photometric Measurements by means of an Electronic Potentiometer," *Trudy GGO*, Issue 153, 1964.
5. Kasatkina (Golikova) O. I. and L. B. Krasil'shchikov: "Automatic Replacement of Filters in Recording Strongly Varying Light Fluxes," *Trudy GGO*, Issue 153, 1964.
6. *"Spravochnaya Kniga Po Svetotekhnike"* [Handbook on Lighting Engineering], *Izv. AN SSSR*, 1956.
7. Soboleva, N. A.; A. P. Berkovskiy; N. O. Chechik and R. Ye. Yeliseyev: *"Fotoelektronnyye Pribory"* [Photo-electronic Instruments], Moscow, 1965.

CERTAIN CHARACTERISTICS OF THE STRUCTURE OF THE INTENSITY FIELD OF PRECIPITATION FALLING IN STEPPE AND DESERT REGIONS

Zh. D. Alibegova

ABSTRACT. In the article the author gives certain characteristics of the structure of the intensity field of liquid precipitation, falling on the territories of the Veliko-Anadol'skiy and Dubovskiy shower gauge groups and also of the Western Turkmenian and Western Kazakhstan discharge stations.
She calculates the recurrences (%) of rains of various intensity , the shares of the precipitation of the given intensity in the total sum of the precipitation fallen. She gives the recurrences of rains of various maximum intensities.

The problem of investigation of precipitation zones from satellites is very pressing. For the practical realization of the program of such investigations it is necessary to develop special measuring equipment. /212

During the flight of a satellite over a certain territory it can record both the distribution of the sources and the intensity of the precipitation. In this case the results of the investigation will depend on the following factors: the precision and sensitivity of the measuring equipment, the dimensions of the sources, and the intensity of the precipitation falling.

What will be the errors of measuring the precipitations from satellites, what will be the distortions produced with various averaging scales with respect to area and time, this is the range of problems, the answers to which depend both on our concept of the structure of precipitation fields,and in particular on the structure of the precipitation intensity field.

In the present article, we give certain results of investigation of the intensity field structure of precipitation falling in Steppe and desert regions of the USSR.

As the initial data we used rain gauge recorder records of the variations of the rains during the warm period of the year, marked over the territories of the Veliko-Anadol'skiy (Donbass region) and Dubovskiy (Sal'skiya Steppes region) groups of shower gauges, and also in the Western Turkmenian and Western Kazakhstan discharge stations.

The selection of these regions is explained by the fact that it is precisely in the regions with the arid climate that the precipitation fields are distinguished by the highest variegation, the precipitation sources are relatively small, and correlation relationships of every type in them die down relatively rapidly.

Apparently, the greatest errors in the measurement of the characteristics of the precipitation fields may be expected in the flights of the satellites over such regions as the Ukrainian and Ural Steppes and also the semi-deserts and deserts of Wester-Turkmenia and Western-Kazakhstan.

All the regions investigated by us are located either in the zone of moderately dry (Veliko-Anadol'skiy shower-gauge group in the southern parts of the foothills of the Donetskiy ridge), or very dry arid climate. Among the latter we can mention the regions of the Dubovskiy shower gauge group in the central part of the Sal'skiya Steppes, the Western-Kazakhstan discharge stations in the semi-desert zone of the Aktyubinskaya oblast of the Kazakh SSR and the western Turkmenian discharge station in the southwestern Turkmenia zone.

Precipitation is one of the elements which is the least stable in space and time. The instability of precipitation is characterized the best by the instantaneous intensity, amplitude of fluctuations of which during the time of the rainfall may reach substantial dimensions. /213

Thus, in the Veliko-Anadol'skiy shower-gauge group region on the second of July 1955, the intensity of precipitation fluctuated between 0.00 and 3.6 mm/min. i.e., the instantaneous intensity during the rain varied by hundreds of times.

Even in such arid regions as Western Kazakhstan and Western-Turkmenia, during relatively brief rainfall, the amplitude of the fluctuations of the intensity of the precipitation falling reached substantial dimensions; thus, in Western-Kazakhstan on 28 June 1959, the intensity of the precipitation reached 2.90 mm/min., and in Western-Turkmenia on 4 July 1954 it reached 2.17 mm/min.

Moreover, it is precisely in the arid regions, where the shower type precipitation predominates, the instability of the precipitation intensity in time and area is the most sharply expressed.

According to data of Table 1, in which we give the recurrences of rains with different maximum intensity, we can judge also on the probability of precipitation with a certain amplitude of intensity fluctuations.

TABLE 1. RECURRENCE (%) OF RAINS WITH DIFFERENT MAXIMUM INTENSITY.

Region	Precipitation Intensity mm/min.								
	0,00–0,10	0,11–0,20	0,21–0,30	0,31–0,40	0,41–0,50	0,51–1,00	1,00–1,50	1,51–2,00	>2,00
Dubovskiy Shower-Gauge Group (1954-58)	21,4	20,6	13,0	6,5	11,0	12,0	7,5	4,0	4,0
Veliko-Anadol'skiy Shower-Gauge Group (1954-57)	10,4	21,0	10,4	8,3	8,3	27,0	6,2	4,2	4,2
West Kazakhstan Discharge Station (1954-59)	8,0	16,0	20,0	12,0	—	32,0	4,0	4,0	4,0
West-Turkmenian Discharge Station (1954-56)	50,0	17,4	6,5	6,5	2,2	6,5	8,7	—	2,2

Tr. Note: Commas indicate decimal points.

From Table 1 we can see that in the regions examined the most probable are the rains with an intensity of fluctuation amplitude from values close to zero to 1.0 mm/min. (85-90%).

The probability of precipitation with an intensity fluctuation amplitude from values close to zero to values of more than 2 mm/min is small; thus, in Western-Turkmania it amounts to only 2% of all the cases of rains, in the Sal'skiya Steppes (Dubovskiy shower gauge group) in the Ukraine (Veliko-Anadol'skiy shower-gauge group) and in Western-Kazakhstan it is about 4%.

We can judge about the share of precipitation of various intensities in the total amount of precipitation fallen during the season according to the data from Table 2. In this table, we can see that the greatest recurrence is observed for rains of low intensity (up to 0.05 mm/min.). Thus, in the region of the Dubovskiy shower-gauge group this recurrence amounts to 74%, in the region of the Western-Kazakhstan discharge station it amounts to 76%, and in the region of the Veliko-Anadol'skiy group it amounts to 80% and in the region of West-Turkmenian station to 87%.

About 10-15% of the length of all the rains in the regions investigated belong to precipitations with intensity of 0.06-0.10 mm/min. Precipitation with intensity higher than 0.10 mm/min. amounts to not more than 10-12% of the total length of rains. /214

The shares of precipitation with weak intensity in the total sum of the precipitation fallen is less than the percentage of their recurrence, however, even they are sufficiently large and amount to about 44% in the region of the West-Turkmenian discharge station, 25% in the region of the Dubovskiy group, 23% in the region of the Western-Kazakhstan station, and about 15% in the region of the Veliko-Anadol'skiy group.

TABLE 2. RECURRENCE (%) OF PRECIPITATION OF VARIOUS INTENSITY (NUMERATOR) AND THE SHARE OF PRECIPITATION OF THE GIVEN INTENSITY IN THE TOTAL SUM (DENOMINATOR).

Region	Precipitation Intensity mm/min						
	0,00–0,05	0,06–0,10	0,11–0,15	0,16–0,20	0,21–0,50	0,51–1,00	1,00
Veliko-Anadol'skiy Shower Gauge Group	80,0 / 14,8	9,1 / 10,4	3,0 / 5,8	0,8 / 2,3	3,6 / 17,7	2,5 / 25,0	1,0 / 24,0
Dubovskiy Shower-Gauge Group	73,6 / 25,0	15,0 / 18,0	4,2 / 9,0	1,7 / 5,0	3,8 / 20,2	1,3 / 15,0	0,4 / 7,8
West-Turkmenian Discharge Stations	87,4 / 44,0	7,8 / 19,5	0,8 / 3,7	0,2 / 1,3	1,1 / 13,4	2,5 / 8,3	0,2 / 9,8
West-Kazakhstan Discharge Stations	76,2 / 23,0	13,8 / 24,0	4,7 / 12,1	0,8 / 3,1	3,3 / 20,2	1,2 / 13,0	0,02 / 4,6

Tr. note: Commas indicate decimal points.

From Table 3, where we present the increasing share of various intensities in the length and total of all the precipitation fallen, we can see that in all the regions precipitations with the intensity of up to 0.50 mm/min. are the most probable (97-98% of the length of all the precipitation). However, the share of these precipitations in all the regions is different. It amounts to 51% in the Ukraine, 77% in the region of the Sal'skiya Steppes, and about 82% in Western-Turkmenia and Western-Kazakhstan.

TABLE 3. THE INCREASING SHARE (%) OF PRECIPITATION OF VARIOUS INTENSITIES IN THE OVER ALL LENGTH (1) AND TOTAL OF PRECIPITATION (2).

Precipitation Intensity, mm/min.	Veliko-Anadolskiy Group		Dubovskiy Group		West-Turkmenian Station		West-Kazakhstan Station	
	1	2	1	2	1	2	1	2
0,0–0,05	80,0	14,8	73,6	25,0	87,4	44,0	76,2	23,0
0,0–0,10	89,1	25,2	88,6	43,0	95,2	63,5	90,0	47,0
0,0–0,15	92,1	31,0	92,8	52,0	96,0	67,2	94,7	59,1
0,0–0,20	92,9	33,3	94,5	57,0	96,2	68,5	95,5	62,2
0,0–0,50	96,5	51,0	98,3	77,2	97,3	81,9	98,8	82,4
0,0–1,00	99,0	76,0	99,6	92,2	99,8	90,2	100,0	95,4
0,0–>1,00	100,0	100,0	100,0	100,0	100,1	100,0		100,0

Tr. Note: Commas indicate decimal points.

We should also note the low recurrence of precipitations of high intensity /215 (0.51-1.0 mm and more), it amounts to only 2-3%. As for their share in the total amount of precipitation, in the region of the Veliko-Anadol'skiy group it is sufficiently large (49%), in the Dubovskiy group region it accounts for about 23%, and in the Western-Turkmenian and Western-Kazakhstan discharge stations it accounts for about 18% of the total.

The maximum intensity of individual rains is of considerable interest for practical purposes.

As we can see from Table 1, in all the regions rains with the maximum intensity of up to 0.40 mm/min. predominate, they account for about 80% of all the cases of rainfall in Western-Turkmenia and 60% in the Sal'skiya Steppes.

In Western-Kazakhstan and in the region of the Veliko-Anadol'skiy station the probability of rains of such intensity is smaller (56 and 50% respectively).

The maximum of recurrence of precipitation in Western-Turkmenia and in the Sal'skiya Steppes belongs to the 0.0-0.10 mm/min. gradation (50 and 21% respectively), in Western-Kazakhstan and in the Ukraine to the 0.51-1.00 mm/min. gradation (32 and 27% respectively).

V. Yu. Kolomiytsev

Viktor Yur'yevich Kolomiytsev, whose works are published in the present collection, was born in Leningrad on 3 April 1937 in a family of physicists. His father Yuriy Ivanovich and mother Tat'yana Sergeyevna are the oldest members of the State Optical Institute named after S. I. Vavilov. Therefore it is natural, that after graduating from school in 1954, he entered the physical faculty of the Leningrad University, which he finished in 1960. In 1961, after one year of work at the State Optical Institute as a physicist enigneer, Viktor Yur'yevich became the Junior Scientific Worker in the Division of Radiation Investigations of the Main Geophysical Observatory. A short time before that the development of the method of meteorological observations from satellites was started at the Main Geophysical Observatory. Viktor Yur'yevich worked actively in the investigations on this theme. The problem on which he worked, consisted of finding the method of determining the luminosity of the earth-atmosphere system, i.e., the full flow of the outgoing shortwave radiation, according to the single value of brightness, measured by the instrument aboard the satellite. Inasmuch as the single value solution of the problem is impossible, the optimum solution was developed, which proposed the most probable value of the luminosity, corresponding to the given brightness value. According to the brightness the albedo of the sector of the terrestrial surface viewed was determined, on which depends to a great extent the shape of the brightness body, and the luminosity was determined further [1]. /216

This system was adopted at the Hydrometeorological Center USSR for Processing the observations of Soviet weather satellites.

In the development of the system mentioned, the hypothesis was made that the reflection from the terrestrial surface occurs according to Lambert's law. This hypothesis however, caused a certain confusion, because it was in direct opposition to the fact that the reflection from the sea, which is the principal underlying surface on the earth, is non-Lambertian. In order to show that actually this situation was not very substantial, it was decided to examine accuratly the problem with the anisotropic reflection from the bottom. The results of this analysis, published in the present collection [2-5], indicate, that the initial system proved to be generally correct. At the same time it was possible to establish the region of the angles around the direction of the mirror ray, where directions are necessary, and to indicate their value. The calculations performed at the same time made it possible to evaluate the screening action of the atmosphere on the possibility of determination of the wind velocity above the sea and the waves according to the measurements of the solar glitter [6]. In general, the totality of Viktor Yur'yevich's investigation, which are consistent and systematic, undoubtedly contains sufficient results for a prominent candidate's dissertation.

Even at the first acquaintance Viktor Yur'yevich left the impression of an educated and thoughtful physicist and this impression was augmented with further joint work with him. He was never in a hurry to answer a question posed, but after a careful analysis arrived at a clear and distinct solution. In spite of the grievous sickness which tormented him for many years, Viktor Yur'yevich always worked persistently. He maintained an even and attentive attitude towards his collaborators, especially to the junior ones. /217

The untimely death of Viktor Yur'yevich, which occurred suddenly on 6 January 1968, was a heavy blow to all those around him. The image of the courageous man and talented physicist will remain in the memory of all those who knew him.

K. S. Shifrin

List of Published Works by V. Yu. Kolomiytsov

1. "Determination of the Flow of Outgoing Shortwave Radiation by means of a Satellite," *Trudy GGO*, Issue 166, 1964 (jointly with K. S. Shifrin, N. P. Pyatovskaya).
2. "Procedure for Calculating the Shortwave Radiation Field During Anisotropic Reflection from the Underlying Surface," See the present collection (jointly with K. S. Shifrin).
3. "Outgoing Shortwave Radiation Field Over the Sea," See the present collection (jointly with K. S. Shifrin).
4. "Contribution of Diffused Reflection by the Water Layer to the Outgoing Shortwave Radiation Field," See the present collection.
5. "Effect of Anisotropy of the Reflection from the Underlying Surface on Determination of the Flow of Outgoing Shortwave Radiation According to Measurements from a Satellite," See the present collection (jointly with K. S. Shifrin).
6. "Determination of Wind Velocity in Waves on the Sea by Measuring the Solar Glitter Parameters from Satellites," See the present collection (jointly with K. S. Shifrin).

Trudy GGO, Issue 221 /219

SATELLITE METEOROLOGY

Editor: Ye. I. Il'yinykh

Technical Editor: I. K. Pelipenko

Proofreader: K. I. Rozinova

Delivered for setting on 16 April 1968.
Signed for printing 1 August 1968
Paper 70 × 108 1/16, Paper sheet 7.125.
Printed sheet 19.95. Textbook publication sheet 18.42.
Number of copies 740. M-12842. Index ML-22.
Hydrometeorological Press, Leningrad. V-53, 2nd line
House No. 23. Order No. 289, Price 1 ruble, 29 kopeks.

Leningrad Printing Office No. 8 of the

Glavpoligrafproma Komittee on Print of the
Council of Ministers of USSR Leningrad,
Prachechnyy Lane, 6.

SCIENTIFIC TECHNICAL HYDROMETEOROLOGICAL PUBLISHING HOUSE /228

GIDROMETEOIZDAT

Preparing for publication in 1969 the following monographs on meteorology

Borisenkov, E. P. and M. Ya. Romanov: "*Algoritmy i programmy statisticheskoy Obrabotki Informatsii na ETsVM*" (Algorithms and Programs of Statistical Processing of Information on Electronic Computers).

23 sheets, price 1 ruble 20 kopeks

Gutman, L. N.: "*Vvedeniye v Nelineynuyu Teoriyu Mezometeorologicheskikh Protsessov*," (Introduction into the Linear Theory of Mesometeorological Processes),

18 sheets, price 95 kopeks

Dikiy, L. A.: "*Teoriya Kolebaniy Zemnoy Atmosfery*", (Theory of Oscillations of the Terrestrial Atmosphere),

12 sheets, price 65 kopeks

Imyanitov, I. M.: "*Elektrizatsiya Samoletov v Oblakakh i Osadkakh Radiatsionnyye Kharakteristiki Atmosfery*", (Electrification of Airplanes in Clouds and Precipitations),

10 sheets, price 55 kopeks

"*Radiatsionnyye Kharakteristiki Atmosfery*", (Radiation Properties of the Atmosphere) Collective of authors edited by K. Ya. Kondrat'yev.

30 sheets, price 1 ruble, 50 kopeks

Logvinov, K. T.: "*Stratosfera*", (The Stratosphere),

12 sheets, price 55 kopeks

Minina, L. S.: "*Praktika Nefanaliza*", (The Practice of Nephanalysis),

17 sheets, price 1 ruble, 10 kopeks

Sazonov, B. I.: and V. F. Loginov: "*Solnechno-Troposfernyye Svyazi*", (The Solar-Tropospheric Relationships),

6 sheets, price 45 kopeks

Khrgian, A. Kh.: *"Fizika Atmosfery,"* (Physics of the Atmosphere)
34 sheets, price 1 ruble 80 kopeks

We request that your orders be delivered into the local bookstores.

In case of refusal we request you to send orders on the following address: Leningrad, P-101, Bol'shoy p.r., House No. 57, Store Number 15 of Lenk

Please remember that the timely delivery of the preliminary orders makes it possible to determine more correctly the number of copies of the books to be printed!

Gidrometreoizdat

Translated for the National Aeronautics and Space Administration under contract No. NASw-1695 by Techtran Corporation, P.O. Box 729, Glen Burnie, Maryland 21061

NATIONAL AERONAUTICS AND SPACE ADMINISTRATION
WASHINGTON, D. C. 20546

OFFICIAL BUSINESS

FIRST CLASS MAIL

POSTAGE AND FEES PAID
NATIONAL AERONAUTICS AND
ADMINISTRATION

04U 001 45 51 3DS 70151 00903
AIR FORCE WEAPONS LABORATORY /WLOL/
KIRTLAND AFB, NEW MEXICO 87117

ATT E. LOU BOWMAN, CHIEF, TECH. LIBRARY

POSTMASTER: If Undeliverable (Section 158 Postal Manual) Do Not Return

---

"The aeronautical and space activities of the United States shall be conducted so as to contribute . . . to the expansion of human knowledge of phenomena in the atmosphere and space. The Administration shall provide for the widest practicable and appropriate dissemination of information concerning its activities and the results thereof."

— NATIONAL AERONAUTICS AND SPACE ACT OF 1958

NASA SCIENTIFIC AND TECHNICAL PUBLICATIONS

TECHNICAL REPORTS: Scientific and technical information considered important, complete, and a lasting contribution to existing knowledge.

TECHNICAL NOTES: Information less broad in scope but nevertheless of importance as a contribution to existing knowledge.

TECHNICAL MEMORANDUMS: Information receiving limited distribution because of preliminary data, security classification, or other reasons.

CONTRACTOR REPORTS: Scientific and technical information generated under a NASA contract or grant and considered an important contribution to existing knowledge.

TECHNICAL TRANSLATIONS: Information published in a foreign language considered to merit NASA distribution in English.

SPECIAL PUBLICATIONS: Information derived from or of value to NASA activities. Publications include conference proceedings, monographs, data compilations, handbooks, sourcebooks, and special bibliographies.

TECHNOLOGY UTILIZATION PUBLICATIONS: Information on technology used by NASA that may be of particular interest in commercial and other non-aerospace applications. Publications include Tech Briefs, Technology Utilization Reports and Technology Surveys.

Details on the availability of these publications may be obtained from:

SCIENTIFIC AND TECHNICAL INFORMATION DIVISION

NATIONAL AERONAUTICS AND SPACE ADMINISTRATION

Washington, D.C. 20546